

043
KRI
15013

DYNAMICS OF LARGE SCALE
HEAT INDUCED CIRCULATIONS
IN THE TROPICAL ATMOSPHERE

R. KRISHNAN

THESIS SUBMITTED FOR THE DEGREE
OF
DOCTOR OF PHILOSOPHY IN PHYSICS
OF
THE UNIVERSITY OF POONA

PHYSICAL RESEARCH LABORATORY
AHMEDABAD
INDIA

043



B15013

APRIL 1993

043
KRI
15013

CERTIFICATE

CERTIFIED that the work incorporated in the thesis entitled 'Dynamics of Large Scale Heat Induced Circulations in the Tropical Atmosphere' submitted by Shri R.KRISHNAN is an authentic record of the work carried out by him at the Physical Research Laboratory, Ahmedabad, under my supervision and that no part thereof has been presented earlier for any other degree. Such material as has been obtained from other sources has been duly acknowledged in the thesis.

April 1993.

R.N. Keshavamurthy
(R.N.Keshavamurthy)
Supervising Guide

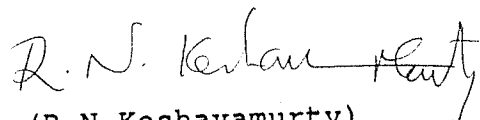
043
KRI
15013

DECLARATION UNDER RULE 4(E) OF THE RULES FOR THE DEGREE OF
DOCTOR OF PHILOSOPHY (Ph.D) OF THE UNIVERSITY OF POONA.

It is certified that in the case of all the joint papers incorporated in the thesis, the major contribution to the papers is by the candidate. Contributions by the co-authors other than the guide has been only in respect of providing supports, like processing of data and assistance in computations.



(R. KRISHNAN)
Candidate



(R.N. Keshavamurty)
Supervising Guide

April 1993.

Dedicated to my
Mother, Father, Sister
and
in memory of my Grandmother

Contents

Acknowledgements	iv
Abstract	vi
1 Introduction	1
1.1 Large scale circulations in the tropical atmosphere	1
1.2 Plan and scope of the thesis	4
1.2.1 The time-mean Walker circulation in the Pacific	4
1.2.2 The winter and summer time-mean circulations during 1979	7
1.2.3 The vorticity balance in the tropical upper troposphere	10
1.2.4 Linear and nonlinear studies of the tropical Hadley cell	12
1.2.5 Northward propagation of the 30-50 day oscillation	15
2 Dynamics of the Time-Mean Walker Circulation	18
2.1 Introduction	18
2.1.1 The diabatic heating in the tropical atmosphere	19
2.1.2 GCM studies of interannual variability	21
2.1.3 Stationary and transient waves in the tropical atmosphere	23
2.2 Aims of the present study	26
2.3 Linear steady state model formulation	28
2.4 Linear steady state solution	30
2.5 The nonlinear global spectral model	32

2.6	Experiments and Results	33
2.6.1	Idealized forcing experiments using heat source and sink . . .	33
2.6.2	Analytical calculations	37
2.6.3	Sensitivity studies with the 2-level model	42
2.6.4	Effects of nonlinearities on the stationary waves	44
2.7	Conclusions	51
3	The Winter and Summer Time-Mean Circulations during 1979	53
3.1	Introduction	53
3.1.1	Observational studies	54
3.1.2	Modelling studies	55
3.1.3	Objectives of the present study	57
3.2	Time-mean circulations during winter 1978-79	58
3.2.1	2-level linear equatorial β -plane model	59
3.2.2	5-level nonlinear global spectral model	64
3.3	Time-mean circulations during summer 1979	68
3.3.1	2-level linear equatorial β -plane model	71
3.3.2	5-level nonlinear global spectral model	73
3.4	Conclusions	77
4	A Study of the Vorticity Balance in the Tropical Upper Troposphere	81
4.1	Introduction	81
4.1.1	Observational and diagnostic studies	82
4.1.2	Theoretical studies based on linearized models	84
4.1.3	Theoretical studies based on nonlinear models	85
4.2	Motivation for the present study	87
4.3	The terms in the vorticity equation	89
4.4	Vorticity balance at 300 mb in a global spectral model	90
4.5	Concluding remarks	94

5	Linear and Nonlinear Studies of the Time-Mean Tropical Hadley Circulation	97
5.1	Introduction	97
5.1.1	Earlier studies	98
5.1.2	Aims of the present study	100
5.2	Model	102
5.3	Experiments with the axisymmetric model	104
5.4	Results and Discussion	105
5.5	Conclusions	112
6	The Tropical Low-Frequency Intraseasonal Oscillation and its Meridional Propagation	115
6.1	Introduction	115
6.1.1	Salient features of the low-frequency 30-50 day oscillation	115
6.1.2	Theoretical explanations for the low-frequency wave	119
6.1.3	Meridional propagation of the low-frequency oscillation	122
6.2	Northward propagation in an axisymmetric global spectral model	127
6.3	Concluding remarks	132
	References	134
	List of Publications	154

Acknowledgements

At the outset, I wish to express my deep sense of gratitude to my thesis supervisor Prof.R.N.Keshavamurty, for taking keen interest and guiding me throughout my Ph.D work. His willingness to discuss the subject, in a simple and effective manner, has given me a proper appreciation of meteorology. I sincerely thank him for the encouragement and the support he has provided to me.

I am extremely thankful to Prof. V.Satyan for the useful discussions I had with him during my Ph.D work. I have been benefitted from the comments of Prof.V.Satyan and Prof.B.H.Subbaraya, during my assessment reviews at PRL. I take this opportunity to thank both of them. It is a pleasure to acknowledge Mr.S.V.Kasture for helping me understand the '5-level global spectral model' code. A substantial portion of my computational work was possible through his sincere help at various stages. I would like to thank him for his simple and friendly nature. I would like to specially thank my friend Kishku, who patiently explained many interesting problems in dynamic meteorology. During the last six years of my association with him, I had very useful discussions on varied topics. I am extremely thankful to him for his nice company.

Discussions with Dr.Sai Iyer have helped me to perform some of my thesis calculations. His help on PC-TEX has been of immense use to me. I acknowledge my sincere thanks to him for his kind help. I would like to thank Dr. B.R.Sitaram, for his Contour and 2D-Plot packages on DEC-10, which were of great use during my Ph.D work. My grateful thanks to Profs.R.K.Verma, J.C.Parikh, A.C.Das, A.R.Prasanna, V.B.Sheorey and J.N.Goswami for taking interest in my progress.

I am left with no words, that can gratify, all my wonderful friends in the hostel. Although I have been away from the hostel for nearly an year, I cannot forget the golden period (1987-1992) of my life. In the first place, I greatly enjoyed the company

of my batchmates Guru, Ganguly, Seema, Supriyo and Manohar Lal, right from the days of our PRL coursework. Lively discussions on academic as well as non-academic issues with Jerry, Viju, Raju, Subrat, Kishku, Aswini, Dipankar, Jitesh, Bhaskaran, Sushant, Mathew, Subba and Sunil Rawat made my stay at PRL very interesting. I shall always cherish the cheerful and unforgettable company of my pals Guru, Sam, Ramani and Ramachandran. My friendship with them has been very unique. The vibrant discussions with Pandey, Sarkar, Bhushan, Anjan and Navin, inside and outside the volley ball court, will always be evergreen in my memory. The joyful company of Mac, Debi, Ashok Sen, Swetketu, Durga, Srinivasan, Manoj, Himadri, Debashish Majumdar, Lambodar, Yadav, Somesh, Gopal, Yags, Gautam, Biswa, Prahlad, Varun, Pal-lam, Mitazi, Sushma, Anshu, Poulouse, Watson, Shibu, Dhinna, Chacko, Debabrata and Sandeep is acknowledged. My thanks to Raju, Subrat, Guru, Ramani and Ramachandran for their help while finalising the thesis.

I accord my thanks to the staff of the PRL computer centre as well as the library, for their excellent support. In addition, I express my thanks to Mr.S.K.Bhavsar, for drafting my thesis diagrams.

I have received encouragement from my parents, sister and brother-in-law, which shall be gratefully remembered always. It is indeed a great pleasure to recall the affection of kids, Sudha, Shruthi and Bishnu. The hospitality provided by my uncle and his family at Delhi, has been of great help and I thank all of them for the same. I am grateful for the company of my friends at NCMRWF during the last one year. In particular, I acknowledge the help I have received from Kishku, Sasi and their families.

Abstract

The most discernible feature in the tropical atmosphere is the strong longitudinal variation in the distribution of the diabatic heating. The zonally asymmetric distribution of heat sources and heat sinks, drives the planetary scale circulations in the tropics. In addition, the heating pattern also exhibits considerable latitudinal variation, especially in the Indian summer monsoon region, which results in meridional circulations. The heat induced east-west (Walker) and meridional (Hadley) circulations offer an excellent opportunity to understand the dynamics of the large scale tropical atmospheric motions. One of our studies is a theoretical investigation of the dynamics of the time-mean Walker circulation in the equatorial Pacific. For this purpose, we have performed idealized forcing experiments, using a 2-level linear equatorial β -plane model and also a 5-level global spectral model. Analytical calculations have also been included to substantiate our results. A comprehensive examination of the nonlinear character of the stationary equatorial Kelvin and Rossby waves has also been carried out. Besides performing experiments with idealized forcings, the steady state circulations based on realistic forcings have also been examined. Here the observed time averaged diabatic heating rates for winter (1978-79) and summer (1979) were used for forcing the 2-level and the 5-level models, and the time-mean Walker and Hadley-type circulations during these seasons were studied. Our study also includes diagnostic calculations of the time-mean vorticity balance in the tropical upper troposphere. These calculations were essentially based on the outputs from the numerical experiments conducted with a 5-level nonlinear global spectral model. Another aspect that has been dealt in this thesis relates to linear and nonlinear studies of the time-mean tropical Hadley circulation, using a 5-level axisymmetric global spectral model. The final aspect of our study is an investigation of the interaction between the tropical 30-50 day oscillation and the Indian summer monsoon. More specifically, we have looked into the issue that concerns the northward movement of

the low-frequency oscillation over the Indian summer monsoon region. A compact chapterwise account of the several questions that have been addressed in the thesis and the key results that were obtained, are presented below.

Chapter I commences with a description of some of the important components of the large scale circulations in the tropics, namely, the structure of the time-mean heating distributions during winter and summer, the dynamics of the major time-mean planetary and synoptic scale circulations, and finally the characteristics of the tropical low-frequency intraseasonal transients. Although these discussions are general, the stress is mostly on the topics directly related to the thesis. A description of some of the earlier studies (observational, diagnostic, theoretical and modelling) has been provided in order to maintain coherence and continuity of the subject. There is a section on the plan and scope of the thesis, which essentially describes the theoretical problems that were studied, followed by a summary of the important results and conclusions.

In **Chapter II**, we deal with idealized theoretical studies of the time-mean Walker circulation in the equatorial Pacific. Observations show the existence of an intense convective heat source over Indonesia, which is most prominent during the northern winter. The heating over Indonesia, drives planetary scale circulations, both to its west and east. The eastward branch over the Pacific, has a longitudinal scale of about 15000-20000 kms. There is also a cloud free region over the eastern Pacific where the longwave cooling is large. This region is characterized by strong subsiding motion and surface easterly winds. The understanding of the variability of the Walker circulation is a challenging problem in the field of climate modelling. One of the key questions that needs to be understood is the time-mean response of the tropical atmosphere forced by the heating over Indonesia and the cooling over the eastern Pacific. We have performed a theoretical investigation of the time-mean

Walker circulation in the Pacific, in respect of the factors that control its longitudinal scale and intensity. Our studies are based on idealized forcing experiments using a) A 2-level linear equatorial β -plane model b) A 5-level global spectral model. The formulation of the 2-level linear equatorial β -plane model has also been discussed in this chapter in a detailed manner. In addition, analytical calculations have been included to strengthen our results.

Gill (1980), in his well-known work, calculated the tropical atmospheric time-mean response, induced by an idealized heat source. He used the long wave approximation and determined the response for a single vertical mode, having a particular equivalent depth. He demonstrated that a heat source symmetric with respect to (w.r.t) the equator, generated stationary Kelvin waves to its east and stationary Rossby waves to its west. He offered an elegant explanation for the Walker circulation in the equatorial Pacific, in terms of the stationary Kelvin waves. The model of Gill (1980) was based on a linearized system of shallow water equations on an equatorial β -plane. However, the main weakness in Gill's model is the fact that the dissipation terms (Rayleigh friction and Newtonian cooling) are tunable parameters in the model. Gill (1980) made use of very strong dissipation terms (e-folding time ~ 2 days), to explain the scale and intensity of the time-mean circulations. Since the cause for such strong damping effects in the tropical atmosphere is not clearly understood, it may not be justifiable to employ them in the model. We have used both the 2-level model and the 5-level model and shown that the radiative cooling in the eastern Pacific is an important factor that determines the zonal scale and intensity of the Walker circulation. It should be noted that we have used weak dissipation terms in our forcing experiments. We find that the longitudinal extent and strength of the Walker circulation primarily depend on the relative positions and intensities of the heat source over Indonesia and the longwave cooling in the eastern Pacific. In fact, our analytical calculations suggest that the Walker circulation in the equatorial

Pacific, can be explained as a superposition of Kelvin waves emanating from the heat source and Rossby waves from the heat sink. It is also found that the changes in the separation between the heat source and the heat sink can produce variability in the scale and intensity of the Walker circulation.

Another aspect that has been examined, utilising both linear and nonlinear models, pertains to the impact of nonlinear terms on the tropical time-mean response forced by idealized diabatic heating. Simple scale analysis suggests that tropical large scale motions are associated with higher Rossby number and significant advective accelerations. Also, the tropical atmosphere possesses several jet streams (eg. the subtropical jet, tropical easterly jet and the somali jet) which can produce strong nonlinear advective effects. Therefore, it is important to study the influence of nonlinear terms on the dynamics of the time-mean motions in the tropical atmosphere. The impact of nonlinear terms on the stationary Kelvin and Rossby waves, has been determined by comparing the equilibrium solutions in the linear and the nonlinear models. It was found that the nonlinearities affect the stationary Kelvin and Rossby waves predominantly near the region of a strong convective forcing. Large eastward shift of the highs at the upward levels was noticed to the west of the forcing region. The maximum eastward shift to the west of the forcing and close to the equator was as large as 20° longitudes. Due to this eastward shift, the anticyclonic circulation over the region of forcing became stronger. We have convincingly demonstrated that the nonlinear terms significantly enhance and to some extent modify the structure of the upper level divergence over the forcing region. In the linear model of Gill (1980), this eastward shift can be explained only when strong dissipation terms are present. On the other hand, we find that even in the presence of weak friction, the nonlinear advection terms can produce realistic phase relation between the upper tropospheric divergence and geopotential distributions. Similar forcing experiments with a heat source having smaller intensity, suggest that the influence due to nonlinear terms

decreases in the case of the weak forcing. We have examined the vertical structure of the time-mean zonal winds, horizontally averaged near the forcing region. It is found that the vertical profiles of the zonal wind in the linear and nonlinear models show important differences, especially in the mid tropospheric levels. In particular, at the level where the heating intensity is maximum, it is seen that nonlinearities appear to favour the generation of westerlies. To the west of the forcing region, an enhancement of the vertical shear in the zonal wind at the upper levels is seen in the nonlinear model. These two important nonlinear effects, i.e., (i) generation of westerlies (ii) the enhancement of vertical shear in the basic flow, may be useful from the point of understanding the propagation characteristics of transient Rossby waves from the tropics to the extratropics and the phenomenon of midlatitude teleconnection. We have also investigated the time-mean response induced by an antisymmetric heat source (heating to the north and cooling to the south of the equator) using both linear and nonlinear models. It is found that the stationary Rossby waves to the west of the forcing region were significantly modified due to effect of nonlinear advection terms. An eastward advection of upper level anticyclone (cyclone), to the west of the forcing region, was noticed to the north (south) of the equator.

In **Chapter III** we have studied the tropical time-mean Walker and Hadley-type of circulations forced by the observed time-mean diabatic heating fields. Using the 2-level linear equatorial β -plane model as well as the 5-level global spectral model, we have calculated the steady-state circulations for winter (1978-79) and summer (1979). The forcings used in the models were based on the heating rates computed by Schaack *et.al* (1990) from the Global Weather Experiment (GWE), for the period December 1978 to November 1979. The observed diabatic heating was prescribed at the 500 mb level as forcing in the 2-level linear equatorial β -plane model. However the 5-level nonlinear global spectral model was forced using the observed heating at all the 5 vertical levels in the model.

The time-mean heating during winter (1978-79) was characterized by convection located along the Inter Tropical Convergence Zone (ITCZ) that extended from South America across the Atlantic, Africa, the Indian ocean and the western Pacific. A well defined cooling maximum (1.0°K per day), was seen in the oceanic regions of the eastern Pacific and to the west of Australia. Both the model responses show the major features, such as the Walker circulation in the Pacific, and the east-west circulations associated with the diabatic heating over continental South America and Africa. However, the circulation features in the case of the 2-level model were weaker than the flow patterns in the 5-level model. The Walker circulation in the Pacific was better reproduced in the case of the 5-level model. This was mainly because of a more accurate vertical representation of the heating field in the 5-level model. On the other hand, the vertical variation of the forcing in the 2-level model was essentially restricted to the first baroclinic mode. In addition, there are no advection terms in the 2-level linear model. On the contrary, the presence of nonlinear advection terms, does account for the realistic time-mean circulations in the 5-level model. Using the maps of velocity potential distribution at 300 mb, we have calculated the intensities of the Walker and Hadley circulations. The longitudinal variation of the Walker circulation suggests that the east-west circulations during winter (1978-79) were strongest in the region of south-eastern and central equatorial Pacific. The Hadley-type of circulation over the western Pacific and the meridional circulation associated with the Australian summer monsoon were strongest near the equator. The Walker and Hadley-type of circulations computed from the velocity potential maps, match well with the observations during winter (1978-79).

During the northern summer of 1979, the major heat zones were located over the Tibetan plateau, Bay of Bengal and northeast India and over the Mexican highlands. Regions of radiative cooling were located over the oceanic north Pacific and

Atlantic. The Indian monsoon region was characterized by a Hadley circulation comprising of a low-level south westerly flow and strong upper level easterlies. Upper level easterlies occurred also over Mexico. In addition to the Hadley circulation over India, there were major east-west circulations associated with the diabatic heating over India and Mexico. Both the 2-level and the 5-level models, reproduced the gross features of the upper level Tibetan and Mexican anticyclones and the upper level easterlies over these regions. However, the easterly speed was weaker in the 2-level model. The upper level easterlies and the low-level southwesterly flow over the Indian monsoon region were more realistic in the 5-level model. The accurate vertical representation of heating and also the inclusion of nonlinear effects are two main factors responsible for the more realistic time-mean circulations in the 5-level model. The velocity potential distribution showed subsidence near northwest India and Pakistan. This subsidence possibly accounts for the poor rainfall which was observed over northwest India during summer (1979). The intensities of the east-west circulations computed from the velocity potential distribution at 300 mb, reveal that the east-west circulations, induced by the heat source over the Indian monsoon region, were quite strong. The intensity of the Hadley circulation over the Indian monsoon region was strongest over the region of Tibetan plateau and the foothills of Himalayas.

Chapter IV is a diagnostic study of the vorticity balance at 300 mb in the tropical atmosphere. The outputs of the forcing experiments with the 5-level global spectral model, were used for this analysis. The vorticity equation is an extremely useful tool for understanding the spatial and temporal evolution of the tropical atmospheric motions. In the past, there have been studies of the vorticity balance, using both linear and nonlinear models. The results from the linear models showed significant differences from those of the nonlinear models. The linear models tried to explain the observed vorticity balance at the upper levels in the tropical atmosphere, by incorporating strong vorticity damping (e-folding time < 1 day) term in

the model. It was conjectured that this large vorticity damping may be due to vertical transport of horizontal momentum by cumulus convection. On the other hand, nonlinear model calculations suggest that, nonlinearities play an important role in determining the vorticity balance in the tropics. Quite contrary to the linearized calculations, the nonlinear models argue that there is no necessity to include strong vorticity dissipation in the model.

In view of the above discrepancies between the earlier linear and the nonlinear calculations, we have re-investigated the nature of vorticity balance in the tropical upper troposphere. The significance of nonlinear dynamical effects on the stationary Kelvin and Rossby waves in the tropics, was already demonstrated in Chapter II. One can also estimate the impact of nonlinear terms on the time-mean vorticity balance in the tropical troposphere by means of diagnostic calculations. The model outputs of three forcing experiments (i.e., an idealized forcing using heat source and sink, forcing for winter (1978-79), and forcing for summer (1979)), with the 5-level global spectral model, were used as datasets for our analysis. The dissipation terms used in the model were very weak and the model was integrated till a steady-state was attained in all the 3 cases. Using the model generated fields, we have explicitly computed all the terms in the vorticity equation, including the vertical advection and twisting terms. In addition, computations of the area averages, of the various terms in the vorticity equation, over different regions, were also carried out. For the case of the idealized forcing, the region between the heat source and the sink was chosen for calculating the area averages. In the case of winter 1978-79, the area averages were calculated in the region of the Walker circulation over the equatorial Pacific. In the case of summer 1979, the averages were calculated for the region covering the northern summer monsoon area. It was found that the dominant balance in the tropical upper atmosphere, was between the nonlinear terms involving the time-mean vorticity stretching and the horizontal advection of absolute vorticity.

The contribution from the vertical advection and twisting terms was found to be small. Similarly, the terms involving the transients were found to be quite small in the tropics. The main conclusion of this study is that nonlinear dynamics plays an important role in the vorticity balance of the tropical upper troposphere.

In Chapter V we present an account of linear and nonlinear studies of the time-mean tropical Hadley circulation using an axisymmetric 5-level global spectral model. In the past there have been quite a few theoretical studies of zonally symmetric flows. In the linear models it was found that the mean-meridional circulation driven by the zonally symmetric distribution of latent heat, matched with the annual mean observed circulation only when cumulus friction was included in the model. However there is still uncertainty regarding the actual estimates of cumulus friction in the tropical atmosphere. In contrast to linear models, the nonlinear calculations and general circulation model (GCM) simulations, suggest that nonlinearities are more important in determining the structure and intensity of the tropical Hadley cell. These studies also showed that cumulus friction effects are not very significant. In the light of the differences between the linear and nonlinear calculations, we have re-investigated the significance of nonlinear dynamics with regard to the time-mean tropical Hadley cell.

Studies of the zonally symmetric response of the tropical atmosphere to idealized forcing, have been carried out using both linear (LM) and nonlinear (NLM) versions of a 5-level axisymmetric global spectral model. We have chosen weak Rayleigh friction and Newtonian cooling terms having long dissipation time scales (e-folding time ~ 15 days). In the first set of experiments, where the diabatic heating was quite strong, it was found that there is a significant transport of easterly momentum from the surface to the upper layers of the atmosphere due to nonlinear vertical advection. This resulted in the slowing down of the low level easterly winds in the NLM.

An explicit calculation of the angular momentum transport terms also revealed this significant vertical transfer of easterly momentum by the nonlinear advection terms near the forcing region. In addition it was seen that the nonlinear meridional advection terms displaced the core of the upper level westerly jets, poleward by about 6° latitude. The equilibrium temperature in the LM was much warmer (max warming $8-10^\circ\text{K}$), in the lower and middle troposphere, as compared to the NLM. The warming in the LM was mainly because of the neglect of nonlinear vertical advection of temperature which resulted in very little adiabatic cooling in the LM. Due to the warmer temperatures in the LM, there was an excess of global mean kinetic energy generation (GMKE). The damping of GMKE in the NLM appears to be mainly related to the nonlinear effects ((a) strong adiabatic cooling associated with vertical ascent and (b) vertical transport of momentum from surface to upper layers). In another set of experiments the intensity of forcing was decreased. It was found that when the heating is weaker, the impact of nonlinear terms becomes smaller resulting in (i) a reduction in the vertical transport of easterly momentum by nonlinear vertical advection (ii) a decrease in the poleward shift of the upper level westerly jets by nonlinear meridional advection (iii) reduced warming, associated with the neglect of nonlinear vertical advection of temperature, in the LM (iv) a decrease in dissipation of GMKE in the NLM. These results indicate that the influence of nonlinear terms on the tropical Hadley cell is quite dependent on the intensity of the forcing.

Chapter VI deals with the study of the tropical low-frequency intraseasonal oscillation and its behavior over India during the northern summer. On the subseasonal time-scale, the tropical atmosphere is characterized by a slow eastward propagation of equatorial convective activity, which has a periodicity of about 30-50 days. This chapter begins with an elucidation of the various observational, diagnostic and theoretical studies, that have extensively documented the 30-50 day oscillation. One of the interesting problems, that is not yet fully understood, is the interaction of this

equatorial 30-50 day mode with the summer monsoon circulation over India. Numerous observational findings indicate that, when this oscillation arrives over the Indian summer monsoon region, a distinct northward propagation of convective activity, with a speed $\sim 1^\circ$ latitude per day, occurs. In fact, observations suggest that there is a strong association between the low-frequency monsoon variability over India and the equatorial 30-50 day mode. A primary step towards understanding the active and break phases associated with the Indian summer monsoon, lies in the explanation of the physical mechanisms that govern the northward movement of the 30-50 day oscillation.

We have used an axisymmetric 5-level global spectral model, to study the northward migration of the tropical low-frequency oscillation. Essentially, we have examined the interaction between the monsoon-type of basic flow and the tropical cumulus convection. A basic flow which closely resembles the time-mean Hadley circulation over the Indian monsoon region, was first generated in the model by forcing it with an appropriate heating distribution. Later on, near-equatorial perturbations were produced in the model by temporarily switching on an equatorial heat source. These perturbations superposed on the monsoon basic flow, represent the arrival of the 30-50 day mode over the Indian monsoon region. We then investigated the impact of cumulus heating (Conditional Instability of the Second Kind (CISK)) on the evolution of the perturbations. The cumulus heating based on CISK was interactively determined from the low-level circulation. It was observed that the perturbations moved northward at the rate of about 0.5° latitude per day. It was further found that the cumulus heating field was meridionally ahead of the low-level zonal wind. This meridional phase difference, induced by the CISK mechanism, resulted in a northward movement of the low-frequency transients. The primary conclusion of this study is that, the interaction between the monsoonal circulation and the cumulus convection associated with the intraseasonal oscillation plays a significant role in producing the

northward progression of the low-frequency intraseasonal transients.

Highlights

The important results, that have been reported in the thesis, are listed below.

- Our idealized forcing experiments (based on a 2-level linear equatorial β -plane model, a 5-level global spectral model and analytical calculations) suggest that the time-mean Walker circulation in the equatorial Pacific can be explained as a superposition of the stationary Kelvin waves emanating from the heat source over Indonesia and the stationary Rossby waves forced by the heat sink in the eastern Pacific.
- A comparison of the low latitude stationary wave response in linear and non-linear models, shows that nonlinear terms significantly affect the Kelvin and the Rossby waves in the vicinity of a strong symmetric heat source. Close to the equator and on the western side of the forcing, it is found that nonlinear advection terms produce an eastward displacement of anticyclonic features at the upper levels, thereby enhancing the anticyclonic circulation over the forcing region. Also the divergence over the forcing region increases and shows some structural changes. When the strength of the forcing is reduced, the impact of the nonlinear terms is smaller. In the case of an antisymmetric heat source, an eastward advection of anticyclone (cyclone), on the western side of the forcing, is noticed in the northern (southern) hemisphere. The vertical structure of the time-mean zonal wind, shows significant differences in the middle tropospheric levels. At the vertical level, where the heating intensity is maximum, nonlinearities favour the generation of westerlies. Nonlinear terms significantly increase

the vertical shear at the upper tropospheric level. The stronger westerlies and the enhanced vertical shear in the basic zonal winds, arising because of nonlinear effects, may be important for midlatitude teleconnection and the propagation of transient Rossby waves from the tropics to midlatitudes.

- The time-mean circulations for winter (1978-79) and summer (1979) were studied, by forcing a 2-level linear equatorial β -plane model as well as a 5-level nonlinear global spectral model with the observed diabatic heating rates during these seasons. The Walker circulation in the equatorial Pacific during winter (1978-79) and the circulations at the lower and upper levels over the Indian monsoon region during summer (1979) were more realistic in the case of the 5-level model. This is mainly because of an accurate vertical representation of diabatic heating in the case of the 5-level model. In addition, nonlinear terms do account for the more realistic time-mean circulations in the 5-level model. The intensity of the Walker and Hadley circulations, computed from the steady state velocity potential distributions in the 5-level model, was rather realistic.
- Diagnostic studies of the vorticity balance at the upper levels of the tropical troposphere indicate that nonlinear terms in the vorticity equation are very important in determining the time-mean vorticity balance in the tropics. The primary balance is between the nonlinear advection of absolute vorticity by the time-mean horizontal wind and the time-mean absolute vorticity stretching term. The vertical advection and twisting terms and the terms involving the transients contribute negligibly to the balance.
- Linear (LM) and nonlinear (NLM) model studies of the tropical time-mean

Hadley circulation show that a significant transport of easterly momentum from the surface to the top of the atmosphere, associated with nonlinear vertical advection, can occur over the region of strong forcing. This presumably results, in the slowing down of the low-level easterlies in the NLM. The meridional advection terms produce a poleward displacement of the upper level westerly jet. A large warming is observed over the forcing region in the LM, which is caused by the neglect of nonlinear vertical advection of temperature. The nonlinear interactions associated mainly with (a) adiabatic cooling due to ascent and (b) vertical transport of easterly momentum, lead to significant dissipation of the global mean kinetic energy in the NLM. When the forcing intensity is reduced, the above mentioned nonlinear effects also decrease.

- Using an axisymmetric version of a 5-level nonlinear global spectral model, we have studied the northward movement of the tropical low-frequency oscillation over the Indian summer monsoon region. It is found that the interaction between the convective heating and the monsoon basic flow is very important in governing the northward migration of the intraseasonal transients. Our study shows that there occurs a meridional phase difference between the low-level zonal wind and the heating field. This phase difference consequently leads to the northward movement of near-equatorial perturbations.

Chapter 1

Introduction

1.1 Large scale circulations in the tropical atmosphere

In this chapter an overview of the large scale characteristics of the tropical atmospheric circulations has been presented. In order to gain a good appreciation of this subject, we first elucidate the main features such as: the structure of the time averaged heating in the tropical troposphere, the dynamics of the time-mean tropical Walker and Hadley circulations and the variability associated with tropical atmospheric motions on different time scales. Although the above discussions are quite general, the emphasis is mainly on the aspects that are directly relevant to the thesis. After presenting a general outline, we have summarized the various theoretical problems that were examined along with the important results.

Much of the large-scale circulations in the tropics are directly driven by convective heating. Considerable insight into the dynamics follows from a study of the response of the atmosphere to tropical heat sources and heat sinks. The diabatic heating is a foremost component of the tropical atmospheric system. The dominant contribution to the diabatic heating in the tropics comes from latent heat release by

cumulus clouds. A broad sketch of the observed time-mean heating in the tropical atmosphere is given below. Observations by Ramage (1968), Krueger and Winston (1974), Liebmann and Hartmann (1982) and many others, indicate that the tropical atmosphere possesses strong longitudinal variations in the distribution of cloudiness and precipitation. The zonally asymmetric distribution of tropical convective activity arises primarily because of the heating associated with the warm sea surface temperature (SST) and equatorial land areas. The regions of intense equatorial convection are located mostly over Indonesia and western Pacific, continental Africa and South America. There are also cloud free zones (eg. eastern Pacific, the deserts of Iran and Saudi Arabia), which are associated with radiative cooling. This longitudinal variation in the heating distribution drives the planetary scale circulations in the tropics. A schematic view of the prominent east-west circulations in the tropical atmosphere is shown in Fig.1.1. The major divergent circulations associated with the convective heat sources over equatorial Africa, western Pacific and South America are well depicted in Fig.1.1. The most striking feature is the east-west circulation in the equatorial Pacific, which is forced by the deep convective heating over Indonesia and western Pacific. The eastward branch of the divergent circulation descends in the eastern Pacific and the westward branch descends near Saudi Arabia. In addition to the east-west circulations, there are large overturnings in the meridional plane caused by north-south heating contrasts. The well known example is the Indian summer monsoon circulation, which results from strong diabatic heating over the elevated Tibetan plateau, the Bay of Bengal and north east India.

The planetary scale features in the tropical atmosphere exhibit variability on various time scales. On the interannual time-scale, the Walker circulation in the equatorial Pacific undergoes significant changes. The phenomenon of changes in the Walker circulation over the equatorial Pacific, caused because of SST anomalies, is called Southern Oscillation. It should be noted that the interannual variations in the

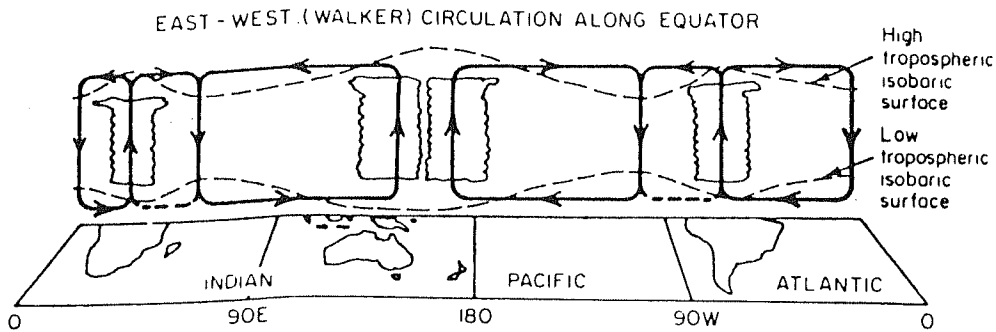


Fig.1.1. Schematic view of the major east-west circulations in the tropical atmosphere. (Adapted from review article of P.J.Webster. Reference: Page 242, Large scale dynamical processes in the atmosphere. Hoskins and Pearce, Academic Press (1983)).

tropical atmosphere are strongly coupled to fluctuations in the tropical SST. For example, during El Niño, a warm SST occurs in the eastern Pacific ocean. The response of the tropical atmosphere to this warm SST anomaly results in a modification of the Walker circulation in the equatorial Pacific. It is found that the zone of maximum convective activity shifts to the central Pacific. Consequently, the rainfall pattern gets displaced to the east of Indonesia resulting in drought over Australia and Indonesia. The structure of the tropical diabatic heating also exhibits distinct seasonal variations. During the northern hemispheric winter, the active zones of convection are located, along the ITCZ, over the equatorial western Pacific and the continents of Africa and South America. The winter Asian monsoon circulation, the Walker circulation in the equatorial Pacific and the east-west circulations associated with the heating over Africa and South America are the outstanding features during the winter months. When a transition from the northern winter to the northern summer occurs, the monsoon rainfall belt (convective heating) shifts from the Indonesian region to the foothills of Himalayas (Krishnamurti (1985)). The prominent circulations during summer are the mean meridional (Hadley) as well as the east-west (Krishnamurti (1971)) circulations associated with the Indian summer monsoon and the circulations induced by the heating over the Mexican highlands. Coming to the subseasonal time-scale, the predominant variability in the tropics has a period of about 30-50 days. The 30-50 day oscillation manifests itself as a slow eastward propagation of equatorial convective activity. Previous studies have shown that this eastward propagation of convective activity arises because of interactions between the planetary scale motions and tropical cumulus convection. During the northern summer, the 30-50 day wave interacts with the Indian summer monsoon circulation thereby producing a slow northward progression of convective activity over India. Observations indicate that as a result of this interaction the rainfall activity over India vacillates between active and break periods.

1.2 Plan and scope of the thesis

In this section, we shall present a gist of the topics covered in the thesis and a brief summary of the main results. A concise review of some of previous studies has been provided, wherever necessary, for the sake of maintaining the continuity of the description.

1.2.1 The time-mean Walker circulation in the Pacific

Observations suggest that large convective heating, which is most prominent during the northern winter, occurs over Indonesia and equatorial western Pacific (Ramage (1968), Krueger and Winston (1974) and Liebmann and Hartmann (1982)). In addition there is a dry zone over the eastern Pacific where the longwave cooling is substantial. This zone is cloud free and is characterized by widespread subsidence and strong surface easterly trades. Gill (1980) theoretically explained the steady state Walker circulation in the equatorial Pacific, by studying the stationary waves forced by an isolated heat source, using a system of shallow water equations on an equatorial β -plane. He showed that a heat source symmetric w.r.t the equator triggered Kelvin waves to its east and Rossby waves to its west. Gill's model offered an elegant explanation for the Walker circulation in the equatorial Pacific in terms of the stationary Kelvin wave response. But the main drawback in Gill's model was the use of large values of the dissipation parameters (Rayleigh friction and Newtonian cooling). Gill (1980) used a very strong dissipation which had an e-folding time-scale of about 2 days. The physical processes which can produce such strong dissipation effects are still not fully understood, although some studies (eg. Holton and Colton (1972),

Stone *et.al* (1974)) speculate that vertical transport of horizontal momentum by deep cumulus convection can act as a damping mechanism. Nevertheless, the use of a strong damping (e-folding time ~ 2 days) by the linear model of Gill (1980) may not be justifiable. However, there are studies based on GCM simulations (e.g. Manabe *et.al* (1974), Kasahara *et.al* (1973)), that have realistically modelled the time-mean flow patterns, without incorporating such strong dissipation terms in the model.

One of the motivations behind our study is to understand, what parameters control the longitudinal scale and intensity of the time-mean Walker circulation. Philips and Gill (1987) proposed that it was the damping term (Rayleigh friction) that accounted for the zonal scale of stationary Kelvin waves. They argued that a strong damping term would localize the stationary waves near the forcing region, while a weak damping term would allow the response to have a greater zonal extent. Philips and Gill (1987), however could not account for the short time-scales associated with the strong values of dissipation. In our study, we have examined the nature of east-west circulations in the equatorial Pacific, induced by the heating over Indonesia and the radiative cooling in the eastern Pacific. We have studied the influence of the radiative cooling over the eastern Pacific in controlling the scale and intensity of the Walker circulation. We have used weak dissipation (Rayleigh friction) in our studies. Idealized forcing experiments were carried using a 2-level linear equatorial β -plane model as well as a 5-level global spectral model. Since idealized studies are also amenable to analytical treatment, we have supplemented the model results with analytical calculations. The steady state equations in the 2-level model reduce to a system of linear algebraic equations. The stationary response to a given forcing is determined by solving this system of equations numerically. In the case of the 5-level global spectral model the prediction equations are integrated, with the forcing kept constant for the entire period of integration and the steady state response is calculated. Our studies indicate that the strength and zonal extent of the Walker

cell, is controlled by the positions and intensities of the heat source over Indonesia and also the heat sink in the eastern Pacific. We have shown that the radiative cooling in the eastern Pacific, which is quite substantial, determines the region of the subsiding branch of the Walker circulation. It is found that the time-mean response forced by the combination of a heat source and a heat sink, results in a superposition of stationary Kelvin waves emanating from the heat source and stationary Rossby waves emanating from the heat sink. The Walker circulation in the equatorial Pacific exhibits variability on the subseasonal, seasonal and interannual time-scales. In our idealized forcing experiments, we varied the relative distances between the diabatic heating and longwave cooling regions and calculated the impact on the east-west circulations. It was found that the intensity of the time-mean Walker circulation exhibited significant variations, as the distance between the heat source and the sink was changed. The circulation pattern was most intense, when the separation between the heating and cooling regions was minimum.

Another aspect that has been investigated pertains to the impact of nonlinearities on the stationary Kelvin and Rossby waves. This was essentially based on a comparison of the stationary wave response in the linear and nonlinear versions of a 5-level global spectral model. It was found that the influence of nonlinear terms was strongly felt in the vicinity of an intense convective heat source. Due to this impact, the structures of the stationary Kelvin and Rossby waves, near the forcing region, were considerably modified. It was also seen, mainly on the western side of the forcing region, that the nonlinear advection terms produced an eastward displacement of the upper level highs. In Gill-type of linear models, one has to employ a very strong damping, in order to obtain an eastward shift of the upper level anticyclones, which may not be realistic. We find that, even in the presence of weak dissipation it is still possible to explain the eastward shift by including nonlinear advection terms in the model. Due to the eastward shift of the highs at the upper levels, there is an

enhancement of the upper level divergence and the anticyclonic circulation over the region of forcing. It is also found that the effects of nonlinear terms become smaller when the intensity of the heat source is reduced. In the case of an antisymmetric heat source, it is found that the stationary Rossby wave pattern to the west of the forcing region shows distinct eastward shift in the NLM. The vertical profiles of the time-mean zonal wind, for the case of the symmetric forcing, reveal that the linear and nonlinear solutions exhibit distinct changes in the mid tropospheric levels. It is found that nonlinear terms favour the generation of westerlies in the equatorial region. Further, it is found that nonlinearities account for an increase in the vertical shear at around 400 mb. The role of nonlinear terms in aiding the generation of westerlies and also modifying the vertical shear of the basic flow, might be useful in understanding the phenomenon of midlatitude teleconnections (see. Lim and Chang (1983), Zhang and Webster (1989), Lim and Chang (1986) and Kasahara and Silva Dias (1986)). The significance of nonlinear dynamics with regard to time-mean circulations in the tropical atmosphere has been again stressed in Chapter IV.

1.2.2 The winter and summer time-mean circulations during 1979

Having so far described the stationary wave response of the tropical atmosphere induced by idealized heating distributions, let us now examine the case of more realistic time-mean circulations in the tropics. We have studied the time-mean circulations during winter (1978-79) and summer (1979), which are described in Chapter III. We have basically examined the equilibrium response, using a 2-level linear equatorial β -plane model as well as a 5-level nonlinear global spectral model, induced by the observed time-mean diabatic heating during winter (1978-79) and summer (1979). We have made use of the observed time averaged diabatic heating computed by Schaack

et.al (1990), during winter (1978-79) and summer (1979), in our forcing experiments. In the case of the 2-level linear equatorial β -plane model, the observed diabatic heating is prescribed at the 500 mb level only. The steady state equations in the 2-level model reduce to a system of linear algebraic equations. The steady state response to a given forcing was determined by solving this system of equations numerically. But in the case of the 5-level nonlinear global spectral model, the observed diabatic heating was prescribed at all the five vertical levels in the model. The 5-level global spectral model was integrated, with the forcing kept constant throughout the period of integration, and the steady state response was calculated.

The gross features of the time-averaged heating field during winter (1978-79) were the active zones of convection located along the ITCZ that extended from South America across the Atlantic, Africa, the Indian ocean and into the western Pacific. The most prominent heat source, associated with the winter Asian monsoon, occurred over the equatorial western Pacific. A well defined cooling maximum exceeding 1.0°K per day, was seen in the oceanic region to the west of South America. We found that both the 2-level linear model and the 5-level nonlinear global spectral model, reproduced most of the gross structural features of the mean circulation during winter (1978-79) reasonably well. The stationary Kelvin and Rossby waves forced by the Indonesian heating were seen in the time-mean flow patterns. The divergent circulations forced by the convective heating over the western Pacific, continental South America and Africa were seen in both the models. However, it was found that the circulation in the 2-level linear model was generally weaker as compared to the response in the 5-level global spectral model. Features such as the Walker circulation in the Pacific and the Hadley-type of circulation in the western Pacific were relatively stronger in the 5-level global spectral model. Further, the circulation features were more close to the observed flow patterns, in the case of the 5-level global spectral model. This is mainly due to the fact that in the 2-level model the prescription of

the forcing was at the 500 mb level alone, thereby restricting the vertical variation of heating to the first baroclinic mode only. Further nonlinear advection terms were absent in the 2-level linear model. On the other hand, the 5-level nonlinear global spectral model has been forced using the heating fields at all the 5 model levels. The more accurate vertical representation of the forcing and also the inclusion of nonlinearities in the 5-level global spectral model, resulted in more realistic flows in the case of the 5-level model. Using the maps of velocity potential distribution at 300 mb, we have calculated the intensities of the Walker and Hadley circulations. It was found the Walker circulation was most intense in the regions of central and eastern Pacific. The Hadley-type of circulation over the western Pacific was strongest in the equatorial region. These results match well with observed circulation patterns during winter (1978-79).

The major heating zones during summer (1979) were located over the Tibetan plateau, the Bay of Bengal and northeast India and the highlands of Mexico. Regions of radiative cooling were located over the oceans of north Pacific and Atlantic. The India summer monsoon region was characterized by a reverse Hadley circulation comprising of low-level south westerly flow and upper level easterlies. In addition to the mean meridional circulation, the strong zonal asymmetry in the distribution of the diabatic heating resulted in major tropical east-west circulations. The gross circulation features at the upper levels, such as the Tibetan anticyclone, the easterlies over the Indian subcontinent and the major east-west circulations were seen in the 2-level linear model response. However, the speeds of the upper level easterlies over the Indian monsoon region were relatively smaller than the observed flows. The 5-level nonlinear global spectral model reproduced the structure of both the upper and lower level circulations quite well. The intensity of the Tibetan anticyclone and the speed of the upper level easterlies in the 5-level model were more realistic. Similarly, the low-level southwesterly flow over the Indian subcontinent, matched well with the

observations. The more realistic upper and lower level circulation features in the 5-level model can be mainly attributed to the accurate representation of the vertical structure of diabatic heating and also the inclusion of nonlinear terms in the model. The major east-west circulations, forced by the heating over the Indian monsoon region, were distinctly seen from the velocity potential maps. Fairly strong subsidence was observed close to Pakistan and Rajasthan which explains the poor rainfall over northwest India during summer 1979. The intensity of the Hadley circulation, computed from the velocity potential distribution at 300 mb, showed that the meridional circulation was quite intense over the Tibetan plateau. The velocity potential maps also displayed prominent east-west circulations at the 300 mb level associated with the heating over the Indian monsoon region and Mexico.

1.2.3 The vorticity balance in the tropical upper troposphere

The vorticity equation is an extremely useful tool for understanding the dynamics of the tropical atmospheric motions. By performing a scale analysis in the tropics, one finds that the divergence equation can be approximated by a balance condition. Similarly, the thermodynamic equation simplifies to a balance between the diabatic heating (cooling) term and the adiabatic cooling (heating) due to ascent(descent). Therefore, the vorticity equation being a prognostic relation is best suited for understanding the dynamics of tropical large scale motions. In the past, there have been quite a few theoretical calculations of the nature of vorticity balance in the tropics (eg. Holton and Colton (1972), Sardeshmukh and Held (1984) and Sardeshmukh and Hoskins (1985)). Holton and Colton (1972) used a barotropic vorticity equation linearized about a zonal mean, to study the observed vorticity balance at 200 mb during summer 1967. They used the observed winds and divergence at 200 mb,

and calculated the vorticity distribution from the linear barotropic vorticity equation. They found that, a large vorticity damping (e-folding time < 1 day) had to be included in the equation, so that the calculated vorticity field matched with the observed vorticity distribution. They speculated that such a large vorticity damping can appear because of vertical transport of momentum, from the surface to the top of the atmosphere, by deep cumulus clouds. The use of such a rapid vorticity decay term at the upper troposphere, which may not be realistic, is the main drawback of the linear model of Holton and Colton (1972). Studies based on nonlinear models (GCMs) present a different view of the vorticity balance in the tropics. For instance, Sardeshmukh and Held (1984) simulated the July mean circulation using the GCM at GFDL. In spite of the fact that the vertical transport of momentum by cumulus convection was not included, the model produced a realistic simulation of the large-scale upper tropospheric circulations. They suggested that the nonlinear advection terms were important in determining the vorticity balance in the tropical upper troposphere. They showed that the linear models had to compensate for the neglected nonlinearities by employing a strong vorticity dissipation term.

We have already demonstrated in Chapter II, the significance of nonlinear dynamical effects on the stationary Kelvin and Rossby waves in the tropics. One can also estimate the impact of nonlinearities on the time-mean vorticity balance in the tropical troposphere by means of diagnostic calculations. In Chapter IV, we have performed budget studies of the vorticity balance in the tropical upper troposphere using the fields generated by three different forcing experiments in a 5-level global spectral model. In the first experiment, the model was forced using an idealized heat source in the western Pacific and a heat sink in the eastern Pacific. The dissipation terms in the model are very weak (e-folding time ~ 15 days). The 5-level global spectral model was integrated, with the forcing kept constant, till a steady state was attained. Similar forcing experiments were performed by forcing the model using the

time-averaged diabatic heating for winter (1978-79) and summer (1979) respectively. Based on the model generated fields, vorticity budget studies at 300 mb, were performed for all the 3 cases. We have explicitly calculated all the terms in the vorticity equation, including the vertical advection and twisting terms. In addition, we have computed area averages for the various terms in the vorticity equation over different regions. For the case of the idealized forcing, the region between the heat source and the sink was chosen for calculating the area averages. In the case of winter 1978-79, the area averages were calculated in the region of the Walker circulation over the equatorial Pacific. In the case of summer 1979, the averages were calculated for the region covering the northern summer monsoon area. We find that the primary vorticity balance at 300 mb, in all the 3 cases, is between the nonlinear terms involving the time-mean vorticity stretching and the horizontal advection of absolute vorticity. This suggests that nonlinear effects are important for the vorticity balance in the tropical upper troposphere. Our result conforms with the findings of Sardeshmukh and Hoskins (1985). The contribution from the vertical advection and twisting terms was found to be small. The terms involving the transients were found to be generally small in the low latitudes.

1.2.4 Linear and nonlinear studies of the tropical Hadley cell

As mentioned earlier, the observed atmospheric general circulation in the tropics owes its existence to the strong longitudinal variation in the distribution of diabatic heating. However, by suppressing the zonally asymmetric components and retaining only the symmetric part, it is possible to study the meridional or Hadley circulations. Zonally symmetric circulations offer a simpler perspective of the more complicated

atmospheric general circulation. Zonally symmetric studies provide valuable information about the transport of momentum, heat and water vapour between the tropics and the midlatitudes. Zonally symmetric flows also serve the role of basic state in instability studies. In Chapter V, we have carried out linear and nonlinear studies of the time-mean tropical Hadley circulation, forced by idealized diabatic heating. By comparing the response in the two models, we have examined the role of nonlinearities in modifying the time-mean meridional circulation in the tropics. In the past, there have been a few interesting linear and nonlinear calculations of the tropical Hadley cell. Schneider and Lindzen (1977) used a linearized axially symmetric model to study the steady-state response induced by the annual mean cumulus convection. They found that the mean meridional circulation driven by the zonally symmetric latent heat distribution, matched with the annual mean observed circulation only when 'cumulus friction' was included. They associated cumulus friction, with the vertical transport of horizontal momentum by cumulus convection. Quite contrary to the linear calculations, the GCM simulations by Manabe *et.al* (1970) and Kasahara *et.al* (1973) and the nonlinear calculations by Held and Hou (1980) showed that cumulus friction was not important in determining the steady-state tropical Hadley circulation. Further it should be noted that there are still uncertainties in the actual estimates of cumulus friction in the tropics. The GCM simulations of Manabe *et.al* (1970) and Kasahara *et.al* (1973) could realistically reproduce the Hadley circulation without specifying cumulus friction. Held and Hou (1980) have pointed out that nonlinear dynamical effects are important in maintaining the tropical Hadley cell.

In Chapter V, we have investigated the impact of nonlinear terms on the time-mean tropical Hadley circulation. The model used for our study is an axisymmetric 5-level global spectral model. We have studied the time-mean zonally symmetric response induced by idealized heating, using both linear (LM) and nonlinear (NLM) versions of this model. By comparing the response of the LM and NLM, we have

isolated the effects of nonlinearities on the time-mean tropical meridional circulation. We have considered two cases of forcing: a strong heat source (max heating 5° K per day) and a weak heat source (max heating 2° K per day). The Rayleigh friction and Newtonian cooling terms were quite weak (decay time ~ 15 days). It was found that the nonlinear vertical advection terms transport considerable flux of easterly momentum upwards in the region of the forcing. The transport of horizontal momentum from the surface to the top of the atmosphere results in the slowing down of the tropical trade winds in the NLM. We have carried out an explicit calculation of the angular momentum transport terms, which also indicates that a significant fraction of the easterly momentum is being transported upwards in the region of the forcing. In addition, it was noted that the nonlinear meridional advection terms displaced the core of the upper level westerly jets, poleward by about 6° latitude. It was found that the term involving the nonlinear vertical advection of temperature produces considerable adiabatic cooling, over the region of forcing. Consequently, the neglect of this nonlinear term in the thermodynamic energy equation, resulted in a large warming in the LM. Thus there was an additional kinetic energy generation in the LM. Infact, it was found that the global mean kinetic energy (GMKE) was significantly damped in the case of the NLM as compared to the LM. The dissipation of GMKE in the NLM is because of the two major nonlinear effects: (a) the large adiabatic cooling produced by the nonlinear vertical advection of temperature (b) the large vertical transport of easterly momentum from the surface to the upper levels. In the case of the weak forcing, it was found that the effects of nonlinear vertical advection (upward transport of easterly momentum and adiabatic cooling effect) were smaller. The poleward shift of the upper level westerly jets was also smaller (3° latitude) in this case. It was noticed that the damping of the GMKE, by nonlinear interactions, was quite small as compared to the strong forcing case.

1.2.5 Northward propagation of the 30-50 day oscillation

Till now our discussions were centered mostly on time-mean circulations in the tropics. However the final chapter of the thesis has been devoted to a theoretical study of the most popular intraseasonal transient in the tropical atmosphere, i.e, the 30-50 day oscillation. On the subseasonal time-scale, the tropical atmosphere is characterized by a slow eastward propagation of equatorial convective activity. This equatorial mode, which takes about 30 to 50 days to go around the globe, was first detected by Madden and Julian (1971). Numerous observations (eg. Lau and Chan (1983), Lorenc (1984), Lau and Phillips (1986), Knutson and Weickmann (1987) and many others) indicate that the intraseasonal fluctuations of convective activity are strongest over the Indian ocean and the western Pacific ocean. Many theoretical studies (eg. Davey (1984), Lau and Peng (1987), Yamagata (1987), Lau and Shen (1988) and others) explain the eastward propagation by a mutual interaction of the equatorial dynamics and convective activity. It is found that the oscillation propagates slowly over regions of warm SST, because the higher saturation moist content lowers the static stability of the atmosphere. Due to this reduced static stability, the Kelvin waves propagate with a slower phase speed (Davey (1984), Miyahara (1987) and Lau and Shen (1988)). But one of the most interesting aspects of the 30-50 day oscillation is its interaction with the Indian summer monsoon. Many observations in the past (eg. Yasunari (1979,1980), Sikka and Gadgil (1980), Krishnamurti and Subrahmanyam (1982), Krishnamurti *et.al* (1985) and others) have shown that the arrival of the equatorial low-frequency 30-50 day mode over the Indian summer monsoon region, is characterized by a northward movement of convective anomalies over the Indian subcontinent. The northward progression rate is roughly about 1° latitude per day. The interaction of the Indian summer monsoon and the 30-50 day oscillation produces a low frequency variability in the monsoon rainfall over India, resulting in active and break phases in the monsoon (eg. Yasunari (1981), Hartmann and Michelson (1989)).

An understanding of the physical mechanism responsible for the northward movement of convective anomalies over the Indian summer monsoon region will go a long way in predicting the monsoon variability.

In Chapter VI, we have performed a theoretical study using an axisymmetric 5-level global spectral model, to understand the interaction of the Indian summer monsoonal circulation and the equatorial 30-50 day oscillation. The treatment of the problem is as follows. A basic flow which closely resembles the time-mean Hadley circulation over the Indian monsoon region, was first generated in the model by forcing it with an appropriate heating distribution. The next step was to produce near-equatorial perturbations in the model, thereby mimicing the arrival of the planetary scale 30-50 day mode over the Indian longitudes. The perturbations were actually generated in the model, by temporarily switching on an equatorial heat source. Later, we investigated the impact of cumulus heating (CISK) on the perturbations. The cumulus heating based on CISK was interactively determined from the low-level circulation. The assumption in CISK is that, the latent heat release by cumulus clouds is enhanced by the low-level frictional convergence of the large scale flow field and the latent heat in turn drives the large scale circulation. It should be noted that over the Indian summer monsoon region, there is a large cyclonic vorticity associated with the low level southwesterly flow. Therefore, Charney's CISK for cumulus heating works in an utmost efficient manner, in this region. Our main interest was to examine the interactions between the time-mean basic flow and the cumulus convection. The model was integrated in the presence of cumulus heating. It was observed that the perturbations moved northward at the rate of about 0.5° latitude per day. It was also found that the low-level zonal wind field lagged meridionally behind the cumulus heating distribution. This meridional phase difference, induced by the CISK mechanism, resulted in the northward movement of the low-frequency intraseasonal convection. Our study suggests that the interaction between the cumulus heating

and the Indian summer monsoon circulation, plays a vital role in establishing the northward propagation of intraseasonal convective activity.

Chapter 2

Dynamics of the Time-Mean Walker Circulation

2.1 Introduction

The most spectacular observational feature in the tropical atmosphere is the strong longitudinal variation in the distribution of heat sources and heat sinks (Ramage (1968), Krueger and Winston (1974), Heddinghaus and Krueger (1981)). This zonally asymmetric distribution of heating drives the planetary scale circulations in the tropical troposphere. The tropical atmosphere is also characterized by meridional circulations which are induced by north-south heating contrasts. A study of the heat induced stationary response of the tropical atmosphere provides valuable information about the dynamics of the time-mean large scale motions in the tropics. In addition to the time-mean motions, the tropical atmosphere also exhibits variability on different time-scales. The year to year variability of the Indian summer monsoon circulation, the Walker circulation in the equatorial Pacific and the phenomenon of El Niño and Southern Oscillation (ENSO) are some of the challenging problems pertaining to the interannual variability in the tropics. Climate transitions on the seasonal time-scale are marked by considerable meridional shifts in the equatorial convective activity.

There is a major need to understand the structure and dynamics of the circulations that are induced by these seasonal shifts in the diabatic heating. On the intraseasonal time-scale, the dominant variability occurs with a periodicity of about 30-50 days in the tropical atmosphere. The tropical low-frequency 30-50 day oscillation manifests itself as a slow eastward propagation of equatorial convective activity. Transients on even smaller time-scale of a few days occur in association with tropical depressions and cyclones. It is the wide range of spatial and temporal scales comprising the tropical atmospheric motions, that renders it an interesting subject. In this chapter, we shall be primarily focussing on the behavior of the time-mean Walker circulation in the equatorial Pacific. Before starting off with our actual problem, we shall turn to some of the relevant details, which will be described in the following subsections.

2.1.1 The diabatic heating in the tropical atmosphere

The diabatic heating in the tropics, which is largely condensational heating due to cumulus convection, is an important component of the tropical atmospheric system. The annual mean diabatic heating, based on ECMWF analyses for 1979-1989, by Hoskins *et.al* (1989) reveals that deep convective heating occurs predominantly over three zones in the tropics located over equatorial South America, equatorial Africa and the 'maritime' continent of Indonesia. These three primary heating zones are responsible for the major east-west circulations in the tropical troposphere. There are also dry and cloud free regions in the tropics, where the radiative cooling in the atmosphere is substantial. For instance the region over central-eastern Pacific, which is characterized by widespread subsidence and strong surface easterly trades, shows considerable longwave cooling. One of the most striking divergent flow patterns in the the tropical atmosphere is the time-mean Walker circulation in the equatorial Pacific. The heat budget study by Cornejo-Garrido and Stone (1977) suggest that zonal variation of condensational heating, caused by moisture convergence, primarily

forces the Walker circulation. The strong upward motions over Indonesia and western Pacific result in upper level divergence and east-west circulations. The eastward branch descends in the eastern Pacific and the westward branch descends near Saudi Arabia. The scale of the eastward branch is typically of the order of 15000-20000 kms. Some of the important theoretical investigations of the thermally forced planetary scale tropical atmospheric circulations are due to Webster (1972), Gill (1980), Geisler (1981), Simmons (1982), Rosenlof *et.al* (1986), Schneider (1987) and Ting and Held (1990).

The heating distribution in the tropics exhibits variability on different time-scales. Observations by Krueger and Winston (1974) and studies based on Outgoing Longwave Radiation (OLR) by Liebmann and Hartmann (1982) reveal that there is a significant year to year variability in the distribution of heat sources and heat sinks in the tropics. Krueger and Winston (1974) found that the Walker circulation in the equatorial Pacific was very strong during February 1971, while it did not intensify much during February 1969. These contrasting flow patterns during the two years was a consequence of distinct changes in the spatial distribution of tropical atmospheric forcing. It was seen that the heat sink in the equatorial Pacific extended far to the west during February 1971 and on the other hand the dry zone was mostly confined over the eastern south Pacific during February 1969. The findings of Krueger and Winston (1974) convincingly demonstrate that the interannual fluctuations in the geometrical distribution of the heat sources and heat sinks and also their intensities crucially determine the year to year variability in the seasonal-mean planetary scale circulations in the tropics. On the seasonal time scale, there is considerable variability in the distribution of convective heating in the tropics. These changes are marked by distinct seasonal shifts, mostly in the meridional direction, in the locations of the centres of tropical convective activity (Hoskins *et.al* (1989)). For example, the transition from northern winter to northern summer is characterized by a northward shift in

the convective belt from Indonesia to the foothills of the Himalayas. These latitudinal displacements are important in determining the seasonal time-mean circulations. Coming to the subseasonal time-scale, observations suggest that the dominant low-frequency variability in the tropical regions occurs with a period of about 30-50 days and is characterized by a slow eastward propagation of equatorial convective activity. This low-frequency wave of equatorial convection, is most intense over the Indian ocean and the western Pacific. One of the interesting phenomena associated with this low-frequency wave, is its northward migration over India during the northern summer monsoon.

2.1.2 GCM studies of interannual variability

There are numerous GCM simulations of the tropical atmospheric interannual variability, of which we shall mention a few well-known studies. Bjerknes (1969) proposed that the sea surface temperature (SST) gradients along and south of the equator in the Pacific are mainly responsible in determining the changes in the Walker circulation on the interannual time-scale. The study of Horel and Wallace (1981) indicates that the SST changes in the equatorial Pacific during El Niño years, produce a shift in the region of major equatorial convective activity. As a result of this displacement, the maximum precipitation zone moves to the east of Indonesia. Consequently, drought conditions prevail over tropical Australia, New Guinea and Indonesia. The study of Horel and Wallace (1981) highlights the significance of tropical SST fluctuations in producing interannual variations in the tropical atmosphere. Conversely, there are also studies dealing with the response of the tropical oceans to atmospheric wind stresses. Wyrtki (1975) demonstrated that El Niño is the result of the response of the equatorial Pacific ocean to atmospheric forcing by trade winds. Barnett *et.al* (1989) have shown that the surface wind is a key factor that affects the climatological distribution and interannual variability of SSTs in the tropical oceans. It is evident from

the above studies, that there is a strong coupling between the tropical atmosphere and the tropical oceans on the interannual time-scale.

Rasmusson and Carpenter (1982) and Philander (1983) have studied the variations in tropical SST and surface winds associated with the ENSO. Rowntree (1972) used the atmospheric model at Geophysical Fluid Dynamics Laboratory (GFDL) to test Bjerknes' hypothesis that fluctuations of ocean temperatures in the tropical east Pacific are responsible for major variations in the position and intensity of the Aleutian surface low. He found that the SST variations had important effects on the model temperatures both tropical and extra-tropical. More recently, Neelin (1990) and Neelin (1991) have studied the interannual oscillations in the tropical atmosphere, arising out of slow temporal changes in the oceanic surface temperature. Julian and Chervin (1978) performed GCM experiments using the National Center for Atmospheric Research (NCAR) atmospheric model. The boundary forcing was prescribed using the ocean surface temperature. They showed that the coupling between the ocean and the atmosphere was essential for determining the interaction between the two systems. Lau (1981) has shown that coupling between large-scale atmospheric and oceanic equatorial Kelvin waves is relevant in the climatic time scale related to the equatorial ocean/atmosphere processes. Cane *et.al* (1990) used a linearized version of an analytical model which combines linear ocean dynamics with a simple version of the Bjerknes hypothesis for El Niño. They found that the most important parameter determining the behaviour of the system was the coupling constant. Lindzen and Nigam (1987), Neelin (1989) and Wang and Rui (1990) have demonstrated that the circulation in the atmospheric boundary layer is strongly influenced by the coupling between the boundary layer and the SST. Neelin (1988) used a simple linear model for studying the circulation in the tropical boundary layer. Strong dissipation, associated with vertical mixing of momentum by boundary layer turbulence, was incorporated in the model. The model simulations of the climatology as well as ENSO-type anomalies

agreed with the corresponding results from GCM.

Using a simple model, Webster (1981) showed that when a SST anomaly was located in a low-latitude basic flow, a strong enhancement of the initial anomaly was produced through a positive feedback between the dynamics and diabatic heating. Some of the well-known GCM simulations of ENSO, are due to Keshavamurty (1982), Blackmon *et.al* (1983) and Fennessy *et.al* (1985). Keshavamurty (1982) studied the atmospheric response to SST anomalies over the equatorial Pacific using the general circulation model (GCM) of GFDL. He showed that the diabatic heating anomalies associated with the central and western Pacific induce large circulation changes over the equatorial Pacific and south Asia. Philander *et.al* (1984) showed that unstable interactions between the atmosphere and ocean lead to an amplification of anomalies observed during ENSO. The study by Weare (1986) reveals that changes in evaporation from the sea surface and the surface layer moisture convergence/divergence crucially influence the tropical atmospheric response. Shukla and Fennessy (1988) have examined the tropical rainfall pattern and time-mean circulation for winter 1982 using a global GCM. They found that when observed SST anomalies over the Pacific ocean during the winter of 1982-83 were added to the climatological SST, the model predicted tropical circulation and rainfall were quite realistic.

2.1.3 Stationary and transient waves in the tropical atmosphere

The tropical atmospheric system is characterized by a rich variety of wave motions. It was Matsuno (1966) who first derived the dispersion relation for the wave solutions in the tropical atmosphere using a shallow water system of equations on an equatorial β -plane. He showed that the normal modes comprise of the equatorially trapped long Kelvin and Rossby waves, and also the high frequency Mixed Rossby-Gravity

and Inertia-Gravity waves. Fig.2.1 is a schematic representation of the frequency versus zonal wavenumber relation for the different equatorially trapped modes. The curve labelled 0 corresponds to the mixed planetary-gravity wave. The upper curves labelled 1 and 2 are the first two gravity wave modes and the corresponding lower curves are the first two Rossby wave modes. Longuet-Higgins (1968) pointed out that Matsuno's solutions are asymptotic approximations of general normal modes on a sphere. Lindzen (1967) extended Matsuno's theory to an isothermal atmosphere. There are quite a few observational findings that have documented the characteristics of these waves. Yanai and Maruyama (1966) showed the existence of the Mixed Rossby-Gravity wave in the lower stratosphere. Wallace and Kousky (1968) and Parker (1973) detected ultra-long stratospheric Kelvin waves with period of about 30 days. The diagnostic study of Hayashi and Golder (1980) showed the appearance of planetary scale Kelvin and Rossby waves in the GFDL GCM. The study by Kalnay *et.al* (1986) suggests that the latent heat in the tropics is important for the maintenance of large amplitude stationary Rossby waves with zonal wavenumber ~ 7 which can be observed in the south Pacific region and east of South America during the northern winter:

It is important to study the physical mechanisms, that trigger and control the spatial evolution and propagation characteristics of the normal modes, from the point of understanding the tropical atmospheric variability. In the context of the tropical atmospheric response to thermal forcing, we briefly describe some of the important theoretical studies. Webster (1972) used a two-layer atmospheric model linearized about a basic state, and demonstrated that the diabatic heating and orography are largely responsible for driving the observed time-mean circulations in the low latitudes. Subsequently, Gill (1980) in his classic work, studied the forced response of a shallow water system on an equatorial β -plane. He considered shallow water equations with a single mode in the vertical having a certain equivalent depth and made use of the

long wave approximation by which he eliminated the short wave components. He showed that an isolated heat source symmetric w.r.t the equator triggered Kelvin waves to its east and Rossby waves to its west. A heat source antisymmetric w.r.t the equator produced a Rossby wave response to the west of the heating region. He demonstrated that the Kelvin wave response generated by a symmetric heat source, had a longitudinal extent thrice that of the Rossby wave because of the faster propagation of the Kelvin waves. The model study by Simmons (1982) suggests that the structure of the tropical response to an isolated heat source is sensitive to the vertical profile of heating. He also showed that the magnitude and spatial and temporal variability of the tropical convective heating crucially determine the stationary motion in the tropics. Silva Dias *et.al* (1983) computed the partition of the thermally forced energy between Kelvin, Mixed Rossby-Gravity, Rossby and Gravity modes. Their model results indicate that many aspects of the summertime upper tropospheric circulation over South America can be explained by the dispersive properties of Rossby and Mixed Rossby-Gravity waves. Kasahara (1984) has studied the forced solutions generated by stationary as well as transient heat sources in the tropics. He found that a stationary heat source could effectively generate Kelvin and Rossby waves, while a transient heat source produced high-frequency gravity waves.

Another interesting aspect pertaining to tropical waves is their interaction with the basic flow. The theoretical studies by Plumb and Bell (1982), Webster and Holton (1982), Wilson and Mak (1984), Kasahara and Da Silva Dias (1986), Webster and Chang (1988), and Chang and Webster (1990) emphasize the significance of the basic flow and also its shear in determining the propagation characteristics and trapping mechanisms for the equatorial waves. Hoskins and Karoly (1981), Lau and Lim (1984) indicated that strong teleconnections from the tropics to midlatitude are possible in a westerly belt over the region of heat source. It can be seen that, during the northern hemispheric winter, the upper troposphere in the mid-Pacific is characterized by a

westerly flow, which enhances the teleconnection between the tropics and extratropics. The studies of Lim and Chang (1983) and Zhang and Webster (1989) indicate that the stationary as well as the transient Rossby wave are less trapped in equatorial westerlies than in an easterly basic state. Lim and Chang (1983), Lim and Chang (1986) and Kasahara and Silva Dias (1986) have pointed out the role of vertical shear in the mean zonal wind in generating external (barotropic) modes which are necessary for teleconnection mechanisms. They have shown that the external modes arise due to interactions between the internal (baroclinic) modes in the presence of vertical shear in the basic zonal wind.

2.2 Aims of the present study

Observations (see Hoskins *et.al* (1989)) of the annual as well as winter time-mean diabatic heating over the equatorial Pacific, reveals that there is a strong convective heat source over Indonesia and western Pacific and a zone of longwave cooling in the southeastern Pacific. A key question that requires attention, is the dynamics of the time-mean response induced by this combination of heat source and heat sink. One of the problems that is examined in this chapter pertains to the impact of the Indonesian heating and the radiative cooling over the eastern Pacific, in controlling the longitudinal scale and intensity of the time-mean Walker circulation in the equatorial Pacific. The motivation for this work came from the studies of Gill (1980) and Philips and Gill (1987). Gill (1980) in his pioneering work explained the stationary wave solutions induced by an isolated heat source, which was symmetric w.r.t the equator. He showed that the heat source generated equatorially trapped long Kelvin waves towards its east and Rossby waves to its west. He demonstrated that at any given instant of time, the Kelvin waves had a greater zonal extent as compared to the Rossby waves, because of the faster speed associated with the Kelvin waves. Gill's model in

spite of its highly simplified formulation successfully explained many aspects of the heat induced Walker and Hadley-type circulations. However, the damping terms (Rayleigh friction and Newtonian cooling) in Gill's model were tunable parameters and the main shortcoming of this model was the use of strong dissipation terms (e-folding time ~ 2 days). In a similar study, Philips and Gill (1987), suggested that the scale of the east-west circulations was dependent on the strength of the dissipation terms. They argued that strong damping terms localized the response near to the heat source, while the use of weak damping terms resulted in stationary waves that extended far away from the heating region. However, at the present, the physical processes that produce large damping effects (e-folding time ~ 2 days) are not yet clearly understood. Therefore, it may not be desirable to employ large damping in models, in order to explain the scale and strength of the observed tropical east-west circulations. In our study we have considered the impact of the radiative cooling over the eastern Pacific, in addition to the convective forcing over Indonesia and western Pacific. The earlier idealized experiments of Gill (1980), Philips and Gill (1987) and many others, have not considered the influence of the radiative cooling over eastern Pacific in determining the scale and intensity of the time-mean Walker circulation. Our goal is to perform idealized forcing experiments, using a simple 2-level linear equatorial β -plane model and also a 5-level nonlinear global spectral model, to understand the nature of the time-mean response generated by a convective heat source in combination with a heat sink.

Another objective of our study is to determine the impact of nonlinear terms on the dynamics of the equatorially trapped Kelvin and Rossby waves. The theoretical studies of the Walker and Hadley circulations by Webster (1972), Gill (1982) and Lau and Lim (1982) are mostly based on linear models. There are, however, several reasons why nonlinear effects should be important at low latitudes. The first is the smallness of the Coriolis parameter, which tends to result in a greater overall influence

of the advective acceleration terms (i.e., a higher Rossby number). Additionally, a number of jet stream systems are present in the tropics, such as the subtropical, tropical easterly and Somali jets; these contain localized regions of very strong winds with significant nonlinear advections. There are other reasons for taking up the study of determining the influence of nonlinear terms on the dynamics of the stationary waves in the tropics. The earlier studies of the tropical time-mean response to heating, calculated by linear and nonlinear models showed some important differences. For example, in Gill-type of linear models, a strong Rayleigh friction had to be employed in order to obtain proper phase relation between the maximum upper level divergence and the geopotential distributions. In the absence of the strong dissipation, the upper level anticyclones in these models appeared on the western side of the heating region. However, Sardeshmukh and Held (1984), Sardeshmukh and Hoskins (1985) and Hendon (1986) have emphasized the role of nonlinearities on the tropical time-mean motions and demonstrated that the inclusion of nonlinearities can yield realistic upper tropospheric circulations even in the absence of strong dissipation terms. In the light of some of the above mentioned studies, we have re-examined the impact of nonlinearities on the stationary waves in the tropics. In order to highlight the role of nonlinear dynamics, we have adopted an approach where a comparison of the stationary solutions in the linear (LM) and nonlinear (NLM) versions of a 5-level global spectral model is made.

2.3 Linear steady state model formulation

The numerical 2-level linear model, on an equatorial β -plane, used for our studies is described below. We denote the zonal velocity, meridional velocity, geopotential and vertical p-velocity by u, v, ϕ and ω respectively. In the vertical, the equations

are discretized. The model levels are shown in Fig.2.2. At levels 1 and 3, we apply the u-momentum equation, the v-momentum equation and continuity equation. The thermodynamic energy equation is applied at level 2. The following are the usual model equations:

$$\frac{\partial u_1}{\partial t} - \beta y v_1 + \frac{\partial \phi_1}{\partial x} = 0 \quad (2.1)$$

$$\frac{\partial v_1}{\partial t} + \beta y u_1 + \frac{\partial \phi_1}{\partial y} = 0 \quad (2.2)$$

$$\frac{\partial u_3}{\partial t} - \beta y v_3 + \frac{\partial \phi_3}{\partial x} = 0 \quad (2.3)$$

$$\frac{\partial v_3}{\partial t} + \beta y u_3 + \frac{\partial \phi_3}{\partial y} = 0 \quad (2.4)$$

The continuity equation at level 1 gives,

$$\omega_2 = -\Delta p \left(\frac{\partial u_1}{\partial x} + \frac{\partial v_1}{\partial y} \right) \quad (2.5)$$

$$\frac{\partial \phi_3}{\partial t} - \frac{\partial \phi_1}{\partial t} - \sigma \Delta p^2 \left(\frac{\partial u_1}{\partial x} + \frac{\partial v_1}{\partial y} \right) = - \left(\frac{R \Delta p}{C_p p} \right) \dot{Q} \quad (2.6)$$

$$\left(\frac{\partial u_1}{\partial x} + \frac{\partial v_1}{\partial y} \right) + \left(\frac{\partial u_3}{\partial x} + \frac{\partial v_3}{\partial y} \right) = 0 \quad (2.7)$$

In the model, the value of the static stability parameter σ is taken as $2.88 \times 10^{-6} \text{ m}^2 \text{ s}^{-2} \text{ pa}^{-2}$ and $\Delta p = 0.5 \times 10^5 \text{ pa}$. By choosing a velocity scale $c = \sqrt{\frac{\sigma \Delta p^2}{2}}$ and a length scale $L = \sqrt{\frac{c}{2\beta}}$ the following nondimensional quantities are defined:

$x^* \left(\frac{x}{L} \right)$ ranges from $\frac{-\pi a}{L}$ to $\frac{\pi a}{L}$, 'a' being the earth's radius.

$y^* \left(\frac{y}{L} \right)$ ranges from $\frac{-\pi a}{4L}$ to $\frac{\pi a}{4L}$, i.e., 45° S to 45° N .

$t^* = \frac{tc}{L}$; $u^* = \frac{u}{c}$; $v^* = \frac{v}{c}$; and $\phi^* = \frac{\phi}{c^2}$

For convenience, we define $\xi^* = \frac{L}{a} \left(x^* + \frac{\pi a}{L} \right)$ which ranges from 0 to 2π . In order

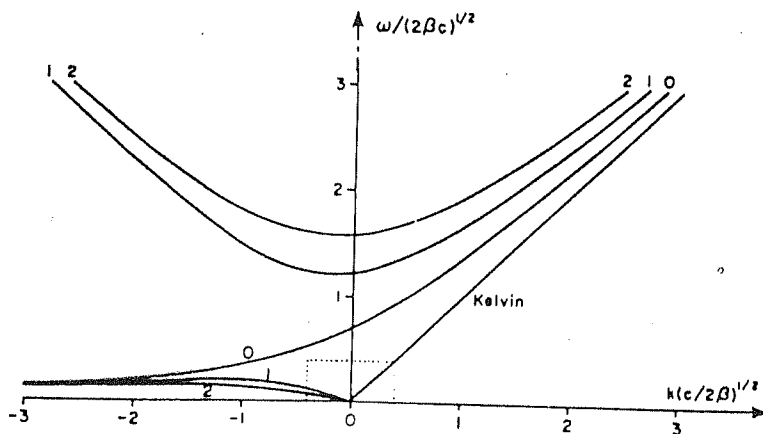


Fig.2.1. Dispersion relation for equatorial waves. The vertical axis is the frequency in units of $\sqrt{2\beta c}$ and horizontal axis is the zonal wave number in units of $\sqrt{2\beta/c}$. (Adapted from A.E.Gill, Page 438, Atmosphere-Ocean Dynamics, Academic Press (1982)).

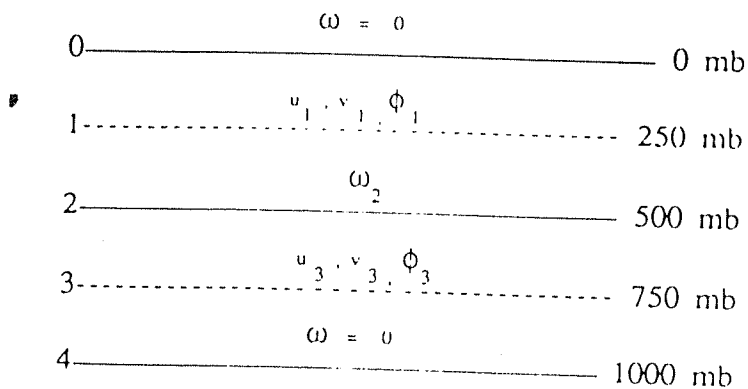


Fig.2.2. Vertical levels in the 2-level linear equatorial β -plane model.

to obtain steady state solution to the above forced problem, we set $\frac{\partial}{\partial t} = \varepsilon$. The nondimensional equations (after dropping the asterisk) are given by:

$$\varepsilon u_1 - \frac{y v_1}{2} + \frac{L}{a} \left(\frac{\partial \phi_1}{\partial \xi} \right) = 0 \quad (2.8)$$

$$\varepsilon v_1 + \frac{y u_1}{2} + \left(\frac{\partial \phi_1}{\partial y} \right) = 0 \quad (2.9)$$

$$\varepsilon u_3 - \frac{y v_3}{2} + \frac{L}{a} \left(\frac{\partial \phi_3}{\partial \xi} \right) = 0 \quad (2.10)$$

$$\varepsilon v_3 + \frac{y u_3}{2} + \left(\frac{\partial \phi_3}{\partial y} \right) = 0 \quad (2.11)$$

$$\varepsilon (\phi_3 - \phi_1) - 2 \left[\frac{L}{a} \left(\frac{\partial u_1}{\partial \xi} \right) + \left(\frac{\partial v_1}{\partial y} \right) \right] = -H(\xi, y) \quad (2.12)$$

$$\frac{L}{a} \left(\frac{\partial u_1}{\partial \xi} + \frac{\partial u_3}{\partial \xi} \right) + \left(\frac{\partial v_1}{\partial y} + \frac{\partial v_3}{\partial y} \right) = 0 \quad (2.13)$$

The form of forcing with the heat source at $A \leq \xi \leq B$ and the heat sink at $C \leq \xi \leq D$ is shown in equation 2.14. The length of the heat source and the sink is 1 unit in the zonal direction. The value of K is 0.07 so that the maximum heating (cooling) is 1° per day.

$$\begin{aligned} H(\xi, y) &= K (B - \xi) (\xi - A) \exp \left(\frac{-y^2}{4} \right) \text{ if } A \leq \xi \leq B \\ H(\xi, y) &= -K (D - \xi) (\xi - C) \exp \left(\frac{-y^2}{4} \right) \text{ if } C \leq \xi \leq D \\ H(\xi, y) &= 0 \text{ otherwise} \end{aligned} \quad (2.14)$$

2.4 Linear steady state solution

We seek a solution that is periodic in the zonal direction and vanishes at the northern and southern boundaries. The variables are split into odd and even components

and expanded by a Fourier series in the zonal direction. In the meridional direction they are expanded using Parabolic Cylinder Functions $D_n(y)$ (Whittaker and Watson (1950)) as the basis function. For instance a variable $\psi(\xi, y)$ is expanded as:

$$\psi(\xi, y) = \sum_{n=0}^{NM} \sum_{m=0}^{MM} [\psi(e)_n^m \cos m\xi + \psi(o)_n^m \sin m\xi] D_n(y) \quad (2.15)$$

We have truncated the above series expansion at $MM = 10$ and $NM = 6$. The $D_0(y)$ component of the heat source and heat sink shown in 2.14 is symmetric w.r.t the equator. It now follows from Gill's (1980) calculations, that it would in fact be sufficient to truncate the meridional expansion at $NM = 2$. This is because the higher meridional wavenumbers associated with the Kelvin and Rossby waves forced by an idealized symmetric heat source are negligibly small.

$$\varepsilon u_1(e)_n^m - [v_1(e)_{n-1}^m + (n+1)v_1(e)_{n+1}^m] + \frac{mL}{a} \phi_1(o)_n^m = 0 \quad (2.16)$$

$$\varepsilon u_1(o)_n^m - [v_1(o)_{n-1}^m + (n+1)v_1(o)_{n+1}^m] - \frac{mL}{a} \phi_1(e)_n^m = 0 \quad (2.17)$$

$$\begin{aligned} \varepsilon v_1(e)_n^m + [u_1(e)_{n-1}^m + (n+1)u_1(e)_{n+1}^m] \\ + \frac{1}{2} [(n+1)\phi_1(e)_{n+1}^m - \phi_1(e)_{n-1}^m] = 0 \end{aligned} \quad (2.18)$$

$$\begin{aligned} \varepsilon v_1(o)_n^m + [u_1(o)_{n-1}^m + (n+1)u_1(o)_{n+1}^m] \\ + \frac{1}{2} [(n+1)\phi_1(o)_{n+1}^m - \phi_1(o)_{n-1}^m] = 0 \end{aligned} \quad (2.19)$$

$$\varepsilon u_3(e)_n^m - [v_3(e)_{n-1}^m + (n+1)v_3(e)_{n+1}^m] + \frac{mL}{a} \phi_3(o)_n^m = 0 \quad (2.20)$$

$$\varepsilon u_3(o)_n^m - [v_3(o)_{n-1}^m + (n+1)v_3(o)_{n+1}^m] - \frac{mL}{a} \phi_3(e)_n^m = 0 \quad (2.21)$$

$$\begin{aligned} \varepsilon v_3(e)_n^m + [u_3(e)_{n-1}^m + (n+1)u_3(e)_{n+1}^m] \\ + \frac{1}{2} [(n+1)\phi_3(e)_{n+1}^m - \phi_3(e)_{n-1}^m] = 0 \end{aligned} \quad (2.22)$$

$$\begin{aligned} \varepsilon v_3(o)_n^m + [u_3(o)_{n-1}^m + (n+1)u_3(o)_{n+1}^m] \\ + \frac{1}{2} [(n+1)\phi_3(o)_{n+1}^m - \phi_3(o)_{n-1}^m] = 0 \end{aligned} \quad (2.23)$$

$$\begin{aligned} & \varepsilon [\phi_3(e)_n^m - \phi_1(e)_n^m] - \frac{2Lm}{a} u_1(o)_n^m \\ & - [(n+1)v_1(e)_{n+1}^m - v_1(e)_{n-1}^m] = -H(e)_n^m \end{aligned} \quad (2.24)$$

$$\begin{aligned} & \varepsilon [\phi_3(o)_n^m - \phi_1(o)_n^m] + \frac{2Lm}{a} u_1(e)_n^m \\ & - [(n+1)v_1(o)_{n+1}^m - v_1(o)_{n-1}^m] = -H(o)_n^m \end{aligned} \quad (2.25)$$

$$\begin{aligned} & \frac{Lm}{a} [u_1(o)_n^m + u_3(o)_n^m] + \frac{1}{2} [(n+1)v_1(e)_{n+1}^m - v_1(e)_{n-1}^m] \\ & + \frac{1}{2} [(n+1)v_3(e)_{n+1}^m - v_3(e)_{n-1}^m] = 0 \end{aligned} \quad (2.26)$$

$$\begin{aligned} & -\frac{Lm}{a} [u_1(e)_n^m + u_3(e)_n^m] + \frac{1}{2} [(n+1)v_1(o)_{n+1}^m - v_1(o)_{n-1}^m] \\ & + \frac{1}{2} [(n+1)v_3(o)_{n+1}^m - v_3(o)_{n-1}^m] = 0 \end{aligned} \quad (2.27)$$

The wavenumber components of the thermal forcing are given by

$$\begin{aligned} H(e)_n^0 &= \left[\frac{1}{\sqrt{2\pi n!}} \right] \frac{1}{2\pi} \int_0^{2\pi} \int_{y_s}^{y_n} H(\xi, y) D_n(y) d\xi dy \\ H(e)_n^m &= \left[\frac{1}{\sqrt{2\pi n!}} \right] \frac{1}{\pi} \int_0^{2\pi} \int_{y_s}^{y_n} H(\xi, y) D_n(y) \cos m\xi d\xi dy \\ H(o)_n^m &= \left[\frac{1}{\sqrt{2\pi n!}} \right] \frac{1}{\pi} \int_0^{2\pi} \int_{y_s}^{y_n} H(\xi, y) D_n(y) \sin m\xi d\xi dy \end{aligned} \quad (2.28)$$

where y_s and y_n are the southern and northern boundaries respectively. The system of linear algebraic equations (2.16)-(2.27) is solved by Singular Value Decomposition Method, Numerical Recipes (1988).

2.5 The nonlinear global spectral model

A brief description of the the 5-level nonlinear global spectral model used in our studies is given below. The model formulation is based on Bourke (1974). This is a dry model having a Rhomboidal truncation at 15 waves. The model equations comprise

of nonlinear prognostic equations for vorticity, divergence, temperature and surface pressure. We have used a weak Rayleigh friction and Newtonian cooling having a damping time scale of 10 days. The initial condition for all the experiments corresponds to an atmosphere at rest. The model equations are integrated until a steady state is attained. The forcing is kept fixed throughout the time of integration. The model equations are integrated using semi-implicit time integration scheme described in Bourke (1974) using a time-step of 3600 seconds.

2.6 Experiments and Results

We shall now describe the different forcing experiments that were carried out using the 2-level linear equatorial β -plane model and the 5-level global spectral model. In order to make our results more concrete, we have also included some analytical calculations. The main stress in these experiments is to examine the time-mean response of the tropical atmosphere, when subjected to different forcing conditions.

2.6.1 Idealized forcing experiments using heat source and sink

The annual mean diabatic heating (see Hoskins *et.al* (1989)) reveals that the tropical atmosphere over the equatorial Pacific is characterized by strong convective heating over Indonesia and western Pacific and a substantial radiative cooling in the eastern Pacific. As mentioned before, our intention is to understand the influence of this heat source and heat sink combination in controlling the zonal scale and strength of the time-mean Walker circulation in the equatorial Pacific. In the model formulation of

Gill (1980), only the heat source was used for forcing the model. He made use of large Rayleigh friction and Newtonian cooling (e-folding time ~ 2 days) in order to explain the scale of the Walker circulation. In our numerical experiments, the model is integrated with the forcing kept fixed throughout the time of integration, till a steady state is attained. For the purpose of obtaining a steady state, we have employed weak damping terms (e-folding time ~ 10 days) in our model. To begin with, we have forced the 5-level nonlinear global spectral model with a strong isolated heat source, which is symmetric w.r.t the equator, located near Indonesia (Fig.2.3a). The heating has a vertical variation of the form $Q(p) = \sin\left(\frac{\pi p}{p_0}\right)$, where p_0 corresponds to the 1000 mb pressure value. This function has a maximum value at 500 mb and is zero at $p = p_0$ and $p = 0$. The maximum amplitude of the forcing is $4^\circ \text{ K per day}$. The heating is switched on and the model is integrated for about 50 days so as to achieve the steady state response. The time-mean zonal winds and velocity potential fields at 300 mb are shown in Figs.2.3b and 2.3c respectively. The east-west circulations at the upper level are characterized by easterlies (shaded) to the west of the heat source and westerlies (solid lines) to the east of the forcing. The response to the west of the forcing corresponds to the stationary Rossby waves and the response on the eastern side corresponds to the stationary Kelvin waves. It can be clearly seen that the stationary Kelvin and Rossby waves are latitudinally confined between 20°S and 20°N . The maximum easterly speed is about -10 ms^{-1} and the westerly speed is 8 ms^{-1} . Gill (1980) has offered an elegant explanation for the zonal extent of the Kelvin and Rossby waves. He explained the greater zonal extent of the Kelvin wave response as compared to the Rossby wave response, by demonstrating that at any given instant of time the Kelvin waves could carry information almost three times faster than the Rossby waves. The velocity potential at 300 mb (Fig.2.3c) illustrates regions of outflow and inflow at the upper level. By looking at the velocity potential maps, one can also infer the approximate regions of ascending and descending motions.

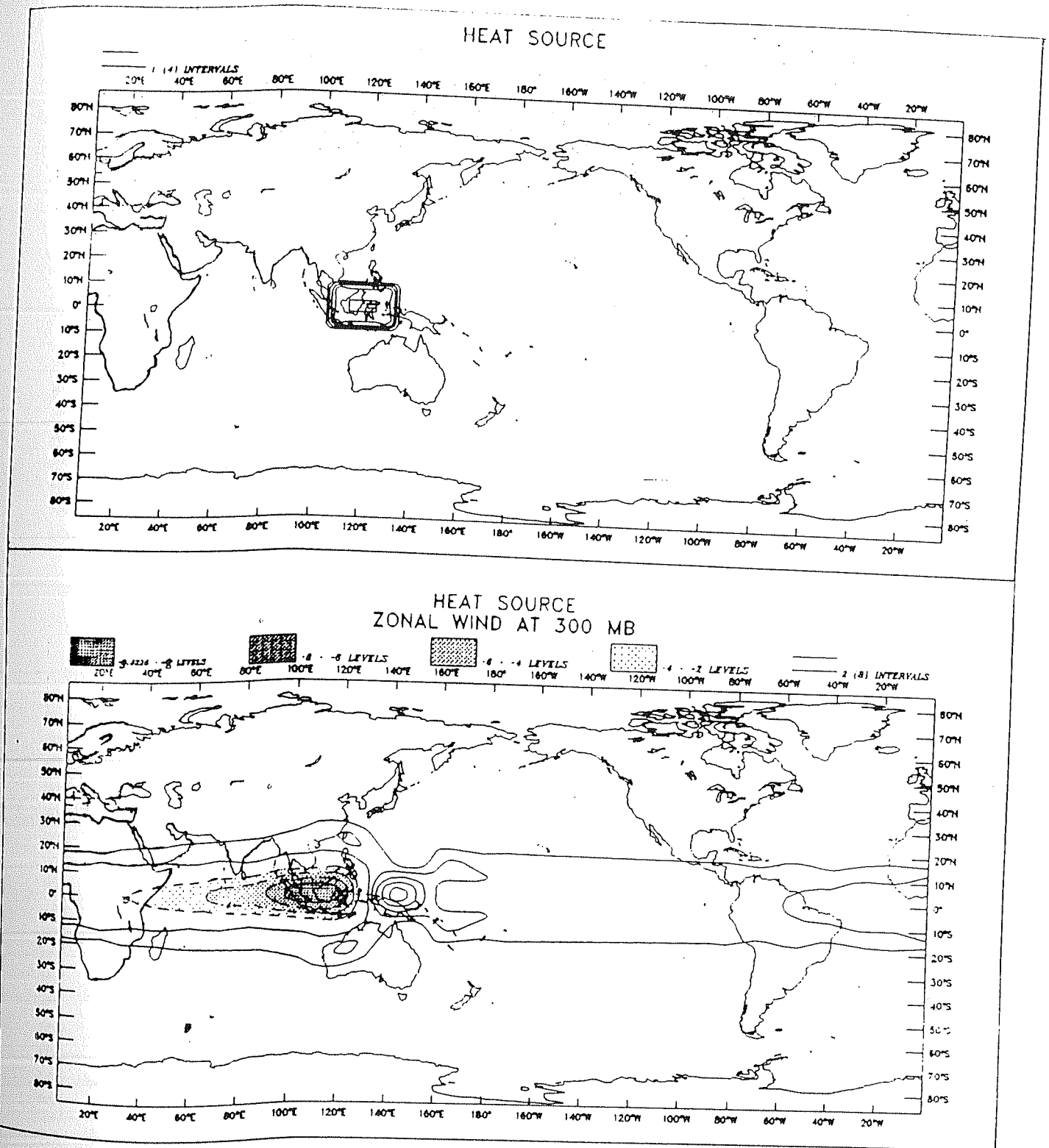
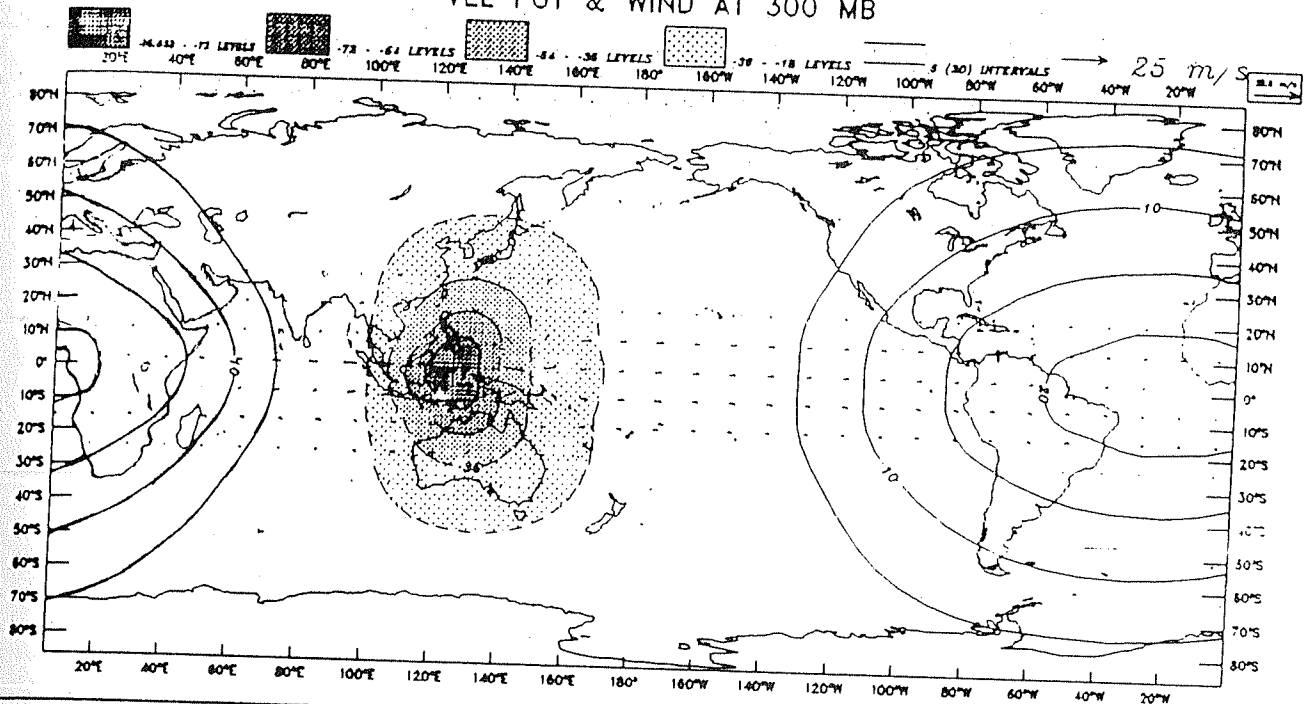


Fig.2.3a. (Top) Horizontal distribution of heat source over Indonesia. Interval 1 °K per day.

Fig.2.3b. (Bottom) Latitude-longitude section of zonal wind at 300 mb (ms^{-1}). Shaded contours (interval 2 units) are easterlies and solid lines are westerlies (interval 2 units). Forcing used as shown in Fig.2.3a.

HEAT SOURCE VEL POT & WIND AT 300 MB



HEAT SOURCE & SINK

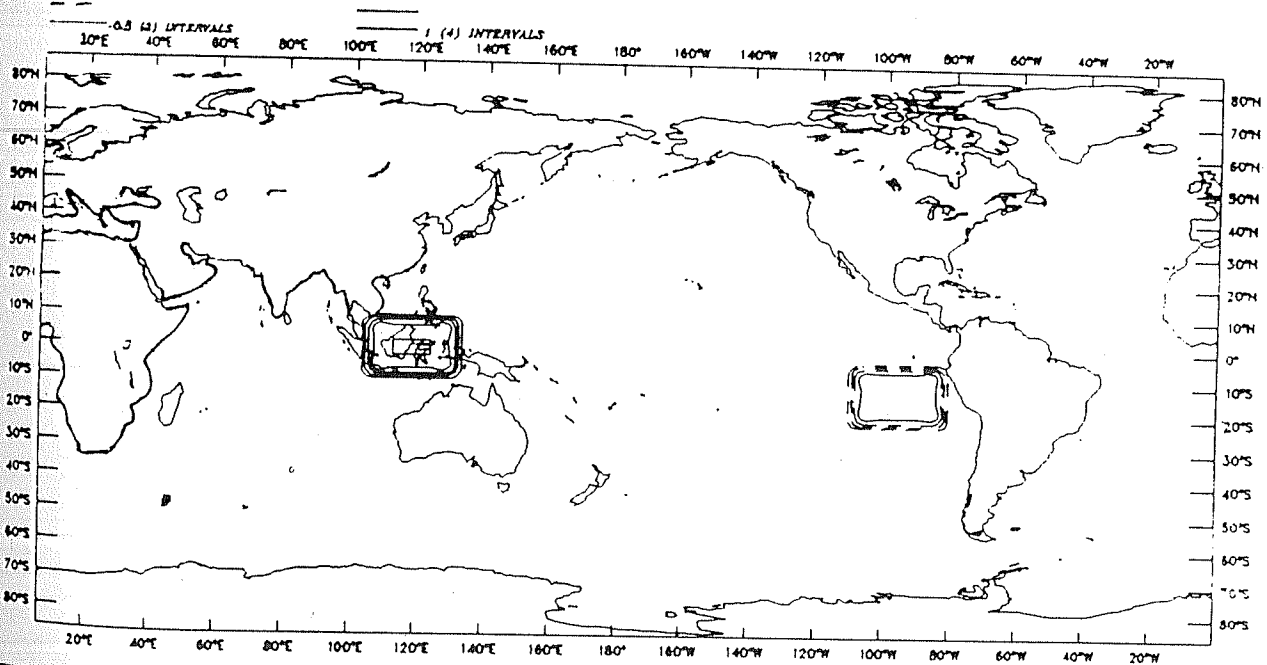


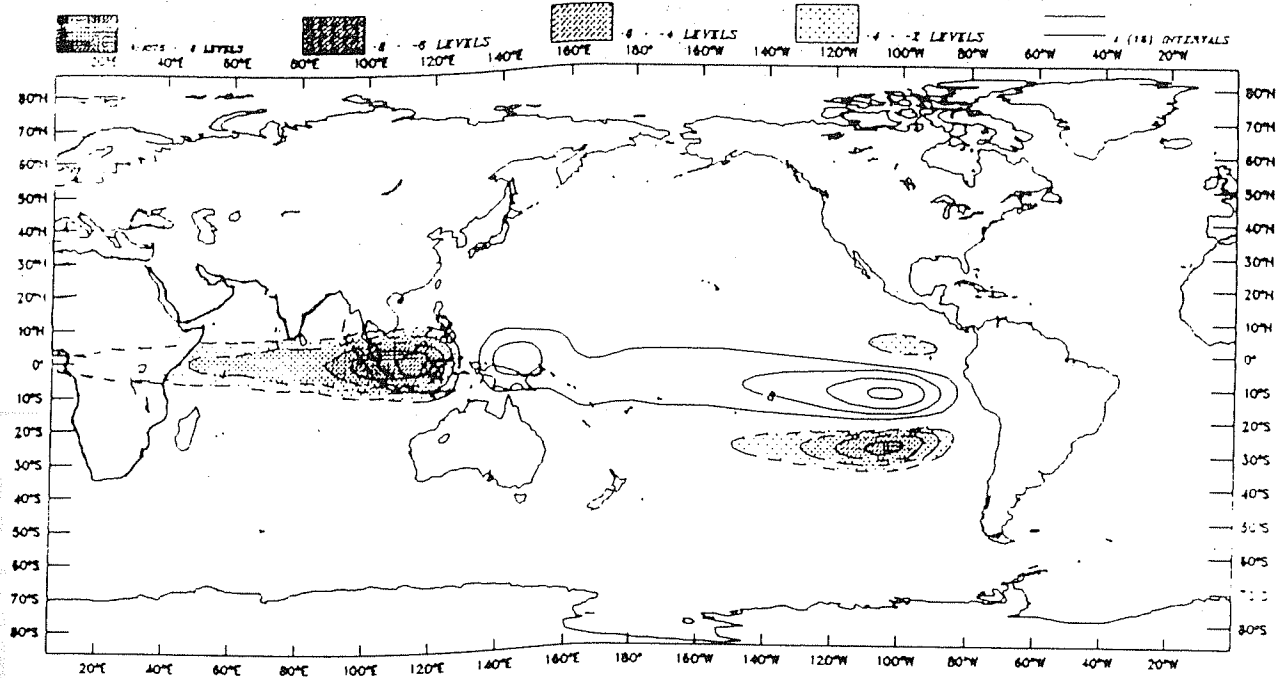
Fig.2.3c. (Top) Latitude-longitude section of velocity potential at 300 mb ($10^5 \text{ m}^2 \text{ s}^{-1}$). Shaded contours are negative (interval 18 units) and solid lines are positive (interval 5 units).

Fig.2.4a. (Bottom) Horizontal distribution of heat source over Indonesia and heat sink in south eastern Pacific (units $^{\circ}\text{K}$ per day). Positive contours (interval 1 unit) and negative contours (interval 0.5 unit).

Regions of $-\chi$ correspond to outflow and regions of inflow can be identified with $+\chi$. From Fig.2.3c, one notices that there is an intense outflow (shaded) over Indonesia, due to strong upward motions over the heat source. The positive contours in Fig. 2.3c indicate that there is upper level convergence in the eastern Pacific and over South America. The upper level westerlies associated with the Walker circulation can be seen extending even to the east of South America. However the westerly speeds are quite small in the region of eastern Pacific ($1-2 \text{ ms}^{-1}$).

Now let us examine the stationary response generated by including the radiative cooling over the south-eastern Pacific. The horizontal distribution of the heat source and heat sink is shown in Fig.2.4a. The heat sink has a maximum cooling of 2° K per day, and is not symmetric w.r.t the equator. It should be noted that the strength of the cooling is only half the intensity of the heat source. This form of thermal distribution is quite realistic. The vertical structure of the heat sink is similar to that of the heat source. The steady state zonal wind distribution at 300 mb (Fig.2.4b) reveals the stationary Kelvin and Rossby waves originating from the heat source. An additional feature is the appearance of strong westerlies in the central and eastern Pacific, indicating the strengthening of the Walker circulation ($\text{max } 16 \text{ ms}^{-1}$). It can be clearly seen that the heat sink limits the upper level westerly flow, which does not extend beyond the eastern Pacific. The velocity potential distribution at 300 mb (Fig.2.4c) shows that there is a strong convergence ($+\chi$) of westerlies over eastern Pacific. Further, one can clearly recognize that the zone of maximum convergence has significantly shifted westward over southeastern Pacific. In the eastern Pacific, the gradient of velocity potential along the zonal direction is positive. Further, the contours are close to one another, indicating that the magnitude of the gradient of the velocity potential in the longitudinal direction is quite large. This large positive gradient in the divergent component of the circulation supports the occurrence of strong westerlies in the equatorial Pacific. We shall later illustrate that the strong

HEAT SOURCE & SINK ZONAL WIND AT 300 MB



HEAT SOURCE & SINK VEL POT & WIND AT 300 MB

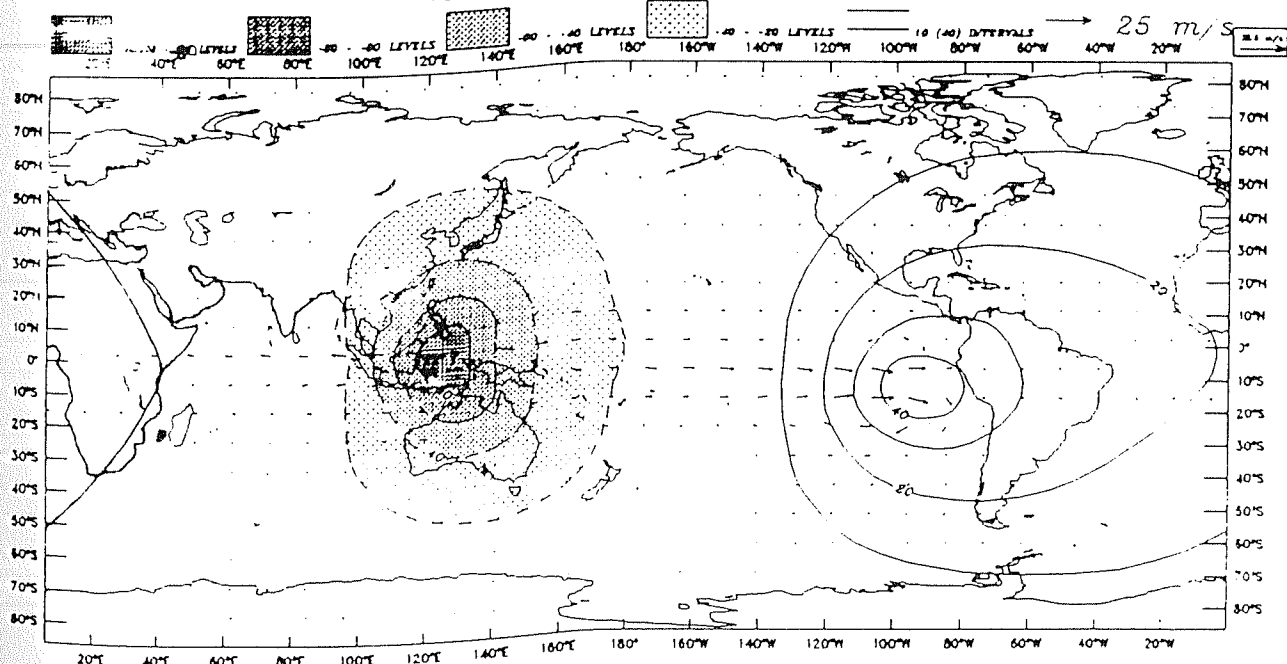


Fig.2.4b. (Top) Same as Fig.2.3b, except for forcing as in Fig.2.4a. Interval (2 units for negative and 4 units for positive contours).

Fig.2.4c. (Bottom) Same as Fig.2.3c, except for forcing as in Fig.2.4a. Interval (20 units for negative and 10 units for positive contours).

upper level westerlies in the equatorial Pacific, arise because of the superposition of the Kelvin waves originating from the heat source and Rossby waves emanating from the heat sink. The conclusion from the above experiments is that the longwave cooling in the eastern Pacific is an important factor that determines the zonal extent (approximately the location of the subsiding branch) and also the intensity of the time-mean Walker circulation in the equatorial Pacific.

In the next set of experiments, we have studied the consequences of decreasing the strengths of the heat source and sink. Fig.2.5a shows a weak heat source, symmetric w.r.t the equator, with a maximum heating of 1° K per day. The steady-state wind vectors, zonal winds and perturbation geopotential at 300 mb are shown in Figs.2.5b, 2.5c and 2.5d respectively. The geopotential at 300 mb shows a high at the equator, which is flanked by anticyclones towards the north and south. In general the stationary wave response is much weaker, which is indicated by the weak easterlies (max speed -2.9 ms^{-1}) to the west of the heat source and weak westerlies (max speed 2.4 ms^{-1}) to its east. The important point to be recognized here is the weakening of the Walker circulation in the equatorial Pacific. Now a weak heat sink (max cooling of 1° K per day), which is separated by about 112.5° from the heat source, is also included in the forcing (Fig.2.6a). Here both the source and sink are symmetric w.r.t the equator. The corresponding steady-state wind vectors, zonal winds and perturbation geopotential at 300 mb are shown in Figs.2.6b, 2.6c and 2.6d respectively. It can be seen that the upper level westerly winds have increased (max value 5 ms^{-1}) and lows have appeared on either side of the equator at about 150°E . The upper level lows near 150°E which are forced by the symmetric heat sink lead to stronger convergence of the upper level westerlies over this longitude. A comparison of Figs.2.5b and 2.6b, suggests that the Rossby wave response is practically unaffected, while the intensity of the westerlies near the central Pacific is stronger. However the strength of the upper level westerlies is still weak as compared to the case of the strong heat

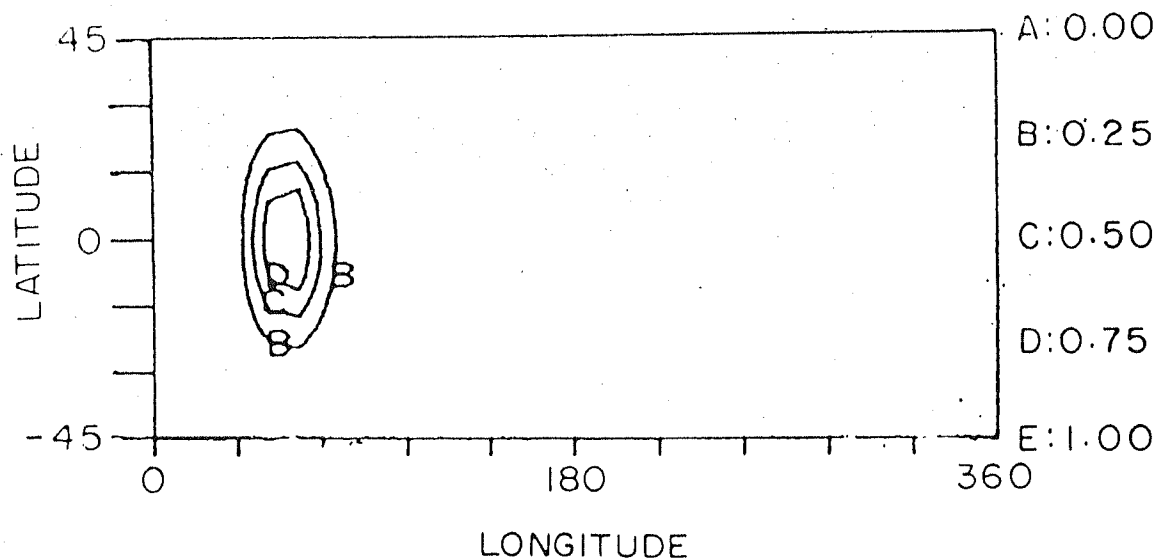


Fig.2.5a. Horizontal distribution of heat source. Interval 0.25 °K per day.

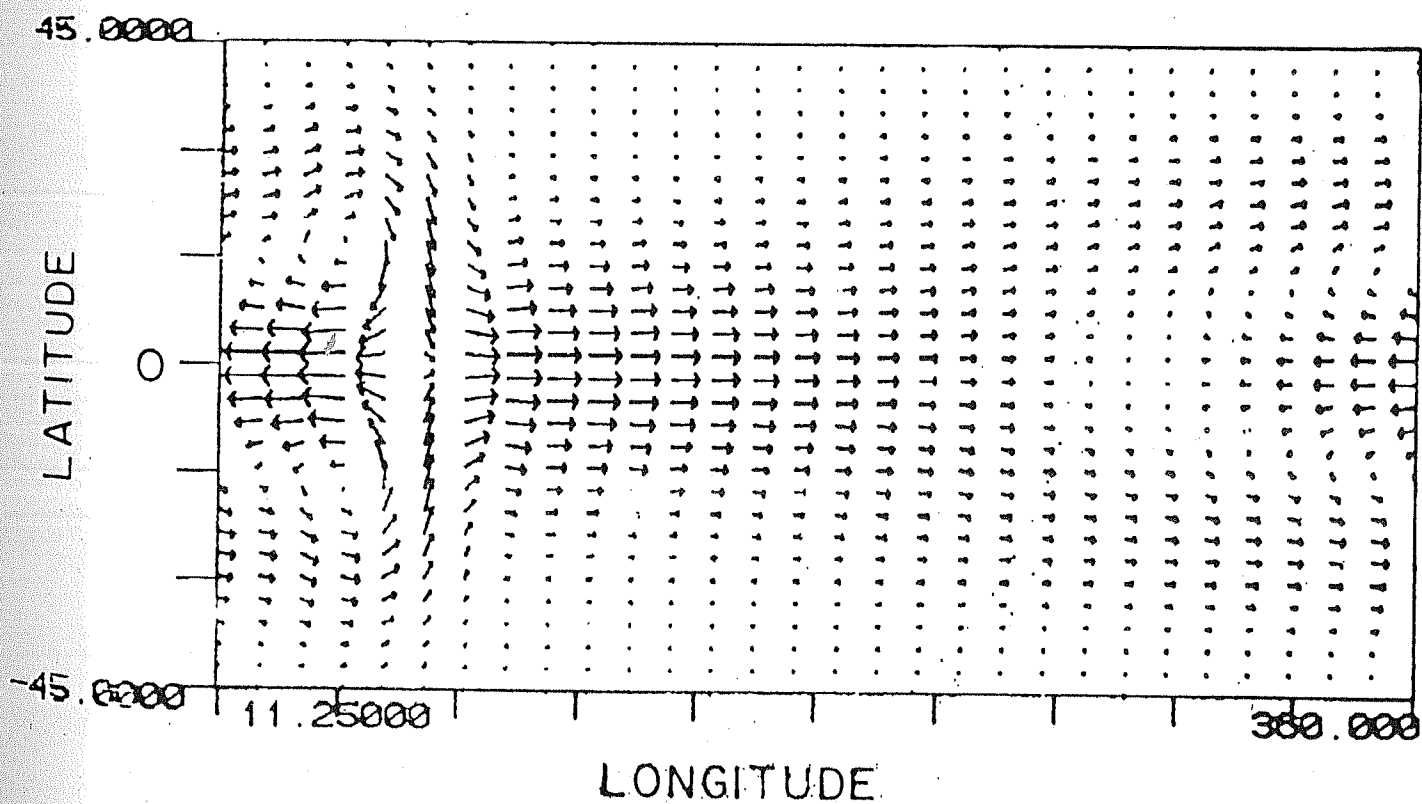


Fig.2.5b. Horizontal wind vectors at 300 mb. Forcing used as in Fig.2.5a.

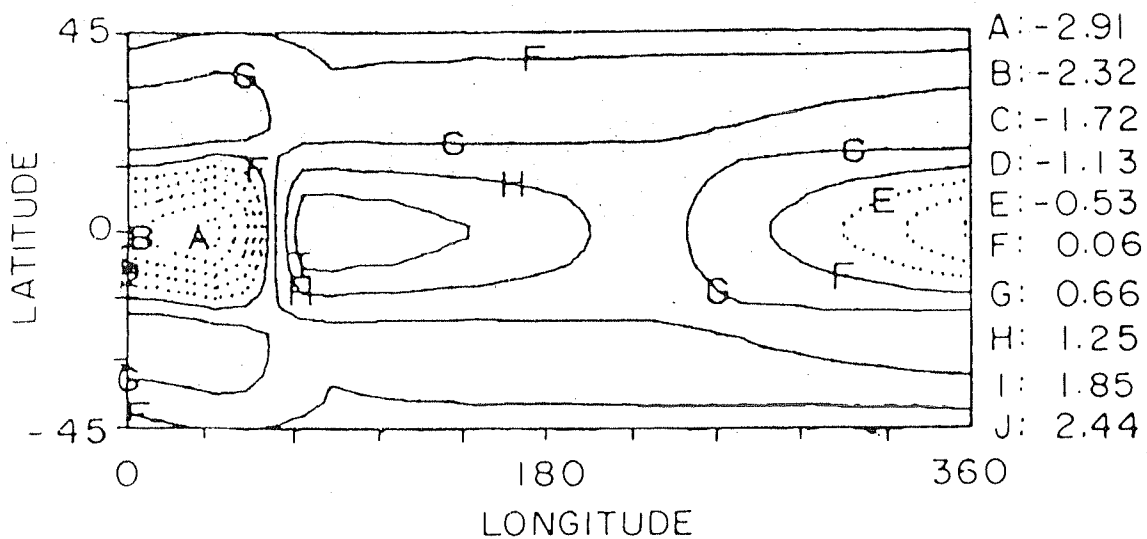


Fig.2.5c. Zonal wind at 300 mb. Interval 0.59 ms^{-1} . Forcing used as in Fig.2.5a.

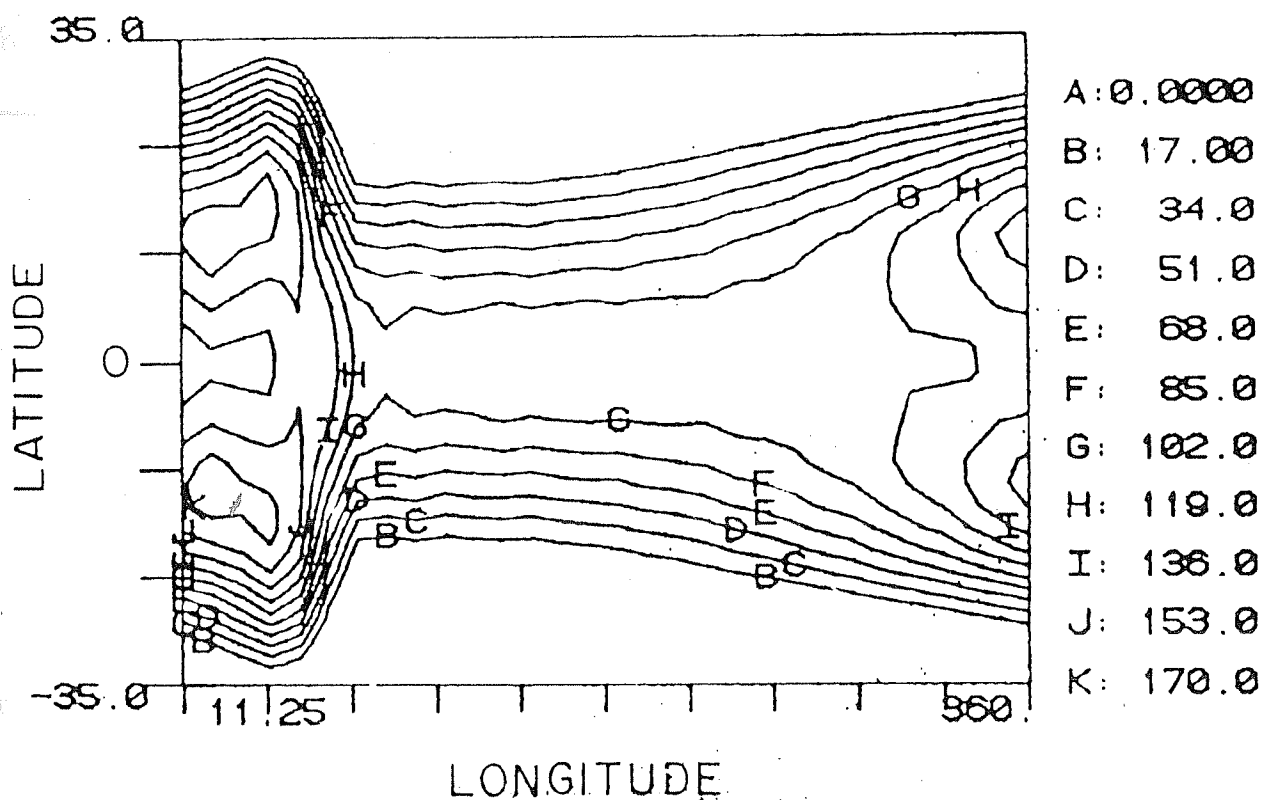


Fig.2.5d. Perturbation geopotential at 300 mb. Interval $17 \text{ m}^2 \text{ s}^{-2}$.

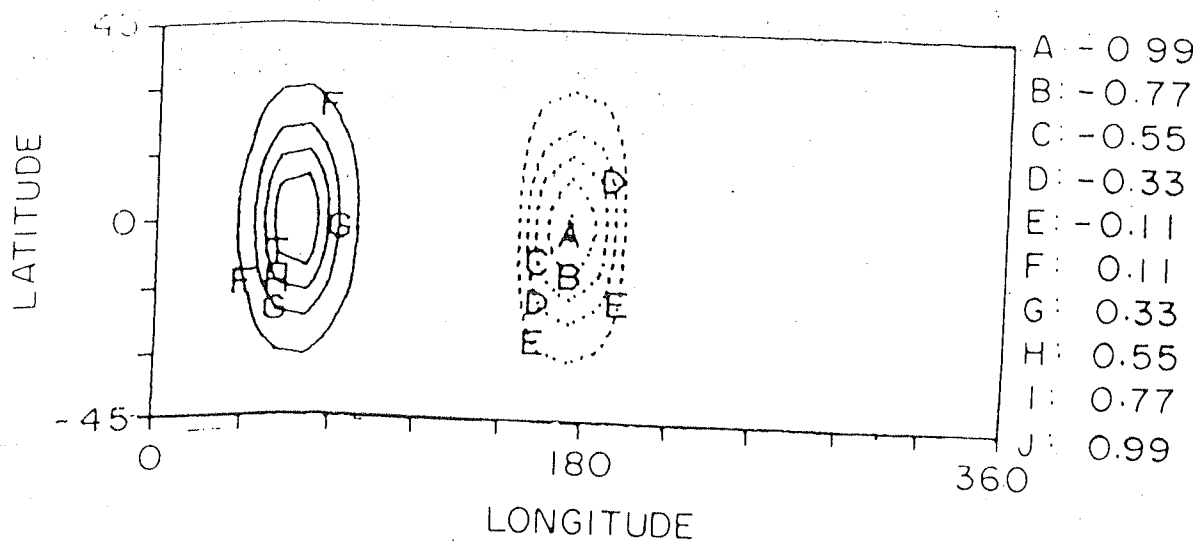


Fig.2.6a. Horizontal distribution of heat source and heat sink separated by 112.5 ° longitudes. Interval 0.22 °K per day.

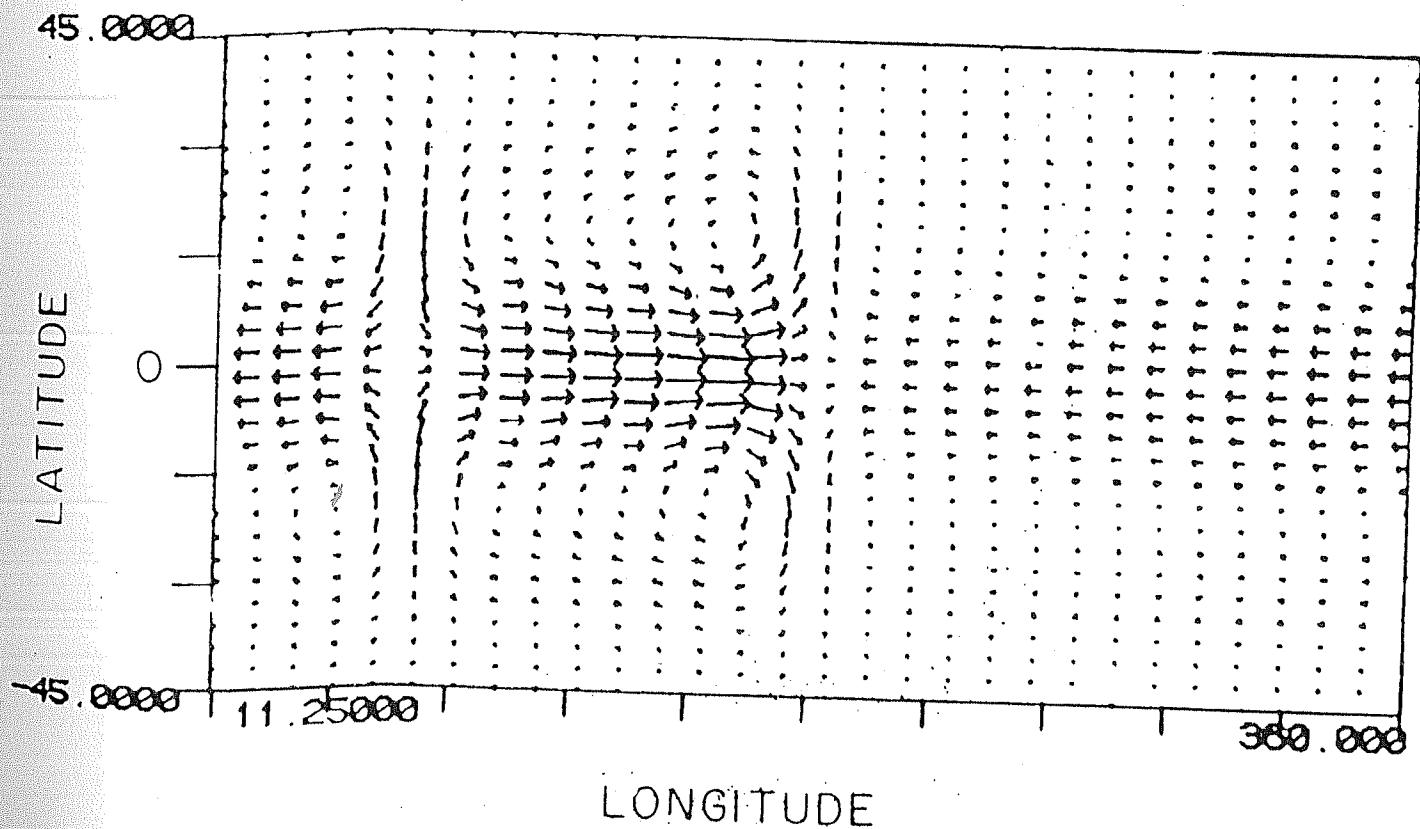


Fig.2.6b. Same as Fig.2.5b, except for forcing as in Fig.2.6a.

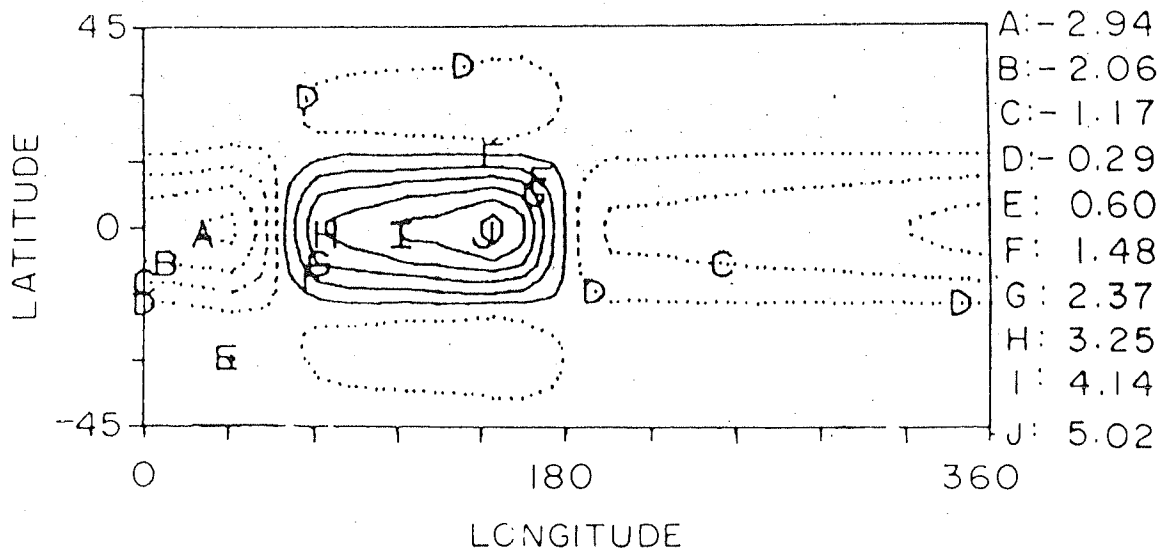


Fig.2.6c. Same as Fig.2.5c, except for forcing as in Fig.2.6a. Interval 0.89 ms^{-1} .

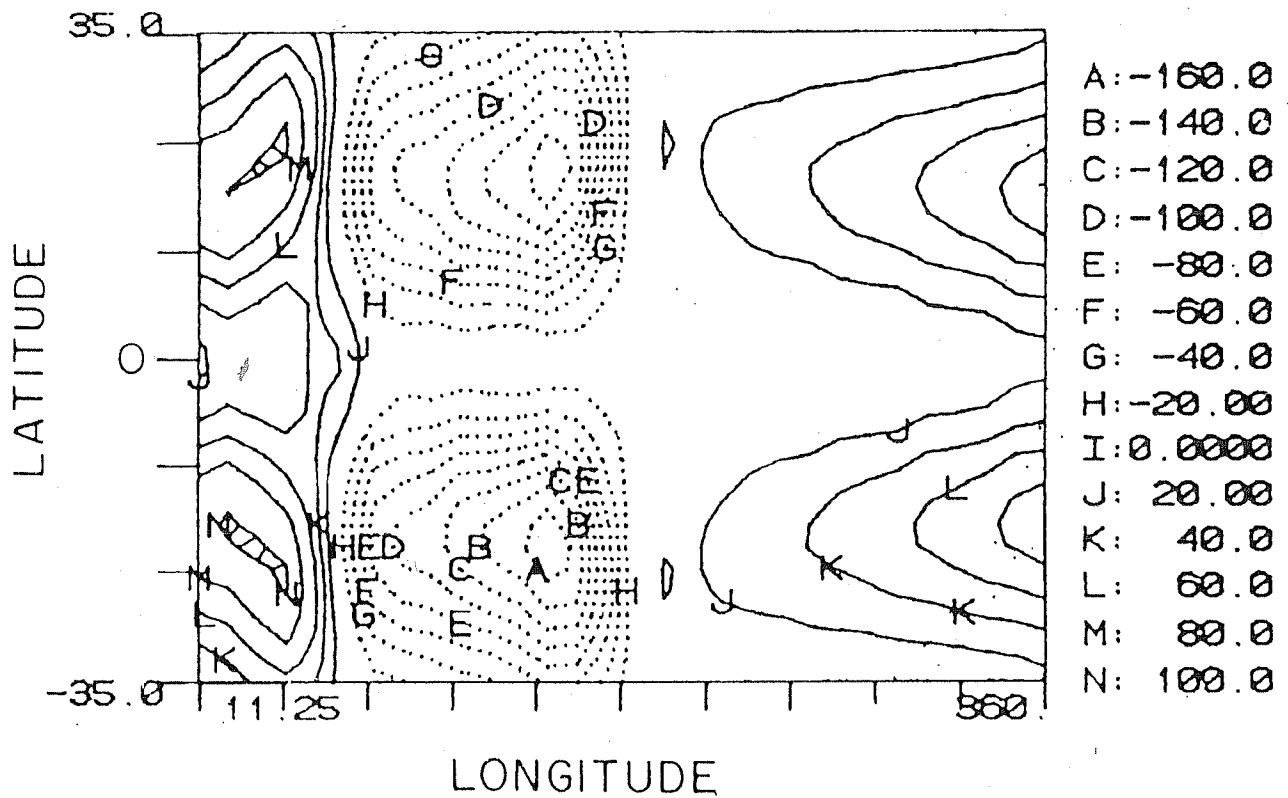


Fig.2.6d. Same as Fig.2.5d, except for forcing as in Fig.2.6a. Interval $20 \text{ m}^2 \text{ s}^{-2}$.

source and heat sink. The main result to be noted is that the radiative cooling in the eastern Pacific, no matter how small, produces an enhancement of the Walker circulation over the central and eastern Pacific. It also leads to the confinement of the time-mean Walker circulation between the heat source and the heat sink.

2.6.2 Analytical calculations

We can analytically work out the time-mean response generated by the combination of a heat source and heat sink (both symmetric w.r.t the equator). This will provide insight into the dynamics of the stationary wave pattern and circulation features, especially in the region between the heat source and heat sink. Analytical expressions can be easily derived by considering the shallow water equations of Gill (1980). The perturbation quantities are expanded in terms of Parabolic Cylinder functions as in Gill (1980). The calculation of the Kelvin and Rossby wave responses induced by a source-sink combination is given below. The thermal forcing is given by 2.29.

$$Q(x, y) = F(x) D_0(y), \text{ where} \quad (2.29)$$

$$F(x) = 0 \text{ if } x \leq A$$

$$F(x) = K(x - A)(B - x) \text{ if } A \leq x \leq B$$

$$F(x) = 0 \text{ if } B \leq x \leq C$$

$$F(x) = -\nu K(x - C)(D - x) \text{ if } C \leq x \leq D$$

$$F(x) = 0 \text{ if } x \geq D$$

where the value of K is chosen such that the maximum heating rate is 1° per day and ν ($0 \leq \nu \leq 1$) is a parameter used to vary the magnitude of the cooling rate. We define $q = u + p$ as in Gill (1980), where u is the perturbation zonal velocity and p is

the perturbation pressure.

The Q_0 component of forcing involves the Kelvin and Rossby wave responses. From equations 3.9 and 4.6 of Gill (1980), the Kelvin wave response is given by q_0 and the Rossby wave response is given by q_2 . The equations governing them are,

$$\frac{dq_0}{dx} + \varepsilon q_0 = -F(x) \quad (2.30)$$

$$\frac{dq_2}{dx} - 3\varepsilon q_2 = F(x) \quad (2.31)$$

The solution of the above equations is obtained by following the treatment for first-order linear inhomogenous equations given by Bender and Orzag (1978).

$$q_0(x) = \alpha \exp(\varepsilon x) - \exp(-\varepsilon x) \int F(x) \exp(\varepsilon x) dx \quad (2.32)$$

$$q_2(x) = \beta \exp(3\varepsilon x) + \exp(3\varepsilon x) \int F(x) \exp(-3\varepsilon x) dx \quad (2.33)$$

where α and β are constants of integration. By using cyclic boundary conditions and matching solutions at the boundaries, we can determine the solution in different regions of the domain. We know that the stationary wave response within the forcing region consists of the free and the forced components and outside the forcing region, the stationary wave response corresponds to the free component alone.

The boundary conditions used by Gill (1980) explicitly make use of the condition that Kelvin waves do not progress to the west of the heat source and Rossby waves do not move to the east of the heat source. However, we do not explicitly impose the above mentioned boundary conditions used by Gill (1980). Since the Kelvin and Rossby wave dynamics are inherently governed by the equations 2.30 and 2.31, their solutions based on cyclic (periodic) boundary condition should consistently bring out the nature of the wave responses. We shall first calculate the stationary Kelvin wave response as shown below:

$$q_0(x) = [g_1(x)] = \alpha_1 \exp(-\varepsilon x) \quad \text{if } x \leq A$$

$$\begin{aligned}
q_0(x) &= [g_2(x)] = \alpha_2 \exp(-\varepsilon x) \\
&- \frac{K}{\varepsilon^3} [(B-x)(x-A)\varepsilon^2 + \varepsilon(2x-A-B)-2] \quad \text{if } A \leq x \leq B \\
q_0(x) &= [g_3(x)] = \alpha_3 \exp(-\varepsilon x) \quad \text{if } B \leq x \leq C \\
q_0(x) &= [g_4(x)] = \alpha_3 \exp(-\varepsilon x) \\
&- \frac{K\nu}{\varepsilon^3} [(D-x)(x-C)\varepsilon^2 + \varepsilon(2x-C-D)-2] \quad \text{if } C \leq x \leq D \\
q_0(x) &= [g_5(x)] = \alpha_5 \exp(-\varepsilon x) \quad \text{if } x \geq D
\end{aligned}$$

By matching the solutions at the boundaries, the constants $\alpha_2, \alpha_3, \alpha_4$ and α_5 are first expressed in terms of α_1 .

From the condition $g_1(A) = g_2(A)$,

$$\alpha_2 = \alpha_1 + \frac{K \exp(\varepsilon A)}{\varepsilon^3} [\varepsilon(A-B) - 2]$$

From the condition $g_2(B) = g_3(B)$,

$$\alpha_3 = \alpha_1 + \frac{K}{\varepsilon^3} [\exp(\varepsilon A) [\varepsilon(A-B) - 2] - \exp(\varepsilon B) [\varepsilon(A-B) - 2]]$$

From the condition $g_3(C) = g_4(C)$,

$$\begin{aligned}
\alpha_4 &= \alpha_1 + \frac{K}{\varepsilon^3} [\exp(\varepsilon A) [\varepsilon(A-B) - 2] - \exp(\varepsilon B) [\varepsilon(A-B) - 2]] \\
&\quad + \frac{K\nu}{\varepsilon^3} [-\exp(\varepsilon C) [\varepsilon(C-D) - 2]]
\end{aligned}$$

From the condition $g_4(D) = g_5(D)$,

$$\begin{aligned}
\alpha_5 &= \alpha_1 + \frac{K}{\varepsilon^3} [\exp(\varepsilon A) [\varepsilon(A-B) - 2] - \exp(\varepsilon B) [\varepsilon(A-B) - 2]] \\
&\quad + \frac{K\nu}{\varepsilon^3} [-\exp(\varepsilon C) [\varepsilon(C-D) - 2] + \exp(\varepsilon D) [\varepsilon(D-C) - 2]]
\end{aligned}$$

We can now determine α_1 by using the cyclic boundary condition $g_1(X_0) = g_5(X_N)$, from which

$$\alpha_1 = \frac{K \exp(-\varepsilon X_N)}{[\exp(-\varepsilon X_0) - \exp(-\varepsilon X_N)] \varepsilon^3} [\exp(\varepsilon A) [\varepsilon(A-B) - 2]]$$

$$\begin{aligned}
& -\exp(\varepsilon B) [\varepsilon(B - A) - 2] - \nu \exp(\varepsilon C) [\varepsilon(C - D) - 2] \\
& + \nu \exp(\varepsilon D) [\varepsilon(D - C) - 2]
\end{aligned}$$

The pressure and velocity components of the flow arising out of the Kelvin wave response are given by,

$$u = p = \frac{1}{2} q_0(x) \exp\left(\frac{-y^2}{4}\right) \quad (2.34)$$

$$v = 0 \quad (2.35)$$

$$w = \frac{1}{2} [\varepsilon q_0(x) + F(x)] \exp\left(\frac{-y^2}{4}\right) \quad (2.36)$$

Similarly, the calculations for the Rossby wave response are shown below,

$$q_2(x) = [h_1(x)] = \beta_1 \exp(3\varepsilon x) \quad \text{if } x \leq A$$

$$\begin{aligned}
q_2(x) &= [h_2(x)] = \beta_2 \exp(3\varepsilon x) \\
& - \frac{K}{27\varepsilon^3} [(B - x)(x - A)9\varepsilon^2 + 3\varepsilon(A + B - 2x) - 2] \quad \text{if } A \leq x \leq B
\end{aligned}$$

$$q_2(x) = [h_3(x)] = \beta_3 \exp(3\varepsilon x) \quad \text{if } B \leq x \leq C$$

$$\begin{aligned}
q_2(x) &= [h_4(x)] = \beta_4 \exp(3\varepsilon x) \\
& + \frac{K\nu}{27\varepsilon^3} [(D - x)(x - C)9\varepsilon^2 + 3\varepsilon(C + D - 2x) - 2] \quad \text{if } C \leq x \leq D
\end{aligned}$$

$$q_2(x) = [h_5(x)] = \beta_5 \exp(3\varepsilon x) \quad \text{if } x \geq D$$

By matching the solutions at the boundaries the constants $\beta_2, \beta_3, \beta_4$ and β_5 are first expressed in terms of β_1 .

From the condition $h_1(A) = h_2(A)$,

$$\beta_2 = \beta_1 + \frac{K \exp(-3\varepsilon A)}{27\varepsilon^3} [3\varepsilon(B - A) - 2]$$

From the condition $h_2(B) = h_3(B)$,

$$\beta_3 = \beta_1 + \frac{K}{27\epsilon^3} [\exp(-3\epsilon A) [3\epsilon(B - A) - 2] - \exp(-3\epsilon B) [3\epsilon(A - B) - 2]]$$

From the condition $h_3(C) = h_4(C)$,

$$\begin{aligned} \beta_4 = \beta_1 + \frac{K}{27\epsilon^3} [\exp(-3\epsilon A) [\epsilon(B - A) - 2] - \exp(-3\epsilon B) [3\epsilon(A - B) - 2]] \\ - \frac{K\nu}{27\epsilon^3} [-\exp(-3\epsilon C) [3\epsilon(D - C) - 2]] \end{aligned}$$

From the condition $h_4(D) = h_5(D)$,

$$\begin{aligned} \beta_5 = \beta_1 + \frac{K}{27\epsilon^3} [\exp(-3\epsilon A) [3\epsilon(B - A) - 2] - \exp(-3\epsilon B) [3\epsilon(A - B) - 2]] \\ - \frac{K\nu}{27\epsilon^3} [\exp(-3\epsilon C) [3\epsilon(D - C) - 2] - \exp(-3\epsilon D) [3\epsilon(C - D) - 2]] \end{aligned}$$

We can now determine β_1 by using the cyclic boundary condition $h_1(X_0) = h_5(X_N)$, from which

$$\begin{aligned} \beta_1 = \frac{K \exp(3\epsilon X_N)}{[\exp(3\epsilon X_0) - \exp(3\epsilon X_N)] 27\epsilon^3} [\exp(-3\epsilon A) [3\epsilon(B - A) - 2] \\ - \exp(-3\epsilon B) [3\epsilon(A - B) - 2] - \nu \exp(-3\epsilon C) [3\epsilon(D - C) - 2] \\ + \nu \exp(-3\epsilon D) [3\epsilon(C - D) - 2]] \end{aligned}$$

The flow fields due to the Rossby wave response are give below,

$$u = \frac{1}{2} q_2(x) (y^2 - 3) \exp\left(\frac{-y^2}{4}\right) \quad (2.37)$$

$$p = \frac{1}{2} q_2(x) (y^2 + 1) \exp\left(\frac{-y^2}{4}\right) \quad (2.38)$$

$$v = [F(x) + 4\epsilon q_2(x)] y \exp\left(\frac{-y^2}{4}\right) \quad (2.39)$$

$$w = \frac{1}{2} \left[F(x) + \varepsilon q_2(x) (1 + y^2) \right] \exp \left(\frac{-y^2}{4} \right) \quad (2.40)$$

We notice that the region between the heat source and the heat sink contains both free Kelvin waves originating from the heat source as well as free Rossby waves originating from the heat sink. The time-mean geopotential at the upper level is characterized by highs near the region of the heat source and lows near the region of the heat sink. The Kelvin wave response of the heat source results in upper level westerlies to the east of the heat source. Similarly, the Rossby wave response of the heat sink produces westerly winds to its west. The lows to the west of the heat sink (Rossby wave response of the heat sink) lead to stronger convergence and strengthening of the westerlies in the region between the heat source and heat sink. This is essentially a superposition of free Kelvin waves (from the heat source) and free Rossby waves (from the heat sink) which leads to reinforcement of the westerly winds at the upper troposphere. Therefore, it will be more appropriate to view the time-mean Walker circulation in the equatorial Pacific as a stationary response resulting from a combination of the Kelvin waves (from the heat source) and Rossby waves (from the heat sink). Apparently the dynamics of this combined wave response, will depend on the intensities of the heat source and the heat sink and also on the separation between them.

2.6.3 Sensitivity studies with the 2-level model

We have used the simple 2-level linear equatorial β -plane model, to study the changes in the time-mean Walker circulation, caused by zonal displacements in the relative positions of the Indonesian heat source and cooling in the eastern Pacific. Krueger and Winston (1974) reported that the Walker circulation in the equatorial Pacific was sensitive to the fluctuations in the spatial distribution of the radiative cooling

zone in the eastern Pacific. They found that during the years, when the heat sink had a greater westward extent, the east-west circulation over the equatorial Pacific exhibited considerable strengthening. We have the following three cases of forcings (Figs.2.7a, 2.8a and 2.9a). In the first case, there is only a heat source (max heating 1° per day) symmetric w.r.t equator. In the second case, a symmetric heat sink (max cooling 1° per day) is situated at a distance of 171° longitude from the heat source. In the third case, the angular separation between the source and sink is further increased to 228° longitude. Figs.2.7b, 2.8b, and 2.9b represent the zonal wind at 250 mb for the three cases. Similarly, Figs.2.7c, 2.8c, and 2.9c represent the perturbation geopotential at 250 mb for the three cases. In the first case, the Rossby and Kelvin wave responses are seen in the zonal wind field, which is also supported by the geopotential field. In the second case, we notice an increase in the westerly speed in the region between the source and the sink and also the appearance of a low (Rossby wave response of the sink) to the west of the heat sink. We have already shown that this intensification of the Walker circulation is the result of the superposition of Kelvin waves from the heat source and Rossby waves from the heat sink. In the third case, when the separation between the source and the sink is further increased, we can observe a decrease in the upper level westerly wind speed. This weakening may be interpreted in the following way. When the distance between the heat source and the heat sink is as large as 228° , the easterly regime (Rossby waves from the heat source and Kelvin waves from the heat sink) starts dominating over the westerly flow in the region between the source and the sink. This essentially leads to a decrease in the upper level westerly flow and consequently a weakening of the Walker circulation in the equatorial Pacific. These simple sensitivity experiments, demonstrate that the changes in the relative separation between the heat source and heat sink can considerably modify the longitudinal scale and strength of the east-west circulations.

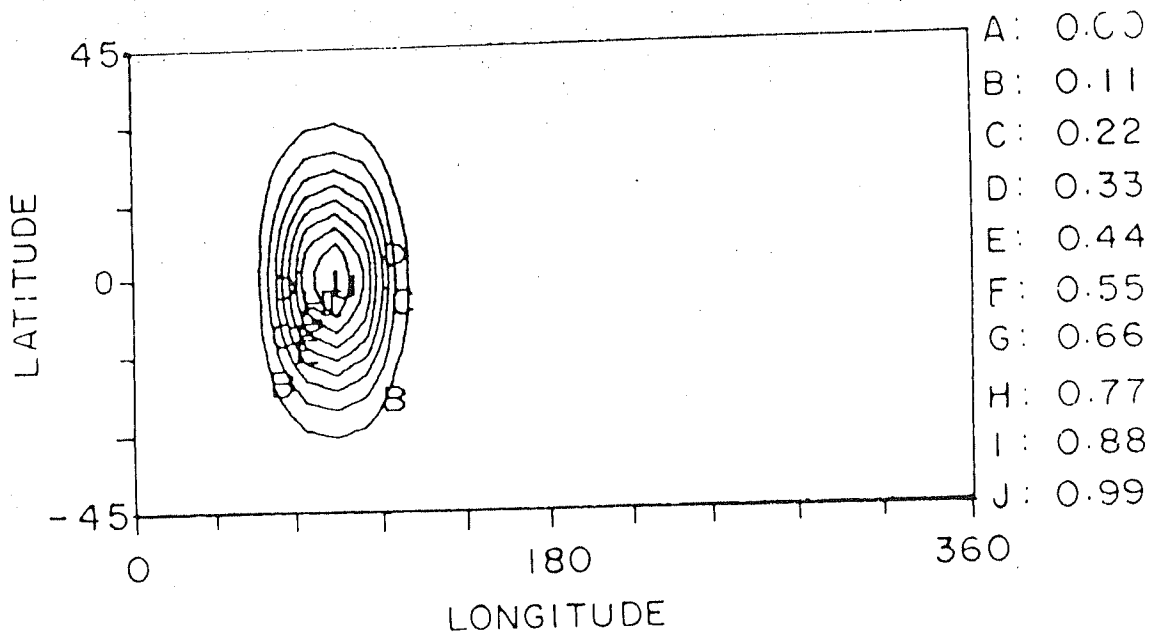


Fig.2.7a. Horizontal distribution of heat source. Interval 0.11 °K per day.

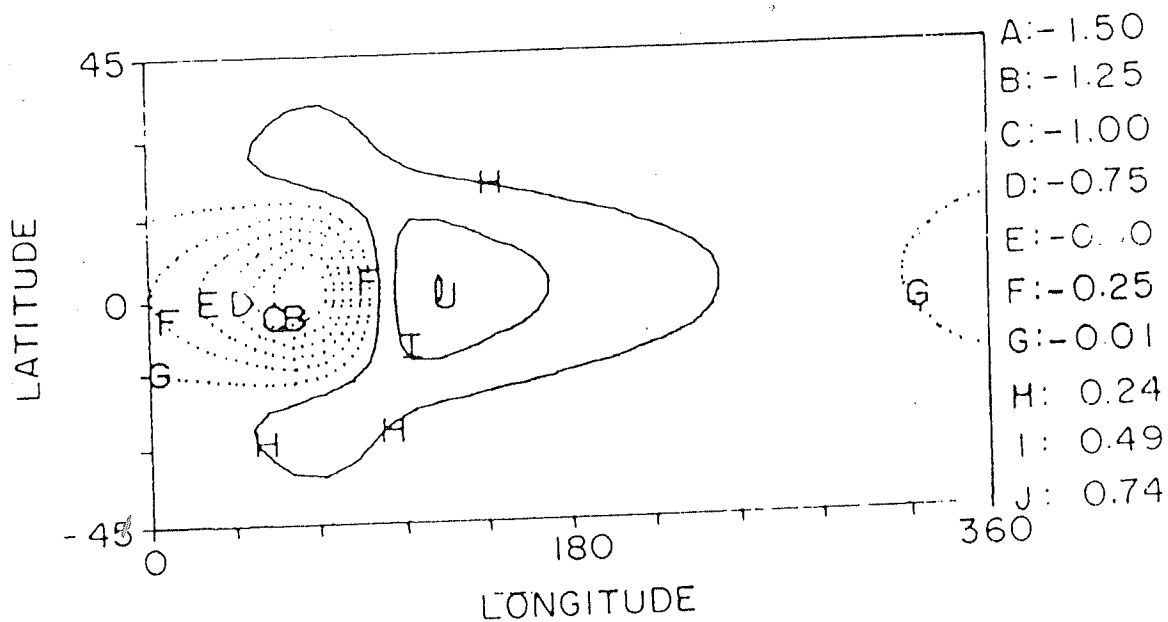


Fig.2.7b. Zonal wind at 250 mb, in the 2-level linear model. Interval 0.25 ms⁻¹. Forcing used as in Fig.2.7a.

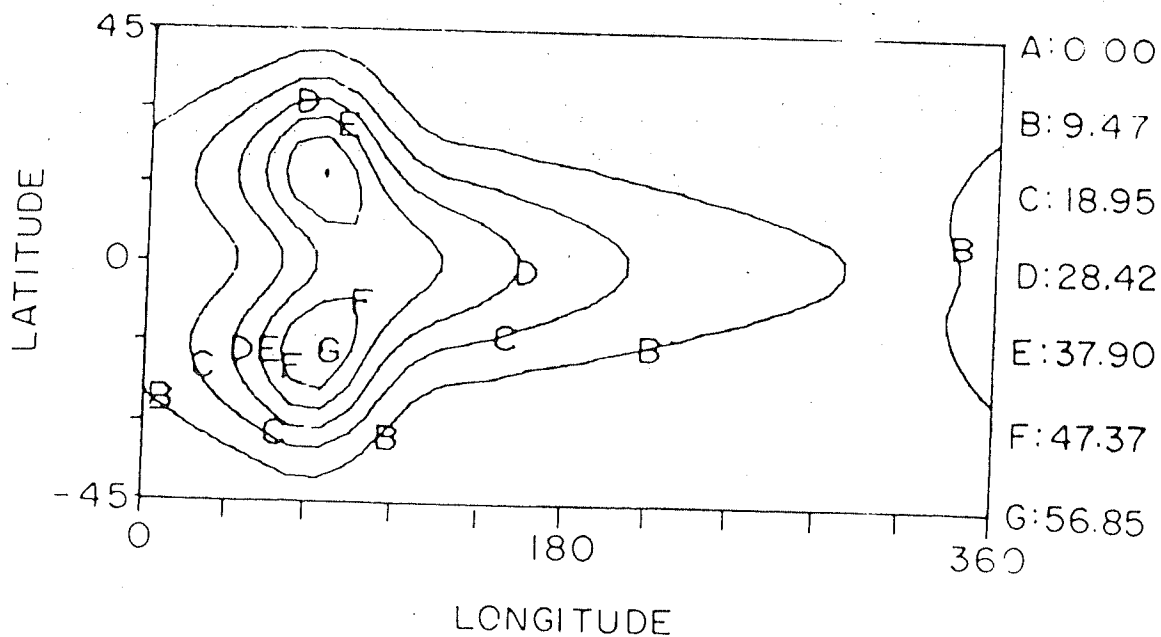


Fig.2.7c. Perturbation geopotential at 250 mb. Interval $9.47 \text{ m}^2 \text{s}^{-2}$. Forcing used as in Fig.2.7a.

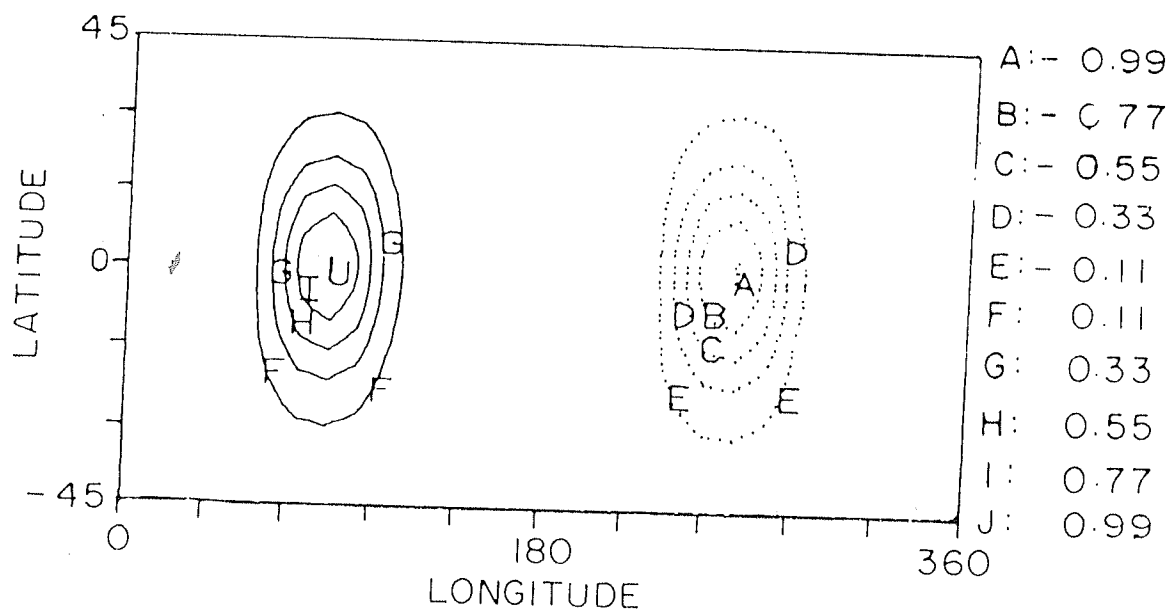


Fig.2.8a. Horizontal distribution of heat source and heat sink separated by 171° longitudes. Interval 0.22°K per day.

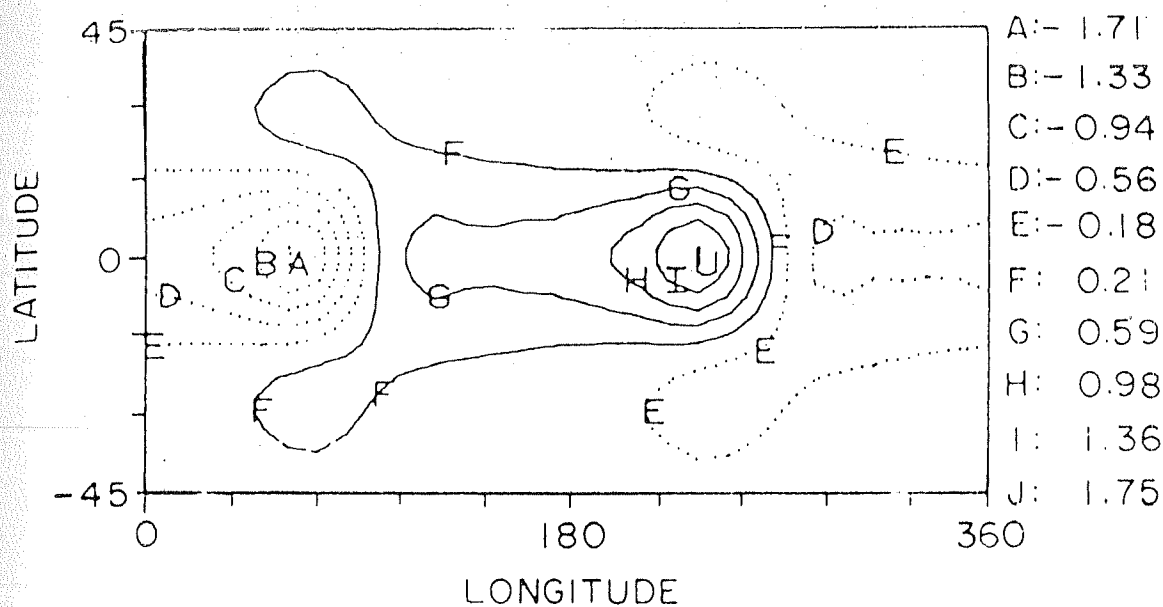


Fig.2.8b. Same as Fig.2.7b, except for forcing as in Fig.2.8a. Interval 0.4 ms^{-1} .

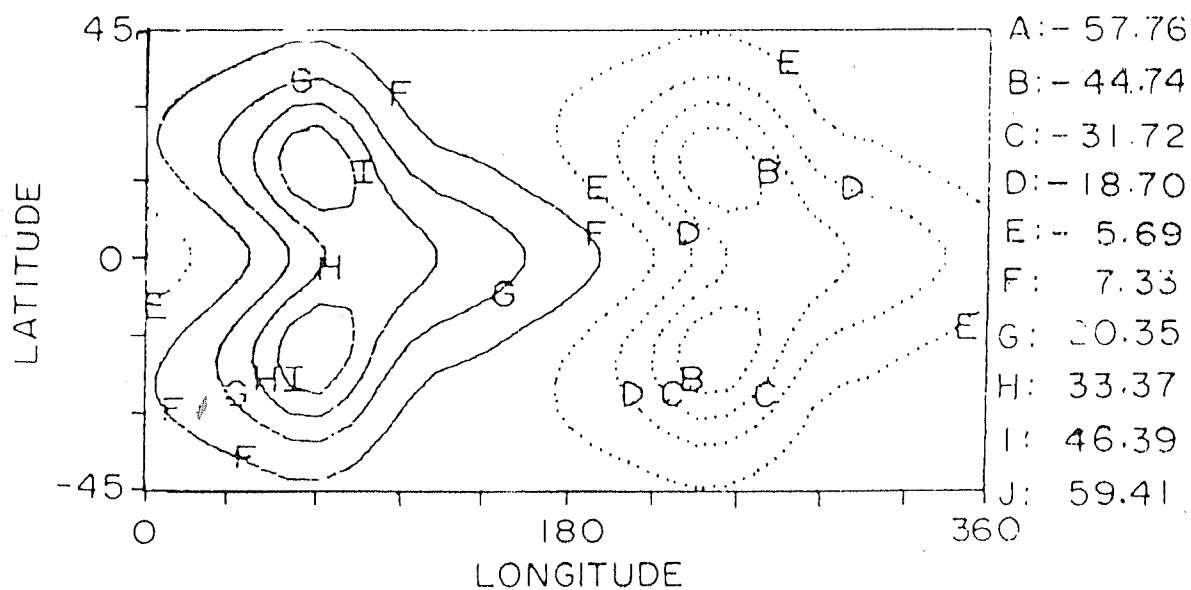


Fig.2.8c. Same as Fig.2.7c, except for forcing as in Fig.2.8a. Interval $13 \text{ m}^2\text{s}^{-2}$.

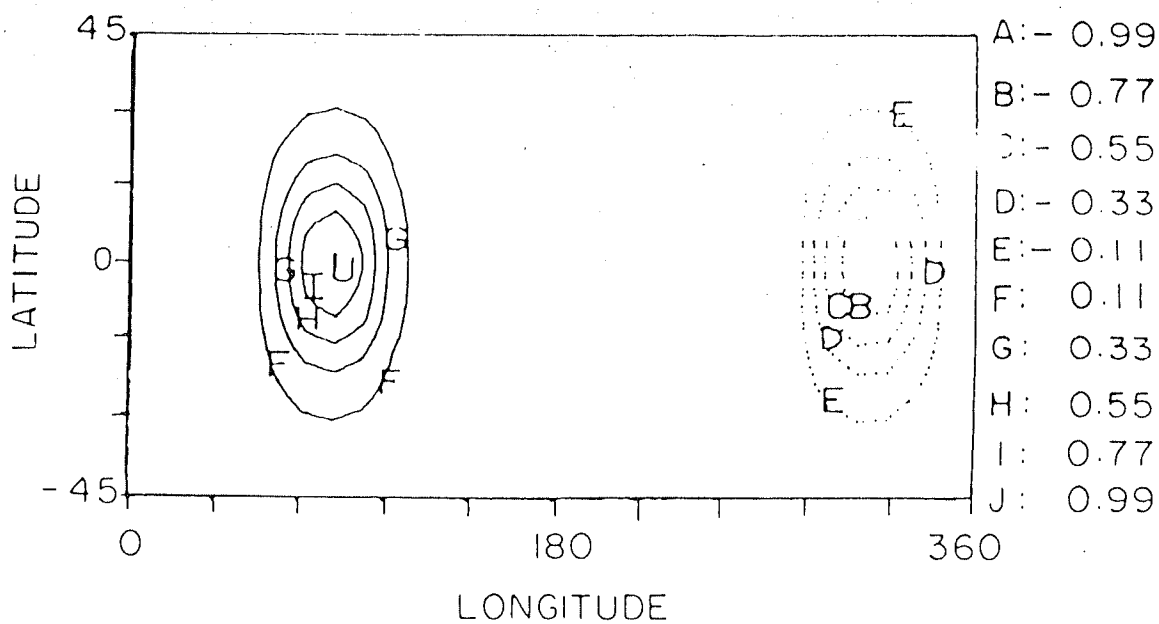


Fig.2.9a. Same as Fig.2.8a, except for separation being 228° longitudes.

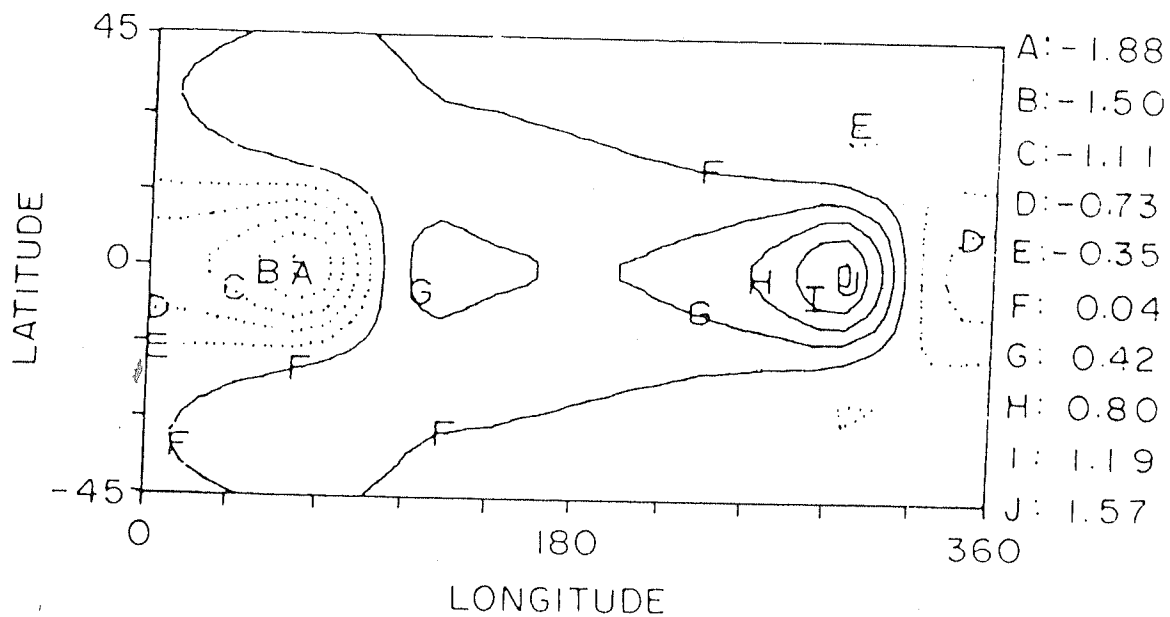


Fig.2.9b. Same as Fig.2.8b, except for forcing as in Fig.2.9a. Interval 0.39 ms^{-1} .

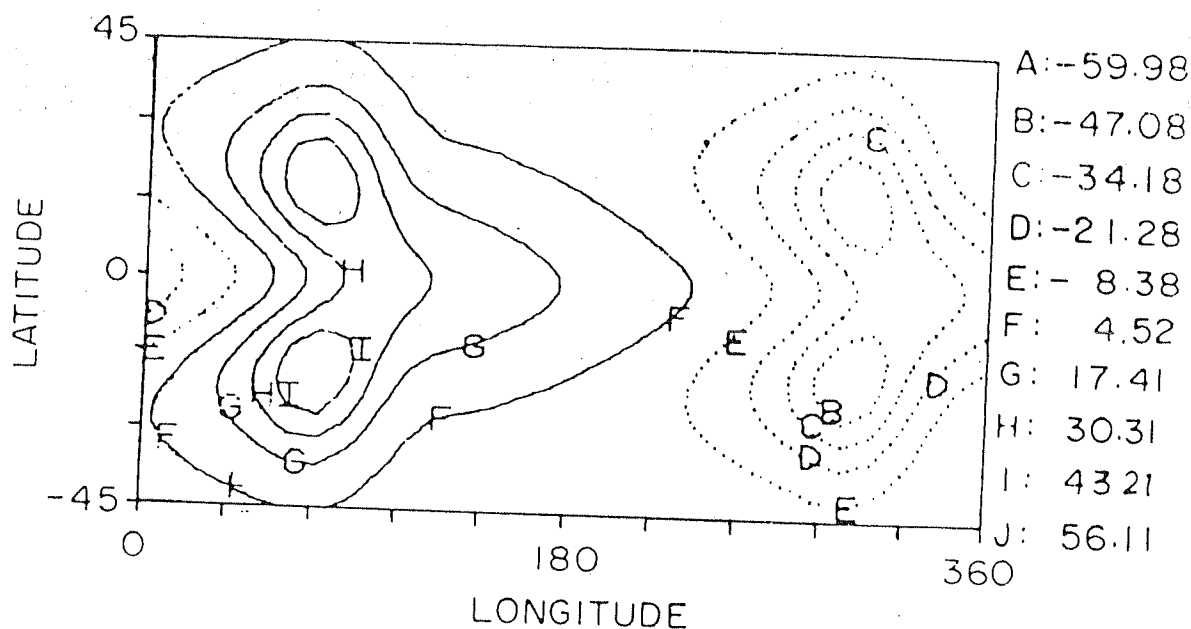


Fig.2.9c. Same as Fig.2.8c, except for forcing as in Fig.2.9a. Interval $13 \text{ m}^2 \text{ s}^{-2}$.

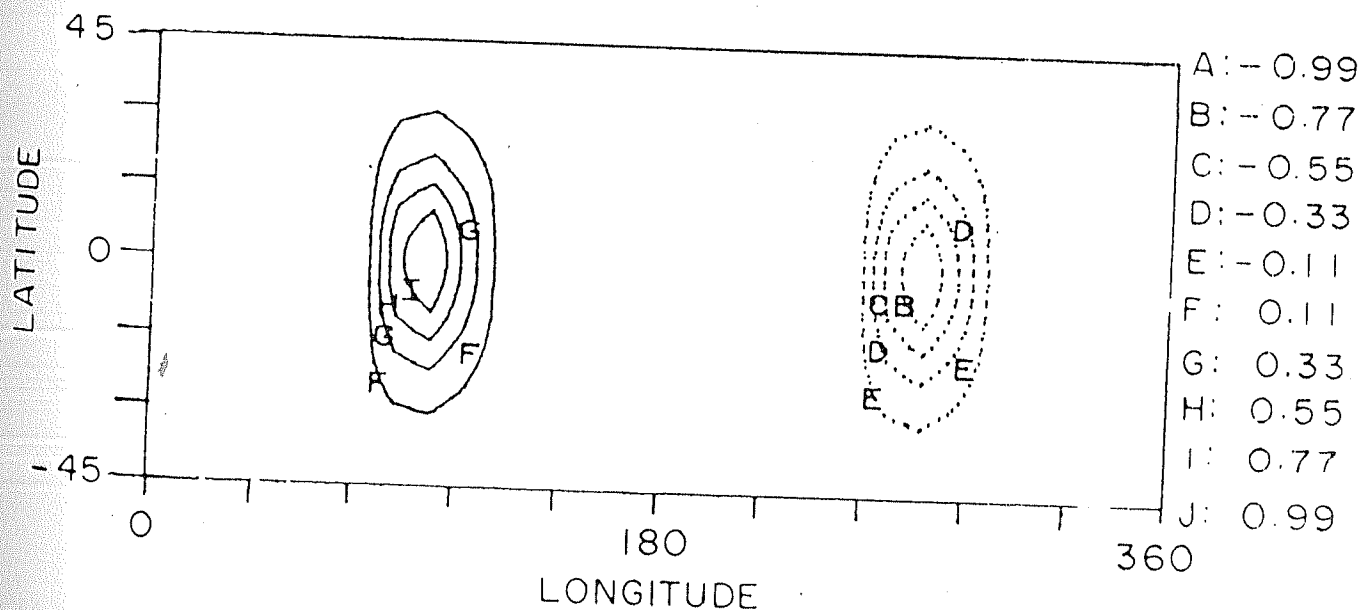


Fig.2.10a. Horizontal distribution of heat source and heat sink separated by 134° longitudes. Interval 0.22°K per day.

The effects of varying the Rayleigh friction term have also been studied. We have considered two different cases of damping, with the forcing remaining the same. The forcing (Fig.2.10a) shows a symmetric source and sink, separated by 134° longitude. The maximum diabatic heating and cooling rates are 1°K per day. In the first case, we choose a strong damping which corresponds to an e-folding time of 2.5 days. In the weaker damping case, the decay time-scale corresponds to 5 days. The zonal winds at the lower level, for the two cases are shown in Figs.2.10b and 2.10c respectively. It can be seen that in the case of the larger damping, the low-level easterly speed in the region of the source and the sink is smaller (-2.55 ms^{-1}) and in the case of the weaker damping the speed is (-3.34 ms^{-1}). We can also notice a substantial reduction in the westerly winds in the case of the strong damping. However, it can be literally seen that the longitudinal scale of the easterlies is essentially the same in the two cases although the strength of the circulation is weak for case of strong dissipation. The implication is that the scale of the Walker circulation in the equatorial Pacific crucially depends on the separation between the heat source and sink.

2.6.4 Effects of nonlinearities on the stationary waves

The final question that we wish to address is the impact of nonlinear terms on the equatorially trapped stationary Kelvin and Rossby waves. The significance of nonlinear advection terms in determining the time-mean response in the tropics has been pointed by Sardeshmukh and Held (1984), Sardeshmukh and Hoskins (1985) and Hendon (1986). Our approach to study the impact due to nonlinearities, is to compare the steady-state response from the linear (LM) and nonlinear (NLM) versions of the 5-level global spectral model. The linear model (LM) is constructed basically by omitting all the nonlinear terms in the model equations. Comparisons of equilibrium solutions of LM and NLM have been performed for two cases of forcing. In the first

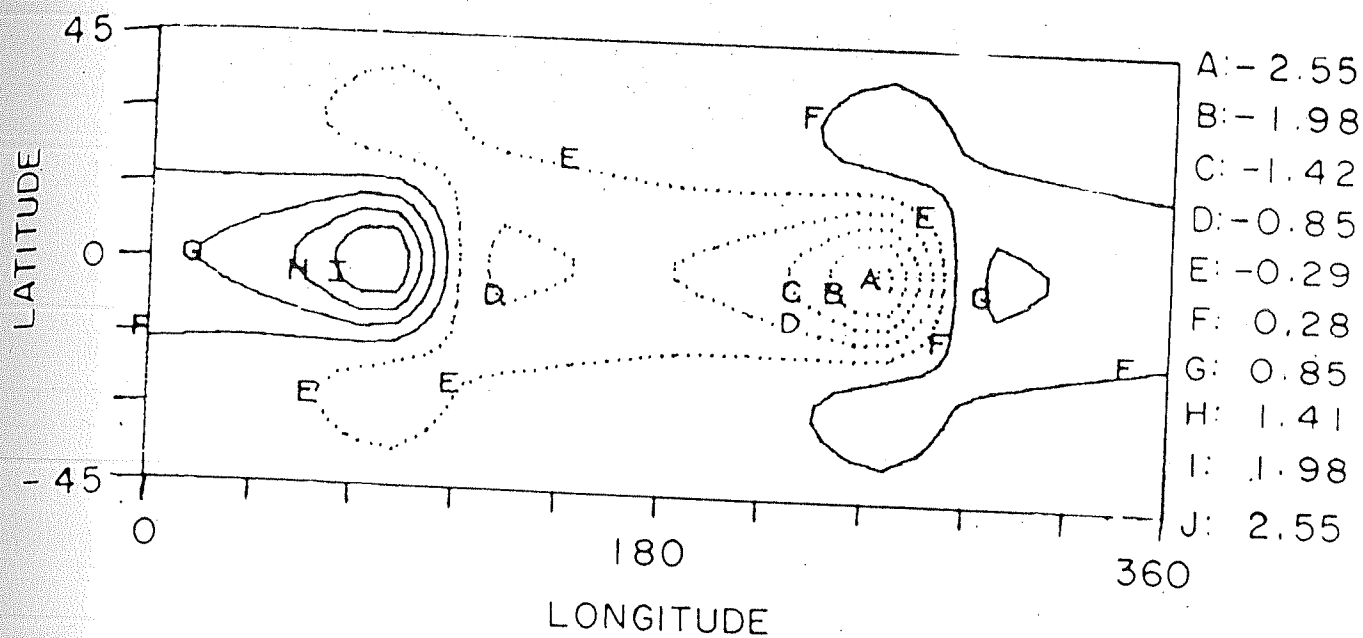


Fig.2.10b. Zonal wind at lower level. Interval 0.57 ms^{-1} . Forcing used as in Fig.2.10a and ϵ corresponds to decay time of 2.5 days.

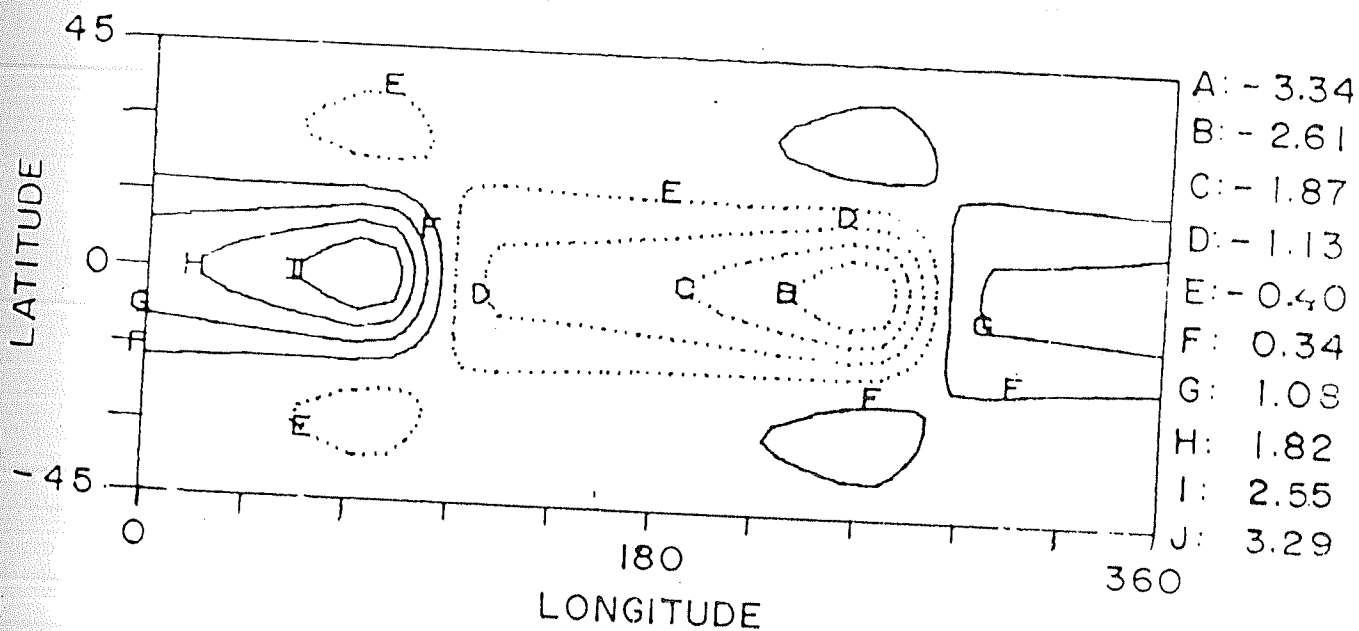


Fig.2.10c. Same as Fig.2.10b, except for ϵ corresponding to decay time of 5 days. Interval 0.74 ms^{-1}

case, the forcing is an idealized heat source symmetric w.r.t the equator and in the second case the forcing is antisymmetric w.r.t the equator.

Fig.2.11a shows a strong heat source symmetric w.r.t the equator and has a maximum heating rate of 4°K per day. The heating has a vertical variation of the form $Q(p) = \sin\left(\frac{\pi p}{p_0}\right)$, where p_0 corresponds to the 1000 mb pressure value. This function has a maximum value at 500 mb and is zero at $p = p_0$ and $p = 0$. We have chosen weak Rayleigh friction and Newtonian cooling terms (damping time-scale ~ 10 days) in the LM and NLM, in order to ensure that the changes in the equilibrium solution produced by nonlinear terms do not get masked by the dissipation effects. Both the models were forced with the heat source shown in Fig.2.11a and the models were integrated until the steady-state was attained. We have analyzed the flow patterns at the 300 mb pressure level in the two cases. The perturbation geopotential at 300 mb for the NLM and LM are shown in Figs.2.11b and 2.11d respectively. The zonal wind field in the two cases are represented in Figs.2.11c and 2.11e. A close examination of the equilibrium solutions in the LM and NLM reveals significant differences in the vicinity of the forcing. These distinct changes that are noticed close to the heating region suggest that the forced component of the stationary waves is strongly influenced by the nonlinearities. Anticyclonic circulations at the tropical upper troposphere can be seen in Figs.2.11b and 2.11d. Within and to the west of the forcing region, one notices that the equatorial high extends more eastward in the NLM as compared to the LM. The eastward shift is very prominently seen to the west of the forcing region and close to the equator. For instance the contour value ($400 \text{ m}^2\text{s}^{-2}$) associated with the equatorial high to the west of the forcing extends upto about 70°E in the NLM. The same contour extends only upto 50°E in the LM. It is clear that the nonlinear advection terms have produced an eastward shift of the upper level anticyclonic features, on the western side of the forcing region, by nearly 20° longitudes. As one proceeds meridionally away from the equator, the eastward shift of

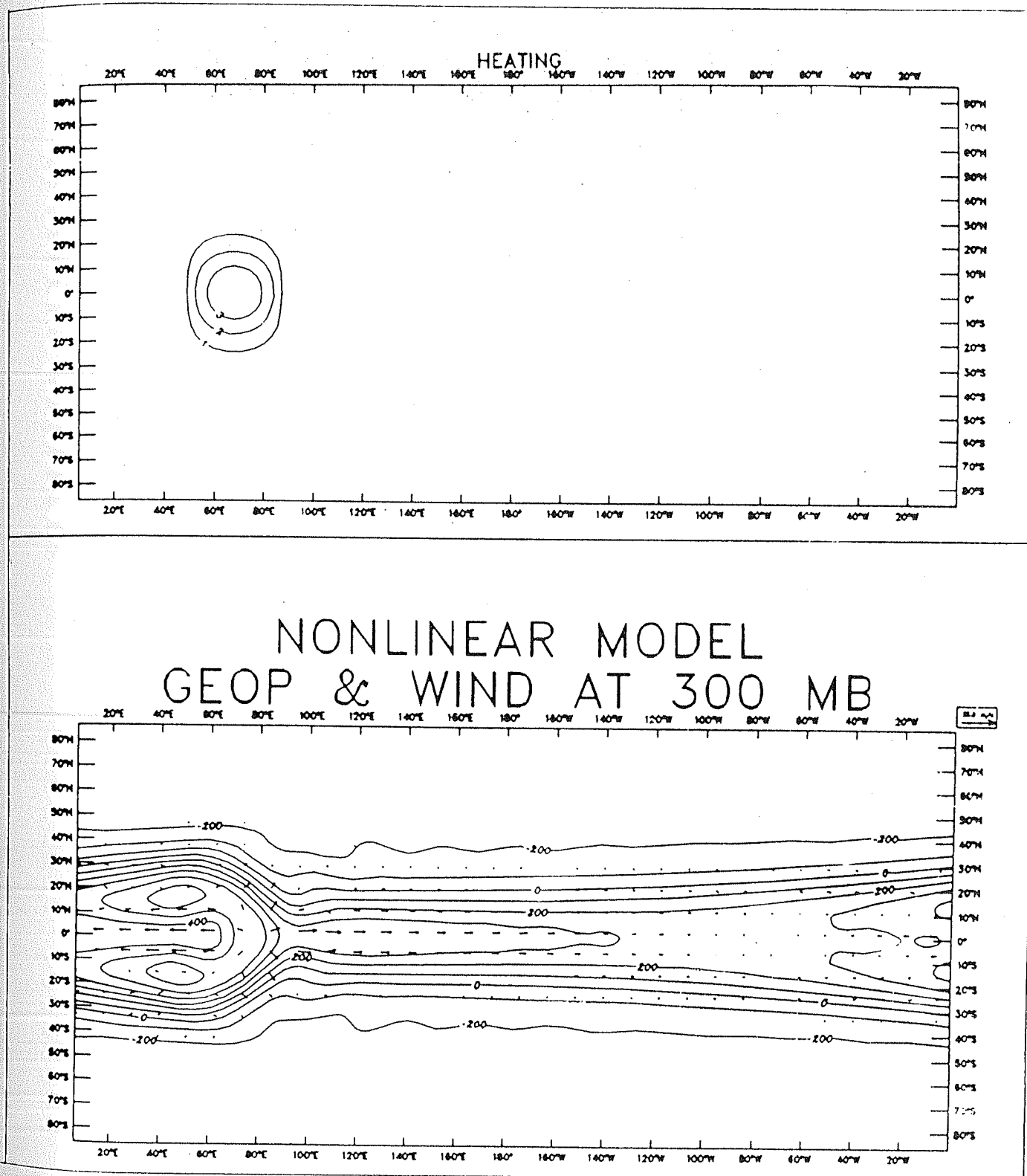
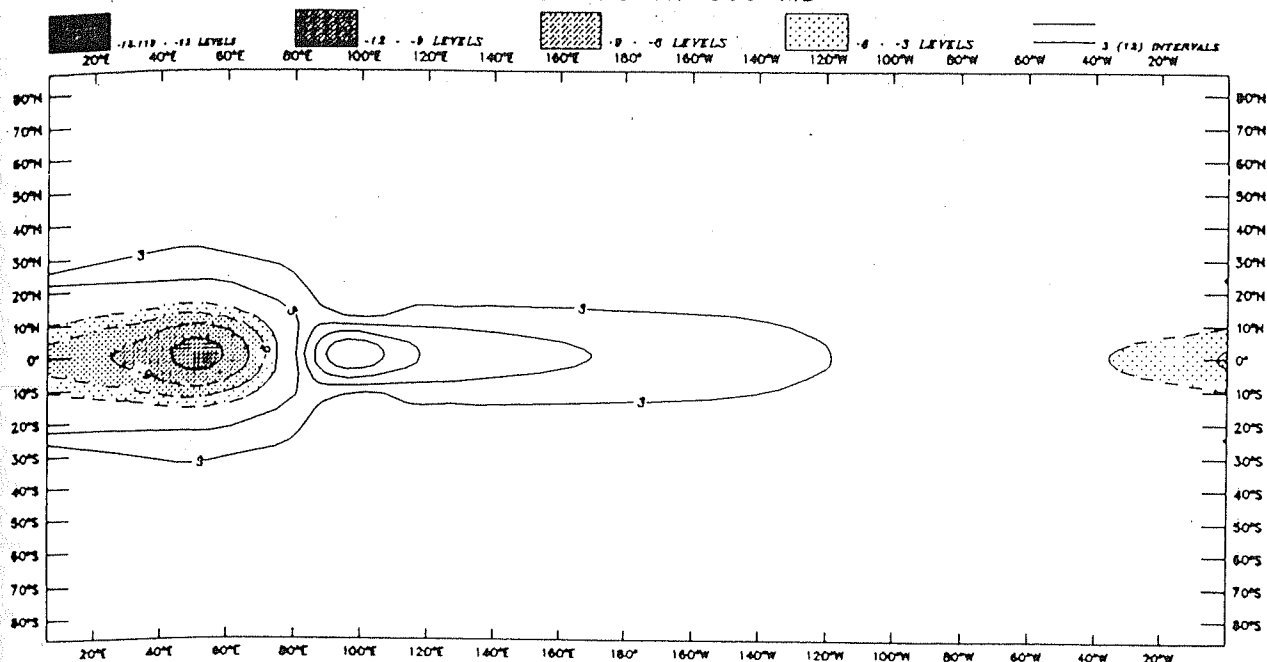


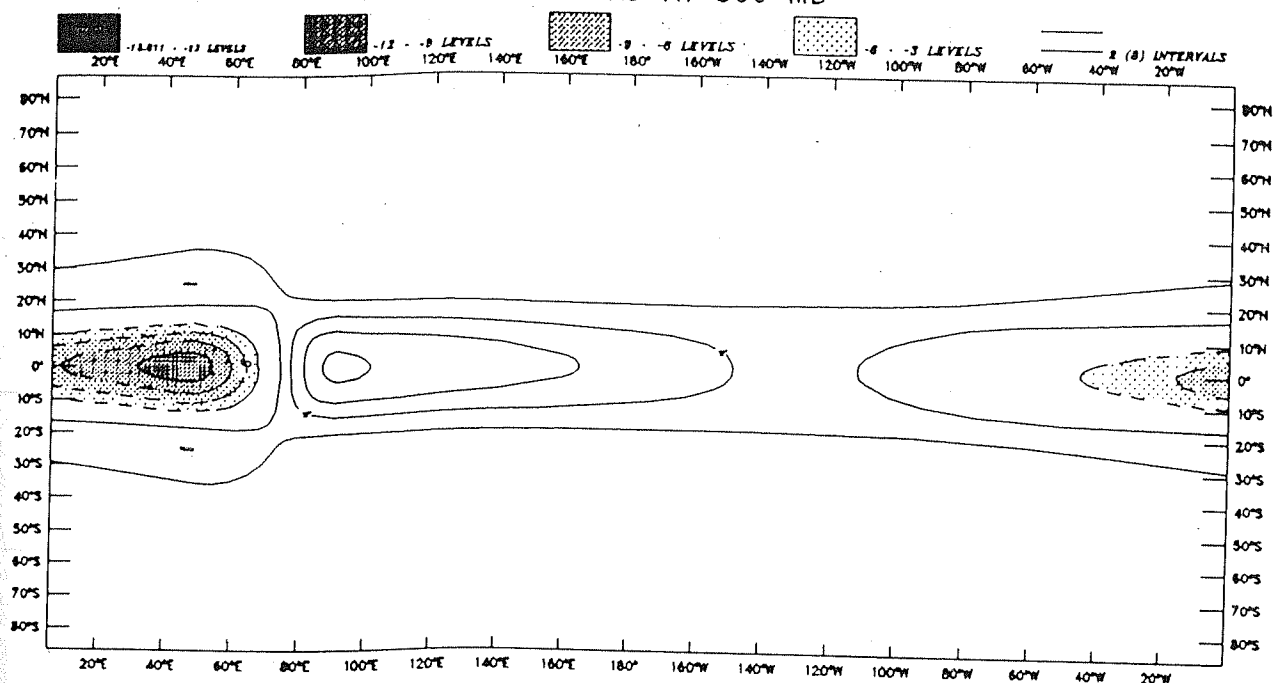
Fig.2.11a. (Top) Horizontal distribution of symmetric heat source. Interval 1 °K per day.

Fig.2.11b. (Bottom) Perturbation geopotential at 300 mb in NLM. Interval 100 $m^2 s^{-2}$. Forcing used as in Fig.2.11a.

NONLINEAR MODEL ZONAL WIND AT 300 MB



LINEAR MODEL ZONAL WIND AT 300 MB



NONLINEAR - LINEAR ZONAL VELOCITY AT 300 MB

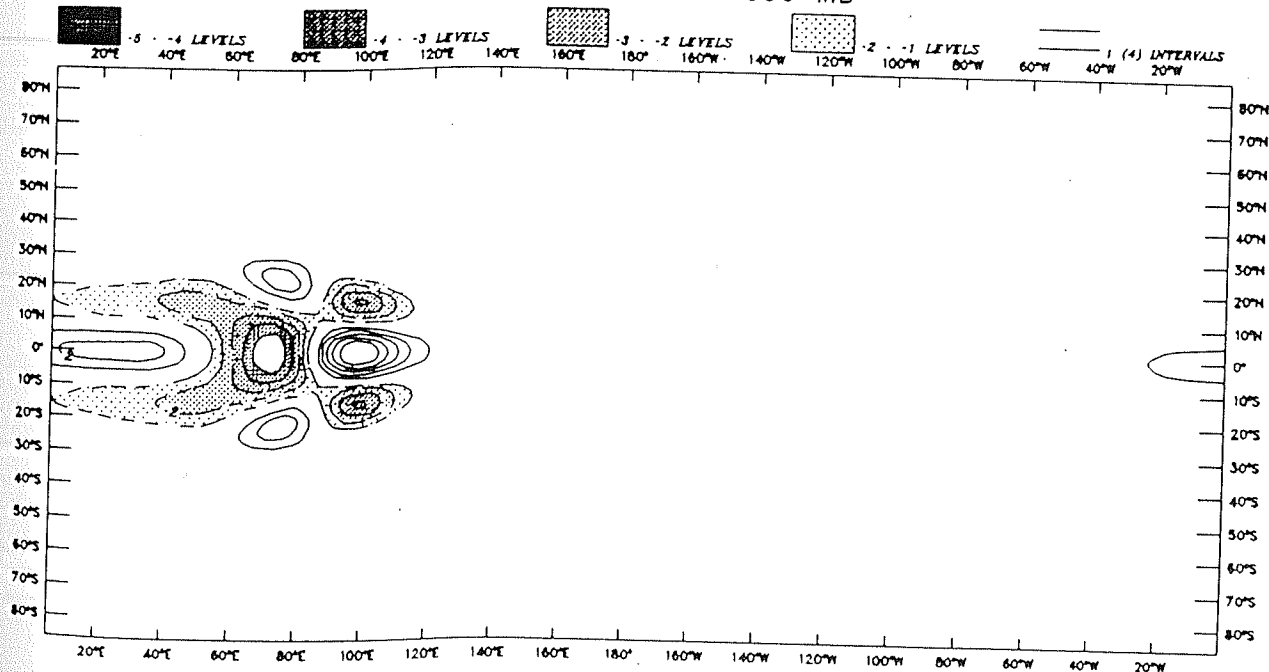
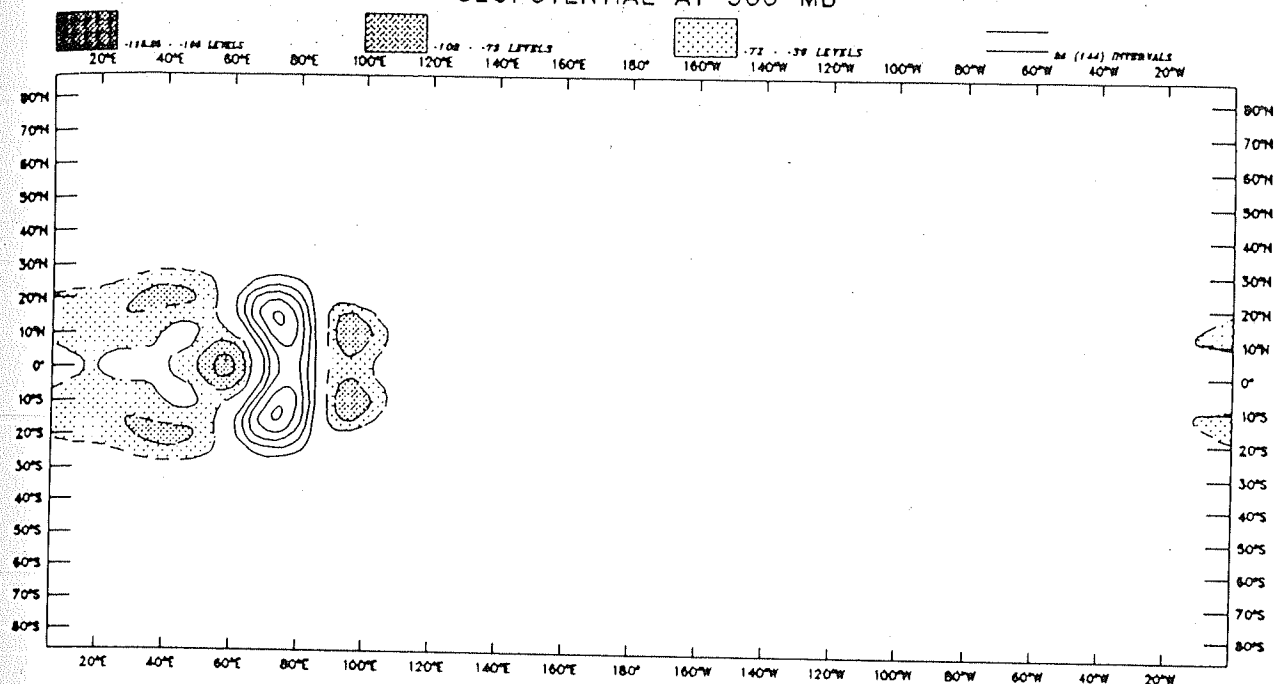


Fig.2.11e. (Top) Same as Fig.2.11c, except for LM and interval for westerlies is 2 ms⁻¹.

Fig.2.11f. (Bottom) Difference (NLM-LM) for zonal velocity at 300 mb. Interval 1 ms⁻¹.

the highs in the NLM becomes smaller. For example, the anticyclonic vortices having value of $600 \text{ m}^2 \text{ s}^{-2}$ which are centered at around 15°S and 15°N show almost the same eastward extents in both the NLM and LM. The zonal winds at 300 mb (Figs.2.11c and 2.11e.) reveal that, within the forcing region the pattern of easterlies (Rossby waves) and westerlies (Kelvin waves) have an eastward displacement of about 8° longitudes in the NLM. The maximum easterly speed in both the models is the same (-13 ms^{-1}) while the westerlies are stronger in the NLM (max speed is 12 ms^{-1}) as compared to the LM (max speed 8 ms^{-1}). The difference (nonlinear - linear) fields, for the zonal velocity, perturbation geopotential and divergence at 300 mb are given by Figs.2.11f, 2.11g and 2.11h respectively. The difference fields indicate that the structures of the stationary Kelvin and Rossby waves near the heat source are considerably affected by nonlinear terms. Fig.2.11g shows highs (solid lines) within the forcing region and lows (shaded) located to the east and west of the high. It was earlier seen in the NLM, that there is an eastward advection of the upper level equatorial high within and to the west of the forcing region. Therefore, the anticyclonic flow over the forcing region becomes stronger in the NLM. Consequently the upper level divergence, right over the forcing region, is stronger in the NLM. In Fig.2.11h, we notice that there is strong divergence (solid lines) right over the forcing region and convergence (shaded) to its west. The maximum divergence over the heating region is $2.0 \times 10^{-6} \text{ s}^{-1}$ and the maximum convergence is $-1.4 \times 10^{-6} \text{ s}^{-1}$. There are also small changes, caused by nonlinearities, in the structure of the upper level divergence within the region of forcing. Linear Gill-type models, cannot explain the eastward shift of upper level highs without including strong linear damping terms. However, our results suggest that even in the presence of weak dissipation, the influence of nonlinear terms can give rise to realistic phase relationship between the upper level divergence and geopotential distributions. From Fig.2.11f, the easterlies (shaded) and westerlies (solid lines) are well supported in the difference fields for perturbation geopotential and divergence.

NONLINEAR - LINEAR GEOPOTENTIAL AT 300 MB



NONLINEAR - LINEAR DIVERGENCE AT 300 MB

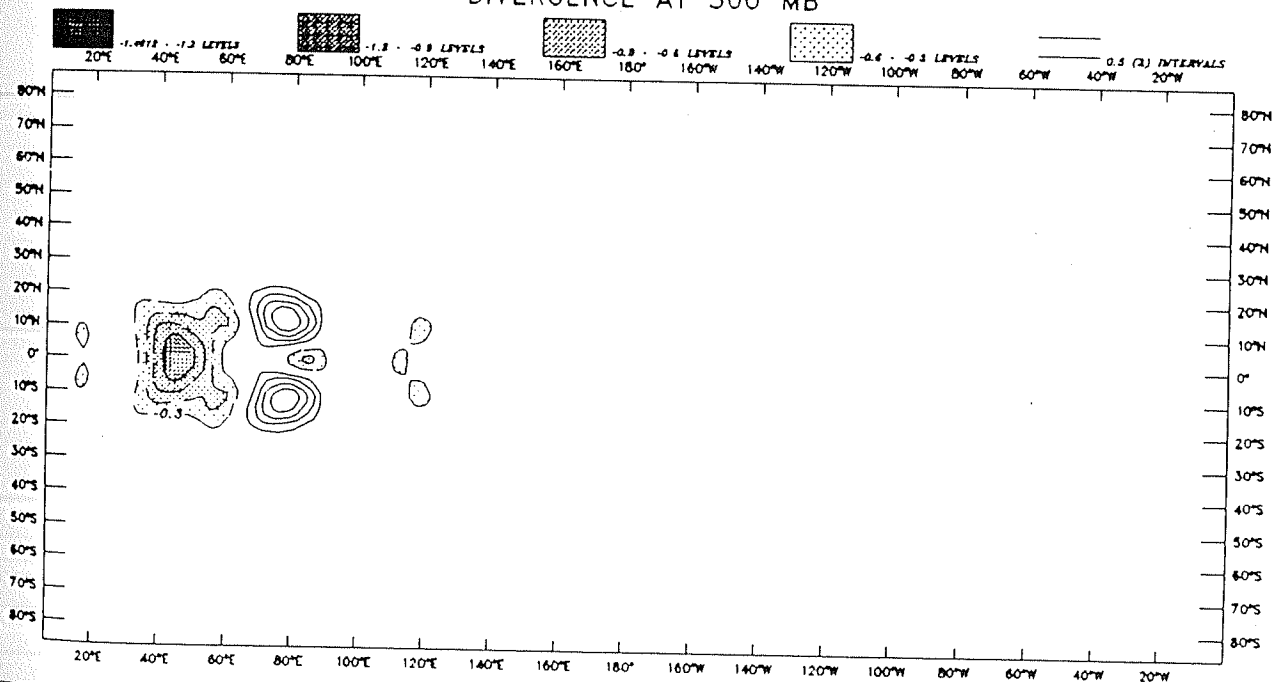


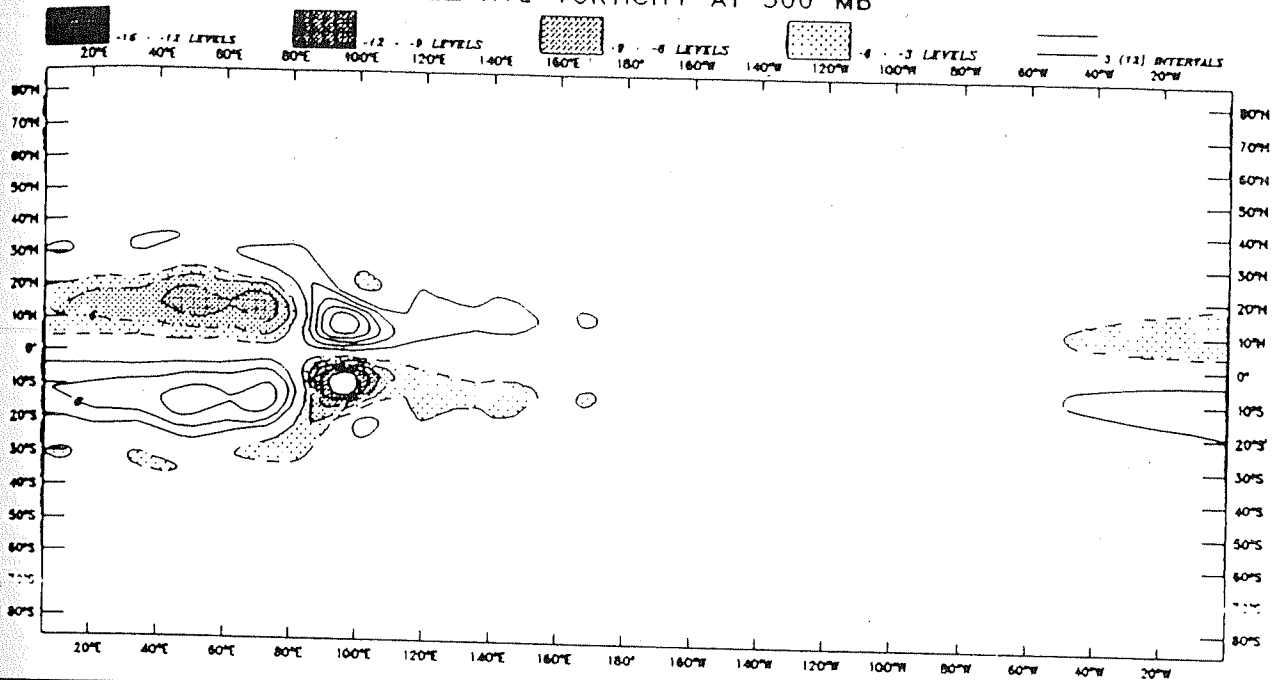
Fig.2.11g. (Top) Difference (NLM-LM) for perturbation geopotential at 300 mb. Interval 36 m²s⁻².

Fig.2.11h. (Bottom) Difference (NLM-LM) for divergence at 300 mb. Interval (0.3x10⁻⁶s⁻¹ for negative and 0.5x10⁻⁶s⁻¹ for positive contours).

The effect on the Kelvin waves is apparent from the equatorial westerlies and the effect on the Rossby waves is seen from the easterlies in Fig.2.11f. We notice that there are equatorial easterlies within and to the west of the forcing region. Likewise equatorial westerlies can be seen to the east of the forcing region. The enhancement of the anticyclonic features, over the forcing region, caused by nonlinear terms results in substantial zonal outflows appearing in Fig.2.11f. The relative vorticity at 300 mb in the NLM and LM are shown in Figs.2.11i and 2.11j respectively. The difference field (NLM - LM) for the relative vorticity at 300 mb is shown in Fig.2.11k. Figs.2.11i and 2.11j very clearly depict an eastward shift of the vorticity features in the NLM. We find that the anticyclonic vorticity (shaded in the northern hemisphere) at the upper levels extends upto about 85°E in the NLM, while it extends upto about 70°E in the LM, indicating an eastward shift of about 15° longitudes in the NLM. Similarly the upper level cyclonic vorticity (solid lines in the northern hemisphere) also shows some eastward shift in the NLM. This nonlinear effect shows up in the difference field (Fig.2.11k) in the form of substantial anticyclonic circulation over the forcing region. To the east of the forcing region, we find that there is an increased upper level cyclonic circulation caused by nonlinear terms.

The vertical structure of the equilibrium solutions in the LM and NLM shows interesting results. The vertical profiles of the zonal wind field were constructed by horizontally averaging the flow at each vertical level. The horizontal averages have been performed over two domains, namely the Kelvin and the Rossby wave domains. The Kelvin wave domain essentially extends eastward from the centre of the heat source and the Rossby wave domain extends westward from the centre of the heat source. In the Kelvin wave domain the averaging in the zonal direction was performed between 67.5°E and 118°E and for the Rossby wave domain the averaging in the zonal direction was performed between 17°E and 67.5°E . In the meridional direction, the averaging was performed between 7°S to 7°N , for both the Kelvin and Rossby wave

NONLINEAR MODEL RELATIVE VORTICITY AT 300 MB



LINEAR MODEL RELATIVE VORTICITY AT 300 MB

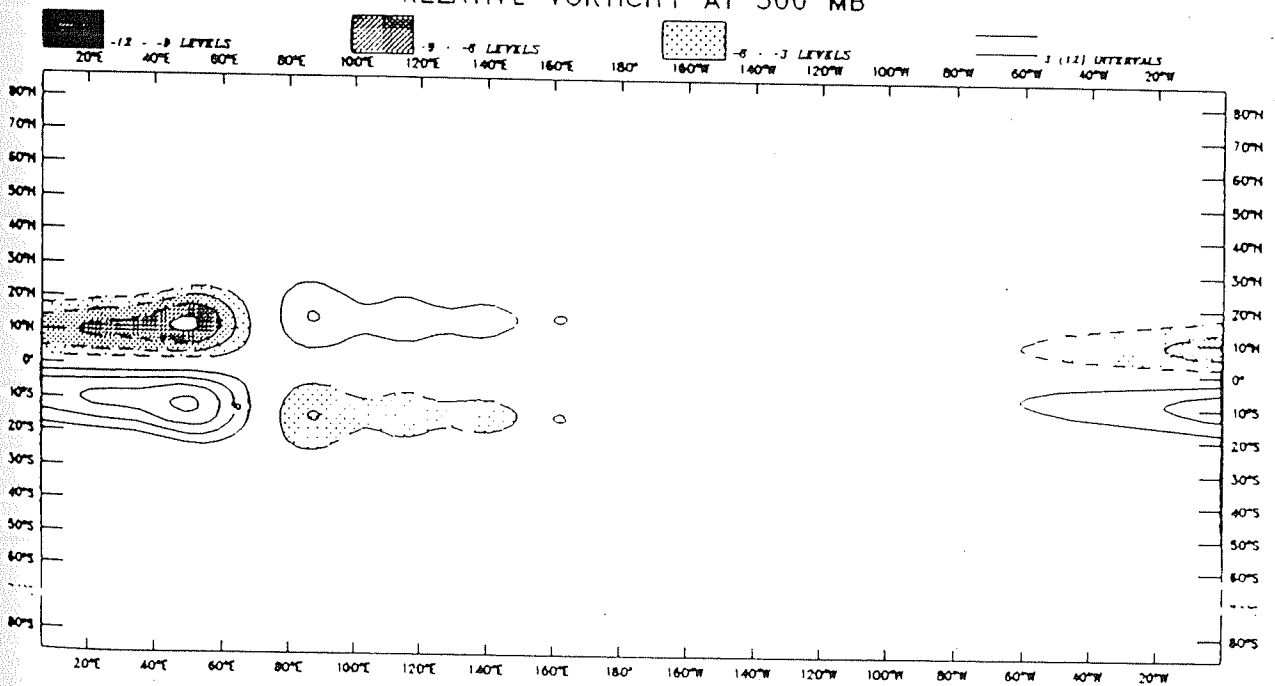
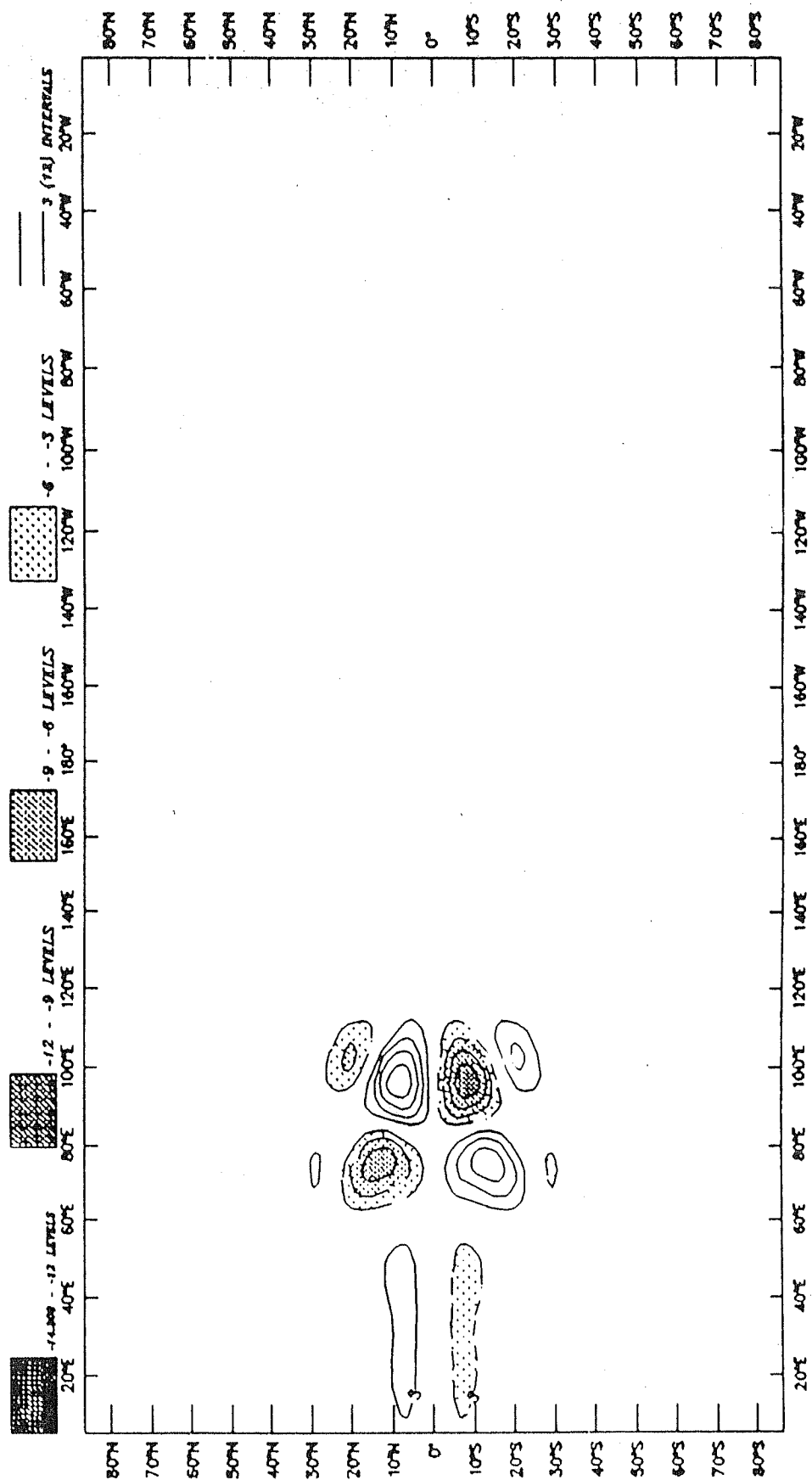


Fig.2.11i. (Top) Relative vorticity at 300 mb in the NLM. Interval $3 \times 10^{-6} \text{ s}^{-1}$.
Fig.2.11j. (Bottom) Same as Fig.2.11i, except for LM.

Fig.2.11k. Difference (NLM-LM) for relative vorticity at 300 mb. Interval $3 \times 10^{-6} S^{-1}$.

NONLINEAR - LINEAR REL VORTICITY AT 300 MB



domains. Figs.2.12a and 2.12b show the vertical profiles of the zonal wind averaged in the Kelvin and Rossby wave domains. From Fig.2.12a, it is seen that the response in the nonlinear model (dotted line) shows considerable difference from the linear response (solid line) at the lower and middle tropospheric levels. The linear response shows a gradual change from a low level easterly flow to a westerly flow in the middle and upper troposphere. However, in the nonlinear model the wind reversal in the vertical direction is more sharper in the lower and middle tropospheric levels. It is also seen in Fig.2.12a that the nonlinear terms tend to weaken the easterlies and strengthen the westerlies in the lower and middle troposphere. The vertical profile of zonal wind in the Rossby wave domain (Fig.2.12b), shows significant differences in the linear and nonlinear response at 500 mb. It can be noticed that the linear model shows easterlies having speed of -6 ms^{-1} at 500 mb, while the nonlinear model shows westerlies having speed of about 3 ms^{-1} . There is a complete change in the direction of flow in the LM and NLM at 500 mb. The zonal velocities at 500 mb for the NLM and LM are shown in Figs.2.13a and 2.13b respectively. One can notice that there are remarkable differences in the linear and nonlinear responses. Easterlies (max speed 8 ms^{-1}) can be seen to the west of the heating region in the LM. However, there is hardly any easterly flow near the equator and to the west of the heating region in the NLM. In fact easterlies can be seen only at around 25°N and 25°S in the NLM. Further, from the nonlinear response it is seen that westerlies extend very much to the west of the forcing region. Also the westerlies in the NLM are stronger (max value 7.5 ms^{-1}) as compared to the LM (max value 4 ms^{-1}). It appears that the nonlinear terms favour the generation of westerlies at 500 mb, which is the level of maximum heating. The role of nonlinear terms in favouring the generation of westerlies may be crucial for teleconnections from the tropics to midlatitudes (Hoskins and Karoly (1981) and Lau and Lim (1984)). Lim and Chang (1983) and Zhang and Webster (1989) have shown that transient Rossby waves are less trapped in equatorial

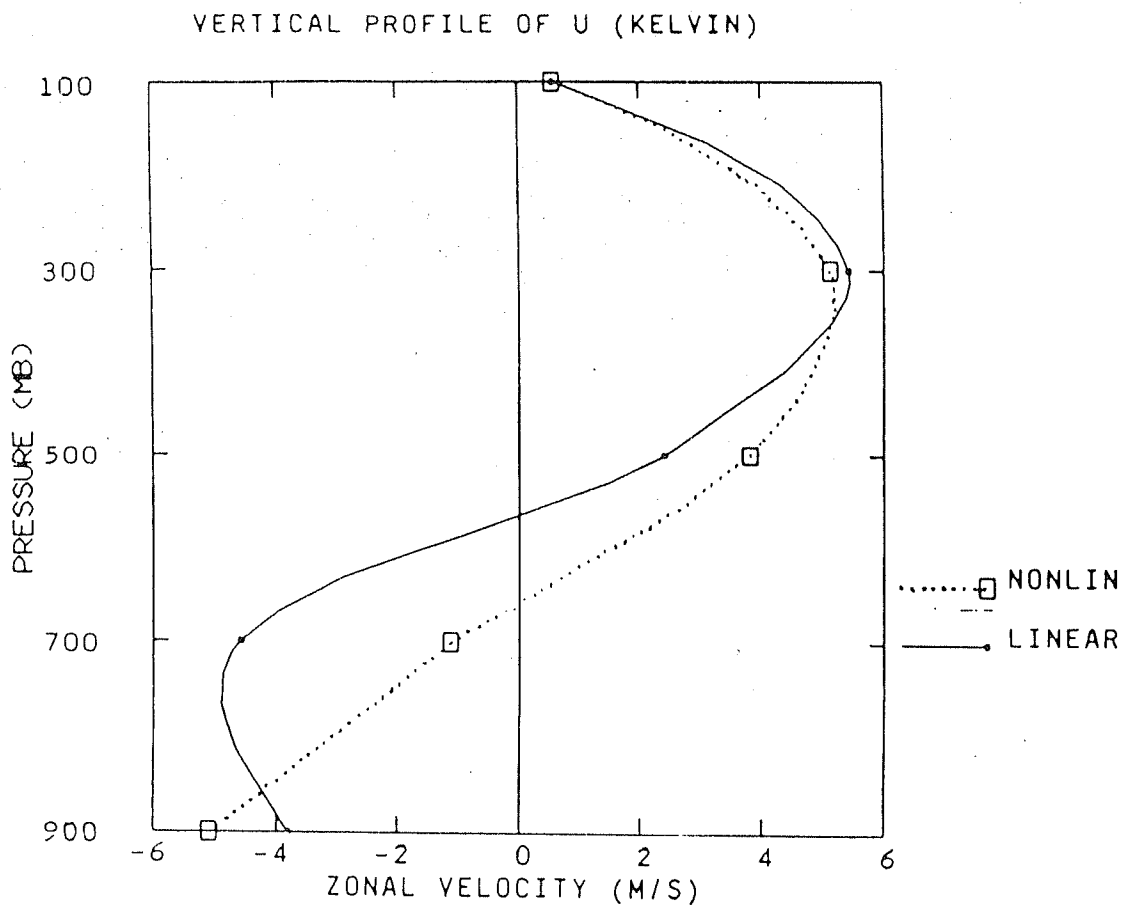


Fig.2.12a. Vertical profile of zonal velocity (Kelvin domain). Dotted line is for NLM and solid line is for LM.

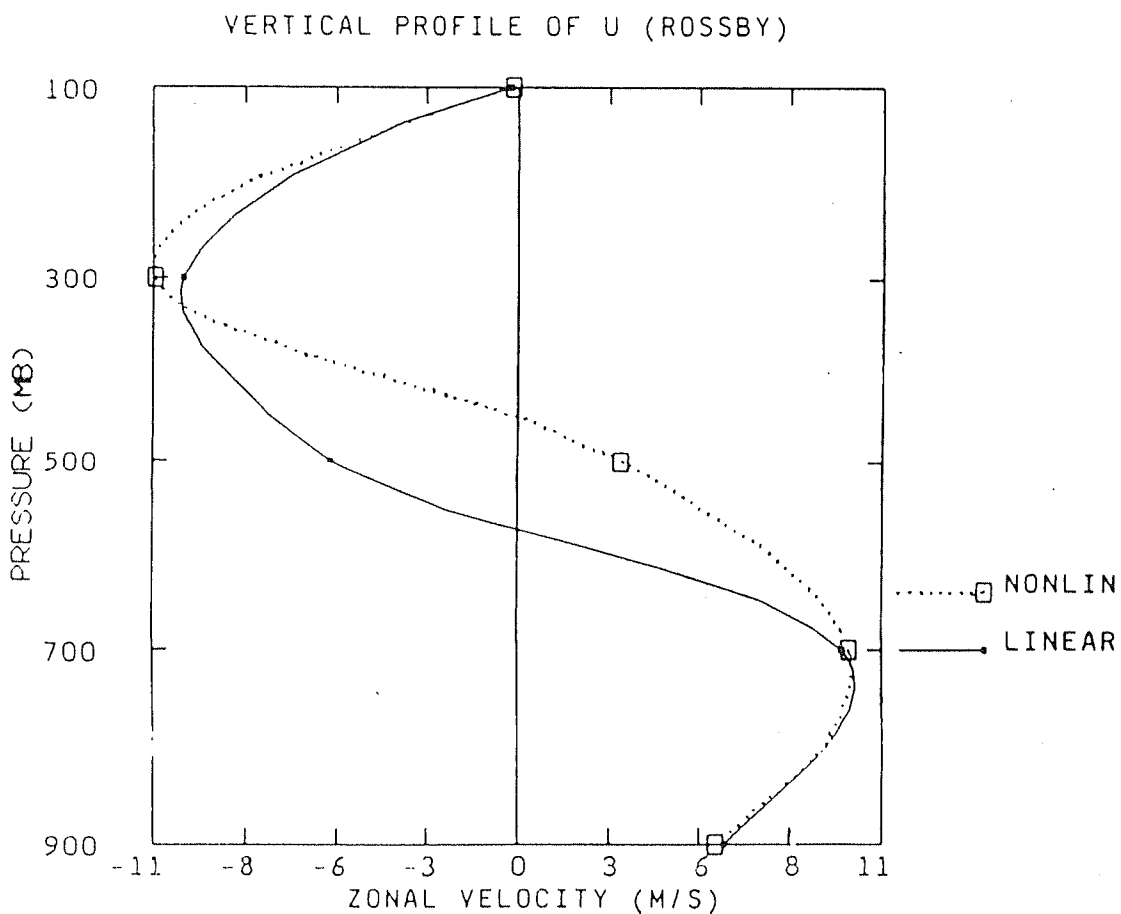
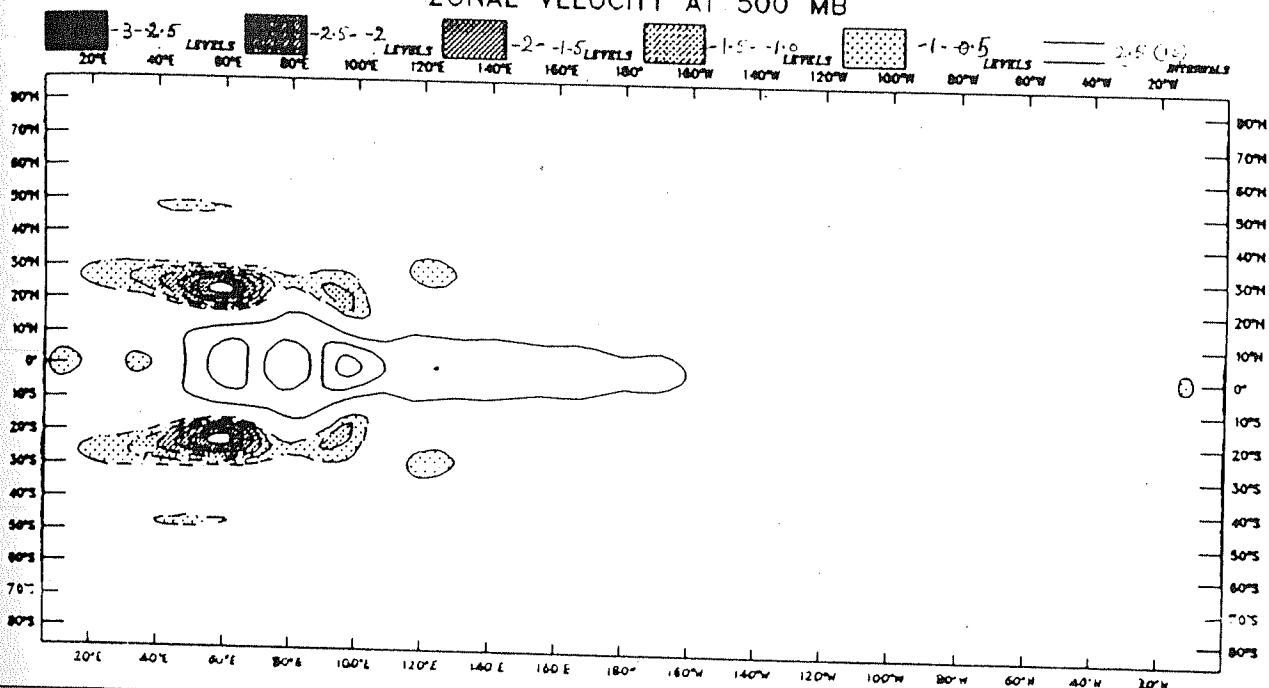


Fig.2.12b. Same as Figure.2.12a, except for Rossby domain.

NONLINEAR MODEL ZONAL VELOCITY AT 500 MB



LINEAR MODEL ZONAL VELOCITY AT 500 MB

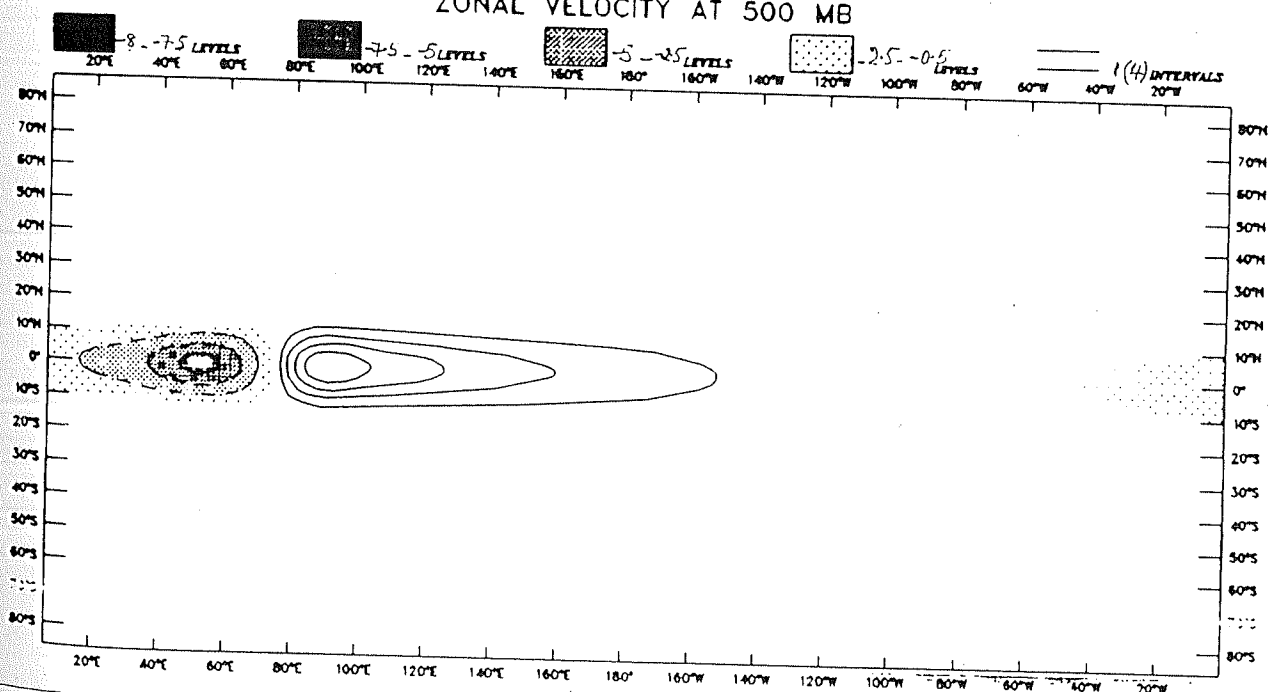


Fig.2.13a. (Top) Zonal velocity at 500 mb in NLM. Interval for westerlies is 2.5 ms^{-1} and easterlies is -0.5 ms^{-1} .

Fig.2.13b. (Bottom) Same as Fig.2.13a, except for LM. Interval for westerlies is 1 ms^{-1} and easterlies is -2.5 ms^{-1} .

westerlies. Therefore, a westerly basic flow near the equatorial regions may serve to radiate Rossby waves from the tropics to the extratropics. One can also notice in Fig.2.12b, that a stronger vertical shear occurs between 500 and 300 mb levels, in the NLM. The studies of Lim and Chang (1983), Lim and Chang (1986) and Kasahara and Silva Dias (1986) highlight the importance of vertical shear in the mean zonal wind in generating barotropic modes which are necessary for teleconnection mechanisms. Therefore, the stronger vertical shear in the NLM at around 400 mb in Fig.2.12b, might be crucial for the propagation characteristics of transient Rossby waves.

We have also investigated the effect of nonlinearities on the Kelvin and Rossby waves, induced by symmetric heat sources of different amplitudes. Figs.2.14a and 2.14b correspond to the difference field (nonlinear - linear) for zonal wind at 300mb for the case of a weak forcing (max heating 1°K per day) and a strong forcing (max heating 5°K per day). It can be easily recognized that the nonlinearities have a much weaker effect when the forcing amplitude is smaller. We also find that the eastward nonlinear advection of the upper level anticyclonic features is smaller in the case of the weaker forcing. Our results agree with the findings reported by Hendon (1986).

We shall now describe the steady-state response in the LM and NLM for the antisymmetric forcing (Fig.2.15a). The maximum heating (cooling) to the north (south) of the equator is 4°K per day. Gill (1980) has shown that an antisymmetric heating generates a stationary Rossby wave response, within and to the west of the forcing, which is characterized by a Hadley type of circulation. The winds and perturbation geopotential at 300 mb for the NLM and LM are shown in Figs.2.15b and 2.15c respectively. We can notice upper level anticyclonic circulation in the northern hemisphere and cyclonic circulation in the southern hemisphere. The flows in the northern and southern hemispheres are mirror images of one another. The central position of the anticyclone (cyclone) is around 15°N ($^{\circ}\text{S}$) in both the models. Another

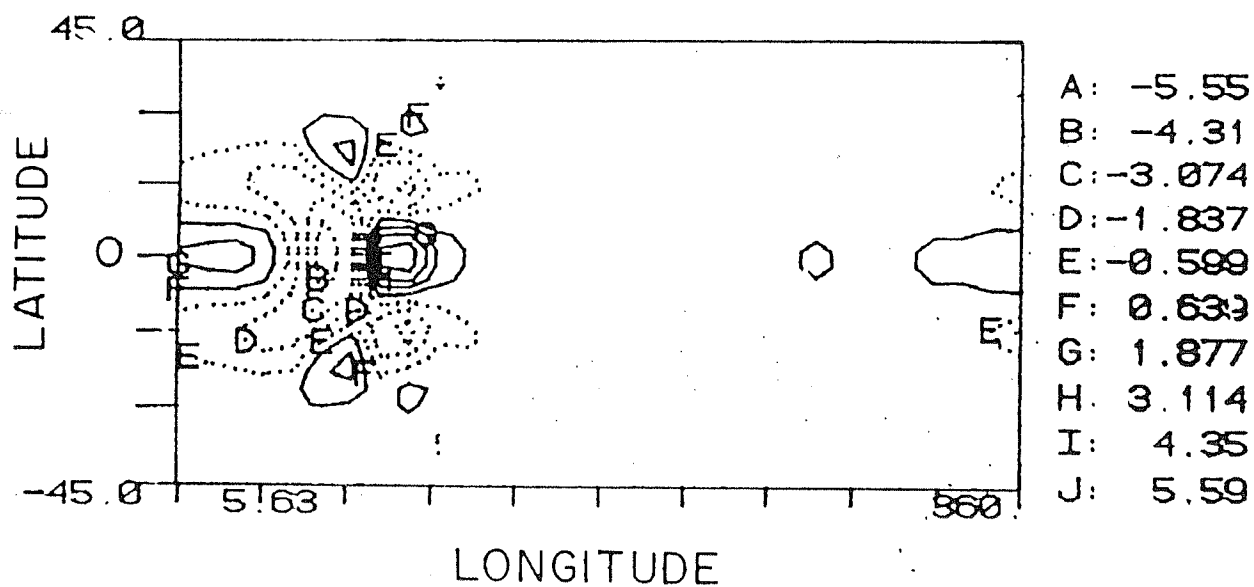
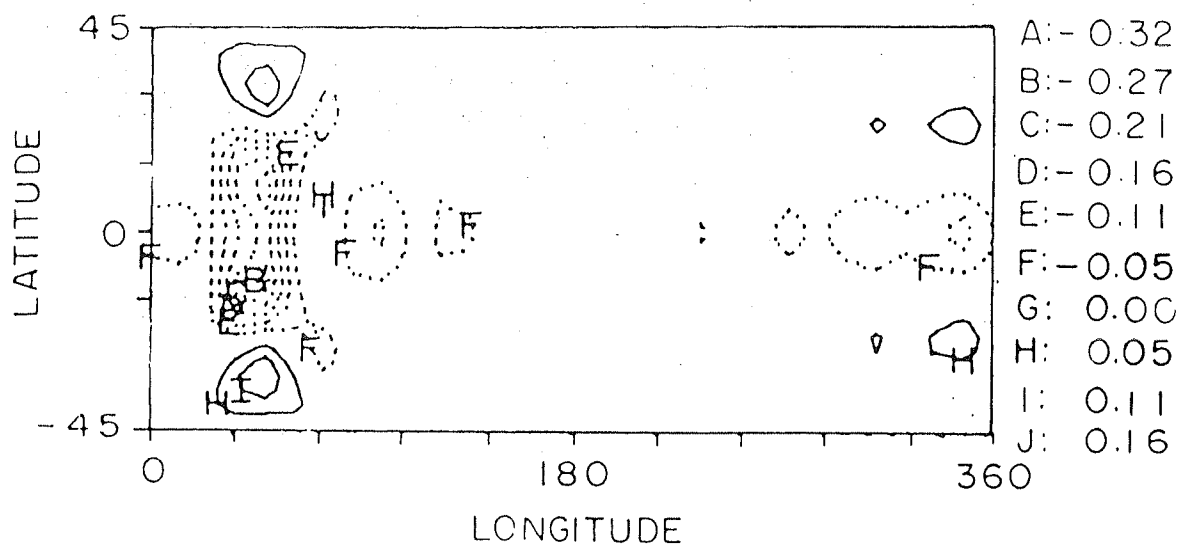


Fig.2.14a. (Top) Difference (NLM-LM) for zonal velocity at 300 mb. Weak forcing case. Interval 0.05 ms^{-1} .

Fig.2.14b. (Bottom) Same as Fig.2.14a, except for the strong forcing case. Interval 1.2 ms^{-1} .

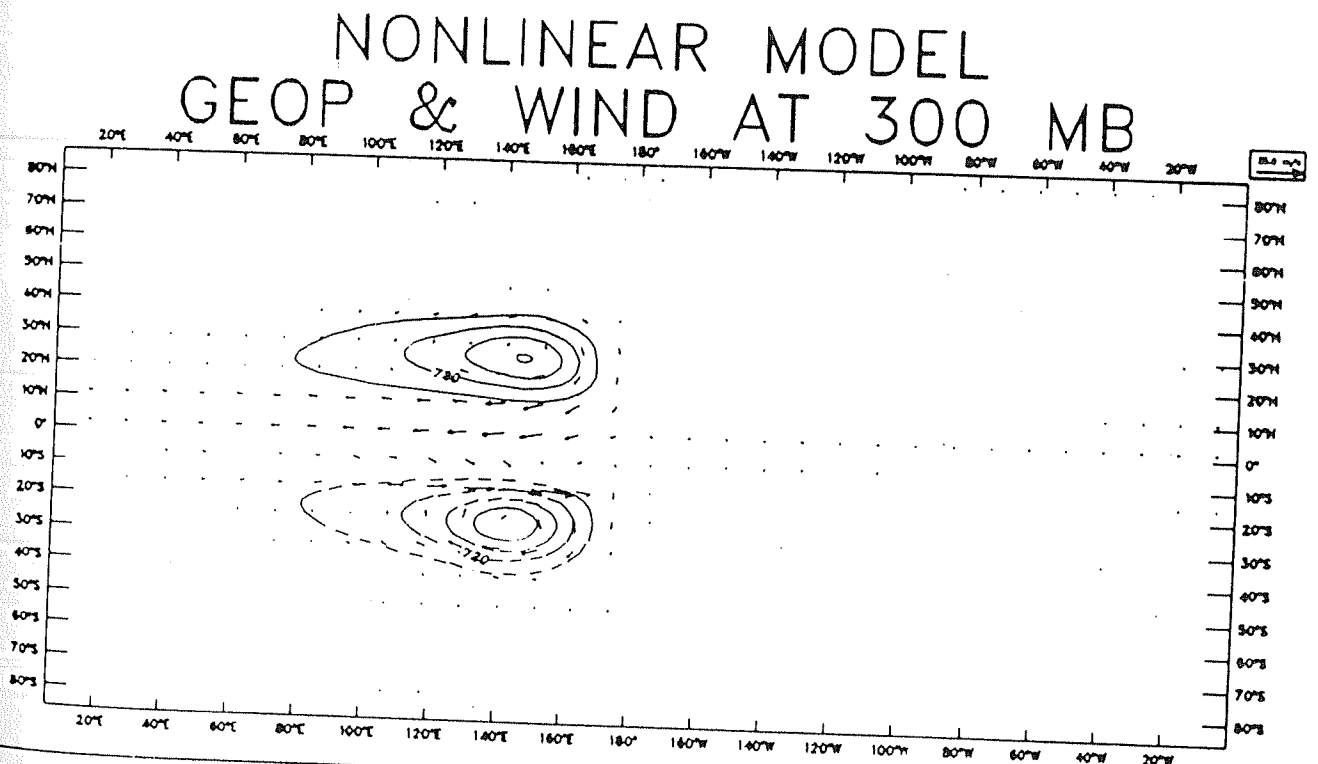
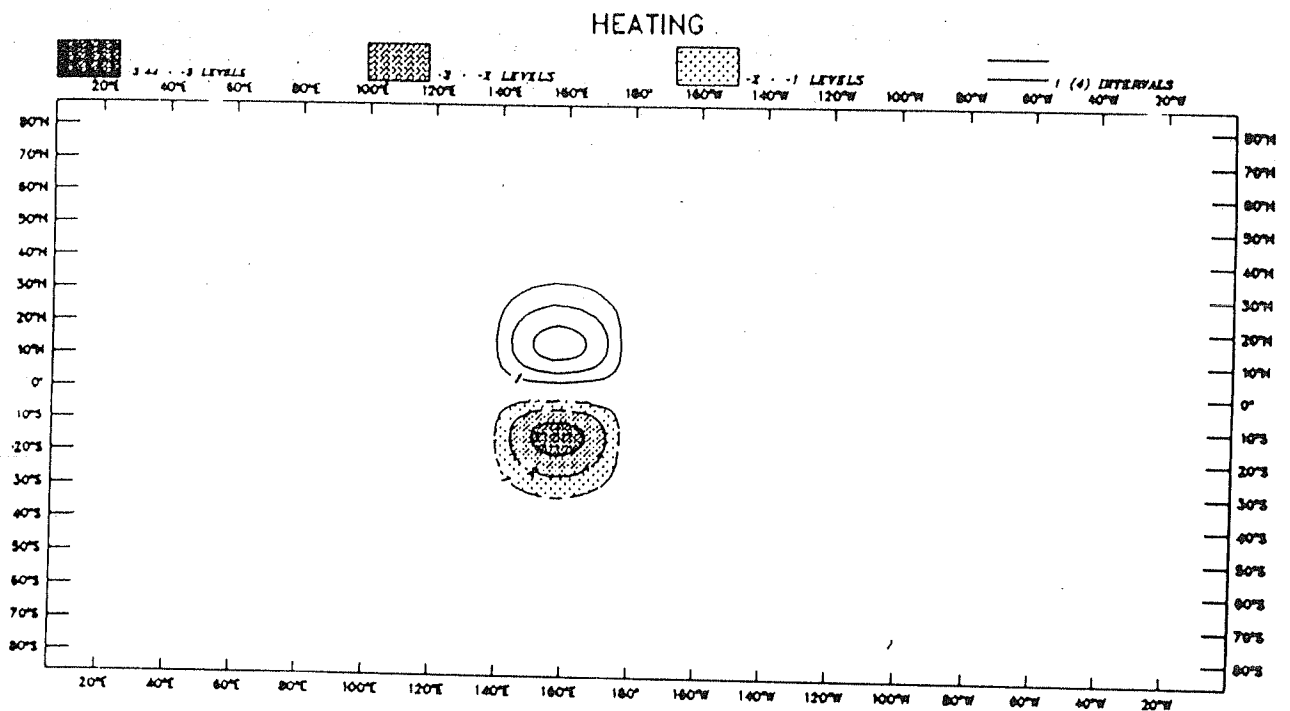
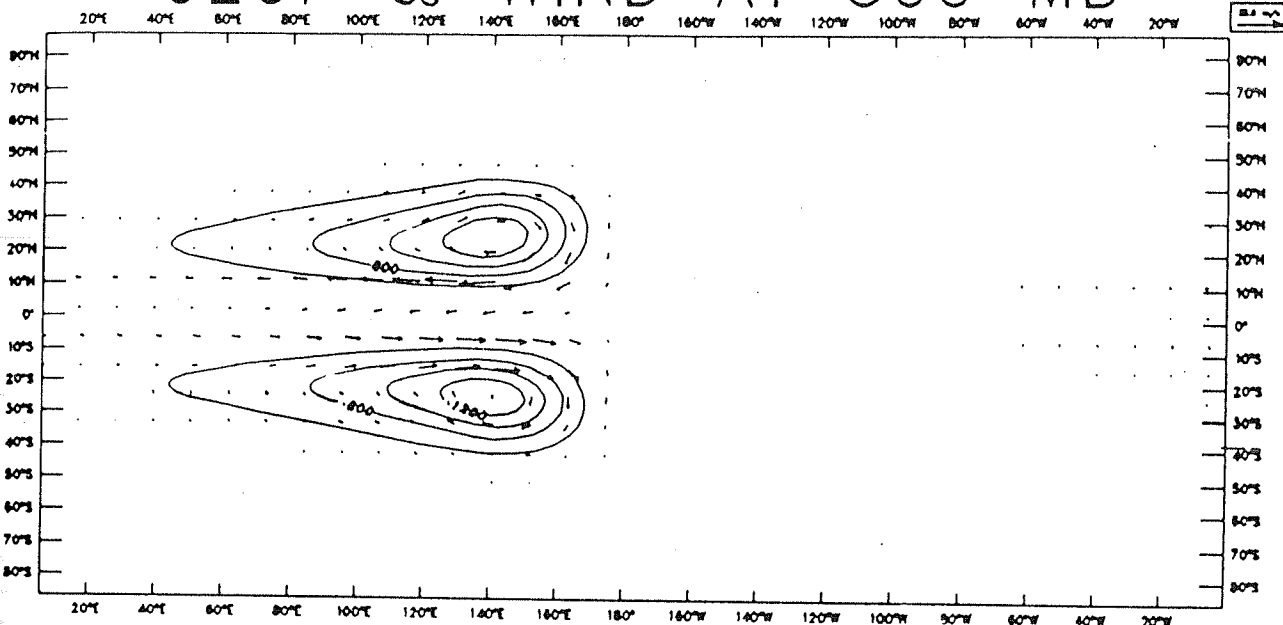


Fig.2.15a. (Top) Horizontal distribution of antisymmetric heat source. Solid lines are positive and shaded contours are negative.
 Fig.2.15b. (Bottom) Same as Fig.2.11b, except for the antisymmetric forcing as in Fig.2.15a. Interval $360 \text{ m}^2 \text{ s}^{-2}$.

important feature is the prominent cross-equatorial flow. At the upper levels, we notice a strong easterly flow to the north and a westerly flow to the south of the equator. From Figs.2.15b and 2.15c, one can notice that there is an eastward shift of the upper level circulation features, on the western side of the forcing, in the NLM. Due to this eastward shift of the upper level anticyclone (cyclone) in the northern (southern) hemisphere, there is an increase in the anticyclonic (cyclonic) flow, over the forcing region, in the NLM. Consequently, the difference (nonlinear - linear) field for the zonal wind (Fig.2.15d) shows strong westerlies (easterlies) at around 10°N (S) respectively. The maximum change in the zonal wind speed, due to nonlinear effect, is as large as 10 ms^{-1} . This substantial change is also noticed in the the difference field for the perturbation geopotential (Fig.2.15e). In the northern hemisphere, we can see that there are highs (solid lines) at around 160°E and 20°N , which lie within the region of forcing. To the west of the high there are lows (shaded) that extend in the east-west direction. In the southern hemisphere, the difference field is more or less the mirror image of the northern hemispheric flow pattern. Strong meridional gradients in the perturbation geopotential can be observed in Fig.2.15e. The difference field for zonal wind (Fig.2.15d) is consistent with the meridional gradient of perturbation geopotential and very roughly satisfy geostrophic relation. In brief, experiments with NLM and LM for the antisymmetric forcing show that the stationary Rossby waves close to the forcing region are significantly affected by the nonlinear advection terms. An eastward advection of upper level anticyclone (cyclone) in the northern (southern) hemisphere is prominently observed within and to the west of the forcing region.

LINEAR MODEL GEOP & WIND AT 300 MB



NONLINEAR - LINEAR ZONAL VELOCITY AT 300 MB

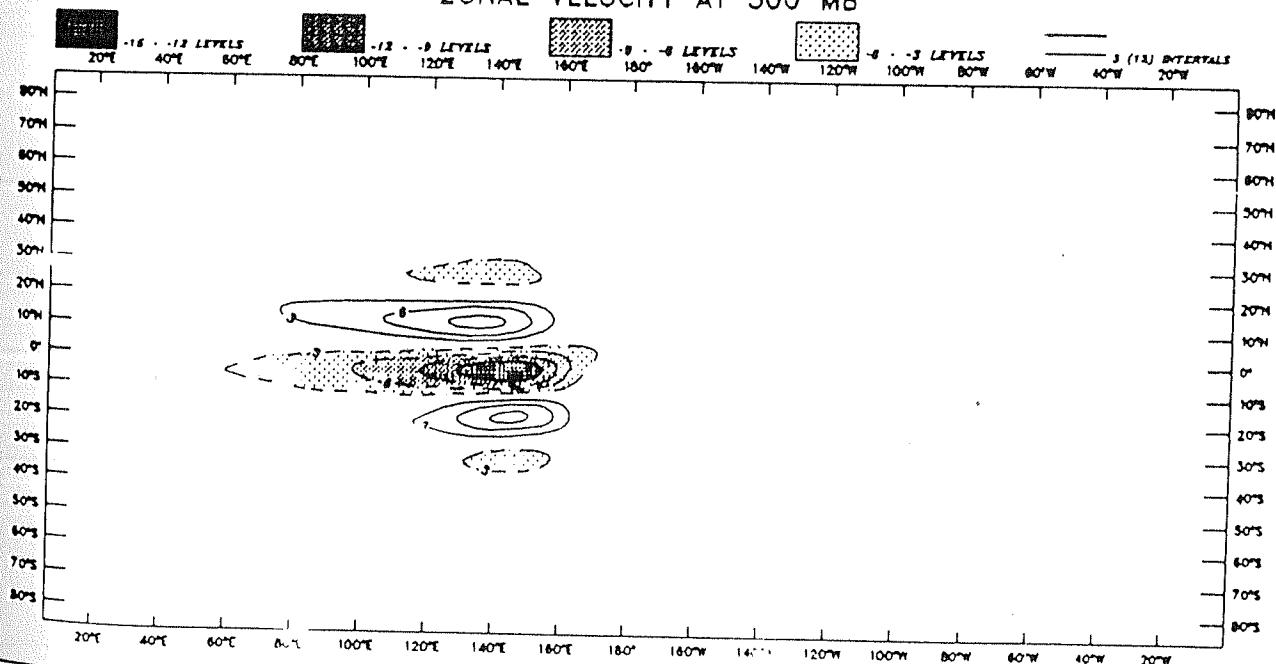
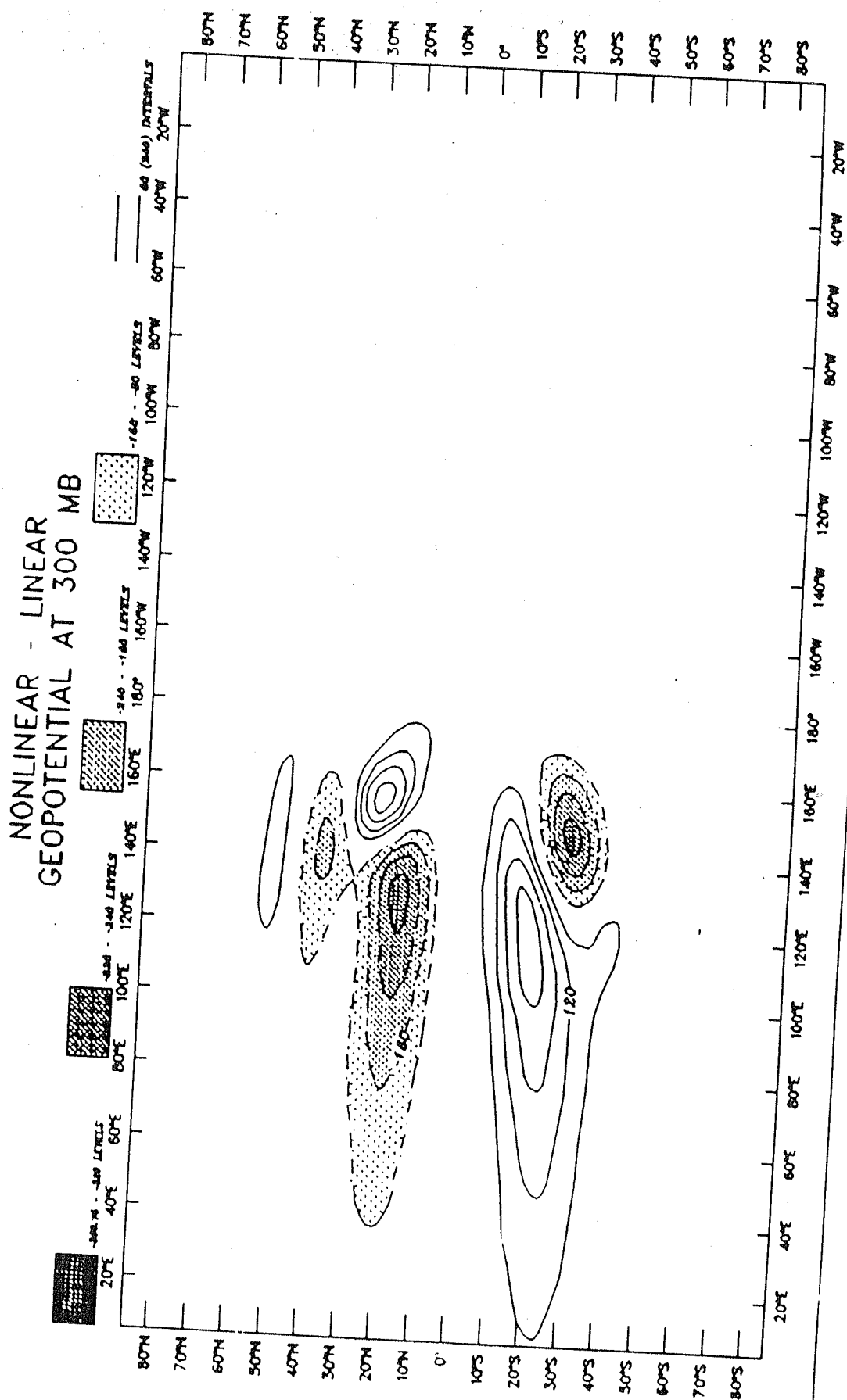


Fig.2.15c. (Top) Same as Fig.2.15b, except for LM. Interval $300 \text{ m}^2 \text{ s}^{-2}$.

Fig.2.15d. (Bottom) Difference (NLM-LM) for zonal velocity at 300 mb. Interval 3 ms^{-1} .

Fig. 2.15e. Difference (NLM-LM) for perturbation geopotential at 300 mb. Interval ($80 \text{ m}^2 \text{ s}^{-2}$ for negative and $60 \text{ m}^2 \text{ s}^{-2}$ for positive contours).



2.7 Conclusions

We have performed a variety of experiments both in the framework of linear as well as nonlinear models, with a motivation to understand the time-mean Walker circulation in the equatorial Pacific. Besides the strong convective heating over Indonesia, it is found that the radiative cooling in the eastern Pacific is an important factor in controlling the time-mean Walker circulation. It has been shown that the longitudinal scale and intensity of the time-mean east-west circulation is crucially dependent on the geometrical location and intensity of the Indonesian heat source and the heat sink in the eastern Pacific. In the region between the heat source and heat sink there is a superposition of Kelvin waves originating from the heat source and Rossby waves originating from the heat sink. This superposition leads to a strengthening of the upper level westerly flow over the equatorial Pacific. There are observational findings (eg. Krueger and Winston (1974)) which suggest that the strength of the time-mean Walker circulation in the equatorial Pacific exhibits interannual fluctuations which primarily arise due to longitudinal shifts in the heating and cooling regions. In our idealized experiments, we have shown that a westward displacement of the heat sink in the eastern Pacific leads to a strengthening of the time-mean divergent circulation in the equatorial Pacific. Our results also reveal that when the heating over Indonesia or the radiative cooling in the Pacific is small, the intensity of the Walker circulation falls down.

By comparing the results from a linear global spectral model and a nonlinear global spectral model, we have studied the impact of the nonlinear advection terms on the equatorially trapped stationary Kelvin and Rossby waves. It has been shown that nonlinearities affect the Kelvin and Rossby waves mostly near the region of strong diabatic heating. An outstanding effect observed to the west of the forcing region is that, the nonlinear advection terms displace the upper level anticyclones eastward.

As a result, there is an enhancement of the upper level divergence over the region of forcing in the NLM. We also find that the upper level divergence over the region of forcing shows minor structural differences within the region of forcing. Linear Gill-type models cannot explain the eastward shift of upper level highs without including strong linear damping terms. However, our results suggest that even in the presence of weak dissipation, the influence of nonlinear terms can give rise to realistic phase relationship between the upper level divergence and geopotential distributions. We also find that the impact of nonlinearities is dependent on the strength of the forcing. The nonlinear effects decrease very much when the forcing amplitude is reduced. When an antisymmetric heat source was used, the nonlinearities affected the Rossby waves on the western side of the forcing. At the upper levels, an eastward advection of the anticyclone (cyclone) was observed in the northern (southern) hemisphere. The vertical structure of the time-mean zonal wind (for the case of the strong symmetric heat source) showed significant differences between the linear and nonlinear responses especially in the mid tropospheric levels. It was found that nonlinearities appear to favour the generation of westerlies particularly at 500 mb, where the forcing was maximum. To the west of the forcing region, an enhancement of the vertical shear in the zonal wind at around 400 mb was seen in the NLM. The generation of the westerlies and also the enhancement of the vertical shear in the basic flow, which are caused by nonlinear terms, may be important for the propagation of transient Rossby waves from the tropics to the extratropics and the phenomenon of midlatitude teleconnection.

Chapter 3

The Winter and Summer Time-Mean Circulations during 1979

3.1 Introduction

In the previous chapter we had studied the stationary wave response induced by idealized diabatic heating in the tropical atmosphere. This chapter is devoted to the study of the time-mean planetary scale circulations forced by the observed time-averaged atmospheric heating. More specifically, we have investigated the time-mean tropical atmospheric response induced by the observed diabatic heating for the periods Dec(1978)-Feb(1979) and June-August (1979), using a 2-level linear equatorial β -plane model and also a 5-level nonlinear global spectral model. We have utilized the time-averaged diabatic heating rates computed by Schaack *et.al* (1990) from the Global Weather Experiment (GWE) dataset, in our forcing experiments.

3.1.1 Observational studies

The global atmospheric circulation data sets from Monsoon Experiment (MONEX) observations, starting from December 1978 through November 1979, were of high quality because of the extensive data coverage and from a large number of observing platforms. Krishnamurti (1985) has given a detailed review of the major components associated with monsoon system based on the MONEX studies. The aspects that he has discussed, deal with the shift of the monsoon rainfall belt from Indonesia to the foothills of Himalayas from the northern winter to the summer, the evolution of the differential heating fields and its influence on the divergent and rotational components of the monsoon circulation. He has also discussed features during the onset, active and break phases of the monsoon and the interaction of the monsoon flow with the low-frequency 30-50 day eastward propagating mode. Using OLR and First Global GARP Experiment (FGGE) data, Murakami and Nakazawa (1985b) studied the shift of the major heat sources associated with the transition from the southern to northern hemispheric summer.

The structure and evolution of the atmospheric circulation is strongly linked to the spatial and temporal distribution of atmospheric heat sources and heat sinks. Therefore, we shall first describe the 3-dimensional time-mean heating distribution during winter (1978-79) and summer (1979) and later on examine the implications of the thermal forcing on the planetary scale time-mean circulations. Schaack *et.al* (1990) have calculated the 3-dimensional global distribution of time-averaged atmospheric heating for January, April, July and October 1979 from the European Centre for Medium Range Weather Forecasts (ECMWF) GWE data set. The heating distribution for January (1979), shows that active zones of convection were located along the ITCZ that extended from South America across the Atlantic, Africa, the Indian ocean and into the mid-Pacific (Fig.3.2.1). A heating maximum greater than 2.5°K

per day, associated with moist convection of the winter Asian monsoon, occurred over the equatorial western Pacific. There was a well defined cooling maximum exceeding 1.0°K per day in the oceanic regions to the west of Australia and South America. During July, the major heating regions were observed to the north of the Bay of Bengal, the foothills of the Himalayas and over the elevated Tibetan plateau (Fig.3.3.1). The maximum heating during July was more than 3.0° per day. Substantial heating ($\sim 2^{\circ}\text{K}$ per day) occurred over the highlands of Mexico. Regions of cooling, with a maximum of 1.0° per day, were seen in the northeastern and southeastern Pacific. Murakami (1983), Nitta (1983) and He *et.al* (1987) have shown that a strong diurnal variation in the diabatic heating occurs over the Tibetan plateau during the northern summer and over the Indonesian region during the northern winter. They found that the latent heat of condensation had a dominant contribution to the net heating distribution. During the northern summer, the contribution by sensible heating in the Tibetan region was found to be equally significant. Krishnamurti (1971) and Krishnamurti *et.al* (1973) demonstrated that the high degree of zonal asymmetry in the thermal forcing during the northern summer and winter months, led to the existence of major east-west and Hadley-type of circulations in the tropics and subtropics.

3.1.2 Modelling studies

There are numerous theoretical studies that have looked into the time-mean as well as the transient nature of the tropical atmospheric response to thermal forcing. The pioneering works of Webster (1972), Gill (1980), Simmons (1982) and others, which deal with the stationary response in the tropics, were discussed quite elaborately in Chapter II. We shall now mention a few other interesting studies. Sankar Rao (1969) obtained the steady-state solutions of the forced quasi-geostrophic perturbation equations. The heating was assumed to be proportional to the difference between

the mean low level air temperature and the prescribed ground surface temperature. He showed that the stationary solutions were sensitive to the vertical variation and also the horizontal scale of heating. Webster (1973a) examined the influence of the stationary extratropical disturbances on the tropical large-scale motions. He found that the tropical response depended both on the climatological basic state and on the magnitude of the forcing. Webster (1973b) studied the seasonal time-mean response in the tropics and midlatitudes, using a 2-layer linearized primitive equation model in the presence of a sheared basic flow. He showed that the development and maintenance of transient disturbances depended on the zonal mean flow and the stationary eddies. Lim and Chang (1981) and Lau and Lim (1982) have studied the winter monsoon circulation changes using a simple shallow water equatorial β -plane model. Hartmann *et.al* (1984) examined quantitatively, the steady-state tropical east-west circulations, forced by different vertical profiles of heating. Their study was based on the observational evidence that mature cloud clusters produce a vertical distribution of diabatic heating with a sharp maximum near 400 mb and very weak heating below 600 mb. Using a vertical distribution of heating which resembled the observed profile, they showed that the simulated east-west circulations were in close agreement with observed flow pattern. Manabe *et.al* (1965) performed numerical experiments with a GCM that incorporated a simple hydrologic cycle. The hydrologic cycle included advection of water vapour by the large-scale motion, evaporation from the surface, precipitation and moist convective adjustment. The quasi-stationary response showed that the hemispheric mean rate of precipitation produced by the model agreed with the observed annual estimates of mean rainfall. In the tropics the precipitation was found to exceed the evaporation while in the subtropics the evaporation was larger than the precipitation. Although this agreed qualitatively with the observations, the difference between the precipitation and evaporation produced by the model was quite different from the observed difference. It was also found that the inclusion of

moist processes produced an increase in the transport of momentum and heat by the tropical meridional circulation. This resulted in the strengthening of the tropical meridional circulation. The January and July GCM simulations (eg. Pitcher *et.al* (1983)) showed that radiative processes played a significant role in producing realistic large-scale circulations in the troposphere and stratosphere. A similar GCM study of the winter and summer global climate by Schlesinger and Gates (1980), suggests that improvements in the treatment of hydrological cycle, cumulus parameterization and radiative transfer, produce a more realistic simulation of precipitation patterns. Kinter *et.al*(1988) simulated the winter and summer circulations using the National Meteorological Center (NMC) global spectral model. The effects of seasonally varying boundary conditions of SST, soil moisture and sea ice were included in the model simulations. The model climatology showed reasonable agreement with the observed sea level pressure, the structure of the tropospheric jets and the stationary wave patterns. However, there was some mismatch between the model precipitation and the observed precipitation (based on OLR).

3.1.3 Objectives of the present study

In the previous chapter, we had mostly confined our attention to the stationary response induced by idealized heat sources and sinks. In this chapter, we shall perform forcing experiments with the actual heating distributions during winter (1978-79) and summer (1979) and examine the nature of time-mean circulations during the above two seasons. Here, we stress on the planetary scale aspects of the heat-induced motions and the primary focus will be on the dynamical interpretation of the Walker and Hadley regimes, during the two seasons. The forcing experiments were carried out using a 2-level linear equatorial β -plane model and also a 5-level nonlinear global spectral model. The formulation of the 2-level model and also the method of solution

have already been described in Chapter II. The formalism of the 5-level nonlinear global spectral model is based on Bourke (1974). It is to be noted that the observed heating is prescribed only at the 500 mb level in the 2-level model, whereas the 5-level model is forced using the observed heating at all the model levels. Therefore, the 5-level model has an accurate representation of the observed vertical modes of heating. On the other hand, the 2-level model contains only the first baroclinic structure in the vertical. In addition, the 2-level model is based on a linear system of equations, while the 5-level model contains a full set of nonlinear equations. Given these differences between the 2-level linear model and the 5-level nonlinear model, it will be interesting to examine the equilibrium response, induced by the observed time-mean diabatic heating, in the two models.

3.2 Time-mean circulations during winter 1978-79

In this section we shall elucidate the main observational features of the steady-state circulations during January (1979). Let us begin with a qualitative description of the salient features of the heating field for winter (1978-79) derived by Shaack *et.al* (1990). The vertically integrated heating distribution for January (1979) (Fig.3.2.1), shows that the primary zones of convection are located along the ITCZ that extends from South America across the Atlantic, Africa, the Indian ocean and into the mid-Pacific. A heating maximum greater than 2.5°K per day, associated with moist convection of the winter Asian monsoon, occurs over the equatorial western Pacific. Well defined cooling maximum exceeding 1.0°K per day occurs over east Asia, northwest India and Pakistan, parts of Saudi Arabia, north of Africa and the oceanic regions to the west of Australia and South America. The upper level flow was characterized by major east-west divergent circulations. The main features of the tropical low-level

circulation during January (1979) were the strong easterly trade winds over central and east Pacific, a well marked cyclonic circulation over Australia, and anticyclonic vortices over east-Asia and west of Australia. Murakami (1983) used the infrared (IR) irradiance data from GMS-1 geostationary satellite and estimated the deep convective activity. He found that during winter 1978-79, the diurnal variation was large over the western Pacific and the northern Australia. Within this area the phase of the diurnal cycle exhibited distinct contrast over land and the adjacent ocean. Sumi and Murakami (1981) studied the monthly and seasonal mean circulations for the 1978-79 winter and found that the heating for winter 1978-79 extended from equator to 10°S latitudinally and had a zonal extent from the Indian ocean to the southcentral Pacific. This pattern was distinctly different from the distribution during the previous years in which the ascending branch of winter monsoon was centered over Indonesia. The upper and lower level circulations, over the equatorial central Pacific, underwent significant intraseasonal changes, leading to the rapid development of the Australian summer monsoon during late December. Similarly, they observed that the circulation over the western south Pacific exhibited considerable intraseasonal variability. Kalnay *et.al* (1986) have shown that prominent cloud bands occurred over the south Pacific and east of South America during January 1979, which were manifestations of large amplitude stationary Rossby waves. They showed that the convective heating associated with the South Pacific Convergence Zone (SPCZ), was responsible in maintaining the Walker circulation and also sustaining the amplitude of the subtropical waves.

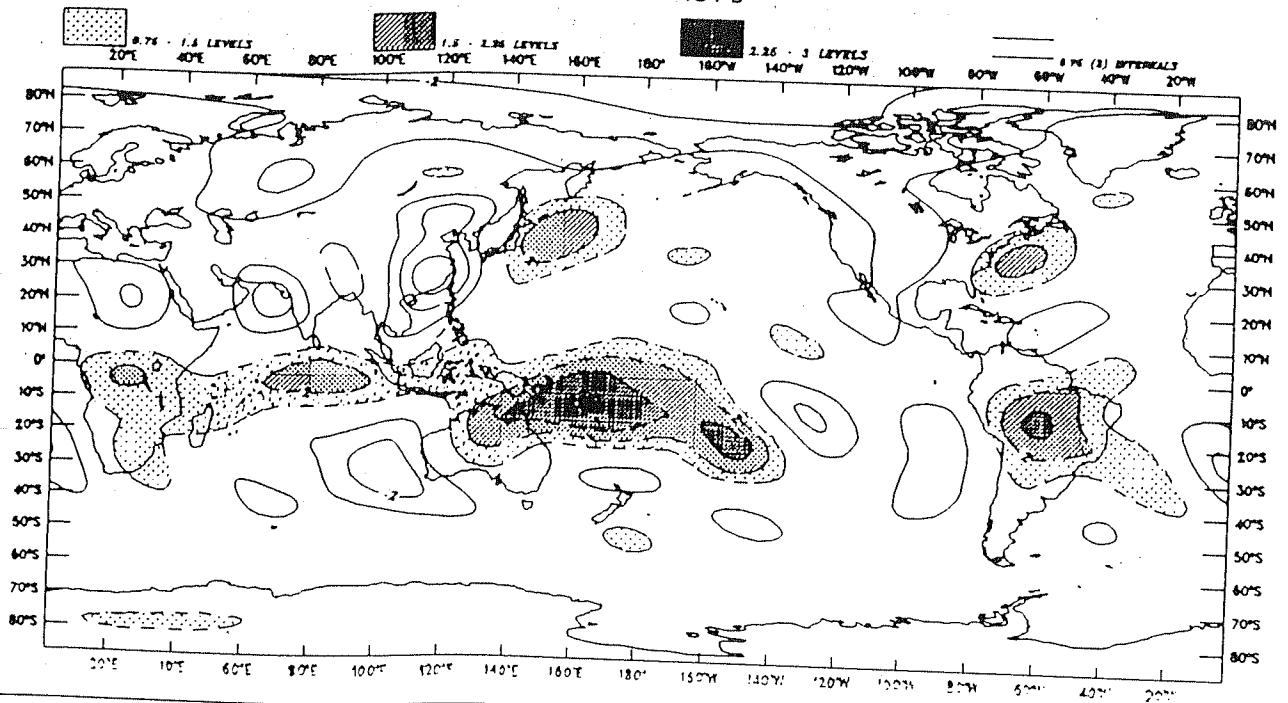
3.2.1 2-level linear equatorial β -plane model

We now describe the forcing experiment for winter (1978-79) using a simple 2-level linear equatorial β -plane model. Simple barotropic models and 2-layer models involve lesser computations and can be of considerable use in understanding the large scale

atmospheric response to forcing. For instance, Washington and Kasahara (1970) performed the January simulation using a two-layer model at National Center for Atmospheric Research (NCAR). The model included a hydrologic cycle, treatment of atmospheric water vapour and radiation. They prescribed a January mean surface temperature distribution which was held constant in time. The initial atmosphere was at rest, dry and isothermal. The gross features of the global atmospheric circulation were simulated quite well. The time-mean response was characterized by Hadley circulation in the tropics and baroclinic waves in the midlatitudes in the form of high and low-pressure patterns. It was found that the Hadley circulation transported heat, angular momentum, moisture and energy both vertically and horizontally in the tropics. In the middle latitude the poleward transport of these variables was achieved by the baroclinic waves.

In Chapter II, we had seen that the stationary response to forcing, in the 2-level linear model, can be studied by prescribing the observed heating at the 500 mb level. We have used the observed diabatic heating at 500 mb for winter (1978-79), from Schaack *et.al* (1990), for investigating the equilibrium response in the 2-level linear model. The vertical variation of the response in a 2-level model possesses the structure of a first baroclinic mode. As a consequence, the flows at 250 mb and 750 mb will be exactly 180 degrees out of phase. Therefore, for the purpose of interpreting the model response, we shall be only considering the circulations at 250 mb. The circulation features at 750 mb will be just the mirror image of the 250 mb flow pattern. The vertically averaged heating for winter (1978-79) is shown in Fig.3.2.1. The dominant heating region over the western Pacific extends longitudinally eastward upto central Pacific and westward across the Indian ocean and Africa. This planetary scale heating is associated with the ITCZ and SPCZ. The maximum heating in the western Pacific is of the order of 3.5°K per day and is located at around 400 mb. Heating in the northwestern Pacific, near Japan, is quite significant and is concentrated below 500

VERTICALLY AVERAGED DIABATIC HEATING WINTER 1979



DIABATIC HEATING AT 500 MB WINTER 1979

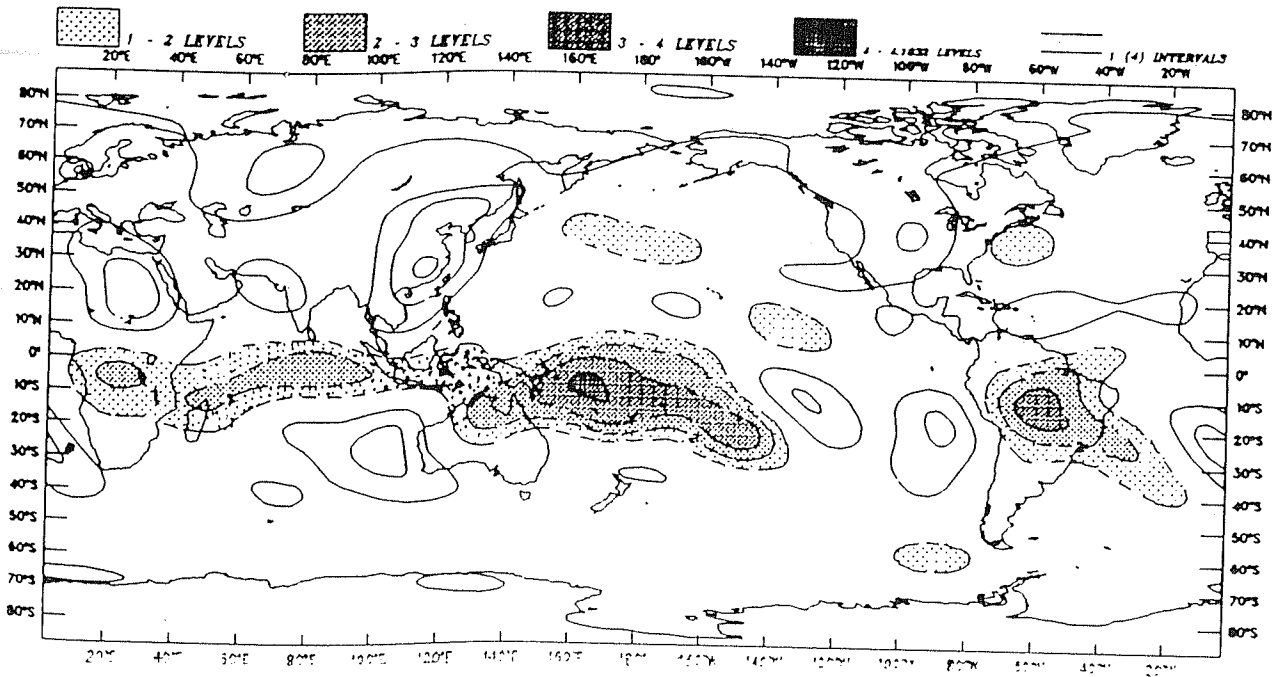


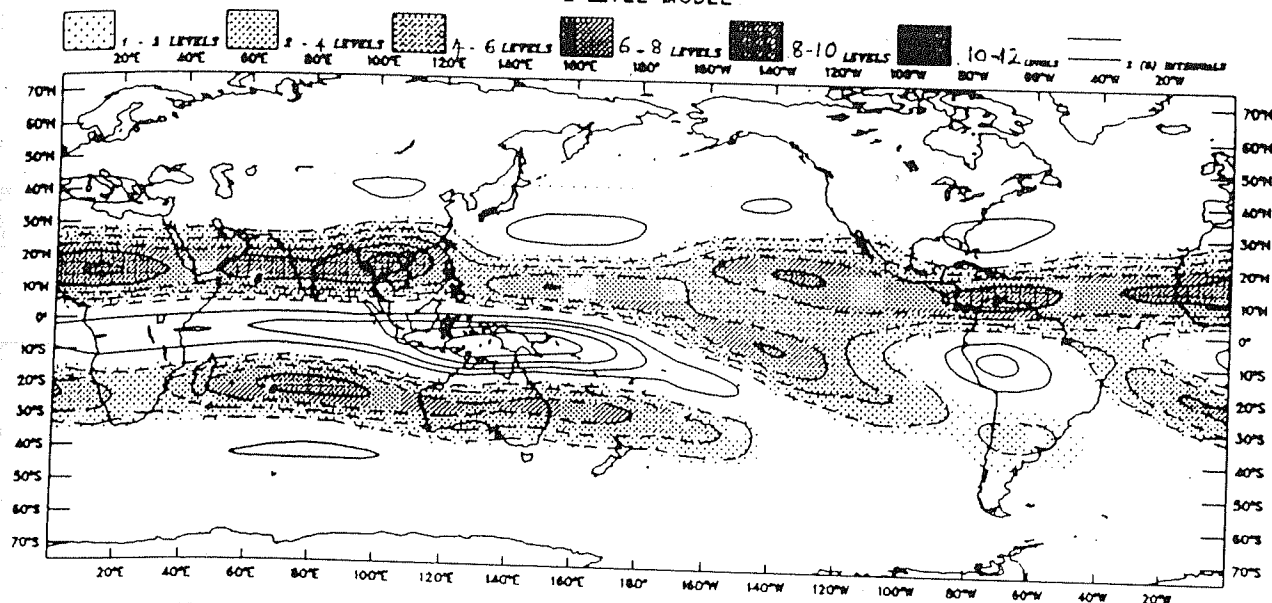
Fig.3.2.1. (Top) Vertically averaged diabatic heating during winter (1978-79). Interval 0.75 °K per day.

Fig.3.2.2. (Bottom) Diabatic heating at 500 mb during winter (1978-79). Interval 1 °K per day.

mb (Schaack *et.al* (1990)). Well defined cooling maxima of about 1.5°K per day over the eastern Pacific, continental North America and east Asia can also be seen. The heating at 500 mb, in Fig.3.2.2, shows a maximum heating of 3.5°K per day in the western Pacific and continental South America. The heating in the western north Pacific is not prominent at the 500 mb level. Cooling rates of about $1-2^{\circ}\text{K}$ per day can be observed over the south central and south eastern Pacific, continental North America and north of continental Africa, Pakistan, northwest India and east Asia. Strong cooling in the oceanic region to the west of Australia can also be noticed. Krishnamurti *et.al* (1973) examined the mean east-west circulations during the northern winter and performed calculations of kinetic energy exchanges between the ultralong waves and the zonal flow. They found that during winter two regions of divergent mass outflow in the upper troposphere occur near the convective zones of Indonesia and northern South America. The east-west circulations were as intense as the Hadley type of circulations. Regions of convergence were located over the mid-oceanic upper tropospheric troughs of the southern oceans in the tropics. They found that the generation of eddy kinetic energy by the mean east-west circulations, was smaller for the northern winter than for the northern summer. It was also found that the energy exchanges during northern winter were opposite to those during northern summer. In northern winter kinetic energy was generally transferred from the zonal flow to the wavenumbers 1-3 in the subtropical jet.

The variables in the 2-level model are expanded in a fourier series having truncation at zonal wavenumber 10 and in terms of parabolic cylinder functions in the meridional direction. We use a Rayleigh friction and Newtonian cooling of 5 days dissipation time-scale. The 500 mb heating is used to force the 2-level model and the method of solution has already been described in Chapter II. Fig.3.2.3a shows the steady state zonal velocity at 250 mb and Fig.3.2.3b shows the perturbation geopotential at 250 mb. Fig.3.2.3a shows easterlies (solid lines) extending from the western

WINTER 1979
ZONAL WIND AT 250 MB
2-LEVEL MODEL



WINTER 1979
GEOP AND WIND AT 250 MB
2-LEVEL MODEL

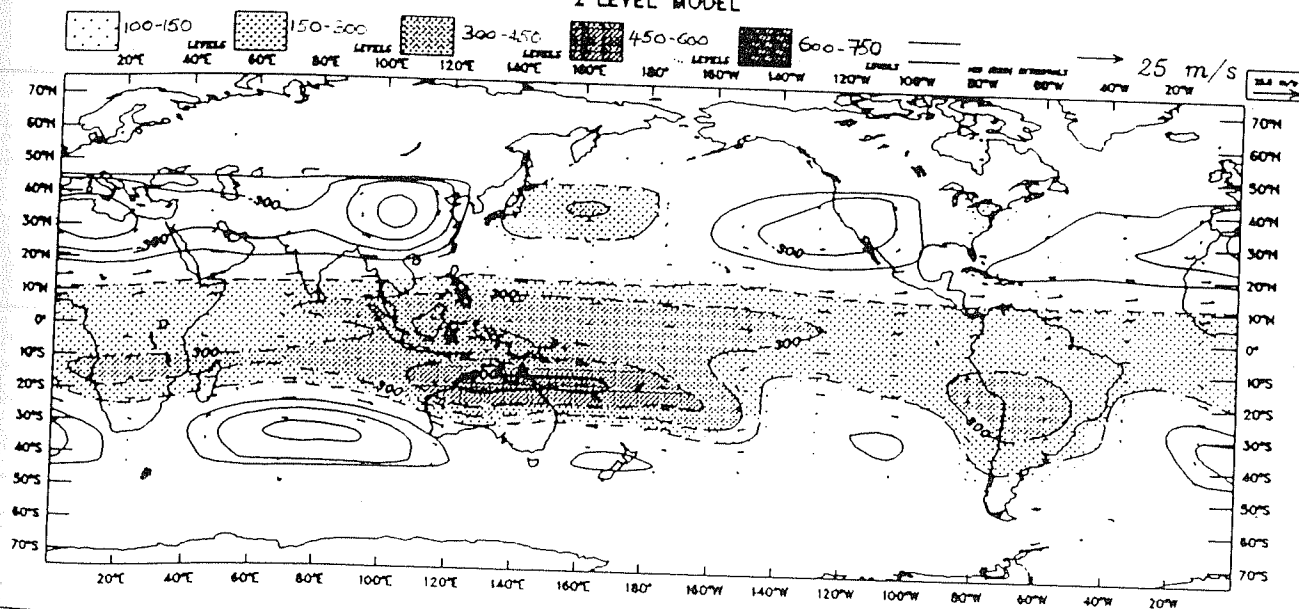


Fig.3.2.3a. (Top) Computed zonal wind at 250 mb for winter (1978-79) using 2-level linear model. Interval 2 ms^{-1} .

Fig.3.2.3b. (Bottom) Computed perturbation geopotential at 250 mb for winter (1978-79) using 2-level linear model. Interval $150 \text{ m}^2 \text{ s}^{-2}$.

Pacific across Africa and Atlantic. The easterly belt is mostly confined to the south of the equator and the maximum easterly wind speed in the western Pacific and further west is about 8 ms^{-1} . These easterlies can be viewed as the stationary Rossby wave response due to the heating over western Pacific. The most striking flow pattern in the tropics, is the westerly belt (shaded) that encircles the whole globe. The westerly flow is more prominent in the northern hemisphere. The Walker circulation in the equatorial Pacific can be identified by the upper level westerlies in the central and eastern Pacific. Strong westerlies that extend from southern parts of Africa upto Australia and central Pacific, can be observed in the southern hemisphere between 20°S and 30°S . The convection over South America also results in east-west circulations. It can be seen that the westward branch of the divergent circulation, which is characterized by a easterly flow is mostly localized near South America and south east Pacific. This is due to the fact that a large cooling occurred to the immediate west of the convective heat source over South America. This heat sink essentially limited the westward extent of the Rossby waves originating from the convective heat source. The geopotential at 250 mb shows a high pressure region (shaded), that extends globally between 10°N and 20°S . The high is most intense over South America, west Pacific and north of Australia. The Australian summer monsoon is well represented by the strong anticyclonic flow aloft. Prominent lows can be seen over east Asia, north India, Pakistan, Saudi Arabia, north Africa and parts of North America and Mexico. A well-defined upper level cyclonic vortex is located to the west of Australia in the south Indian ocean. Lim and Chang (1981) used a system of linearized shallow water equations on an equatorial β -plane and performed forcing experiments, to study the northeasterly monsoon surges and associated tropical motions over southeast Asia during northern winter. They explained the features of the observed circulation pattern during the winter monsoon in terms of the Rossby wave response produced by the forcing.

Generally, it can be seen that the structure and location of the time-mean circulation features are reasonably realistic in the 2-level model. But the strength of the circulations has been underestimated. For instance, the upper level easterlies over the western Pacific, continental South America and Africa are quite weak. Similarly, the maximum westerly wind speed of about $8-10 \text{ ms}^{-1}$, associated with the Walker circulation in the central and eastern Pacific is quite weak. One of the reasons for the weak divergent circulations, in the linear steady state model, is because of the use of a zero-basic state. Another reason is that the 2-level model is forced using the heating at 500 mb level, thereby allowing only the first baroclinic mode. The inadequacy in the vertical representation of heating mainly accounts for the weaker east-west circulations in the case of the 2-level model. The importance of the vertical structure of the 3-dimensional heating distribution has been pointed out by many earlier studies. The study by Hartmann *et.al* (1984) suggests that the maximum convective heating by mature cloud clusters, over the western Pacific, occurs at around 400 mb. They have shown that the equatorial Walker circulation is quite sensitive to the vertical distribution of heating. De Maria (1985) calculated the linear response of a stratified tropical atmosphere to convective forcing and compared the model results with the observed circulations during January 1979 over tropical South America. He found that the upper-level anticyclonic flow over South America could be simulated well, only when the maximum heating was located at 400 mb or above. This shortcoming of the 2-level model can be overcome in a multilevel model, where it is possible to include higher vertical modes by prescribing the observed heating at various vertical levels. In fact, we shall be showing in the next section that the 5-level nonlinear global spectral model reproduces the Walker circulation in the equatorial Pacific more realistically, when forced using the observed 3-dimensional heating distribution. In short, we find that the 2-level model captures the gross structural features of the time-mean circulations during winter (1978-79), but the strength of

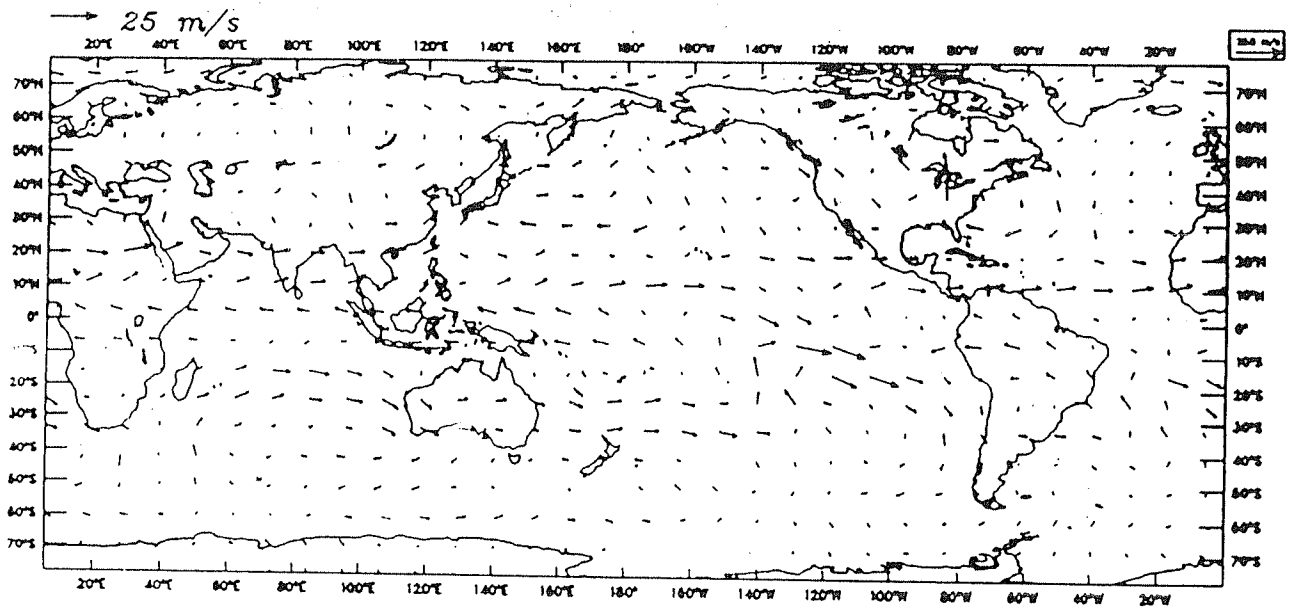
the major divergent circulations appears to be rather weak.

3.2.2 5-level nonlinear global spectral model

We shall now discuss the results of the winter (1978-79) forcing experiment with the 5-level nonlinear global spectral model. The model has a Rhomboidal truncation at 15 waves and the formulation is based on Bourke (1974). The model does not include parameterization of any of the physical processes. This model is designed primarily to study problems related to atmospheric dynamics and is well suited for carrying out forcing experiments. The model prognostic equations comprise of the vorticity, divergence, temperature and surface pressure equations. The model is forced using the observed heating rates for winter (1978-79) (Schaack *et.al* (1990)) at 900 mb, 700 mb, 500 mb, 300 mb and 100 mb. A Rayleigh friction and Newtonian cooling of 5 days dissipation time-scale have been used. The model is integrated for 35 days, with the heating held constant in time, so as to attain a steady state.

The wind fields at 300 mb and 900 mb are given in Figs.3.2.4a and 3.2.4b respectively. The zonal velocity fields at 300 mb and 900 mb are given in Figs.3.2.5a and 3.2.5b respectively. The salient circulation feature at 300 mb level is the strong easterly flow to the south of the equator extending right from the central Pacific across the Indian ocean, Africa upto the Atlantic. The maximum easterly speed over the western Pacific is about $8-10 \text{ ms}^{-1}$ which agrees well with the observations of Sumi and Murakami (1981). The Walker circulation in the equatorial Pacific is quite prominently seen and is more realistic in the 5-level model simulation. The westerlies associated with the Walker circulation have a maximum speed of about 20 ms^{-1} in the region of the eastern Pacific. The strong northwesterlies in the south eastern Pacific which extend upto 25°S compare well with the observations of Sumi and

WINTER 1979
WINDS AT 300 MB



WINTER 1979
WINDS AT 900 MB

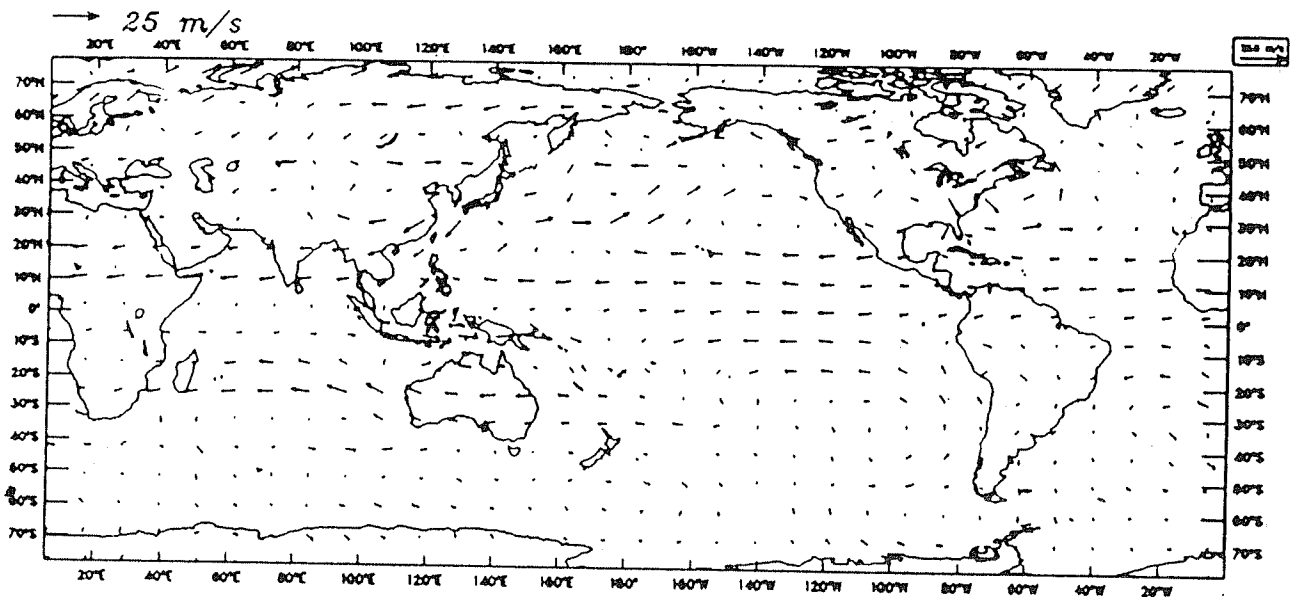


Fig.3.2.4a. (Top) Computed horizontal wind vectors at 300 mb for winter (1978-79) using 5-level nonlinear model.
Fig.3.2.4b. (Bottom) Same as Fig.3.2.4a, except for 900 mb.

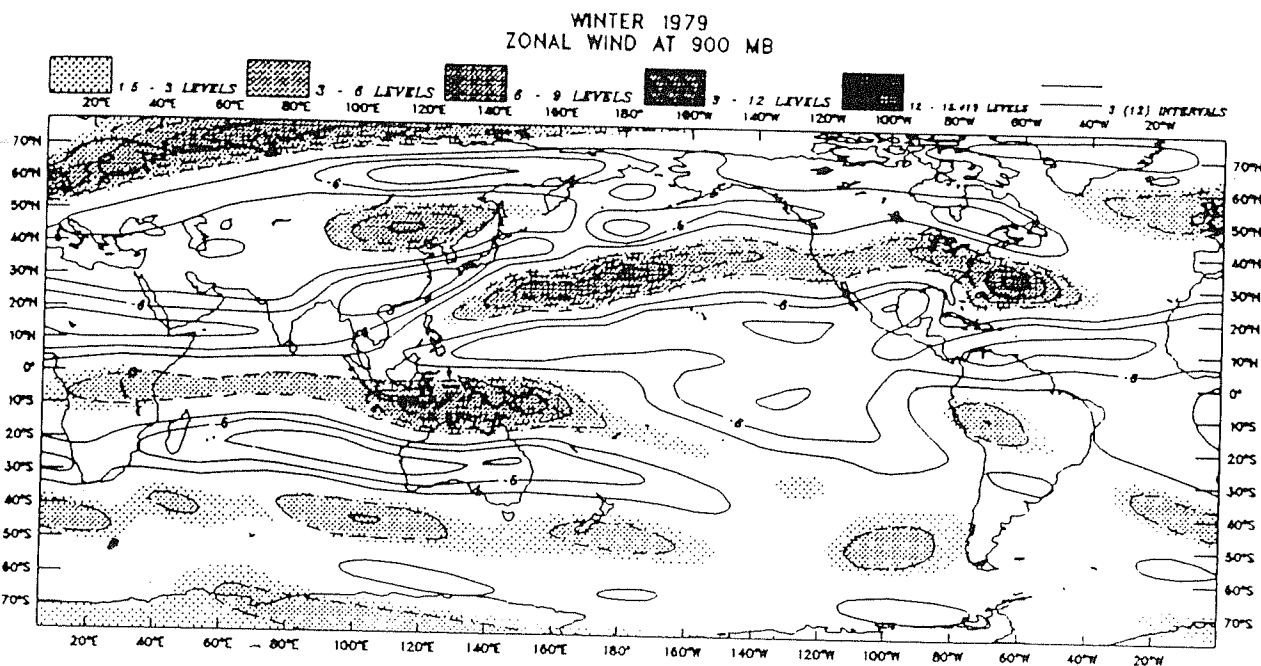
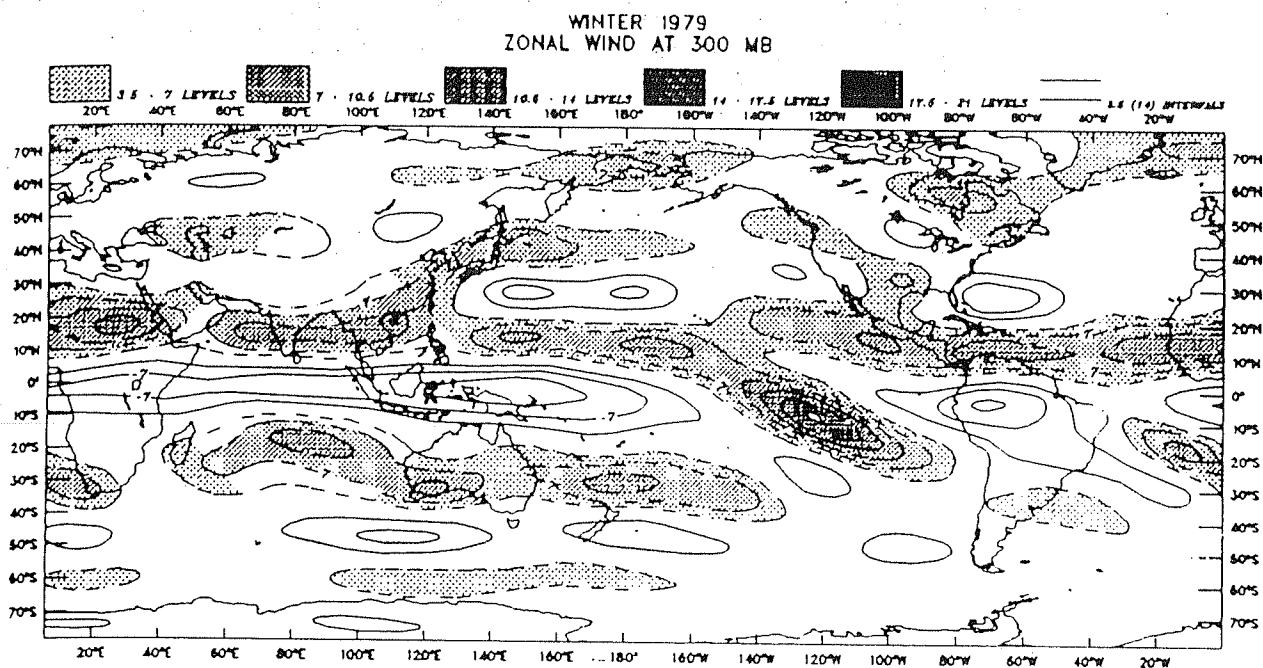


Fig.3.2.5a. (Top) Computed zonal wind at 300 mb for winter (1978-79) using 5-level nonlinear model. Interval 3.5 ms^{-1} .

Fig.3.2.5b. (Bottom) Same as Fig.3.2.5a, except for 900 mb. Interval 3 ms^{-1} .

Murakami (1981). Similarly, the upper level westerlies over east Asia, India, Saudi Arabia and northern Africa are reproduced well. The Rossby wave response due to the heat source over South America and the associated upper level easterlies are fairly intense and have a larger zonal extent as compared to the 2-level model simulation. Kalnay *et.al* (1986) found the region over south eastern Pacific and east of South America, was characterized by strong Rossby wave activity during January 1979. Our 5-level model simulation shows that the upper level easterlies over South America and the strong north westerlies over south-eastern Pacific, have been reproduced quite well. In the case of the 5-level nonlinear model, a realistic time-mean flow pattern was achieved mainly because of the accurate vertical representation of the diabatic heating. Additionally, the 5-level model is based on a nonlinear system of equations while the 2-level model is based on a linear system of equations. Since, nonlinear advection effects, are quite important in the tropics, they do contribute significantly towards the more realistic tropical time-mean response in the case of the 5-level model.

The low-level circulation during winter months is characterized by interesting events. Lau and Lim (1982) examined the heat-induced monsoon circulations, during southeast Asian northeasterly cold surges, using an equatorial β -plane model. During the winter season of the northern hemisphere, an intense high pressure system develops over central Asia and Siberia. This leads to a large influx of surface cold air from the cold Siberian region into central and south east China, causing a rapid cooling of the lower troposphere and a rise in the surface pressure. This is followed by strong northeasterly surface flow over the south China sea. The low level convergence leads to convective motions in the equatorial region. The convective heating over Borneo-Indonesia sets up a strong Walker circulation in the Pacific and a local Hadley-type circulation. They showed that the equatorial heating exerts significant influence on the Rossby wave response to the west of the forcing region. The Kelvin waves to the east of the forcing and the strength of the associated Walker circulation in the Pacific

are strongly related to the heating contrast between the Indonesian heating and the heat sink over the central and eastern Pacific. Let us examine the model simulation of the circulations at the lower levels. The 900 mb circulations (Fig.3.2.4b) show the appearance of a broad easterly trade belt over central and east Pacific which is in good agreement with the observations of Sumi and Murakami (1981). The tropical easterly trade winds can be seen encircling the whole globe. One can notice the westerly winds from the Siberian region blowing towards China and strong northerly winds blowing from east Asia towards south China sea. The low-level convergence enhances the convective activity in the region of western Pacific which later on drives the major east-west and Hadley-type of circulations. The flow at 900 mb shows well defined cyclonic circulation over northern Australia and two anticyclonic vortices over central and east Asia (30°N and 100°E) and in the oceanic region to the west of Australia.

The geopotential and velocity potential distributions at 300 mb are given in Figs.3.2.6a and 3.2.6b respectively. The negative contours of velocity potential in the western and central Pacific suggests that there is strong outflow at 300 mb over this region. One can notice that there is upper level divergence associated with the heating in the southern hemisphere over continental Africa and South America. The positive contours (shaded) of velocity potential at 300 mb indicate that there is strong subsidence in the eastern Pacific, Mexico, east Asia and parts of north Africa. The enhanced subsidence over the south eastern Pacific corresponds to the descending branch of the Walker circulation in the equatorial Pacific. The geopotential distribution at 300 mb also indicates that the region over the Australia, western Pacific, equatorial Africa and South America are characterized by outflow at the upper levels. The highs at the upper levels in the north western Pacific ocean and to the east of USA are forced by convective heat sources which are mostly confined below the middle troposphere. Well defined upper level lows are located in the eastern Pacific, Mexico, east Asia, north Africa and west of Australia.

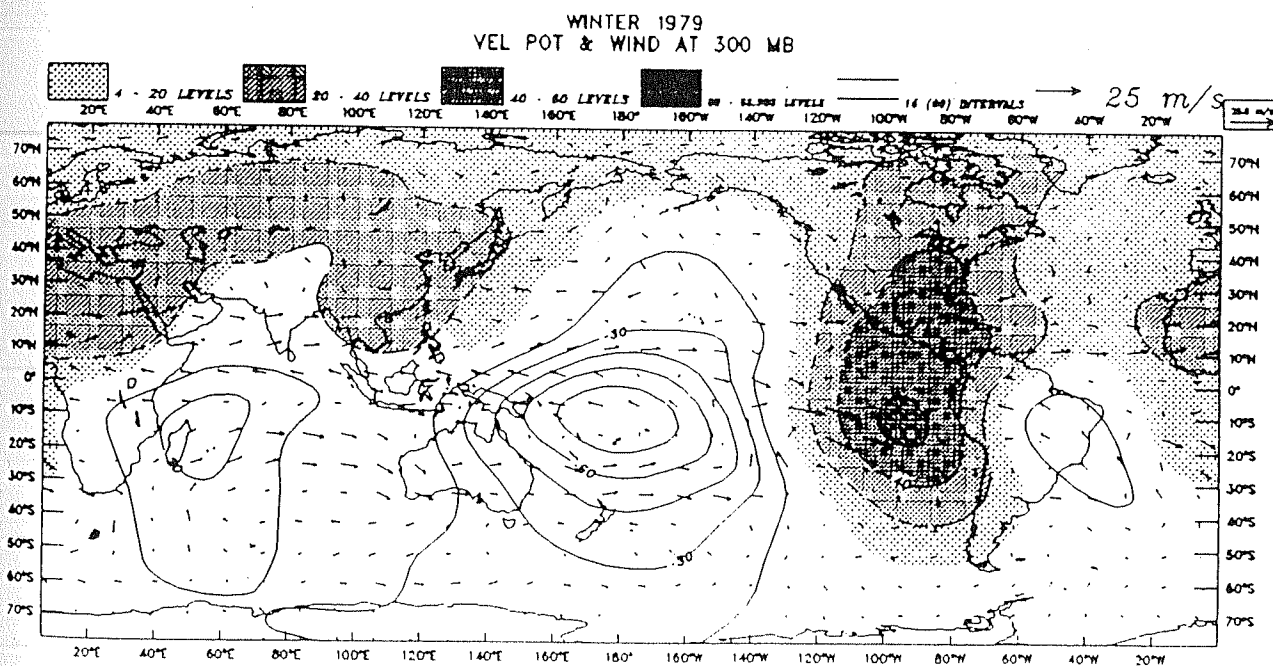
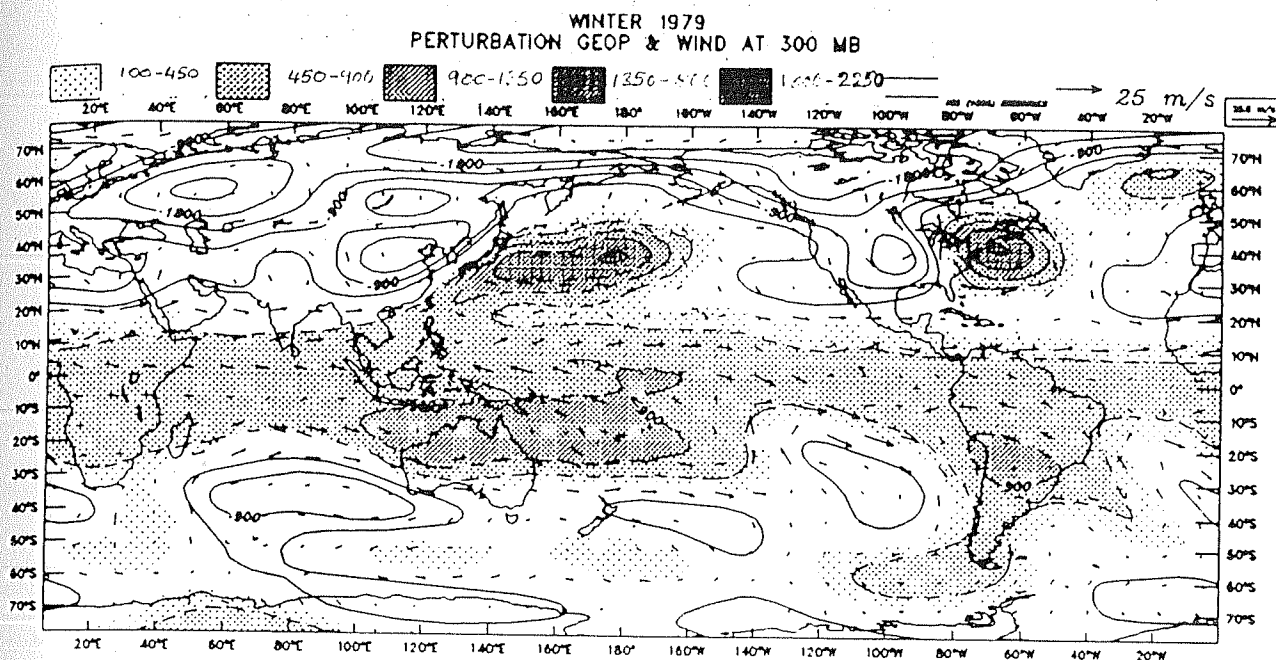


Fig.3.2.6a. (Top) Computed perturbation geopotential at 300 mb for winter (1978-79) using 5-level nonlinear model. Interval $450 \text{ m}^2 \text{ s}^{-2}$.
 Fig.3.2.6b. (Bottom) Computed velocity potential at 300 mb for winter (1978-79) using 5-level nonlinear model. Interval $(20 \times 10^5 \text{ m}^2 \text{ s}^{-1}$ for positive and $15 \times 10^5 \text{ m}^2 \text{ s}^{-1}$ for negative contours).

The velocity potential distribution at 300 mb can be used to calculate the intensities of the east-west and the Hadley-type of circulations at this level. Following Krishnamurti *et.al* (1973), we have computed the intensities of the equatorial Walker circulation and the Hadley-type of circulation in the western Pacific for the case of winter (1978-79). The intensity of the Walker circulation (I_w), averaged for a latitudinal belt, is given by $\frac{1}{a(\phi_2 - \phi_1)} \int_{\phi_1}^{\phi_2} \frac{1}{\cos\phi} \frac{\partial\chi}{\partial\lambda} d\phi$ and the intensity of the Hadley circulation (I_h), averaged between two longitudes, is given by $\frac{1}{a(\lambda_2 - \lambda_1)} \int_{\lambda_1}^{\lambda_2} \frac{\partial\chi}{\partial\phi} d\lambda$. In the above expressions 'a' stands for the radius of the earth, λ for longitude, and ϕ for latitude. I_w and I_h for winter (1978-79) have been calculated and are shown in Figures 3.2.7a and 3.2.7b respectively. Fig.3.2.7a shows the longitudinal variation of the intensity of Walker circulation at 300 mb averaged between 29°S and 29°N. As the gradient of the velocity potential field corresponds to the divergent part of the wind, the negative peaks of I_w indicate regions where easterlies dominate and the positive peaks represent regions where westerlies dominate. There are three negative and three positive peaks of I_w at 300 mb, corresponding to the three active regions of convection during winter (1978-79). The first convective zone was located over Africa, the second one over western Pacific and Australia and the third convective zone over South America. We can see from Fig.3.2.7a that the strongest easterlies at the upper levels, were associated with the convective heating over South America. Observational findings by Kalnay *et.al* (1986) do suggest that the region over south eastern Pacific and east of South America, was characterized by strong easterlies during January 1979. It can be further seen that (Fig. 3.2.7a) the westerlies at the upper levels were strongest in the region of central Pacific. This means that the stationary Kelvin waves originating from the convective heating over the western Pacific were associated with large amplitudes. The position of the convective heat source over the western Pacific during January 1979 is an important feature to be noted. Sumi and Murakami (1981) also found from observations that the heat source was situated in the western Pacific

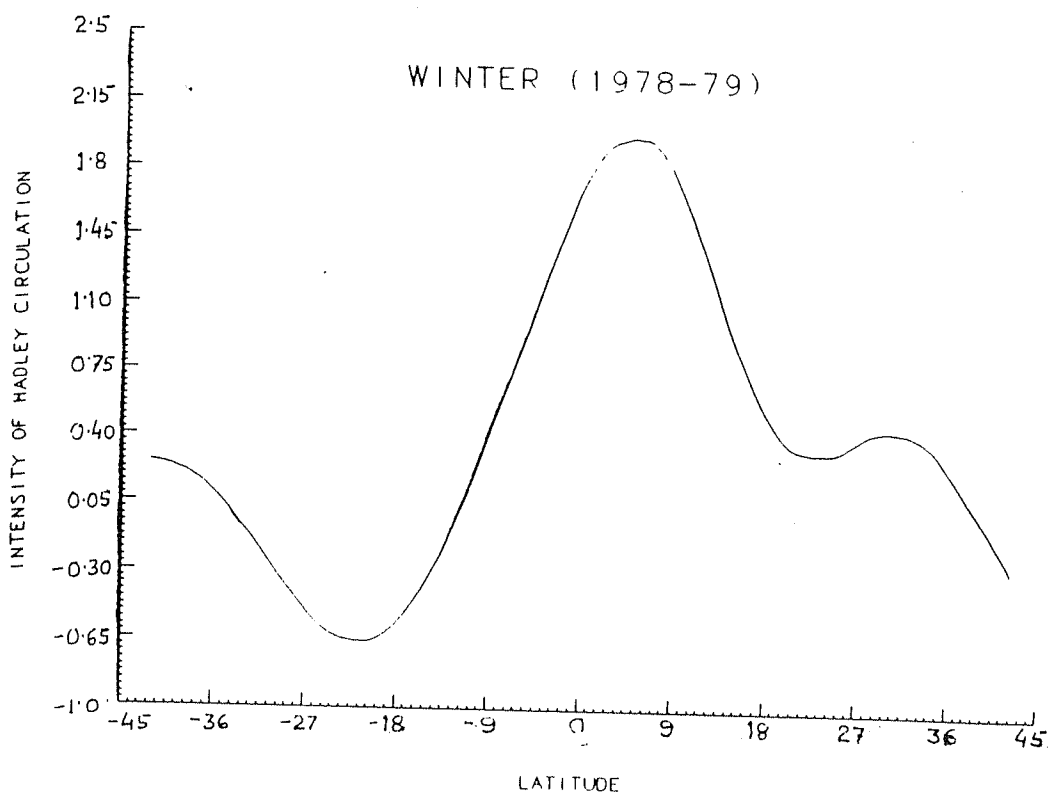
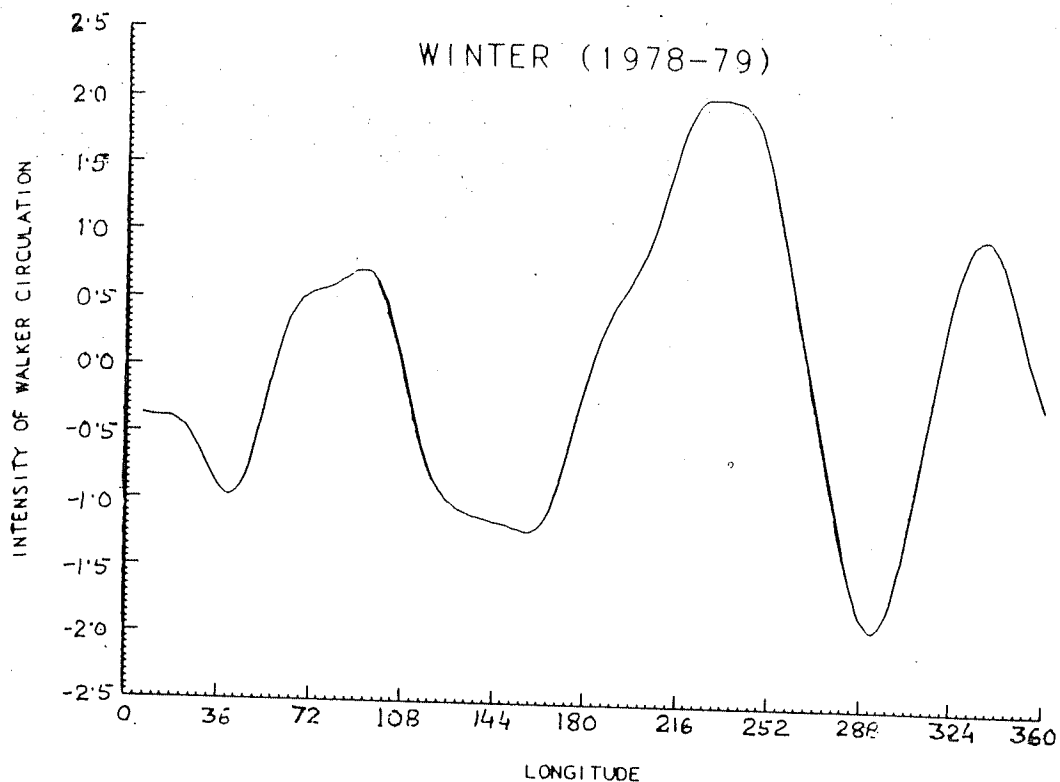


Fig.3.2.7a. (Top) Longitudinal variation of the intensity of Walker circulation at 300 mb for winter (1978-79). Units ms^{-1} .

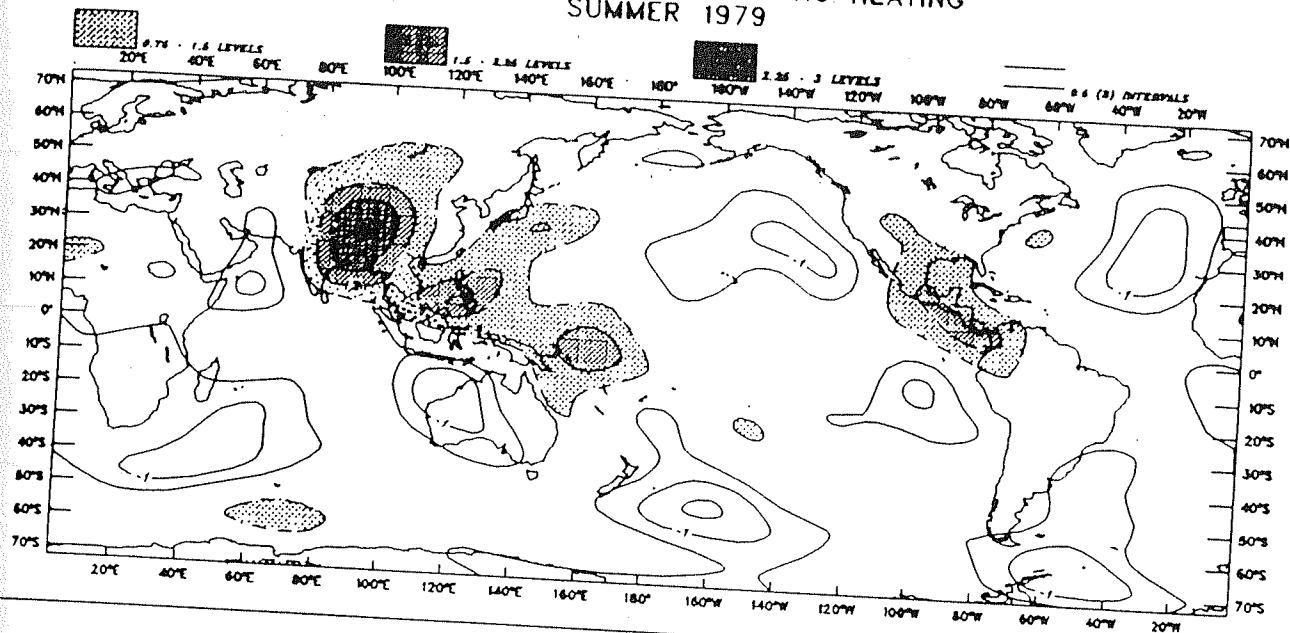
Fig.3.2.7b. (Bottom) Latitudinal variation of the intensity of Hadley circulation at 300 mb for winter (1978-79). Units ms^{-1} .

during January 1979, while during the previous years it was situated over Indonesia. Fig.3.2.7b shows the meridional variation of the intensity of the Hadley circulation averaged for the longitudes between 118°E and 140°E . It can be seen that the Hadley-type circulation was quite intense between 25°S and 8°N . Fig.3.2.7b indicates that the southern hemisphere was dominated by northerly winds associated with the upper level circulation to the west of Australia. The strong southerly winds at around 5°N are related to the Rossby waves in the equatorial western Pacific and the upper level flow associated with the Australian summer monsoon.

3.3 Time-mean circulations during summer 1979

Let us now take a look at the salient features of the time-mean motions during summer 1979. The vertically integrated heating for summer 1979 (Fig.3.3.1), shows that there is an intense heating ($\sim 3.0^{\circ}\text{K}$ per day) to the north of the Bay of Bengal, the foothills of the Himalayas and over the elevated Tibetan plateau. One also notices that there is significant heating over the Mexican highlands and to some extent in the equatorial western Pacific. Substantial cooling ($\sim 1.0^{\circ}\text{K}$ per day) is observed over Saudi Arabia, Iran, Pakistan, Australia and the oceanic regions of the Atlantic and north and south eastern Pacific. Estimates of convective activity based on satellite observations by Murakami (1983) indicate that during the northern summer (1979), the amplitude of the diurnal variation was large (1° - 2° per day) over the Tibetan plateau and the western Pacific. Nitta (1983) used the FGGE upper-air observations during summer MONEX in 1979 and analyzed the spatial and temporal variations of the heat source over the eastern Tibetan plateau. He found that both the elevated surface heating and the latent heat release, contributed nearly equally to the net total heating of about 4° per day. The moisture budget analysis showed that the water vapour lost by condensation over the plateau was generally balanced by the surface evaporation.

VERTICALLY AVERAGED DIABATIC HEATING SUMMER 1979



DIABATIC HEATING AT 500 MB SUMMER 1979

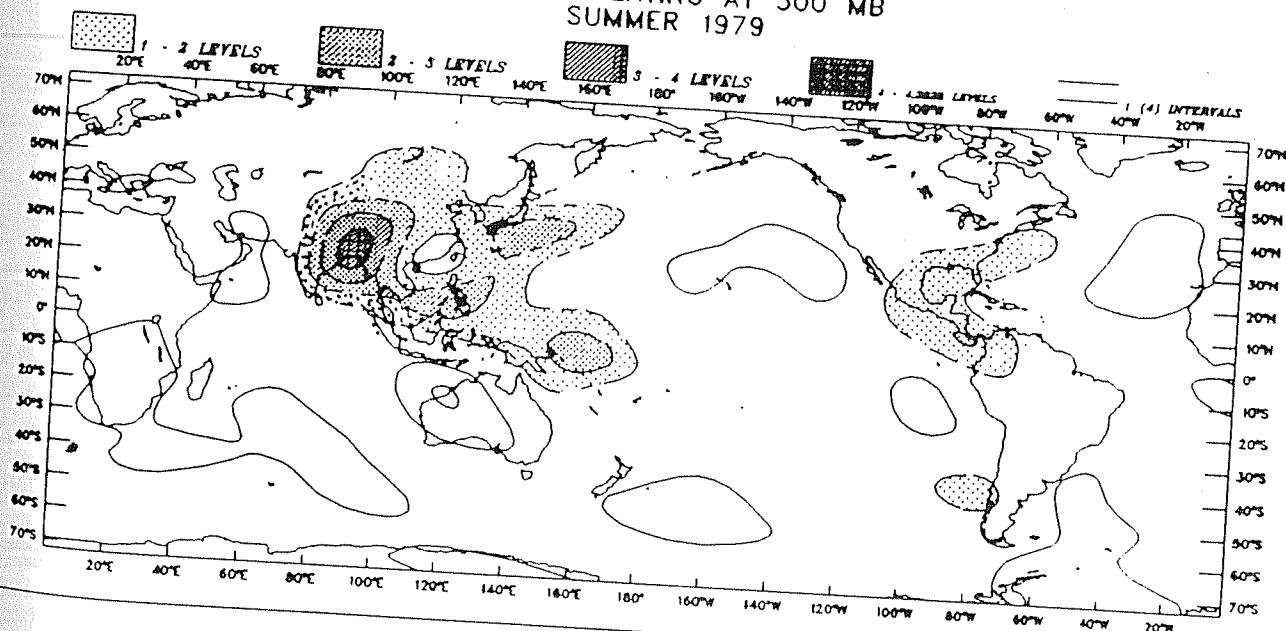


Fig.3.3.1. (Top) Same as Fig.3.2.1, except for summer (1979). Interval (0.75°K per day for positive and 0.5°K per day for negative contours).

Fig.3.3.2. (Bottom) Same as Fig.3.2.2, except for summer (1979).

Water vapour transport was mainly by the south westerly monsoon flow and the maximum condensational heating occurred at around 400 mb level.

A brief description of the circulation patterns during this season is given below. He *et.al*(1987) analyzed the evolution of the Asian summer monsoon circulation and the effect of the Tibetan plateau on the monsoon onset during 1979 using the FGGE data. They found that the condensational heating was primarily responsible for driving the Asian summer monsoon circulation. The sensible heating over the Tibetan plateau was also significantly large. The development of the mean monsoon circulation in July has been simulated by Kuo and Qian (1982). It was found that the diabatic heating distribution had a profound influence on the low-level circulation pattern. They found that the precipitation was mainly determined by the diabatic heating, orography and the initial condition. The roles of convection, cloud-radiation and evaporation feedback processes on the July simulation, have been studied by Sud and Molod (1988). They found that cumulus parameterization with dry convective mixing produced a realistic ITCZ over North Africa. The model did not produce any rainfall over the Sahara, which agreed with the observations.

We now briefly describe some synoptic scale aspects related with the monsoon onset over India and its subsequent evolution. The onset of the summer monsoon over India is characterized by a sequence of interesting changes in the synoptic scale circulation, which are well documented by Krishnamurti and Ramanathan (1982). They performed numerical experiments to investigate the sensitivity of the monsoon onset to differential heating. The results of their experiments explained some of the observational aspects of the evolution of the differential heating and energy exchanges during the MONEX. They showed that there is a substantial increase in the kinetic energy of the monsoon circulation and the nondivergent component of the flow over the Arabian sea, prior to the onset of monsoon rains over central India. It is found

Water vapour transport was mainly by the south westerly monsoon flow and the maximum condensational heating occurred at around 400 mb level.

A brief description of the circulation patterns during this season is given below. He *et.al*(1987) analyzed the evolution of the Asian summer monsoon circulation and the effect of the Tibetan plateau on the monsoon onset during 1979 using the FGGE data. They found that the condensational heating was primarily responsible for driving the Asian summer monsoon circulation. The sensible heating over the Tibetan plateau was also significantly large. The development of the mean monsoon circulation in July has been simulated by Kuo and Qian (1982). It was found that the diabatic heating distribution had a profound influence on the low-level circulation pattern. They found that the precipitation was mainly determined by the diabatic heating, orography and the initial condition. The roles of convection, cloud-radiation and evaporation feedback processes on the July simulation, have been studied by Sud and Molod (1988). They found that cumulus parameterization with dry convective mixing produced a realistic ITCZ over North Africa. The model did not produce any rainfall over the Sahara, which agreed with the observations.

We now briefly describe some synoptic scale aspects related with the monsoon onset over India and its subsequent evolution. The onset of the summer monsoon over India is characterized by a sequence of interesting changes in the synoptic scale circulation, which are well documented by Krishnamurti and Ramanathan (1982). They performed numerical experiments to investigate the sensitivity of the monsoon onset to differential heating. The results of their experiments explained some of the observational aspects of the evolution of the differential heating and energy exchanges during the MONEX. They showed that there is a substantial increase in the kinetic energy of the monsoon circulation and the nondivergent component of the flow over the Arabian sea, prior to the onset of monsoon rains over central India. It is found

that the field of the differential heating migrates to a favorable position during the onset phase. The differential heating generates the eddy available potential energy which enhances the eddy kinetic energy of the divergent circulations. This is followed by a rapid transfer of energy from the divergent flow to the nondivergent circulation. Analyses of moisture fields by Pearce and Mohanty (1984), based on FGGE data for summer 1979, revealed that the onset phase of the Asian summer monsoon is characterized by a moisture build up over the Arabian sea during which synoptic and mesoscale transient disturbances develop. They also found that during the onset phase, there is a rapid intensification of the Arabian sea winds and a significant increase in the latent heat release because of large-scale feedback effects. The strong cross-equatorial flow is maintained by the latent heat release in the tropical atmosphere.

The interaction of the summer monsoon (1979) circulation with the tropical low-frequency intraseasonal oscillation has been studied quite extensively. Chen (1985) carried out detailed energetics in the tropical region during the FGGE summer and showed that the eddy kinetic energy of the flow, exhibited a pronounced quasi-periodic variation with a period of about 45 days. Murakami and Nakazawa (1985a) used the FGGE data to study the intraseasonal oscillations over the tropical belt during the 1979 summer. They found a strong association between the monsoon activity over south Asia and changes in the intensity of the equatorial Walker circulation. During active monsoons over south Asia, the Walker circulation was stronger and characterized by prominent 850 mb easterlies over the eastern Pacific, strong westerlies over the Indian ocean and western Pacific and strong equatorial convective activity. During the break monsoon phase, the strength of the equatorial Walker circulation was below normal. Chen(1987) observed a coherent seesaw fluctuation of 200 mb temperature and 850 mb height fields between the Tibet-India region and over north Pacific during summer 1979. The T (200 mb) and Z (850 mb) fields were seen to oscillate with opposite phases. This oscillation was related to the eastward

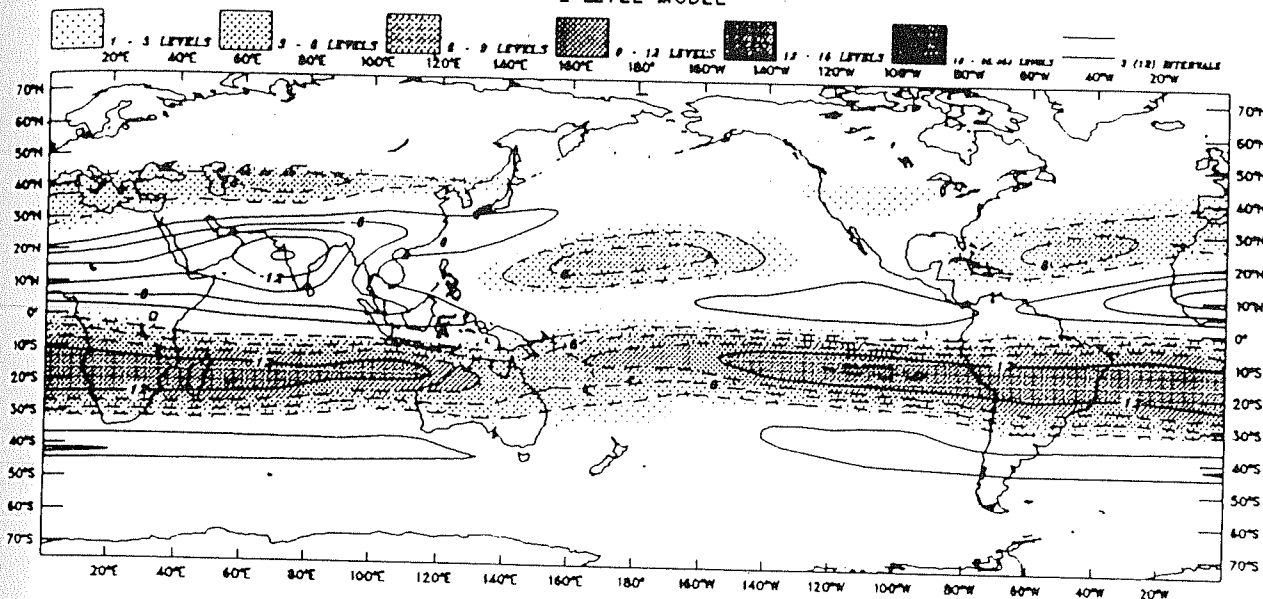
propagating 30-50 day mode. Chen *et.al* (1988a) studied the water vapour transport over the entire Asian monsoon region using the FGGE data set. They found that the movement of the water vapour convergence zone was linked with the eastward propagating 30-50 day oscillation.

3.3.1 2-level linear equatorial β -plane model

The results of the forcing experiments for summer 1979 using the 2-level linear equatorial β -plane model are discussed below. The model was forced using the heating distribution at 500 mb, for July 1979, given in Schaack *et.al* (1990). The variables in the 2-level model were expanded in a fourier series having truncation at zonal wavenumber 10 and in terms of parabolic cylinder functions in the meridional direction. A weak Rayleigh friction and Newtonian cooling of 15 days dissipation time-scale was used. The heating at 500 mb, which is shown in Fig.3.3.2, has a large meridional gradient over the Indian summer monsoon region. The maximum heating at around 90°E and 23°N is about 4.0° K per day. Besides the heating near the Bay of Bengal, the foothills of Himalayas and the Tibetan plateau, there is considerable heating over the Mexican highlands and to some extent in the western Pacific. Zones of cooling are located over Iran, Pakistan, Australia and the Pacific and Atlantic oceans. Abbot (1977) simulated the northern hemisphere summer monsoon and showed that the zonally asymmetric distribution of heating creates the available potential energy on the planetary scale. Most of this energy, is then baroclinically converted into kinetic energy which maintains the atmosphere's ultralong waves. The planetary scale waves subsequently transfer energy barotropically to both the zonal flow and the smaller synoptic scale waves. Kanamitsu (1977) showed that the tropical quasi-stationary ultralong waves which are nonlinear and non-geostrophic, are maintained by the land-ocean heating contrast.

Fig.3.3.3a shows the steady state zonal velocity at 250 mb and Fig.3.3.3b shows the perturbation geopotential at 250 mb. The zonal wind pattern at 250 mb indicates that there are major east-west circulations associated with heating over the Indian monsoon region and the Mexican highlands. Upper level westerlies can be seen converging into the regions of the upper tropospheric troughs located over the Pacific and Atlantic oceans. The southern hemisphere is characterized by westerlies in the latitudinal belt between (10°S and 25°S), which cover the entire globe. The geopotential distribution at 250 mb shows anticyclonic circulations over the Tibetan plateau, Himalayas and near Mexico. Highs can be seen extending even over Arabia and northern parts of continental Africa. The maximum speed of the upper tropospheric easterlies, over the Indian summer monsoon region, is about 15 ms^{-1} and is comparatively lower than the observed wind speed. It can also be seen that the upper level easterlies associated with the heating over Mexico, are poorly represented. The subtropical westerlies in the southern hemisphere are rather weak (max speed $\sim 15 \text{ ms}^{-1}$). In brief, the 2-level linear model simulates the structure of the upper level circulations reasonably well, while their intensities appear to be quite weak. One of the main shortcomings of the 2-level linear model is its inadequacy to take into account the observed vertical structure associated with the 3-dimensional heating distribution. The effect of using heating at a single level, permits the inclusion of a single vertical mode only. For instance, a first baroclinic mode of heating (maximum heating at 500 mb) produces a flow at the upper and lower levels, which are exactly opposite in phase. However, observations indicate that over the Indian monsoon region there is a large vertical variation of heating distribution. Consequently the structure of the flows at the upper and lower levels are totally different. Therefore, one needs to use a model with higher vertical resolution in order to take into account the impact of all the vertical modes associated with the complicated 3-dimensional heating over the Indian monsoon region. Further, since nonlinear advection terms are absent in the

SUMMER 1979
ZONAL WIND AT 250 MB
2-LEVEL MODEL



SUMMER 1979
GEOP AND WIND AT 250 MB
2-LEVEL MODEL

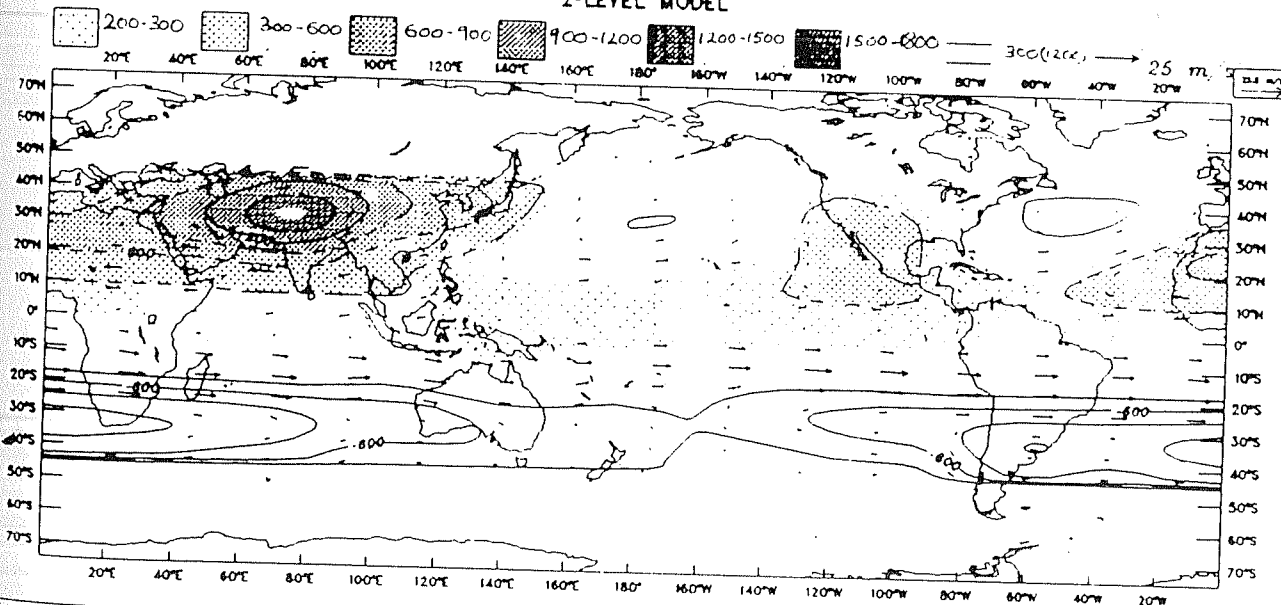


Fig.3.3.3a. (Top) Same as Fig.3.2.3a, except for summer (1979). Interval 3 ms^{-1} .
Fig.3.3.3b. (Bottom) Same as Fig.3.2.3b, except for summer (1979). Interval $300 \text{ m}^2 \text{ s}^{-2}$.

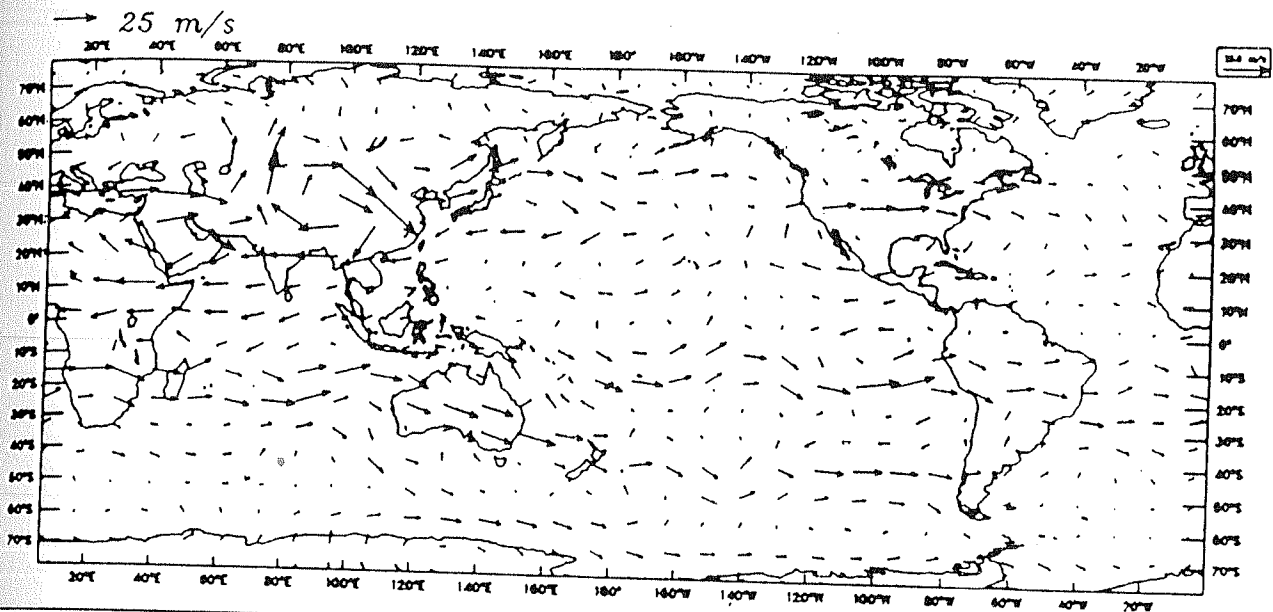
2-level model, the tropical time-mean response may not be very realistic. In the following subsection, we shall study the stationary response during summer-1979 using the 5-level nonlinear global spectral model.

3.3.2 5-level nonlinear global spectral model

We shall now discuss the results of the summer 1979 forcing experiment using the 5-level nonlinear global spectral model having a Rhomboidal truncation at 15 waves. The model was forced using the observed heating rates at 900 mb, 700 mb, 500 mb, 300 mb and 100 mb for summer 1979, computed by Schaack *et.al* (1990). A weak Rayleigh friction and Newtonian cooling of 15 days dissipation time-scale was used. The model was integrated for 100 days, with the heating kept constant in time, so as to attain a steady state.

We now describe the model simulation of the steady-state circulations for the case of summer (1979). The wind vectors at 300 mb and 900 mb are shown in Figs.3.3.4a and 3.3.4b respectively. The contours of zonal velocity at 300 mb and 900 mb are given in Figs.3.3.5a and 3.3.5b respectively. The upper level flow over the Indian monsoon region shows well defined easterlies and the strong anticyclonic flow associated with the Tibetan high. The easterlies extend westward into southern Saudi Arabia and Africa and penetrate upto south of the equator. The maximum easterly wind speed around 20°N is about 26-28 ms⁻¹. Observations (eg. Krishnamurti (1985)) indicate that during July 1979, the 200 mb easterlies over the Indian monsoon region had speeds of the order of 25 ms⁻¹. Similarly, the upper level easterlies over the Mexican highlands having speed of about 8-10 ms⁻¹ and the associated anticyclonic vortex are reproduced quite well. Westerlies in the northern hemisphere are prominently seen over northern regions of Africa and Saudi Arabia and over USA. The subtropical westerlies in the southern hemisphere are quite strong (~20 ms⁻¹)

SUMMER 1979
WINDS AT 300 MB



SUMMER 1979
WINDS AT 900 MB

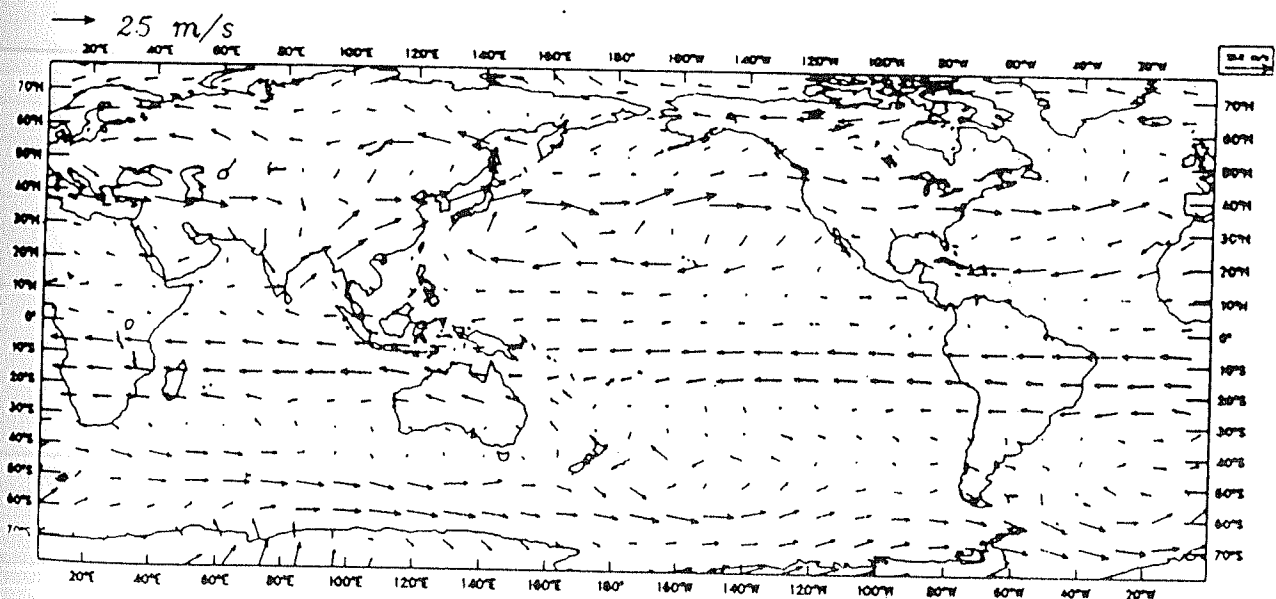


Fig.3.3.4a. (Top) Same as Fig.3.2.4a, except for summer (1979).

Fig.3.3.4b. (Bottom) Same as Fig.3.2.4b, except for summer (1979).

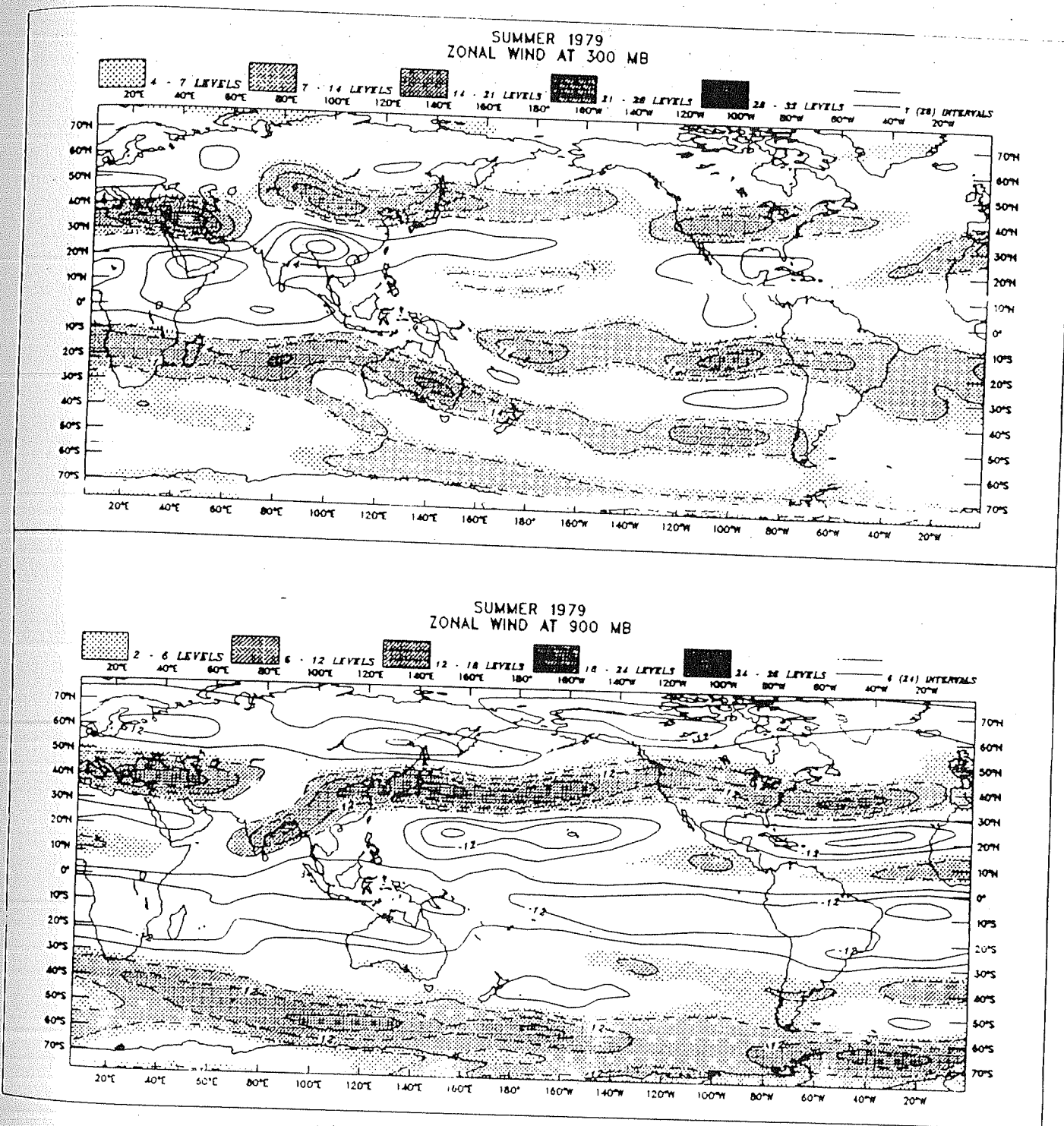
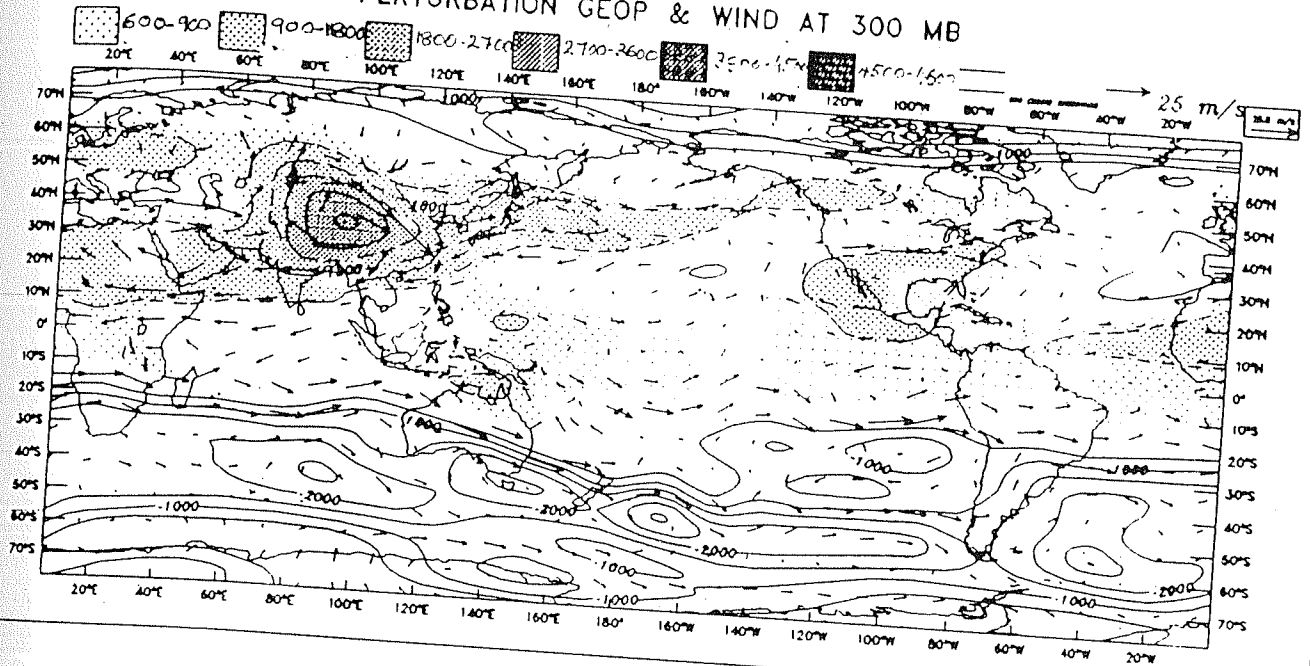


Fig.3.3.5a. (Top) Same as Fig.3.2.5a, except for summer (1979). Interval 7 ms^{-1} .
 Fig.3.3.5b. (Bottom) Same as Fig.3.2.5b, except for summer (1979). Interval 6 ms^{-1} .

over Australia and south eastern Pacific. The prominent features at 900 mb are the strong south westerly winds over India, the midlatitude westerlies over west and central Asia and the oceanic regions of north Pacific and Atlantic. The maximum speed of the south westerly winds over India is about 18 ms^{-1} . The southwesterly wind speeds agree with the July 1979 observations of Krishnamurti (1985). The southern hemispheric easterly trades (max speed $\sim 12 \text{ ms}^{-1}$) are nearly zonal and extend all round the globe. The cross-equatorial flow near the Indian longitudes is distinctly seen at the 900 mb level. Sashegyi and Geisler (1987) have simulated the cross-equatorial flow during the summer monsoon using a linear model. The computed geopotential and the velocity potential distributions at 300 mb are given in Figs.3.3.6a and 3.3.6b respectively. The negative contours of velocity potential in the regions near the Bay of Bengal, the Tibetan plateau and to some extent in the western Pacific, indicate that there is a strong divergence over these places. The geopotential field also shows a prominent anticyclone over the Tibetan plateau. Prominent oceanic lows, associated with regions of longwave cooling can be seen over the northern Pacific and Atlantic oceans (Fig.3.3.6a). The upper level divergence over the Mexican highlands is clearly seen in Figs.3.3.6a and 3.3.6b. The negative contours of velocity potential at 300 mb (shaded), suggest that there is large subsidence over Pakistan, Iran, Africa and oceanic regions in the Pacific and Atlantic.

The intensity of the Hadley-type and east-west circulations during summer (1979) has been calculated by using the velocity potential distribution. The diagnostic study of the 200 mb circulation patterns for summer 1967 by Krishnamurti (1971) revealed the existence of prominent east-west cells. These major east-west overturnings were caused because of land-ocean thermal contrasts and a zonally asymmetric distribution of heating. These east-west cells were located at around 20°N and were quite different from the traditional equatorial Walker circulation. He found that the intensity of the east-west circulation, in the Indian summer monsoon region, was

SUMMER 1979 PERTURBATION GEOP & WIND AT 300 MB



SUMMER 1979 VEL POT & WIND AT 300 MB

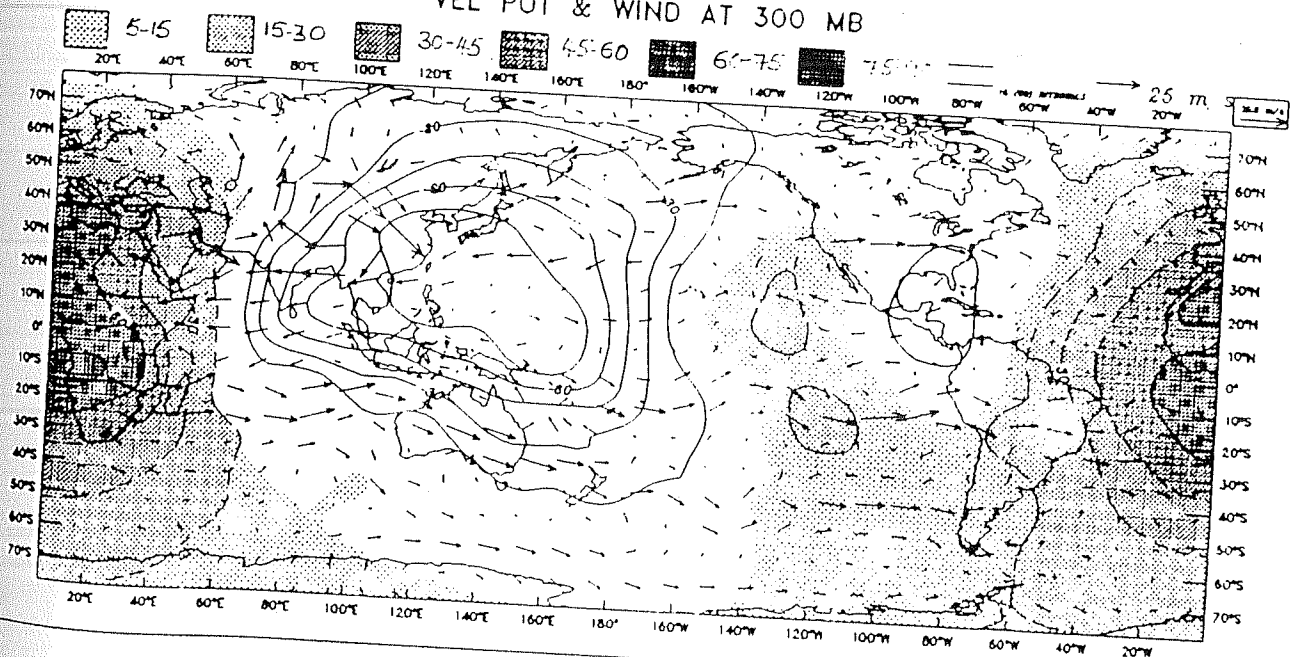


Fig.3.3.6a. (Top) Same as Fig.3.2.6a, except for summer (1979). Interval $900 \text{ m}^2 \text{ s}^{-2}$.
Fig.3.3.6b. (Bottom) Same as Fig.3.2.6b, except for summer (1979). Interval $15 \times 10^5 \text{ m}^2 \text{ s}^{-1}$.

comparable to that of the Hadley circulation. The mean flow at the upper levels was characterized by the Tibetan and Mexican anticyclones and mid-oceanic troughs over the Atlantic and the Pacific. He showed that the east-west circulations were important in generating kinetic energy of the quasi-stationary planetary scale waves. Significant amount of kinetic energy was transferred by wavenumber 1 to the zonal flows during the northern summer.

I_w and I_h for summer 1979 have been calculated and are shown in Figures 3.3.7a and 3.3.7b respectively. Fig.3.3.7a shows the longitudinal variation of the intensity of east-west circulation at 300 mb averaged between 2°N and 29°N . The negative peaks of I_w indicate regions of easterly predominance and the positive peaks represent regions of westerly predominance. There are two negative peaks and two positive peaks, suggesting the existence of two major convectively active regions during summer (1979) (i.e., heating over the Indian monsoon region and over Mexico). The sharp negative peak at around 70°E corresponds to the strong easterlies associated with the Tibetan anticyclone. A second negative peak at around 250°E is associated with the anticyclonic flow over Mexico. The positive peaks around 200°E and 300°E correspond to the eastward branch of the divergent circulations forced by these two heat sources. Fig.3.3.7b shows the meridional variation of the intensity of the Hadley circulation averaged for the longitudes between 61°E and 118°E . This longitudinal span covers the Arabian sea, the Indian ocean and the northern summer monsoon region. The positive peak (southerly flow) of I_h at around 33°N indicates that the Hadley circulation was most intense over the Tibetan plateau. At around 3°S , there is a negative peak which represents the northerly component of the Tibetan anticyclone.

The east-west circulations induced by the heat source over the Indian summer monsoon region play a crucial role in determining the monsoonal activity over

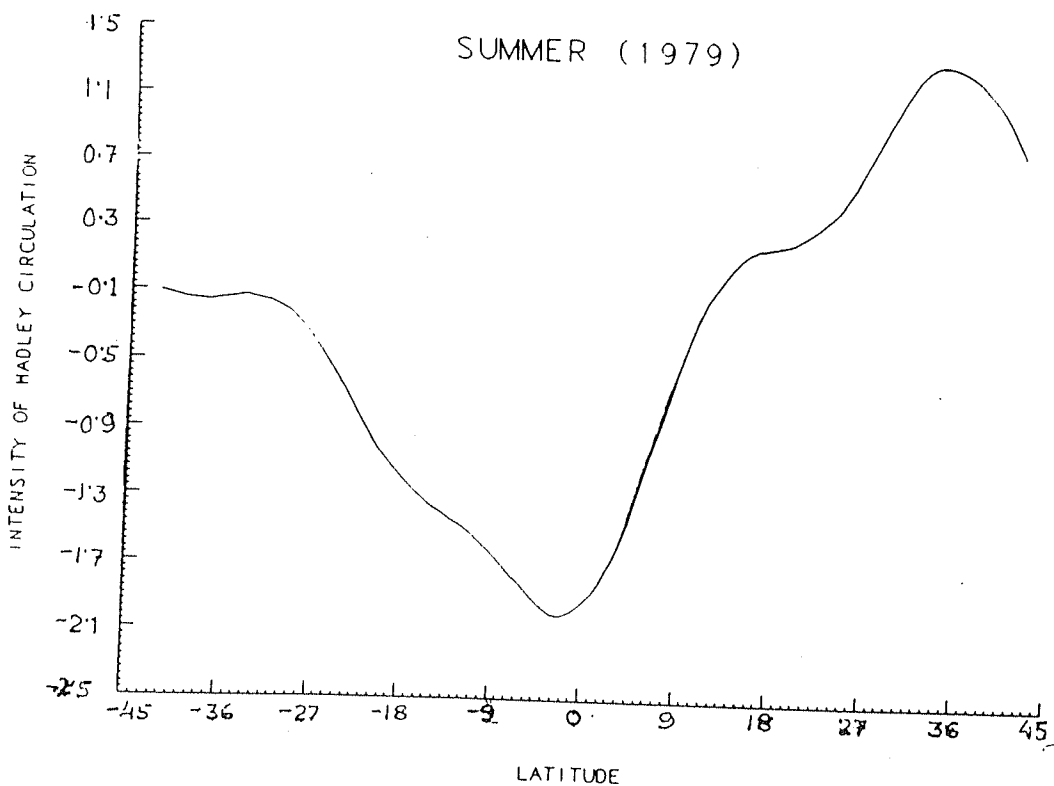
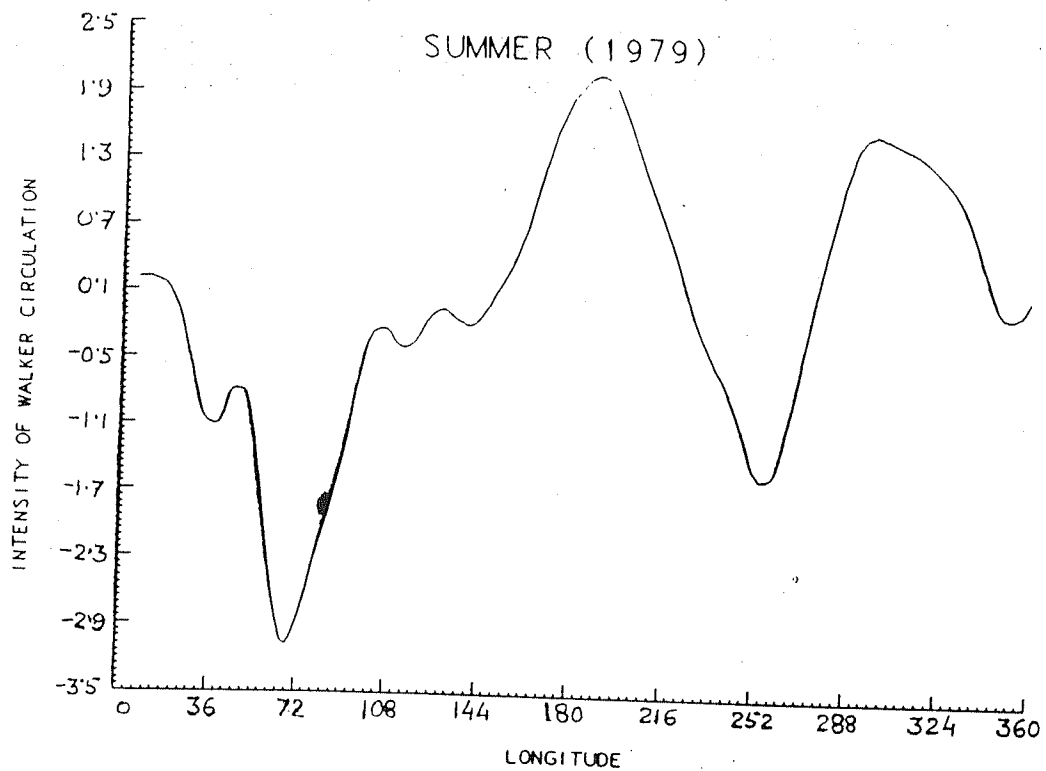


Fig.3.3.7a. (Top) Same as Fig.3.2.7a, except for summer (1979).
 Fig.3.3.7b. (Bottom) Same as Fig.3.2.7b, except for summer (1979).

north west India. The diabatic heating during summer months is generally characterized by convective heating over northeast India and radiative cooling over Rajasthan, Pakistan and Iran. This zonally asymmetric heating pattern sets up divergent circulations, with vertical ascent taking place over northeast India and sinking motion over Rajasthan and further west. Krishnamurti (1971) has shown that this east-west circulation is as intense as the monsoon meridional circulation. Observations indicate that during certain years there is an east-west shift in the relative positions of the heat source over northeast India and the heat sink over the desert regions in the west. As a consequence of this longitudinal displacement, the subsidence over Rajasthan and Pakistan becomes stronger. This enhanced subsidence creates stable atmospheric condition which inhibits upward motions and convective activity. This leads to poor rainfall over Rajasthan and northwest India and hence drought conditions prevail over the region.

The summer of 1979 was characterized by poor rainfall over northwest India. A magnified view of the circulation patterns during summer 1979 reveals some interesting circulation features associated with the weak monsoon situation over northwest India. The vertically integrated heating for summer 1979, for the domain 40°E and 120°E ; 45°S and 45°N , is shown in Fig. 3.3.8a. Strong heating rates of the order of 3°K per day occur at around 27°N and 95°E . Radiative cooling of the order of 1.0°K per day extends longitudinally between 40°E and 72°E . The July mean velocity potential at 300 mb and the winds at 300 mb and 900 mb, computed from the 5-level nonlinear global spectral model, are shown in Figs. 3.3.8b, 3.3.8c and 3.3.8d respectively. The Tibetan anticyclone at the upper levels is well reproduced and the core of upper level easterly jet is seen at around 20°N (Fig. 3.3.8c). The cross-equatorial flow and the south westerly monsoon flow at 900 mb are well depicted in Fig. 3.3.8d. The region of strong outward flow, which is indicated by the negative contours of velocity potential, extends from about 75°E to about 120°E and the maximum divergence takes place

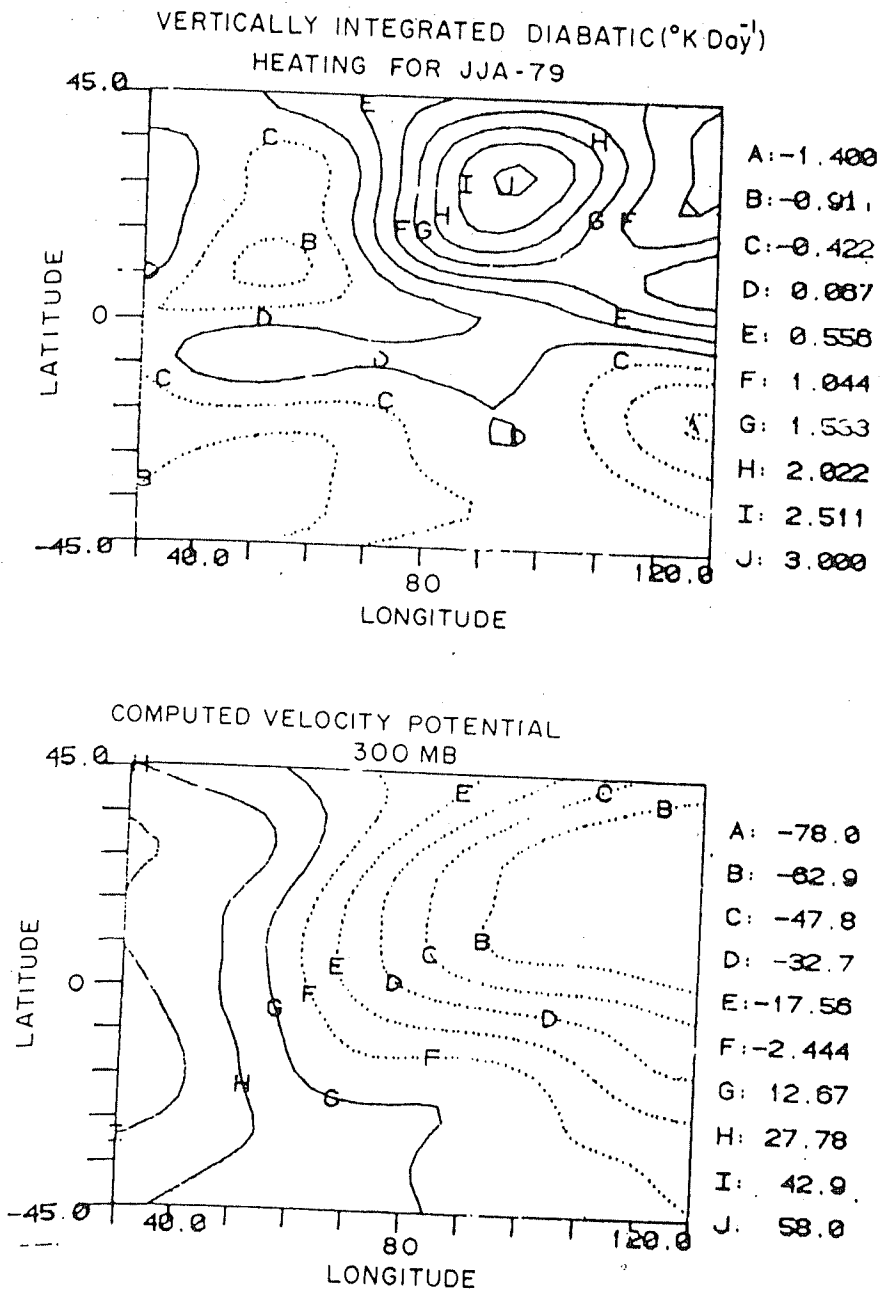
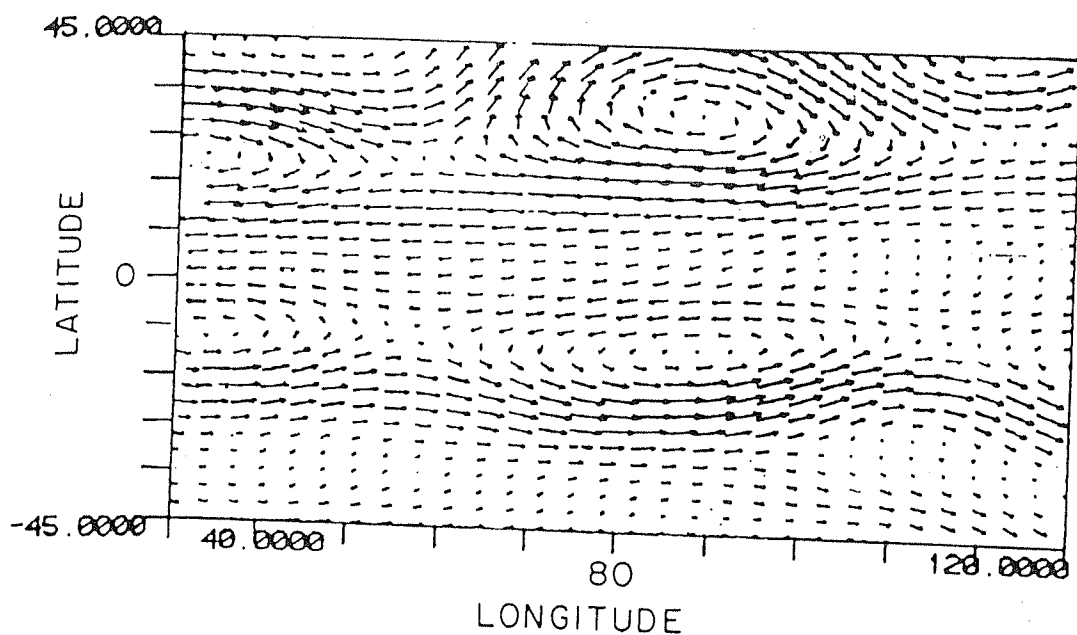


Fig.3.3.8a. (Top) Vertically averaged diabatic heating during July (1979), over the northern summer monsoon region. Interval 0.5°K per day.

Fig.3.3.8b. (Bottom) Computed velocity potential at 300 mb over the summer (1979) monsoon region, using 5-level nonlinear model. Interval $15 \times 10^5 \text{m}^2 \text{s}^{-1}$.

WIND VECTOR AT 300 MB



WIND VECTOR AT 900 MB

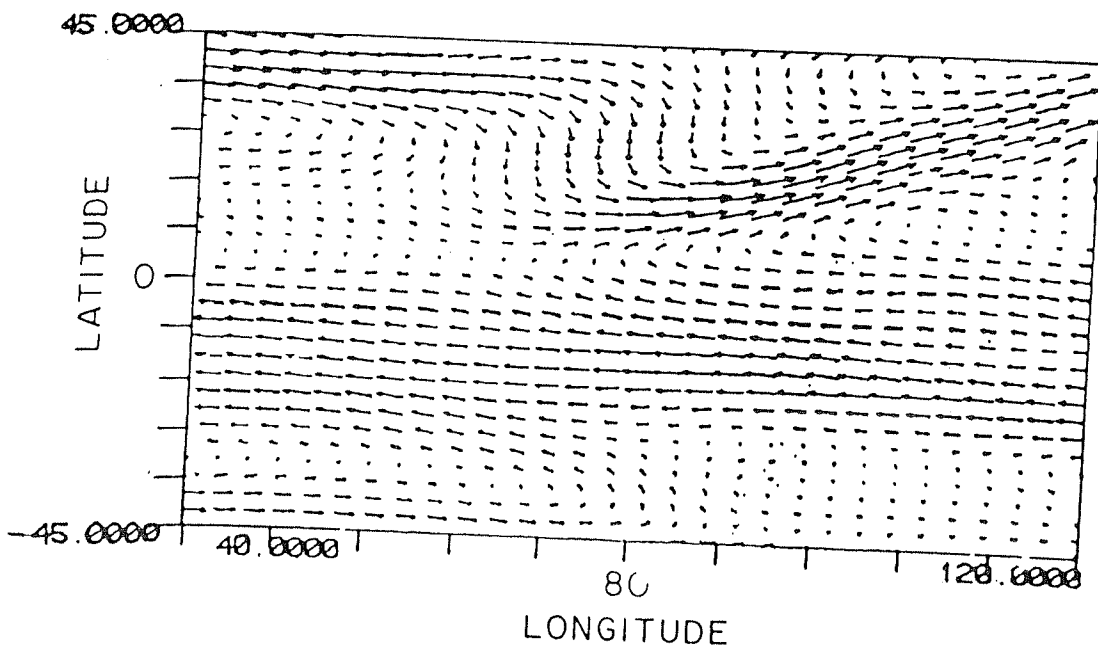


Fig.3.3.8c. (Top) Computed horizontal wind vectors at 300 mb over the summer (1979) monsoon region, using 5-level nonlinear model.
 Fig.3.3.8d. (Bottom) Same as Fig.3.3.8c, except for 900 mb.

at around 110° . The positive contours of velocity potential represent upper level convergence followed by descending motions. It can be seen that there is an enhanced subsidence taking place at around 72°E and further west. This strong subsidence is unfavourable for convective activity and possibly explains the poor rainfall scenario in the northwest India during summer 1979.

3.4 Conclusions

A summary of the main results of the winter (1978-79) and summer (1979) forcing experiments is given below. The objective of this study was to understand the time-mean Walker and Hadley-type circulations during the above seasons, within the framework of a 2-level linear equatorial β -plane model and a 5-level nonlinear global spectral model. The models were forced using the observed time-mean heating for winter (1978-79) and summer (1979), based on Schaack *et.al* (1990), and the steady-state responses were calculated for both the seasons.

Observations suggest that during January (1979), intense convection occurred over the western Pacific, Australia, equatorial South America and Africa. Substantial longwave cooling was observed over the south central and south eastern Pacific oceans, west of Australia, east Asia, Pakistan and Iran and north Africa. This large zonally asymmetric heating resulted in strong Walker circulation over the equatorial Pacific, Atlantic and Indian oceans. It was found that both the 2-level linear model and the 5-level nonlinear model reproduced the gross structure of the time-mean circulations, such as the Walker circulation in the equatorial Pacific, the upper level anticyclone over Australia and the upper level lows over east Asia, Mexico and over the oceanic region to the west of Australia. However, the intensities of the Walker circulations and the stationary waves were weak in the case of the 2-level model. In the 2-level model the

vertical variation of the forcing is essentially restricted to the first baroclinic mode. On the other hand the 5-level nonlinear global spectral model was forced using the heating at all the five model levels. The time-mean circulations were quite strong and realistic in this case. Sumi and Murakami (1981) noted that the maximum convective activity was centered in the western Pacific and Australia during winter (1978-79) whereas it was mostly located over Indonesia in the previous years. The low level cyclonic circulation over Australia and the anticyclonic vortex to its west were simulated quite well in the 5-level model and conformed with the observations of Sumi and Murakami (1981). The structure and intensity of the Walker circulation in the equatorial Pacific and the upper level easterlies, associated with the Rossby waves, to the west of South America matched well with the observations. The accurate vertical structure of the prescribed forcing and also the presence of nonlinear advection terms were mainly responsible for the more realistic simulation of the tropical time-mean response in the 5-level nonlinear model. Using the velocity potential at 300 mb, the strengths of the Walker and Hadley-type of circulations have been computed. The zonal variation in the intensity of Walker circulation, based on the velocity potential field at 300 mb, clearly exhibited the intense east-west circulation to the west of South America and the strong upper level westerlies associated with the Walker circulation over the central equatorial Pacific. The major tropical divergent circulations associated with the three primary convective zones were distinctly evident from the longitudinal variation of the intensity of Walker circulation. The Hadley-type circulation in the region of western Pacific was strongest near the equator. In the southern hemisphere, the meridional circulation associated with the circulation to the west of Australia exhibited a strong northerly component.

During July (1979) the primary heat sources were located over the Bay of Bengal, Tibetan plateau, northeast India and the highlands of Mexico. Significant cooling was seen over Pakistan, Iran, Australia and the oceanic regions of south and north

Pacific and Atlantic. The time-mean response of the 2-level linear equatorial β -plane model to the heating during July (1979), brought out the gross upper level features like the Tibetan and Mexican anticyclones and their associated easterlies. Similarly, the southern hemispheric subtropical westerlies and the westerlies associated with the east-west circulations in the northern hemisphere agreed qualitatively with observations. However, the speed of the upper level easterlies over the Indian monsoon region and the westerlies associated with the major divergent circulations were quite weak. The 5-level nonlinear global spectral model, on the other hand, reproduced the structure and intensity of the upper as well the lower level circulations quite well. The Tibetan and Mexican highs were quite intense and the upper level easterlies over these regions were strong. The east-west circulations at the 300 mb level was characterized by outflow over northeast India and Mexico and convergence in the regions of Pakistan, Iran, Saudi Arabia, Africa and the mid-oceanic regions of Pacific and Atlantic oceans were quite realistic. In addition, the low-level southwest monsoon flow and also the cross-equatorial flow simulated by the 5-level model matched well with the observed flow patterns given in Krishnamurti (1985). The accurate vertical structure of heating in the 5-level nonlinear model was mainly responsible for the better simulation of the summer (1979) circulation. In addition, the equations in the 5-level model were fully nonlinear while those in the 2-level model were linearized w.r.t a zero basic state. The inclusion of nonlinear terms in the 5-level model was also an important factor that contributed for the realistic time-mean circulations especially in the low latitude regions. A calculation of the intensities of the east-west and Hadley circulations during summer (1979), based on the velocity potential at 300 mb, suggests that the strongest east-west circulation was associated with the rising motion over northeast India and sinking motion over the Rajasthan, Pakistan and further west. This enhanced subsidence supports the fact that poor rainfall conditions prevailed over northwest India during summer 1979. The longitudinal variation of the

east-west circulation, showed two distinct westerly peaks corresponding to the two convective heat sources over northeast India and Mexico respectively. The intensity curve of the Hadley circulation over the northern summer region showed that southerlies dominated in the region of Tibet, while strong northerly winds were prevalent in the equatorial region.

Chapter 4

A Study of the Vorticity Balance in the Tropical Upper Troposphere

4.1 Introduction

A simple scale analysis, of the large scale motions in the tropical atmosphere, suggests that the primary thermodynamical balance occurs between the diabatic heating (cooling) term and the adiabatic cooling (warming) due to vertical ascent (descent). This essentially means that, in the tropics, the thermodynamic energy equation can be approximated as a diagnostic balance relation. Similarly, if one considers the tropical atmospheric motions having large spatial and temporal scales, it can be shown that the divergence equation also reduces to a balance condition. We are therefore effectively left with a single prognostic relation (i.e., the vorticity equation) which contains vital information regarding the spatial and temporal evolutionary characteristics of the large scale circulations in the tropical atmosphere. Hence, a diagnostic analysis of the various terms in the vorticity equation can be used as a powerful tool to understand the dynamics of the atmospheric motions in the tropics. The relevance of this study is to examine the nature of vorticity balance that governs the time-mean

circulations in the tropical atmosphere.

4.1.1 Observational and diagnostic studies

Let us begin our discussion with some of the important observational features associated with large scale motions in tropics. Krishnamurti (1971) and Krishnamurti *et.al* (1973) have given a comprehensive account of the planetary scale east-west circulations and quasi-stationary waves, during the northern summer and winter months. The salient features of the upper tropospheric circulations during the northern summer, are the Tibetan and Mexican anticyclones, the easterly jet over south east Asia, the mid-oceanic troughs over the Atlantic and Pacific and finally the southern hemispheric westerly subtropical jet. Krishnamurti (1971) found that the thermally direct east-west overturnings, caused by land-ocean heating and zonal asymmetries, were more pronounced in the northern summer than during other seasons. It was found that the convective latent heat release, which was the major component of heating, had maximum intensity over the Tibetan and Mexican highlands. The zonal temperature contrast at the upper levels between the warm southwest monsoon circulation over Asia and the oceanic trough over the Pacific was shown to be as large as 25°C . Krishnamurti (1971) found that the intensity of the east-west circulations was comparable to that of the Hadley type circulation. During winter, intense convective heating occurs over the maritime continent of Malaysia-Indonesia resulting in upper tropospheric anticyclones over south China sea and western Pacific. In addition, two weak highs appear over equatorial eastern Africa and the northern part of South America. Oceanic troughs can be seen extending from the equator to the southern subtropics. The most outstanding feature during the winter as well as the summer months is an almost exact out of phase relation between the observed vorticity and divergence fields in the upper troposphere.

Many observational and diagnostic studies have examined the vorticity dynamics in the tropical atmosphere and estimated the significance of vertical transport of vorticity by cumulus convection. Williams and Gray (1973), Reed and Johnson (1974), Hodur and Fein (1977) and Chu *et.al* (1981) have performed vorticity budget analyses over the tropical western Pacific. Reed and Johnson (1974) found that there existed an apparent vorticity sink for the large-scale motions in the lower half of the troposphere and an apparent vorticity source in the upper troposphere. They attributed this to the removal of vorticity-rich air from the lower layers and its deposition at the upper layers by deep convection. Hodur and Fein (1977) found that subgrid scale cumulus convection processes played an important role in the vertical transport of vorticity in the tropical oceanic region. Similar diagnostic studies over the eastern Atlantic ocean have been carried out, using the data from GARP Atlantic Tropical Experiment (GATE), by Shapiro (1978), Stevens (1979) and Reeves *et.al* (1979). Shapiro (1978) and Stevens (1979) studied the synoptic scale wave disturbances over Africa and eastern Atlantic and found that the disturbances were governed by linear dynamics. Reeves *et.al* (1979) examined the interrelationship between the convective scale precipitation and the large scale wind field using the upper air and surface data from the GATE. They concluded that vorticity was transported from the surface to the top of the atmosphere due to cumulus convection. In a similar study, Sui and Yanai (1986) have shown that organized cumulus convection affects the large scale vorticity budget, resulting in the deceleration of upper tropospheric flow. Fein (1977) evaluated the large scale terms in the vorticity equation using the summer mean fields at 200 mb from Krishnamurti's (1971) analysis. His study showed that there is a requirement for a subgrid scale mechanism which rapidly removes negative vorticity from the regions of strong divergence (Tibetan and Mexican highlands) and removes positive vorticity from the regions of strong convergence (mid-oceanic troughs) at 200 mb. He concluded that over regions of strong and persistent convection such as

the Tibetan plateau, deep cumulus clouds can account for the transport. However, the mechanism for removing positive vorticity in the vicinity of upper tropospheric mid-oceanic troughs was still not clearly understood.

4.1.2 Theoretical studies based on linearized models

Holton and Colton (1972) employed a linearized barotropic steady state vorticity equation to study the vorticity balance at the upper troposphere during JJA 1967. The barotropic vorticity equation, linearized about the zonal mean wind $[\bar{u}]$, is given below. The zonal mean is denoted by $[\]$ and the deviation from the zonal mean by $*$. Similarly, an overbar denotes the time-mean and a prime denotes the deviation from the time-mean.

$$\frac{[\bar{u}]}{a \cos \phi} \frac{\partial \nabla^2 \psi^*}{\partial \lambda} + \frac{1}{a \cos \phi} \frac{\partial \psi^*}{\partial \lambda} \left(\beta + \frac{1}{a} \frac{[\partial \bar{\zeta}]}{\partial \phi} \right) = - \left(f + [\bar{\zeta}] \right) \nabla \cdot \vec{V} - \epsilon \nabla^2 \psi^* \quad (4.1)$$

They linearized the vorticity equation about a zonal mean flow at 200 mb and forced it by the observed time-mean horizontal divergence. In (4.1), $-(f + \bar{\zeta}) \nabla \cdot \vec{V}$ is the time-independent forcing at 200 mb. The zonal mean flow at 200 mb ($[\bar{u}]$ and $[\bar{\zeta}]$) and the time-mean horizontal divergence for JJA 1967 were obtained from Krishnamurti's (1971) analysis. They calculated the response to the observed forcing, by solving (4.1) for different values of ϵ . It was found that the calculated streamfunction resembled the observed streamfunction only for the values of ϵ corresponding to damping times of less than one day. However when a weak vorticity dissipation was used, the mismatch between the calculated and observed streamfunction distribution at 200 mb was large. It can be seen from Figs. 4.1a and 4.1b that, in the presence of a strong viscous damping of vorticity ($1.5 \times 10^{-5} S^{-1}$), the structure and intensity of the upper level easterlies and the Tibetan anticyclone closely match with the observed flow field.

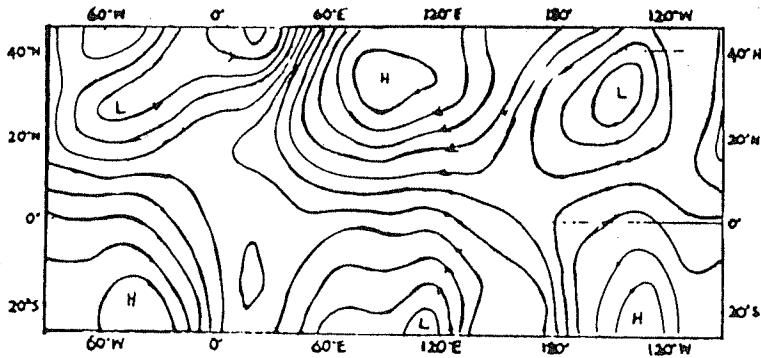
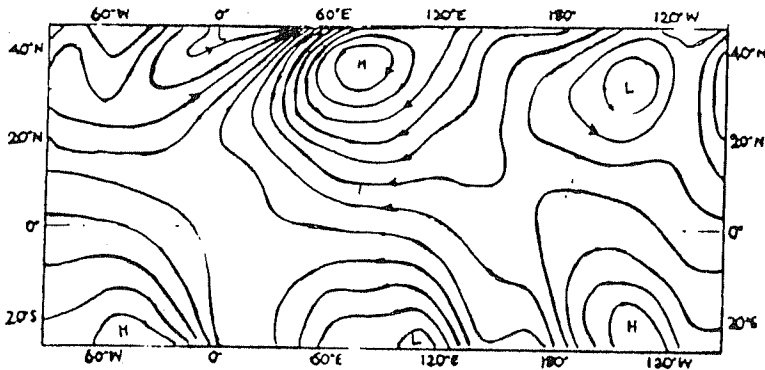


Fig.4.1a. (Top) Observed 200 mb perturbation streamfunction during summer 1967. (Adapted from Holton and Colton (1972)). Interval $5 \times 10^6 m^2 s^{-1}$.

Fig.4.1b. (Bottom) Computed perturbation streamfunction using linear barotropic vorticity model, for damping rate of $1.5 \times 10^{-5} S^{-1}$. (Adapted from Holton and Colton (1972)). Interval $5 \times 10^6 m^2 s^{-1}$.



It was proposed that the vorticity damping at the upper layers could arise because of vertical transport of horizontal momentum due to deep cumulus convection. They conjectured that the deep cumulonimbus towers in the tropics could transport vorticity directly from the boundary layer to the outflow level at 200 mb within a time scale of one day. The vorticity is subsequently deposited at 200 mb which later on decays quite rapidly.

4.1.3 Theoretical studies based on nonlinear models

The significance of nonlinear dynamics in the tropical upper troposphere has been pointed out by several investigators. Colton (1973) examined the nonlinear interactions between quasi-stationary long waves and transient synoptic waves in the tropical upper troposphere. He showed that a nonlinear barotropic energy exchange between large scale quasi-stationary forced waves and transient synoptic scale waves was important in producing several features of the upper tropospheric general circulation (for example, the vortices and small scale waves present in the mid-oceanic troughs and the disturbances that form along the easterly jet over the Indian ocean). He also found that the nonlinear transfer of energy to smaller scales of motion acted as a damping mechanism to the large scale forced circulation. Chang (1977) has shown that the barotropic instability associated with the planetary scale summer monsoon leads to a strong nonlinear energy transfer which appears to be quite relevant to the damping of planetary scale flows during the summer monsoon. Kanamitsu (1977) performed model studies and obtained a reasonable position of the Tibetan high even without the inclusion of strong damping. His vorticity budget study at 200 mb suggested that the advection of relative vorticity by the divergent part of the flow is one of the leading terms of the vorticity equation. His study indicated that the tropical quasi-stationary ultralong waves are fully nonlinear and nongeostrophic during the

Indian Summer Monsoon. Cho *et.al* (1983) studied the vorticity dynamics of tropical easterly waves obtained in GATE using a simplified vorticity equation and found that horizontal advection of vorticity by the African easterly jet considerably influenced the evolution of the vorticity field. Sardeshmukh and Held (1984) studied the vorticity budget in the upper tropospheric levels of the tropical atmosphere based on GCM simulations of the northern summer monsoon performed at Geophysical Fluid Dynamics Laboratory (GFDL). The model did not have explicit momentum transfer in the cumulus parameterization. The model could still simulate the 200 mb circulation and the Tibetan anticyclone quite realistically. However, on forcing the linearized barotropic vorticity equation using the model's zonal mean flow and mean divergence, the Tibetan anticyclone could be reproduced only when large values of the damping coefficient were used. This damping was found to crudely account for the neglected nonlinear horizontal advection. Their study showed that nonlinear interactions in the tropics could possibly play the role of vorticity damping.

In a subsequent study, Sardeshmukh and Hoskins (1985) carried out detailed budget analysis of the vorticity balance at 150 mb in the tropics during December 1982 to February 1983. This season was characterized by warm SST anomalies over the central and east equatorial Pacific ocean. There was a shift of the maximum tropical rainfall and cloudiness from Indonesia - New Guinea to the central Pacific. The observations of 1982-83 El Niño-Southern Oscillation (ENSO) by Quiroz (1983), Rasmusson and Wallace (1983) clearly indicate anomalous low level westerlies to the west of the heating anomaly. Anticyclones were seen straddling the equator at the same longitude as the heating anomaly. They found that the observed anomalies at 150 mb could not be modelled within the frame work of a steady state model linearized about a basic flow at rest, where the vorticity equation takes the form:

$$\beta v = -f \nabla \cdot \vec{V} - \epsilon \zeta \quad (4.2)$$

where $f = \beta y$. For small ϵ , the vorticity source $f \frac{\partial \omega}{\partial p}$ is balanced by βv with a result that the high at the upper level always occurs to the west of the heating region. But observations (eg., Krishnamurti (1971)) suggest that the upper level anticyclone is almost in phase with the heating distribution. Therefore linear models have no option but to employ a strong vorticity damping, as a result of which, a balance between the vorticity source term and the friction term occurs, thus overcoming the phase-shift problem. The strong damping, used in the linear models, is often associated with the vertical transport of vorticity in cumulus towers. It should however be noted that the GCM simulations of Blackmon *et.al* (1983), Sardeshmukh and Held (1984) and the nonlinear model calculation of Hendon (1986) have overcome the phase-shift problem inspite of not incorporating vertical momentum transport in the cumulus convection parameterization. Using a nonlinear model, Hendon (1986) calculated the steady state response due to an isolated heat source symmetric w.r.t the equator. He showed that when the forcing was quite large, the nonlinear advection terms displaced the upper level anticyclones eastwards to the same longitude as the heating. The vorticity budget calculations of Sardeshmukh and Hoskins (1985) revealed that the dominant vorticity balance in the tropics was between the stretching and advection of absolute vorticity by the time-mean horizontal flow. In another study, Sardeshmukh and Hoskins (1988) have shown that the advection of vorticity by the divergent component of the flow is very important in determining the response to tropical heating.

4.2 Motivation for the present study

From the above mentioned studies of the vorticity balance in the tropics, we have seen that there are differences between the linear and nonlinear calculations. The

linear calculations assume a large vorticity damping, which is associated with vertical transport of momentum by cumulus convection, in order to explain the observed circulation features. In other words, the linear models assume that deep cumulus clouds rapidly transport vorticity from the boundary layer to the top of the atmosphere in < 1 day. However, such a rapid decay of the upper tropospheric vorticity may not be quite physical. On the contrary, the nonlinear calculations indicate that nonlinearities play a more fundamental role in determining the observed time-mean vorticity balance in the tropics. The nonlinear studies also indicate that the vertical transport of momentum by cumulus convection has only secondary effects on the time-mean large scale circulation in the tropics.

In Chapter II, we had studied the impact of nonlinear terms on the quasi stationary waves in the tropical atmosphere. It was shown that nonlinearities can significantly modify the structure of the time-mean response in the vicinity of a strong convective heat source. One can actually estimate the nonlinear effects in the tropical atmosphere, by performing diagnostic calculations of the vorticity equation. In this chapter, we shall carry out vorticity budget calculations, using the output fields generated from steady state forcing experiments with a 5-level nonlinear global spectral model. Our intention is to understand the nature of vorticity balance in the tropical upper troposphere. The analysis will be carried out for the data sets generated by three different forcing experiments with the 5-level nonlinear global spectral model.

- Model forced with an idealized heating distribution.
- Model forced with the diabatic heating for DJF-(1978-79).
- Model forced with the diabatic heating for JJA-(1979).

Sardeshmukh and Hoskins (1985) assumed that the vertical advection and twisting terms are quite small in the tropics. In our study we have made an assessment of the

various terms in the vorticity equation, including the vertical advection and twisting terms, and their contribution towards the vorticity balance in the tropical upper troposphere.

4.3 The terms in the vorticity equation

Let us now consider the vorticity equation in pressure coordinates. The external sources and sinks and subgrid-scale processes are ignored in the equation.

$$\frac{\partial \zeta}{\partial t} + \vec{V} \cdot \nabla (\zeta + f) + \hat{k} \cdot \nabla \times \left(\omega \frac{\partial \vec{V}}{\partial p} \right) = -(\zeta + f) \nabla \cdot \vec{V} \quad (4.3)$$

In (4.3) ω is the vertical p velocity, $\vec{V} \cdot \nabla (\zeta + f)$ represents the advection of absolute vorticity by the horizontal wind and $\hat{k} \cdot \nabla \times \left(\omega \frac{\partial \vec{V}}{\partial p} \right)$ is the vertical advection and twisting term. The term $-(\zeta + f) \nabla \cdot \vec{V}$ represents the stretching term. Equation (4.3) is now averaged over a period of time. The vorticity balance reduces to

$$\overline{\vec{V} \cdot \nabla (\zeta + f)} + \hat{k} \cdot \nabla \times \overline{\left(\omega \frac{\partial \vec{V}}{\partial p} \right)} = -\overline{(\zeta + f) \nabla \cdot \vec{V}} \quad (4.4)$$

One can rewrite 4.4 as:

$$\begin{aligned} \bar{\vec{V}} \cdot \nabla (\bar{\zeta} + f) + \overline{\vec{V}' \cdot \nabla \zeta'} + \hat{k} \cdot \nabla \times \left(\bar{\omega} \frac{\partial \bar{\vec{V}}}{\partial p} \right) + \hat{k} \cdot \nabla \times \overline{\left(\omega' \frac{\partial \vec{V}'}{\partial p} \right)} \\ = -(\bar{\zeta} + f) \nabla \cdot \bar{\vec{V}} - \overline{\zeta' \nabla \cdot \vec{V}'} \end{aligned} \quad (4.5)$$

For convenience we shall refer the terms involving the time-mean namely, $\bar{\vec{V}} \cdot \nabla$

$(\bar{\zeta} + f)$ as M1, $-(\bar{\zeta} + f) \nabla \cdot \bar{\vec{V}}$ as M2 and $\hat{k} \cdot \nabla \times \left(\bar{\omega} \frac{\partial \bar{\vec{V}}}{\partial p} \right)$ as M3. The terms involving the transients namely, $\overline{\vec{V}' \cdot \nabla \zeta'}$ as T1, $-\overline{\zeta' \nabla \cdot \vec{V}'}$ as T2, and $\hat{k} \cdot \nabla \times \left(\overline{\omega' \frac{\partial \vec{V}'}{\partial p}} \right)$ as T3.

4.4 Vorticity balance at 300 mb in a global spectral model

We first consider the case of an idealized forcing which essentially is a combination of a heat source and heat sink symmetric w.r.t the equator (Fig.4.2a). The centres of the heat source and the heat sink are separated by 112.5° longitudes. This form of forcing very crudely mimics the heating in the western Pacific and the longwave cooling in the eastern Pacific. The vertical distribution of the forcing is of the form $\sin\left(\frac{\pi p}{p_0}\right)$ which has a maximum value at 500 mb and a minimum at the surface and top of the atmosphere. Using the above forcing the model was integrated for a period of 70 days until a steady state was reached. A weak Rayleigh friction having a dissipation time scale of 15 days was used in the model. The stationary Kelvin and Rossby waves induced by this form of forcing have already been discussed thoroughly in Chapter II. The region of the Walker circulation between the heat source and the heat sink is characterized by upper level westerlies and lower level easterlies. There is rising motion over the heating region and subsidence over the heat-sink. The steady-state streamfunction and velocity potential at 300 mb are shown in Figs.4.2b and 4.2c respectively. It can be seen from Fig.4.2b, that in the region between the source and the sink, the streamfunction at 300 mb has the structure of a dipole in the meridional direction. From the velocity potential distribution at 300 mb, one can infer the regions of divergence and convergence at the upper level. The negative (positive) contours of velocity potential correspond to regions of outflow (inflow). It is evident

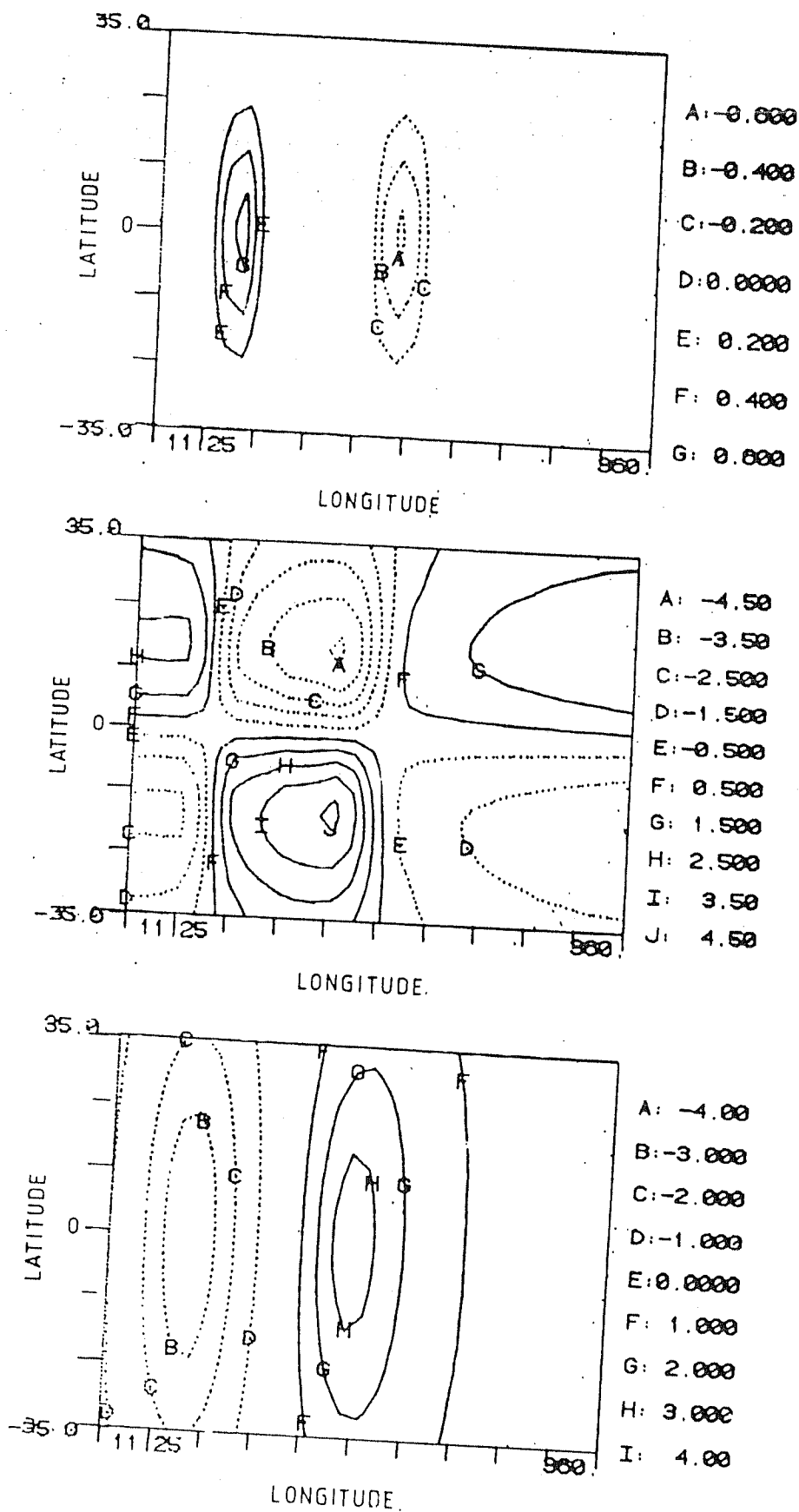


Fig.4.2a. (Top) Latitude-longitude section of vertically averaged heating (idealized case). Interval 0.2°K per day.

Fig.4.2b. (Middle) Computed streamfunction at 300 mb using 5-level nonlinear global spectral model. Forcing in Fig.4.2a used. Interval $1 \times 10^6 \text{m}^2 \text{s}^{-1}$.

Fig.4.2c. (Lower) Same as Fig.4.2b, except for velocity potential. Interval $1 \times 10^6 \text{m}^2 \text{s}^{-1}$.

from Fig.4.2c that at the upper levels, there is strong divergence in the region of the heat source and a converging flow over the heat sink. The meridional gradient of the streamfunction, in between the heat source and heat sink, is negative. In addition, the longitudinal gradient of the velocity potential is positive. The meridional gradient of the streamfunction and the zonal gradient of the velocity potential, in the region between the heat source and the heat sink, consistently support the westerlies at 300 mb.

The time mean and transient terms of the vorticity equation are constructed using the fields from day 50 to day 70. The different terms of the equation 4.5 are shown in Figs.4.3a-4.3f. Area average values for these terms are shown in Table.4.1. These averages are calculated for the domain: 67.5°E to 157°E in the zonal direction and 3.4°N to 44.1°N in the meridional direction, which represents the region between the heat source and the heat sink. It can be clearly seen from the area average values that the advection of absolute vorticity by the time-mean horizontal wind ($M1 = 5.3 \times 10^{-12} S^{-2}$) and the vorticity stretching term due to the time-mean wind ($M2 = 4.4 \times 10^{-12} S^{-2}$) are the dominant terms in the vorticity equation. In addition it can be noted from Fig.4.3a and Fig.4.3b that the structure and magnitude of the terms $M1$ and $M2$ nearly match. This indicates that the predominant vorticity balance, in the tropical upper troposphere, is between the horizontal advection of absolute vorticity and the vorticity stretching term. It should be recognized that this balance has been achieved in the presence of a very weak Rayleigh friction in the model. The advection of absolute vorticity by horizontal wind ($M1$) and the absolute vorticity stretching by the horizontal divergence ($M2$) are basically nonlinear terms in the vorticity equation. Therefore, a primary balance between the terms $M1$ and $M2$ as seen from Figs.4.3a and 4.3b, highlights the significance of nonlinear dynamics in the tropical upper troposphere. It is further seen from Fig.4.3c that the term representing the time-mean vertical advection and twisting of vorticity ($M3$) is three

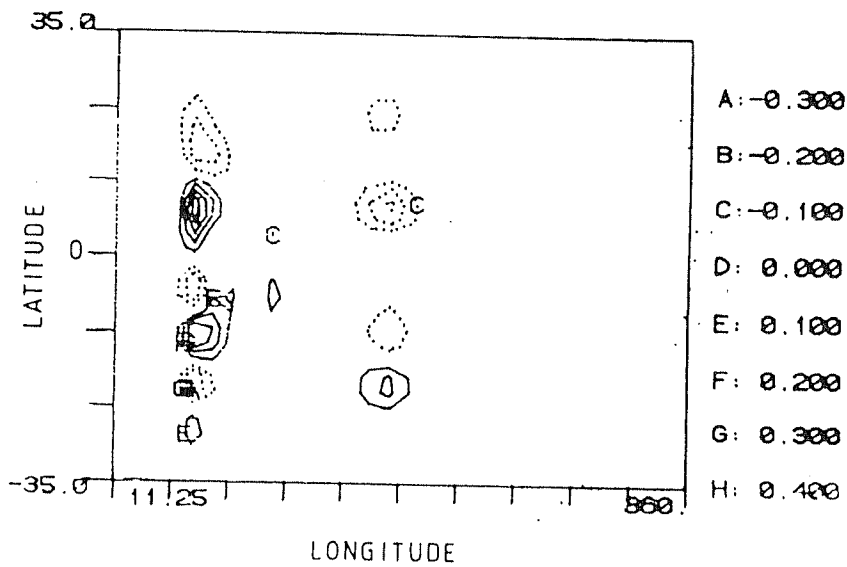
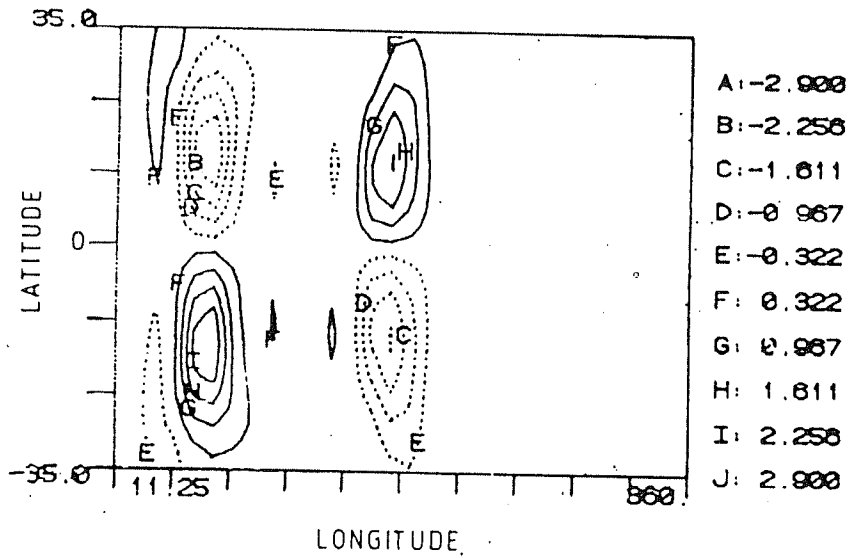
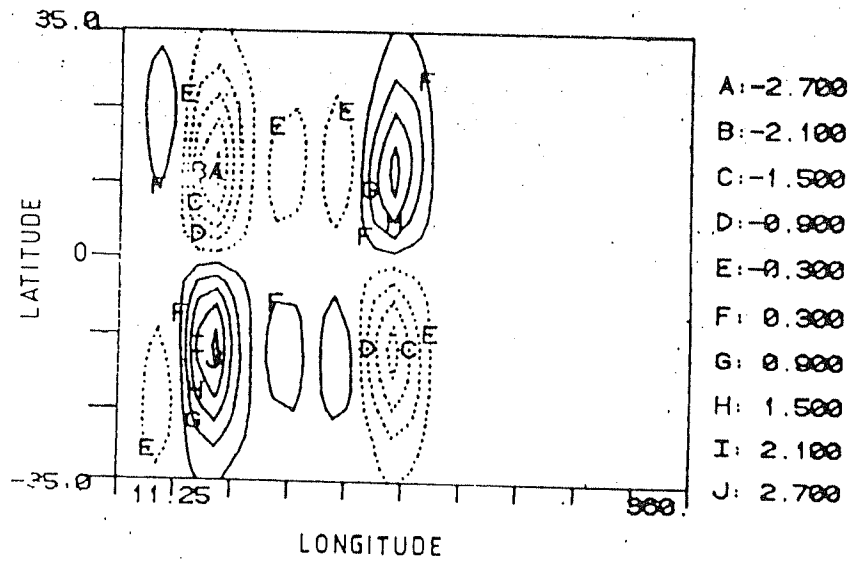


Fig.4.3a. (Top) Latitude-longitude section of Term M1. Case of Idealized forcing. Interval $0.6 \times 10^{-11} s^{-2}$.

Fig.4.3b. (Middle) Same as Fig.4.3a, except for term M2. Interval $0.64 \times 10^{-11} s^{-2}$.

Fig.4.3c. (Lower) Same as Fig.4.3a, except for term M3. Interval $0.1 \times 10^{-11} s^{-2}$.

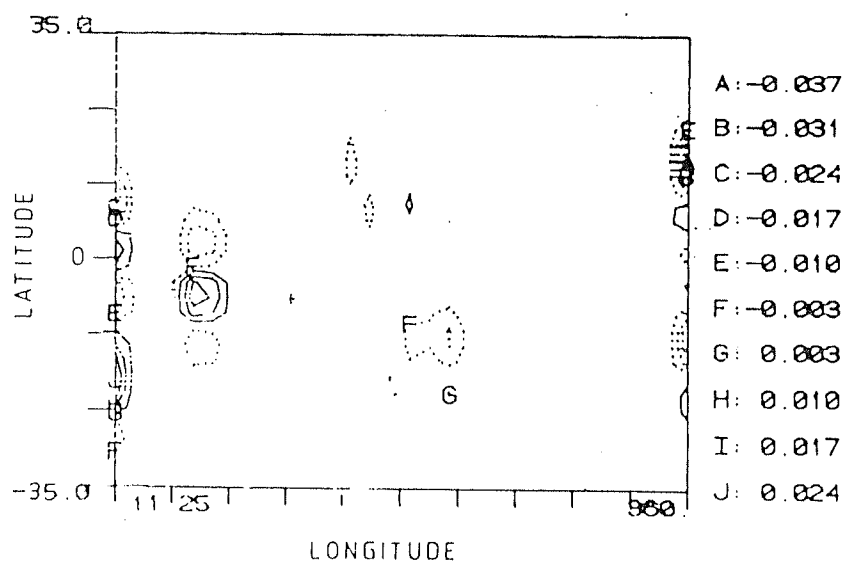
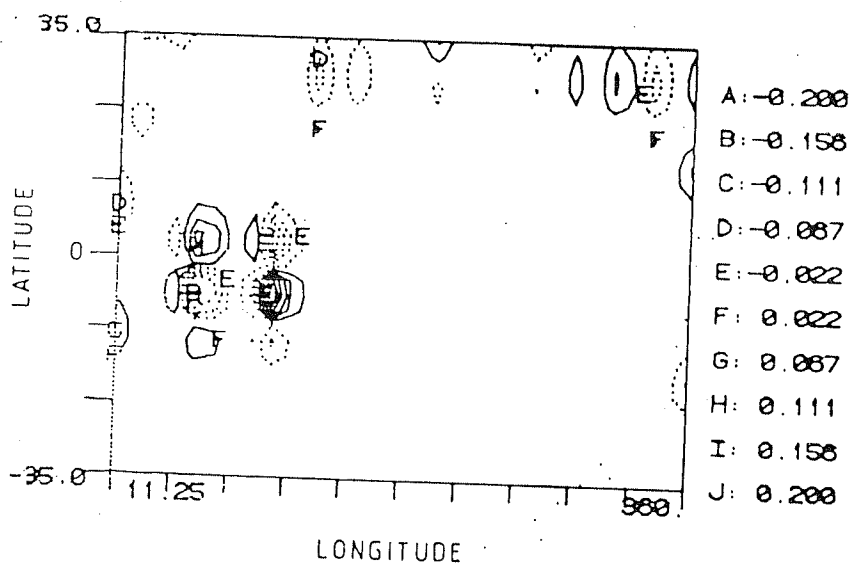
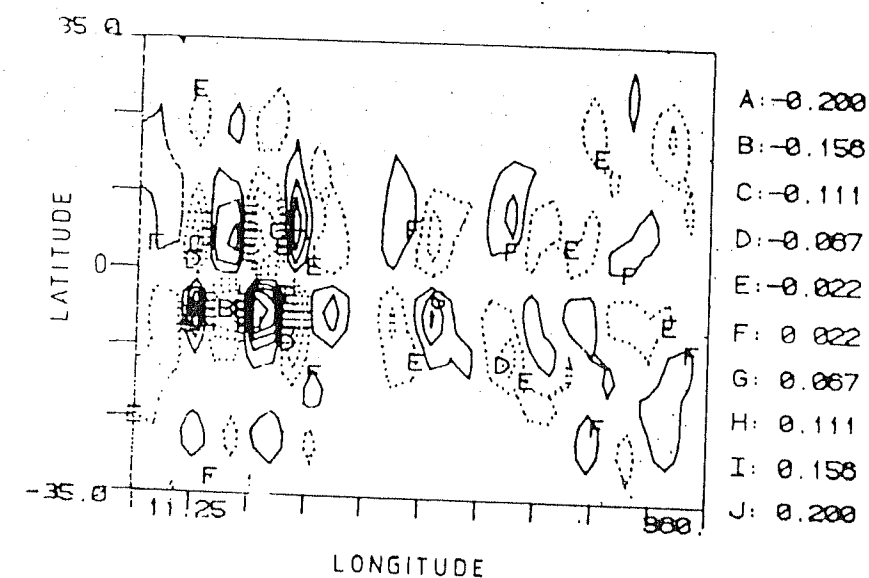


Fig.4.3d. (Top) Same as Fig.4.3a, except for term T1. Interval $0.044 \times 10^{-14} s^{-2}$.
 Fig.4.3e. (Middle) Same as Fig.4.3a, except for term T2. Interval $0.044 \times 10^{-14} s^{-2}$.
 Fig.4.3f. (Lower) Same as Fig.4.3a, except for term T3. Interval $0.006 \times 10^{-14} s^{-2}$.

TABLE 4.1: AREA AVERAGES OF THE TERMS OF THE VORTICITY EQUATION

FORCING	AVERAGING REGION	M1	M2	M3	T1	T2	T3
Idealized Source-Sink combination	67.5°E-157.5°E 3.4°N - 44.1°N	$5.3 \times 10^{-12} \text{S}^{-2}$	$4.4 \times 10^{-12} \text{S}^{-2}$	$3.0 \times 10^{-16} \text{S}^{-2}$	$4.6 \times 10^{-17} \text{S}^{-2}$	$1.14 \times 10^{-17} \text{S}^{-2}$	$4.4 \times 10^{-19} \text{S}^{-2}$
DJF-1979	101.25°E-101.25°W -15.5°S - 28.8°N	$2.3 \times 10^{-11} \text{S}^{-2}$	$2.4 \times 10^{-11} \text{S}^{-2}$	$1.08 \times 10^{-12} \text{S}^{-2}$	$1.9 \times 10^{-14} \text{S}^{-2}$	$1.03 \times 10^{-14} \text{S}^{-2}$	$3.8 \times 10^{-15} \text{S}^{-2}$
JJA-1979	45°E-123.75°W -11.1°S - 33.3°N	$2.6 \times 10^{-11} \text{S}^{-2}$	$1.8 \times 10^{-11} \text{S}^{-2}$	$1.13 \times 10^{-12} \text{S}^{-2}$	$1.18 \times 10^{-12} \text{S}^{-2}$	$1.5 \times 10^{-12} \text{S}^{-2}$	$9.4 \times 10^{-16} \text{S}^{-2}$

to four orders smaller than the terms M1 and M2. The smallness of M3 is also seen in its area average value, in the region between is heat source and sink, which is $3 \times 10^{-17} \text{S}^{-2}$. Terms involving the transients T1, T2 and T3 are given in Figs. 4.3d, 4.3e and 4.3f respectively. It is clearly evident that the terms T1, T2 and T3 and also their respective area averages are negligible as compared to the terms M1 and M2.

A similar vorticity budget study has been carried out for the winter 1978-79 dataset. The 5-level nonlinear global spectral model was forced using the observed time-mean 3-dimensional atmospheric heating for DJF (1978-79). The observed diabatic heating distribution was prescribed at all the model levels. The vertically averaged heating is shown in Fig. 4.4a. The large scale features consist of the heating over Indonesia and western Pacific, continental heating over South America and Africa. The time-mean response induced by the observed diabatic heating for winter (1978-79) was calculated in the 5-level nonlinear global spectral model. In the last chapter, we had given a detailed account of the planetary scale circulations during DJF (1978-79). The model generated streamfunction and velocity potential at 300 mb are shown in Fig. 4.4b and Fig. 4.4c respectively. The most prominent planetary scale circulation during the northern winter is the Walker circulation in the equatorial Pacific. Large scale divergence over Indonesia and subsidence over the eastern Pacific can be seen in Fig. 4.4c. The equatorial Pacific is characterized by upper level westerlies and lower level easterlies. The upper level westerly flow in the equatorial Pacific is evident from the positive values of the zonal gradient associated with velocity potential at 300 mb.

The different terms of the equation 4.5 for the winter 1979 analysis are shown in Figs. 4.5a-4.5f. The area average values for the different terms are calculated in the region between 101.25°E and 101.25°W and -15.5°S and 28.8°N , which corresponds to the Walker circulation in the equatorial Pacific. It can be seen from the area

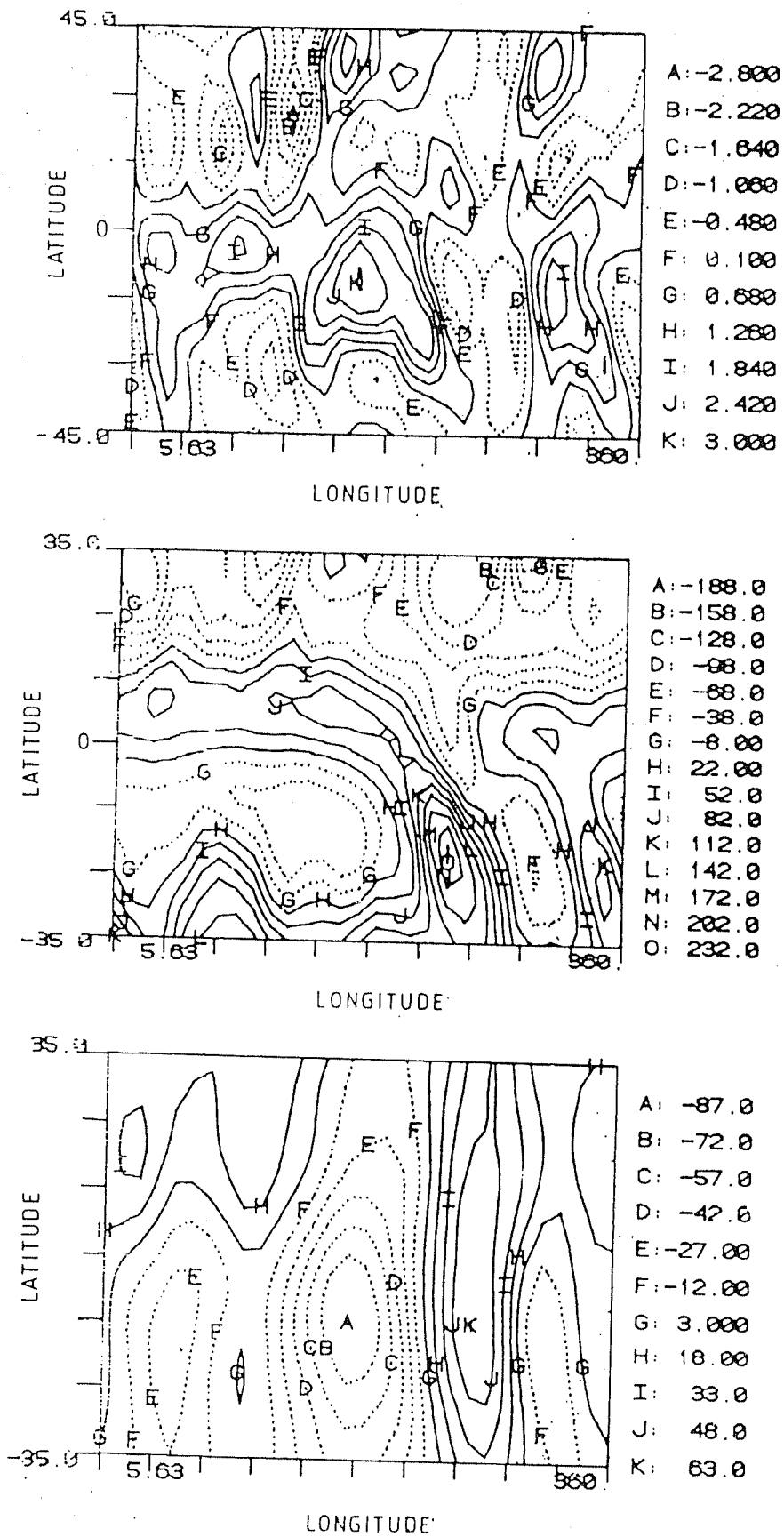


Fig.4.4a. (Top) Same as Fig.4.2a, except for the case of winter (1978-79). Interval 0.58 °K per day.
 Fig.4.4b. (Middle) Same as Fig.4.2b, except for the case of winter (1978-79). Interval $30 \times 10^5 m^2 s^{-1}$.
 Fig.4.4c. (Lower) Same as Fig.4.2c, except for the case of winter (1978-79). Interval $15 \times 10^5 m^2 s^{-1}$.

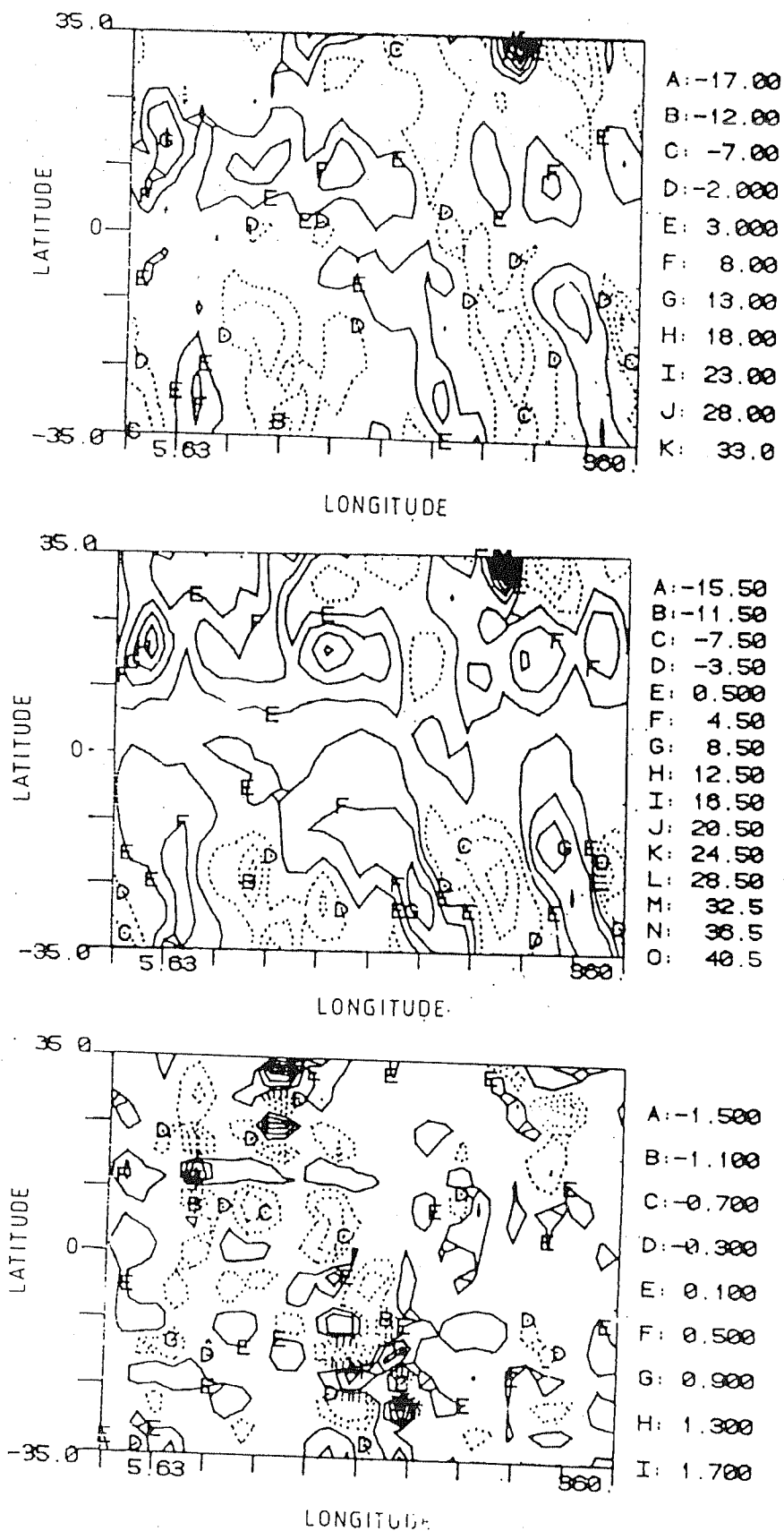


Fig.4.5a. (Top) Same as Fig.4.3a, except for the case of winter (1978-79). Interval $5 \times 10^{-11} s^{-2}$.

Fig.4.5b. (Middle) Same as Fig.4.3b, except for the case of winter (1978-79). Interval $4 \times 10^{-11} s^{-2}$.

Fig.4.5c. (Lower) Same as Fig.4.3c, except for the case of winter (1978-79). Interval $0.4 \times 10^{-11} s^{-2}$.

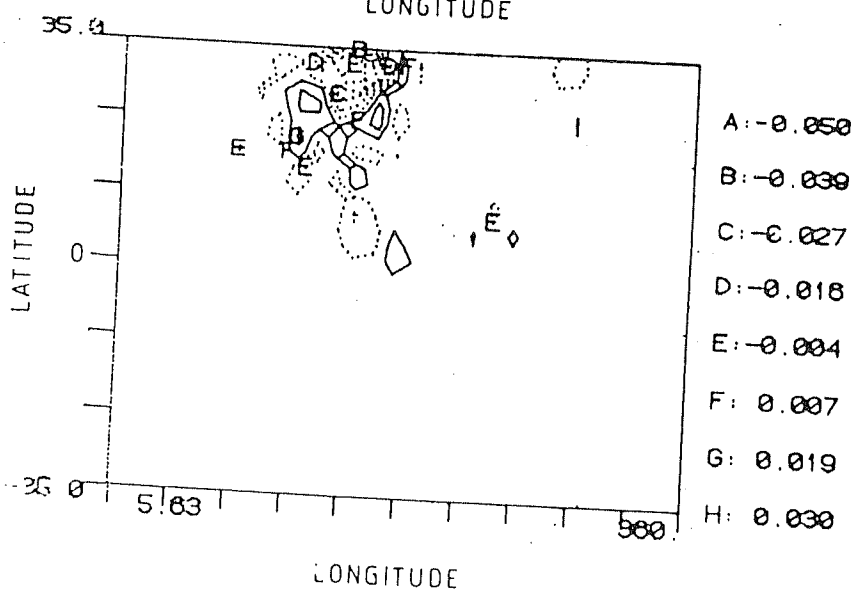
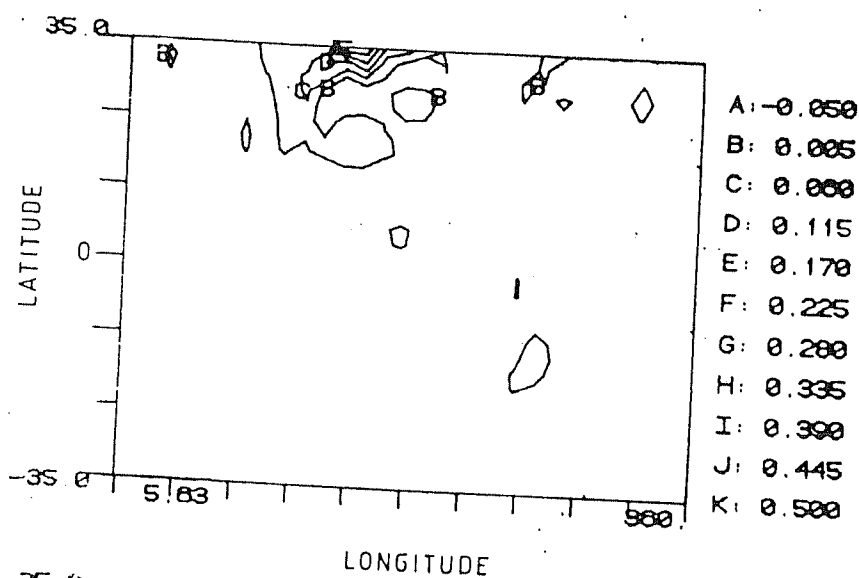
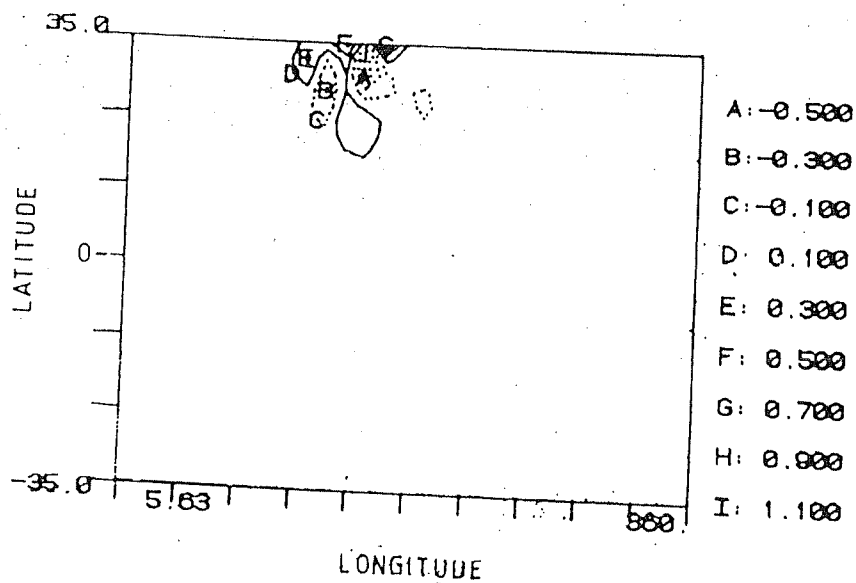


Fig.4.5d. (Top) Same as Fig.4.3d, except for the case of winter (1978-79). Interval $0.2 \times 10^{-11} s^{-2}$.

Fig.4.5e. (Middle) Same as Fig.4.3e, except for the case of winter (1978-79). Interval $0.055 \times 10^{-11} s^{-2}$.

Fig.4.5f. (Lower) Same as Fig.4.3f, except for the case of winter (1978-79). Interval $0.012 \times 10^{-11} s^{-2}$.

average values and from Figs.4.5a and 4.5b that the terms involving the advection of absolute vorticity by the time-mean horizontal wind and the time-mean absolute vorticity stretching are of comparable magnitudes. The horizontal structures of the terms M1 and M2 are quite similar. The area average values of M1 and M2 are $2.3 \times 10^{-11} \text{S}^{-2}$ and $2.4 \times 10^{-11} \text{S}^{-2}$ respectively. The time-mean vertical advection and twisting terms shown in Fig.4.5c are about one to two orders smaller than the terms M1 and M2. The terms involving the transients T1, T2 and T3 (Figs.4.5d, 4.5e and 4.5f) and also their area average values are negligibly small as compared to the terms time-mean terms M1 and M2. The terms M1 and M2 being the dominant terms during winter (1978-79), suggest that nonlinear effects associated with the advection and stretching of absolute vorticity by the horizontal winds are quite important in determining the vorticity balance over the region of the Walker circulation in the equatorial Pacific.

We shall now examine the vorticity balance associated with the summer (1979) monsoon circulation. Fig.4.6a shows the vertically integrated time-mean heating during JJA (1979). The large heating over the Bay of Bengal, the foothills of Himalayas and the elevated Tibetan plateau, drives the summer monsoon circulation over India. The mean meridional circulations as well as the major east-west circulations forced by the time averaged heating during summer (1979) were extensively discussed in the previous chapter. The dataset for the vorticity budget study was obtained by forcing the 5-level nonlinear global spectral model with the observed three dimensional time-mean diabatic heating for JJA (1979). A weak Rayleigh friction of 15 days dissipation time scale was used in the model. The model was integrated for 100 days so as to attain a steady state. The steady-state streamfunction and velocity potential at 300 mb are shown in Fig.4.6b and Fig.4.6c respectively. The most striking feature in the upper levels is the anticyclonic flow over the Tibetan region. In addition to the Hadley circulation of the Indian summer monsoon, there are prominent planetary

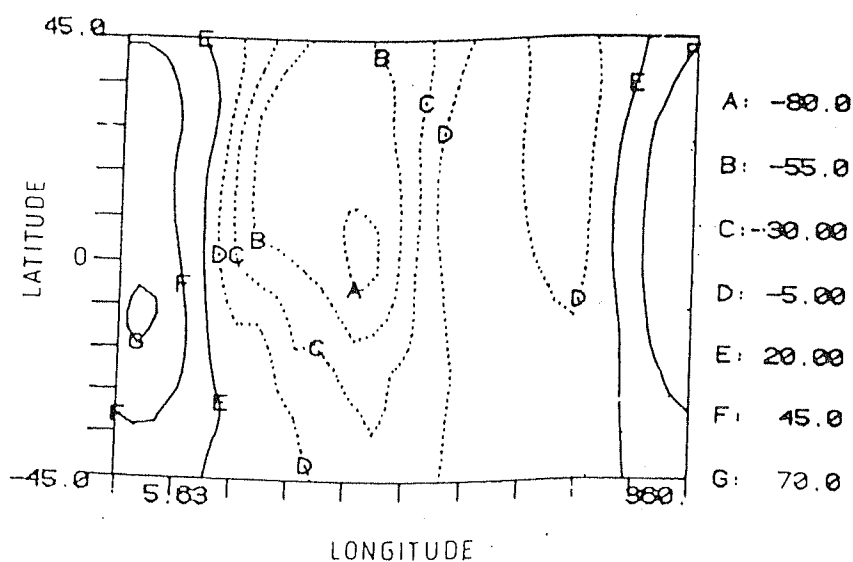
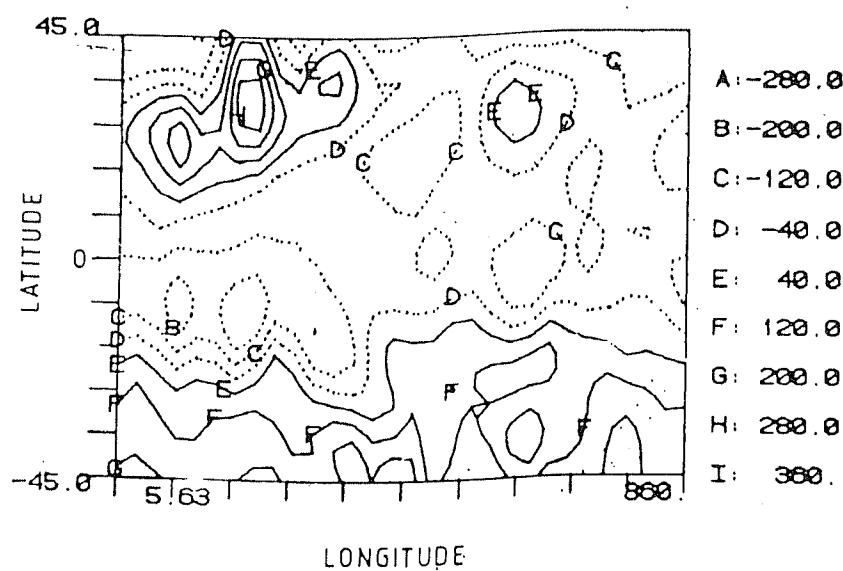
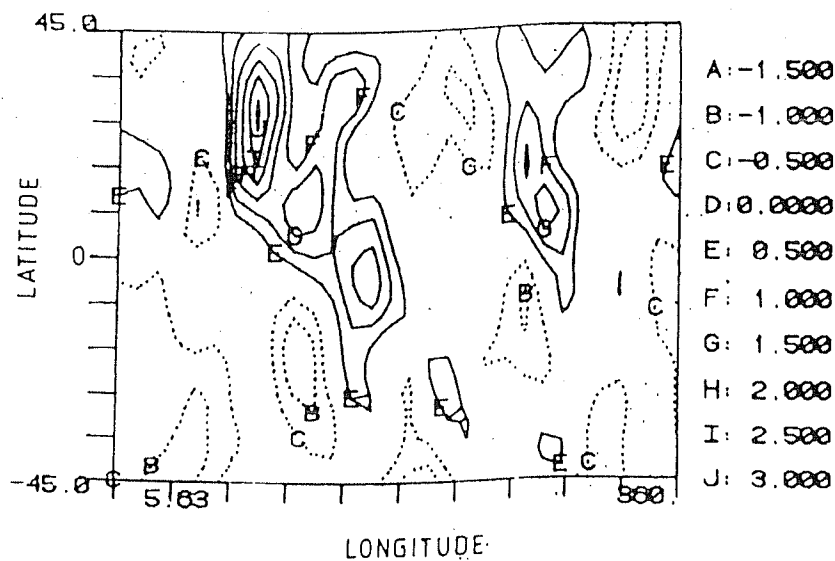


Fig.4.6a. (Top) Same as Fig.4.2a, except for the case of summer (1979). Interval 0.5 °K per day.

Fig.4.6b. (Middle) Same as Fig.4.2b, except for the case of summer (1979). Interval $80 \times 10^5 m^2 s^{-1}$.

Fig.4.6c. (Lower) Same as Fig.4.2c, except for the case of summer (1979). Interval $25 \times 10^5 m^2 s^{-1}$.

scale east-west circulations associated with the heating in the Tibetan and Mexican highlands. The velocity potential at 300 mb shows outflow over the Indian summer monsoon region and the highlands of Mexico.

The time mean and transient terms of the vorticity equation were constructed using the fields of the last 20 days. The different terms of the equation 4.5 for the summer 1979 analysis are shown in Figs.4.7a-4.7f. It is seen from Figs.4.7a and 4.7b, that the magnitude and structure of the time-mean terms associated with horizontal advection and stretching of absolute vorticity, match well especially over the highlands of Tibet and northern central Pacific. The time-mean vertical advection and twisting terms are about one order smaller than M1 and M2 over the Indian monsoon region. The transient terms T1, T2 and T3, shown in Figs.4.7d, 4.7e and 4.7f are small in the low latitudes. The magnitude of the transient term T1 over the Tibetan plateau is nearly the same as the time-mean term M3. The area average values for the different terms have been calculated in the region between 45° E and 123.75° E and 11.5° S and 33.3° N, which is the region of the northern summer monsoon. The area average values of M1, M2 and M3 are $2.6 \times 10^{-11} \text{S}^{-2}$, $1.8 \times 10^{-11} \text{S}^{-2}$ and $1.13 \times 10^{-12} \text{S}^{-2}$ respectively. It can be observed that the area average values of M1 and M2 are of comparable magnitudes while M3 is one order smaller than M1 and M2. The area average values of transient terms T1 and T2 are 1-2 orders smaller than the corresponding time-mean terms.

4.5 Concluding remarks

We have performed a diagnostic study of the vorticity balance in the tropical upper troposphere using the datasets generated from steady-state forcing experiments with

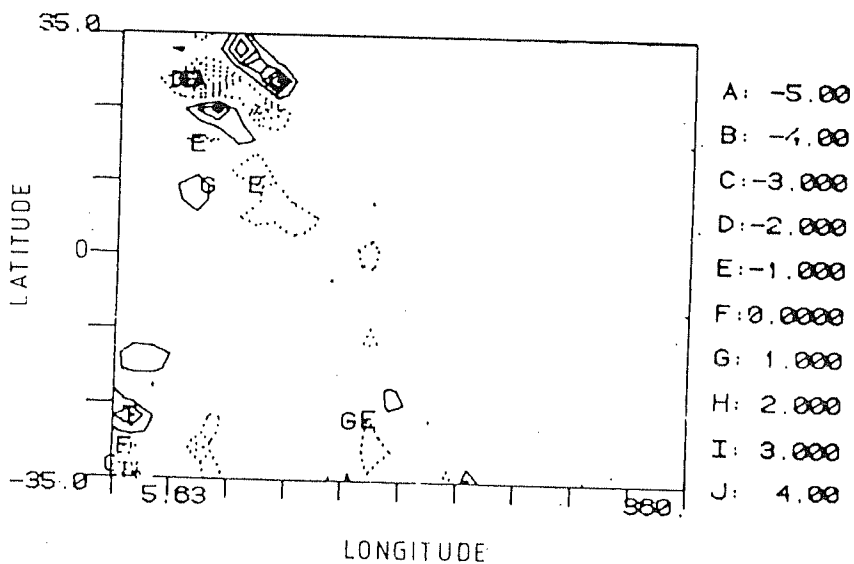
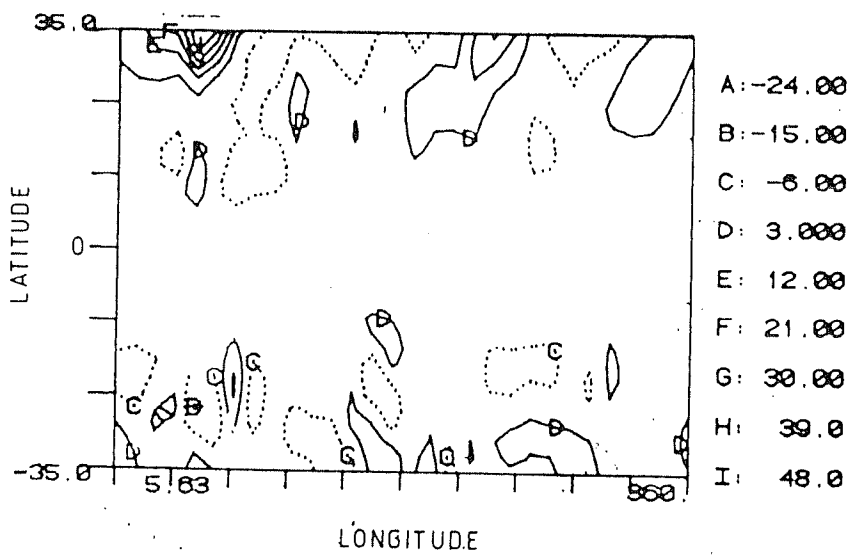
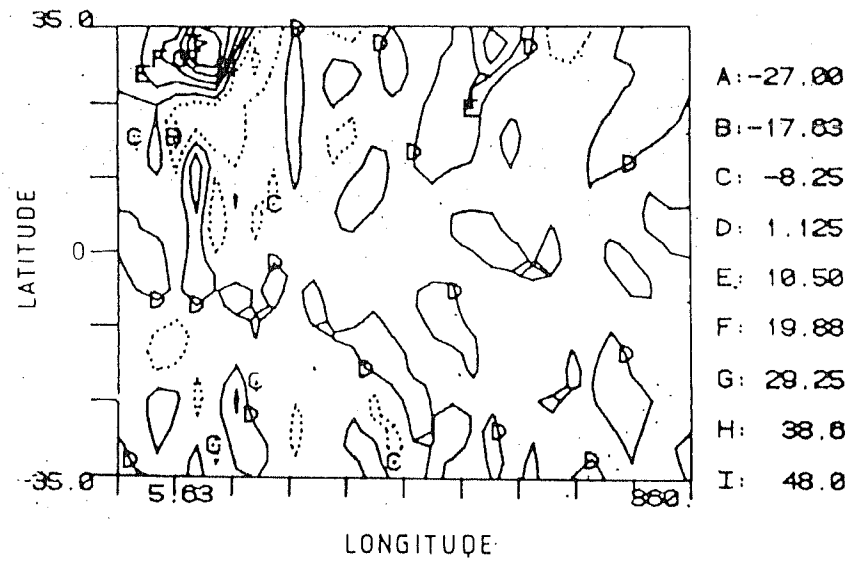


Fig.4.7a. (Top) Same as Fig.4.3a, except for the case of summer (1979). Interval $9.4 \times 10^{-11} s^{-2}$.

Fig.4.7b. (Middle) Same as Fig.4.3b, except for the case of summer (1979). Interval $9 \times 10^{-11} s^{-2}$.

Fig.4.7c. (Lower) Same as Fig.4.3c, except for the case of summer (1979). Interval $1 \times 10^{-11} s^{-2}$.

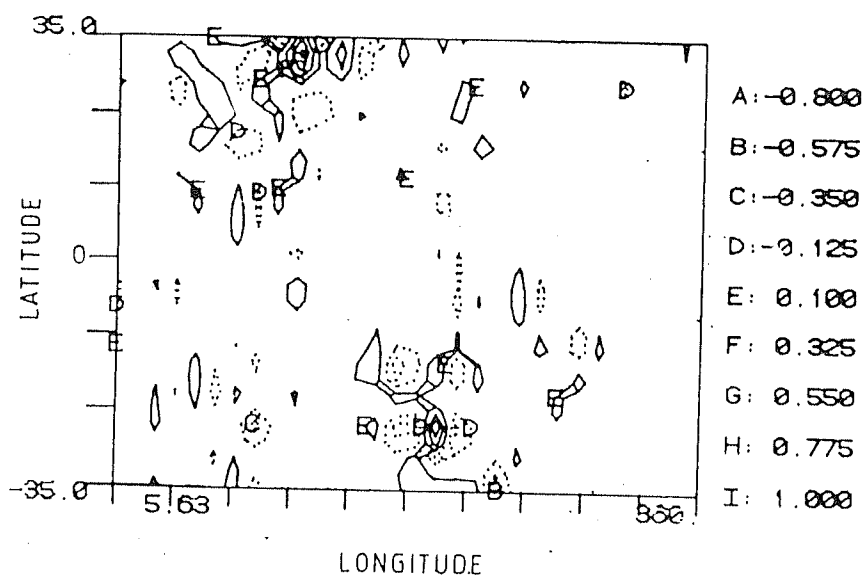
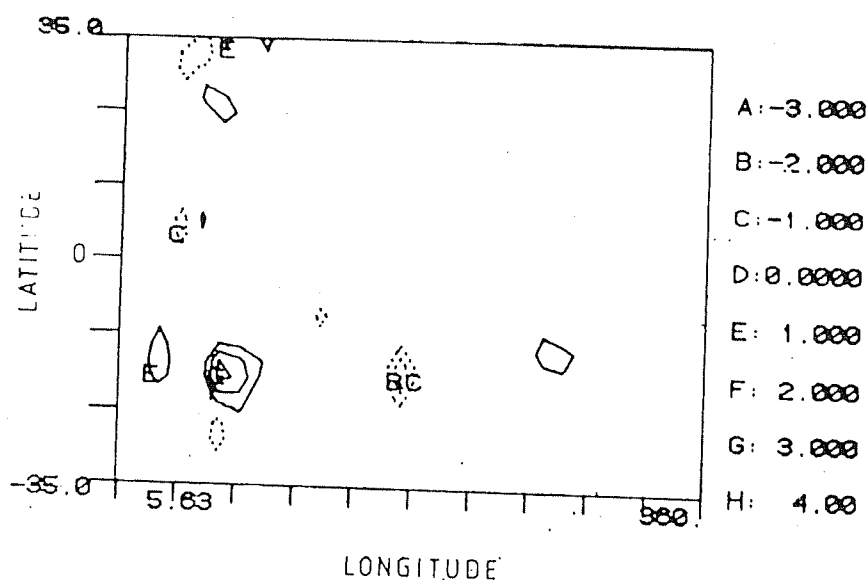
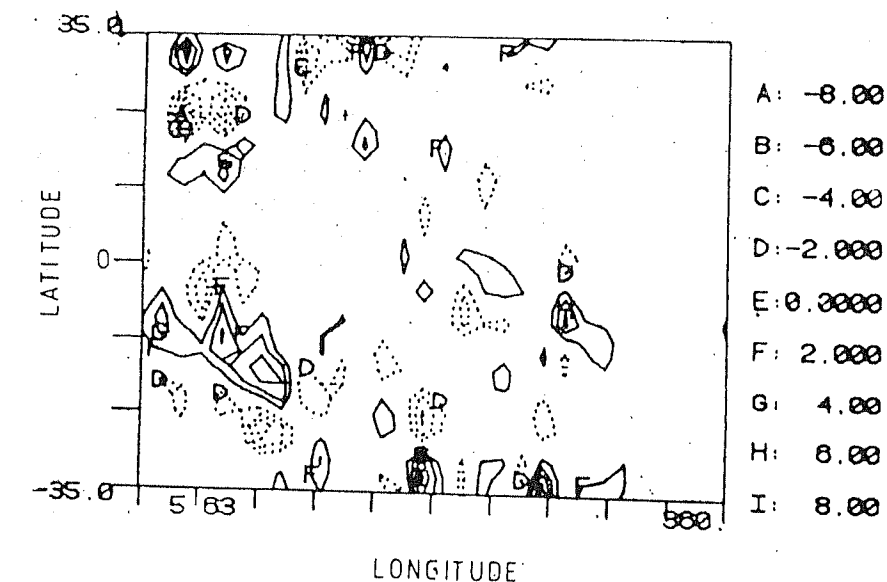


Fig.4.7d. (Top) Same as Fig.4.3d, except for the case of summer (1979). Interval $2 \times 10^{-11} s^{-2}$.

Fig.4.7e. (Middle) Same as Fig.4.3e, except for the case of summer (1979). Interval $1 \times 10^{-11} s^{-2}$.

Fig.4.7f. (Lower) Same as Fig.4.3f, except for the case of summer (1979). Interval $0.23 \times 10^{-11} s^{-2}$.

in the tropics, it can be concluded that nonlinear effects associated with horizontal advection and vorticity stretching, can greatly affect the large-scale motions in the tropical upper troposphere.

Chapter 5

Linear and Nonlinear Studies of the Time-Mean Tropical Hadley Circulation

5.1 Introduction

In the earlier chapters, it was seen that the diabatic heating in the tropics, exhibits a high degree of longitudinal variation. It is this strong zonal asymmetry, that renders a large complexity to the observed motions in the tropical atmosphere. However, by eliminating the complex behaviour introduced by the zonal asymmetries and retaining only the zonally symmetric component, one can gain a deeper understanding of the dynamics of tropical atmospheric circulation. Zonally symmetric flows also serve the role of basic state in instability studies, where one examines the spatial and temporal evolution of the perturbations superposed on a given basic state. More importantly, zonally symmetric circulations are of considerable interest from the perspective of modelling climate especially on long time-scales. In this chapter, we shall study the time-mean zonally symmetric circulations in the tropical atmosphere, using both linear and nonlinear models. The emphasis will be to understand the dynamics of the tropical Hadley circulation induced by diabatic heating. Further, we shall compare

the linear and nonlinear equilibrium solutions and investigate the role of nonlinear dynamics on the mean-meridional motions in the tropics.

5.1.1 Earlier studies

The subject of zonally averaged atmospheric circulation has a sufficiently long history which dates back to the time of Hadley (1735). A complete historical treatment of this topic as well as the important observational and theoretical findings, is given in Lorenz (1967). He has presented a comprehensive review of the various transport (angular momentum, heat and water vapour) processes and the energy conversion mechanisms associated with the tropical Hadley cell. The classical works of Eliassen (1952) and Kuo (1956), which deal with the response of a simplified zonally symmetric atmosphere to thermal forcing, suggest that the mean meridional circulations in the atmosphere are strongly controlled by heat and momentum transport by the eddies and dissipation by friction.

We shall first describe some of the well known observational, diagnostic, theoretical and modelling studies. During the northern summer, there is a strong meridional gradient of heating over the Indian monsoon region, which sets up a reverse Hadley cell. Keshavamurty (1968) studied the nature of angular momentum balance over the Indian southwest monsoon region and found that the Coriolis term mainly contributes towards the maintenance of the lower tropospheric westerlies against frictional effects. Keshavamurty and Awade (1970) studied the maintenance of the monsoon trough over north India. Their energetic calculations suggest that the work done by the horizontal pressure forces is primarily responsible for maintaining the monsoon trough against frictional dissipation. Oort and Rasmussen (1970) have studied the annual cycle of the monthly mean meridional circulations in the atmosphere. They found that during the months of April-May and October-November, the mean

meridional circulation was symmetric w.r.t. the equator. During the other months of the year, the Hadley cell of the winter hemisphere appeared to dominate the circulation. They also computed the transport of angular momentum, potential energy, sensible and latent heat by the mean meridional circulations during January and July. Vernekar (1967) investigated the mean meridional circulations forced by eddy transports of heat and momentum and carried out an energetic study for the zonally averaged flow. He found that eddy transport of momentum is twice as effective as the eddy transport of heat in forcing the meridional circulations. During the winter months, he found that the mean meridional circulation was mainly influenced by the planetary-scale (long) waves, whereas the baroclinically unstable waves (medium and short scale) waves had a dominant impact during the other seasons. Dickinson (1971a) carried out analytical calculations to study the maintenance of the zonal mean atmospheric circulations by momentum and thermal sources in the tropical rainbelt. Detailed calculations of the observed global angular momentum and energy balance are given in Newell *et.al* (1972) and Oort and Piexoto (1983).

There are many GCM simulations as well as semi-analytical calculations of the tropical Hadley circulation. The GCM experiments by Manabe *et.al* (1965) and Hunt (1973) suggest that moist processes affect the tropical Hadley circulation significantly. Manabe *et.al* (1965) incorporated a simple hydrologic cycle consisting of advection of water vapour by the large-scale motion, evaporation from the surface, precipitation and moist convective adjustment in a GCM. They found that the inclusion of moist processes produced an increase in the transport of momentum and heat by the tropical Hadley cell. This resulted in the strengthening of the tropical meridional circulation. Dickinson (1971b) examined the vertical variation of Rayleigh friction and Newtonian cooling in the model. He obtained realistic extratropical circulations when the rate of damping was larger near the ground and gradually decreased till the tropopause. The circulation changes caused by the seasonal and hemispheric variation of the

tropical rainbelt were also investigated. He showed that the asymmetry caused by the northward shift of the rainbelt resulted in the winter Hadley cell being more intense in July than in January. Goswami *et.al* (1984) calculated the symmetric response due to zonally averaged latent heating fields for equinox condition, northern hemispheric summer and winter cases. They found that the strength of the circulation was sensitive to changes in vertical eddy viscosity. They showed that the position and structure of the ITCZ was determined by the imposed SST and latent heating by CISK mechanism. The studies of Webster(1983) and Goswami and Shukla (1984) emphasize the roles of surface hydrology and land surface processes in determining the meridional propagation of the tropical convective anomalies on the intraseasonal time-scale.

5.1.2 Aims of the present study

The main objective of our study is to examine the steady-state Hadley circulation in the tropics, using both linear and nonlinear versions of an axisymmetric 5-level global spectral model. Some of the past studies reveal that the dynamics of the time-mean Hadley circulation calculated from linear models differs considerably from those based on nonlinear calculations. For instance, Stone *et.al* (1974) used the GCM at Goddard Institute for Space Studies (GISS) and found that a rather large amount of subgrid-scale turbulent mixing of horizontal momentum (eddy viscosity $\sim 100 \text{ m}^2\text{s}^{-1}$ was required in the low-latitude troposphere, in order to account for the observed Hadley circulation. Schneider and Lindzen (1977) used a linear axially symmetric model to study the steady-state response induced by the annual mean cumulus convection. They found that the mean meridional circulation driven by the zonally symmetric latent heat distribution, was similar to the annual mean observed circulation only when 'cumulus friction' was included. They attributed cumulus friction, with the vertical transport of horizontal momentum by cumulus convection.

In a subsequent study, with a nonlinear axially symmetric model, Schneider (1977) found that both nonlinear advection terms and cumulus friction produce an increase in the intensity of the upper level zonally symmetric circulation. In general, most of the linear calculations emphasize the need for incorporating vertical transport of horizontal momentum by cumulus convection (cumulus friction) so as to explain the observed time-mean meridional circulations in the tropics. Observations by Riehl and Soltwisch (1974), over the Atlantic and Pacific, do indicate that an appreciable fraction of the momentum is transported from the surface trades to the upper layers of the atmosphere. However, there still remains a lot of uncertainty in the numerical estimates of cumulus friction in the tropics. Houze (1973) and Schneider and Lindzen (1976, 1980) have parameterized vertical transports of horizontal momentum by cumulus clouds and their estimated magnitudes of cumulus friction were found to be as large as the large-scale vertical momentum flux. On the other hand, Thomson and Hartmann (1979, 1980) estimated the effects of cumulus friction on the tropical mean meridional circulation, using the observed precipitation and 200 mb winds and showed that they are not significant. Thus, there is uncertainty in using cumulus friction in models, owing to the large discrepancies in its estimated value. Therefore there is still ambiguity regarding the small decay time-scales (large cumulus friction) which are employed by linear models.

Quite contrary to the studies based on linear models, the GCM simulations by Manabe *et.al* (1970) with the Geophysical Fluid Dynamics Laboratory (GFDL) model and Kasahara *et.al* (1973) with the National Center for Atmospheric Research (NCAR) model, indicate that cumulus friction is not important in determining the steady-state tropical Hadley circulation. The above two GCM simulation studies employed moist convective adjustment for their cumulus heating parameterizations. The GCM simulations of Manabe *et.al* (1970) and Kasahara *et.al* (1973) were able to reproduce the Hadley circulation realistically without specifying cumulus friction. Held

and Hou (1980) performed nonlinear calculations for a nearly inviscid atmosphere using conservation laws for angular momentum and potential temperature. Their theoretical calculations also included the total poleward heat flux and the position of the upper level jet in the zonal wind. They found that the momentum transport due to the nonlinear meridional advection was very important in considering the Hadley circulation. They showed that the meridional width of the Hadley cell depends primarily on the thermal Rossby number. From the previous investigations it is evident that there are certain important differences between the linear and nonlinear model calculations. In the light of these differences, we propose to re-examine the time-mean tropical Hadley circulation using both linear and nonlinear models. It is well known that the large scale circulations in the low latitudes are associated with large values of Rossby number, indicating that nonlinear advection effects are quite important in the tropical regions. Therefore, by comparing the equilibrium solutions in the linear and nonlinear models, we intend to investigate the impact of nonlinear terms on the dynamics of the steady-state tropical Hadley cell. In the next section, we shall describe the formulation of the axisymmetric model which will be used for our studies.

5.2 Model

We have constructed an axially symmetric 5-level nonlinear global spectral model, basically by discarding the zonal variations from the complete set of model equations described in Bourke (1974). The vertical σ levels in the model are shown in Fig.5.1a. The axially symmetric equations are obtained by setting $\frac{\partial}{\partial \lambda} = 0$. The prognostic and diagnostic equations are given below:

$$\frac{\partial \zeta}{\partial t} = -\frac{1}{a \cos \phi} \frac{\partial B}{\partial \phi} - 2\Omega \left(\sin \phi D + \frac{V}{a} \right) + K_h \left[\frac{1}{a^2} \frac{\partial^2 \zeta}{\partial \phi^2} + 2 \frac{\zeta}{a^2} \right] - \varepsilon \zeta \quad (5.1)$$

$$\begin{aligned}\frac{\partial D}{\partial t} = & -\frac{1}{a \cos \phi} \frac{\partial A}{\partial \phi} + 2\Omega \left(\sin \phi \zeta - \frac{U}{a} \right) - \frac{1}{a^2} \frac{\partial^2}{\partial \phi^2} (E + \Phi' + RT_0 q) \\ & + K_h \left[\frac{1}{a^2} \frac{\partial^2 D}{\partial \phi^2} + 2 \frac{D}{a^2} \right] - \epsilon D\end{aligned}\quad (5.2)$$

$$\frac{\partial q}{\partial t} = \frac{\bar{V}}{a} \frac{\partial q}{\partial \phi} + \bar{D}\quad (5.3)$$

$$\begin{aligned}\frac{\partial T}{\partial t} = & -\frac{1}{a \cos \phi} \frac{\partial (VT')}{\partial \phi} + T'D + \dot{\sigma} \gamma + \frac{RT}{c_p} \left[\bar{D} + (V + \bar{V}) \frac{1}{a} \frac{\partial q}{\partial \phi} \right] \\ & + \frac{H_c}{c_p} + \frac{K_h}{a^2} \frac{\partial^2 T}{\partial \phi^2} - \delta T\end{aligned}\quad (5.4)$$

The diagnostic equation for vertical velocity $\dot{\sigma}$ is

$$\dot{\sigma} = \left[(1 - \sigma) \bar{D} - \bar{D}^\sigma \right] + \left[(1 - \sigma) \bar{V} - \bar{V}^\sigma \right] \frac{1}{a} \frac{\partial q}{\partial \phi}\quad (5.5)$$

The terms in the above equations are explained below:

'a' is the radius of the earth, ϕ is latitude, p_* is the surface pressure, $\sigma = \frac{p}{p_*}$ is the vertical coordinate; Ω is the earth's rotation rate; R is the gas constant; c_p is the specific heat at constant pressure, $\gamma = \frac{RT}{\sigma c_p} - \frac{\partial T}{\partial \sigma}$ is the static stability; H_c is the prescribed rate of heating; ϵ is the Rayleigh friction and δ is the Newtonian cooling and K_h is the horizontal diffusion coefficient.

u is the zonal velocity; v is the meridional velocity; $U = u \cos \phi$; $V = v \cos \phi$; ζ is the vertical component of relative vorticity; D is the horizontal divergence; q is $\log p_*$; T is the absolute temperature; Φ is the geopotential height; $\dot{\sigma}$ is the total time derivative of σ . A subscript zero denotes a horizontal mean value and the superscript prime the deviation from the mean.

$$\begin{aligned}A &= \zeta U + \dot{\sigma} \frac{\partial V}{\partial \sigma} + \frac{RT'}{a} \cos \phi \frac{\partial q}{\partial \phi} \\ B &= \zeta V - \dot{\sigma} \frac{\partial U}{\partial \sigma} \\ E &= \frac{U^2 + V^2}{2 \cos^2 \phi}\end{aligned}\quad (5.6)$$

$$\begin{aligned}(\bar{\cdot})^\sigma &= \int_1^\sigma (\cdot) \partial\sigma \\(\bar{\cdot}) &= \int_1^0 (\cdot) \partial\sigma\end{aligned}$$

The boundary conditions are $\dot{\sigma} = 0$ at $\sigma = 1$ and $\sigma = 0$. The prognostic and diagnostic variables at each vertical level are expanded in terms of legendre polynomials in the meridional direction. For instance the stream function ψ at a given model level is expanded as

$$\psi = \sum_{l=0}^{l=LMAX} \psi_l(t) P_l(\sin \phi)$$

The series is truncated at $LMAX = 30$. The nonlinear advection terms are first calculated at grid points and later on transformed into the meridional wavenumber domain. The model equations are integrated using Semi-Implicit time integration scheme. A time-step of 24 minutes is used in the model and the horizontal diffusion has been parameterized following Bourke *et.al* (1977). The horizontal diffusion coefficient K_h is chosen to be $6.25 \times 10^4 \text{ m}^2 \text{ s}^{-1}$. The mean hemispheric temperatures at the different model levels are as follows: $T_{0900mb} = 277.5^\circ\text{K}$, $T_{0700mb} = 268.0^\circ\text{K}$, $T_{0500mb} = 250.7^\circ\text{K}$, $T_{0300mb} = 226.5^\circ\text{K}$ and $T_{0100mb} = 203.0^\circ\text{K}$. The initial condition corresponds to an atmosphere at rest. The initial temperatures at the different model levels correspond to their respective mean hemispheric values already mentioned.

5.3 Experiments with the axisymmetric model

The idealized experiments performed with the linear (LM) and nonlinear (NLM) versions of the 5-level axisymmetric global spectral model are described below. The LM is constructed, essentially by omitting all the nonlinear terms (eg. derivatives of product terms of two prognostic (diagnostic) variables) in the model equations. We have considered two cases of forcing i.e., (i) a strong heat source (max value 5°K

per day) (ii) a weak heat source (max value 2° K per day). It should be noted that the structure of the heating is identical in both the cases (Fig.5.1b). The heating distribution is symmetric w.r.t the equator and has a vertical structure of the form $\sin(\pi\sigma)$, with the maximum heating occurring at $\sigma = 0.5$ (500 mb). A weak Rayleigh friction and Newtonian cooling of 15 days dissipation time scale have been used. The main purpose of using weak dissipation terms in the model, is to fully ensure that the changes produced by the nonlinear terms are well projected. If this is not taken into account the effects due to nonlinearities may get masked because of the strong damping terms. Both the NLM and LM have been integrated for 150 days after switching on the heat source. The forcing is kept fixed throughout the time of integration so as to attain a steady state. The steady state Hadley circulations in the NLM and the LM are compared and the changes caused by the nonlinear terms are isolated.

5.4 Results and Discussion

We shall first discuss the equilibrium response when the NLM is forced by the strong heat source (Fig.5.1b). The strong equator to pole heating contrast forces a convective cell which is characterized by upper level westerlies and lower level easterlies. By and large, this convective overturning can be viewed as a thermodynamical balance between the terms involving the diabatic heating and adiabatic cooling due to ascent. The time-mean zonal velocity distribution associated with the Hadley circulation in the NLM is shown in Fig.5.2a. The latitudinal and vertical structure of zonal winds is well depicted in Fig.5.2a. But, the Hadley circulation is quite intense at the upper and lower levels. Since, we have employed very weak dissipation terms and at the same time the forcing amplitude is also quite large, the meridional circulation appears to be very intense. As mentioned before, the very purpose of choosing small damping terms

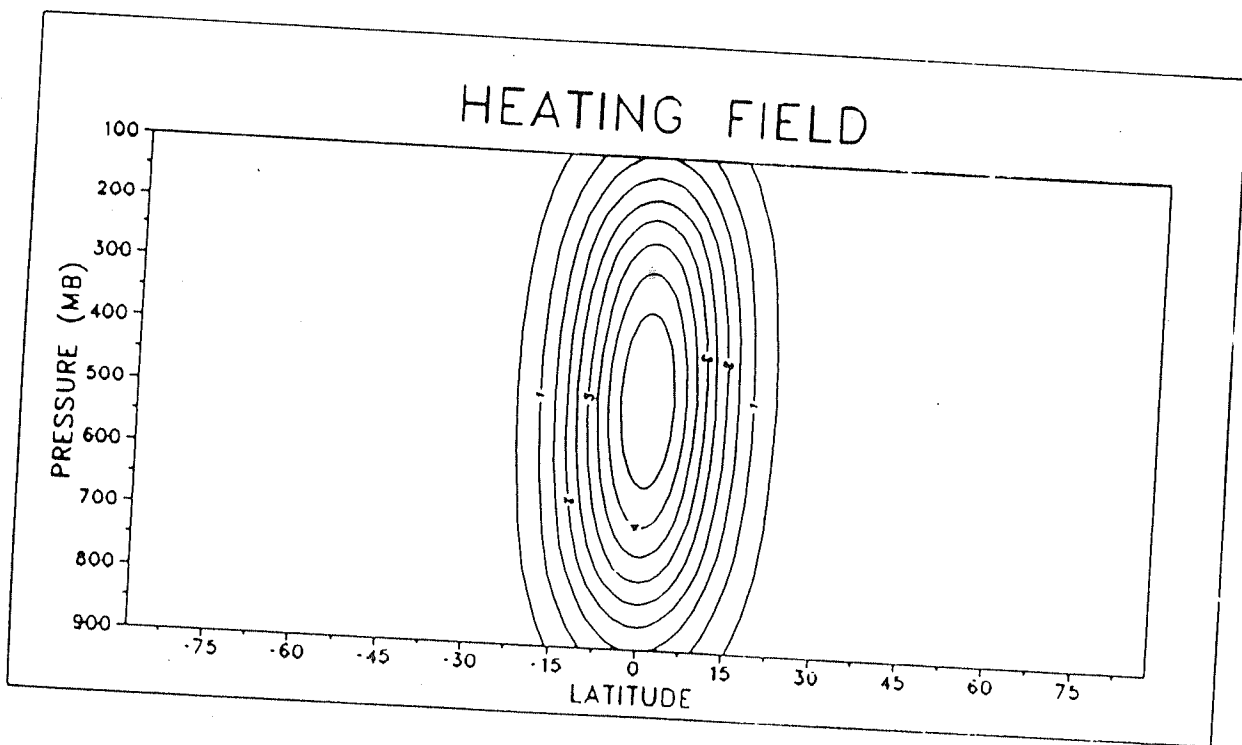
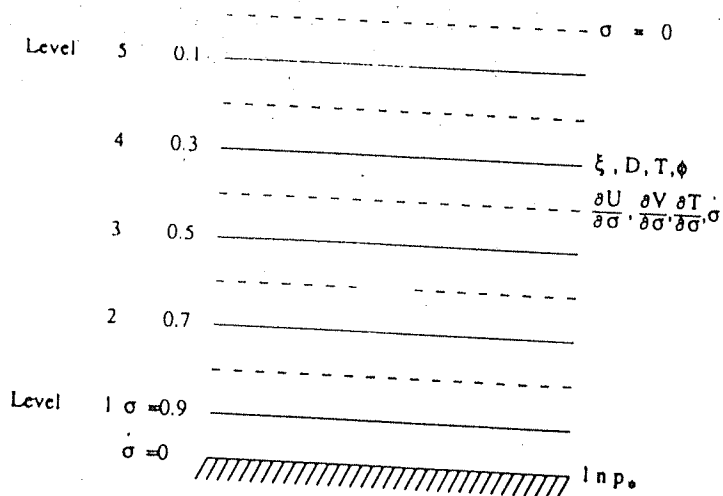


Fig.5.1a. (Top) Vertical sigma levels in the 5-level axisymmetric model.

Fig.5.1b. (Bottom) Latitude-pressure section of heating. Interval 0.5°K per day.

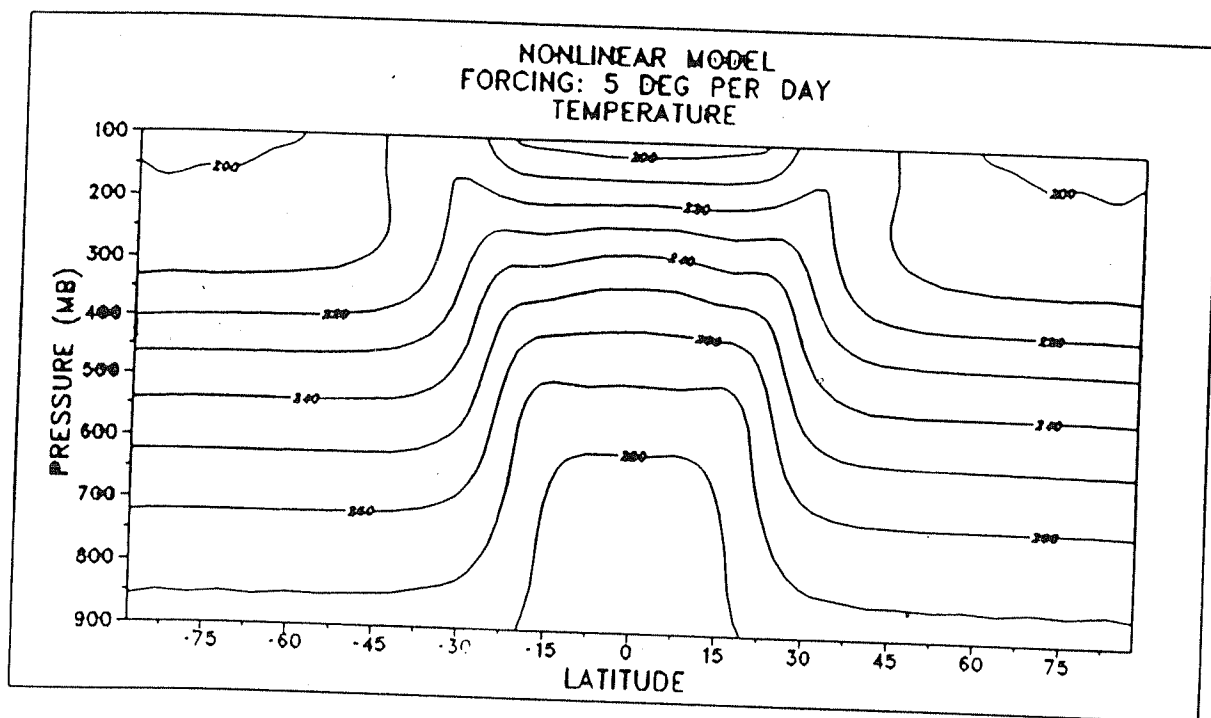
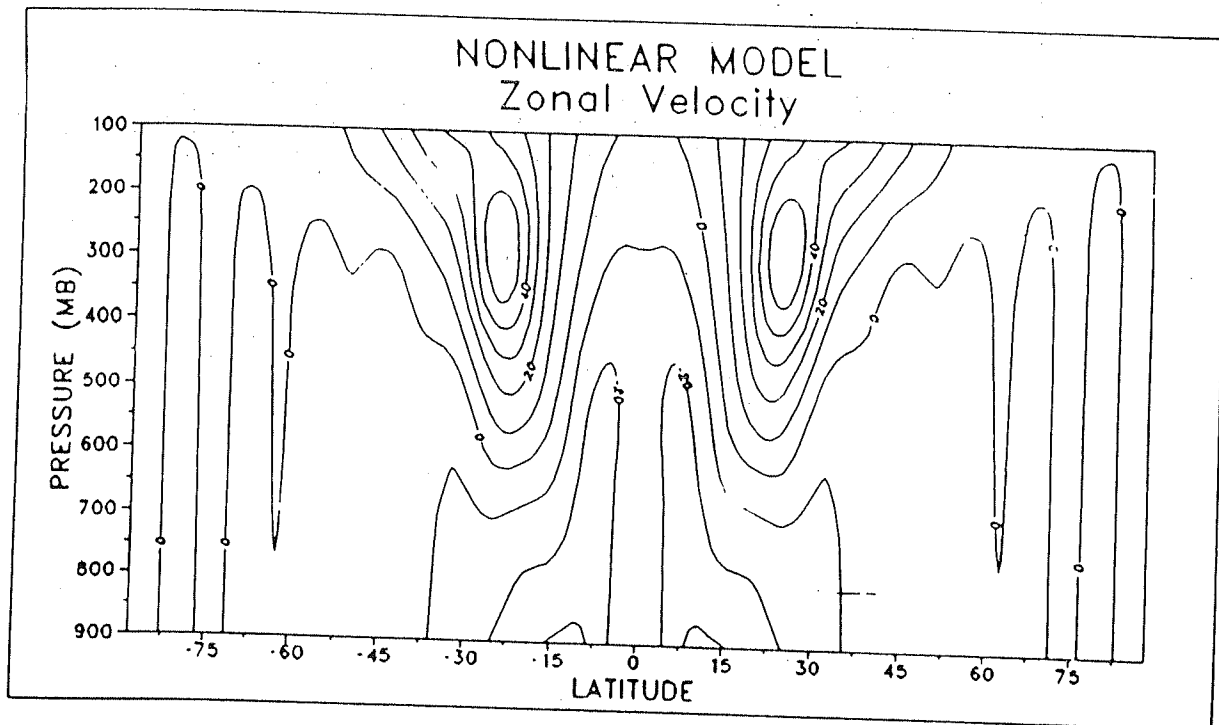
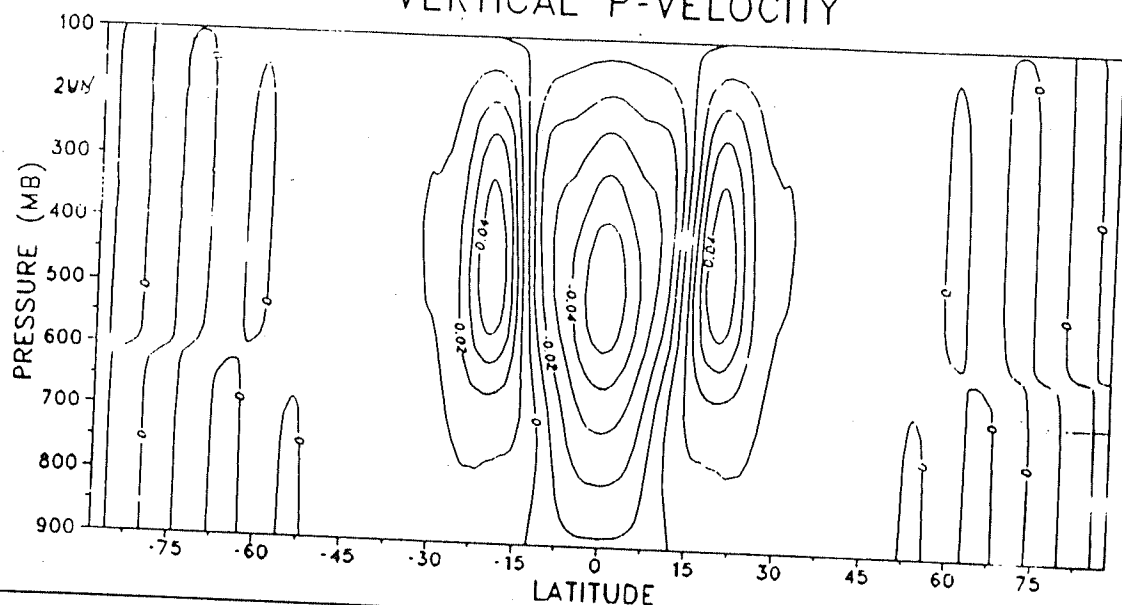


Fig.5.2a. (Top) Latitude-pressure section of zonal velocity in NLM. Strong forcing in Fig.5.1a used. Interval 10 ms^{-1} .
 Fig.5.2b. (Bottom) Same as Fig.5.2a, except for temperature. Interval $10 \text{ }^{\circ}\text{K}$.

NONLINEAR MODEL VERTICAL P-VELOCITY



LINEAR MODEL. Zonal Velocity

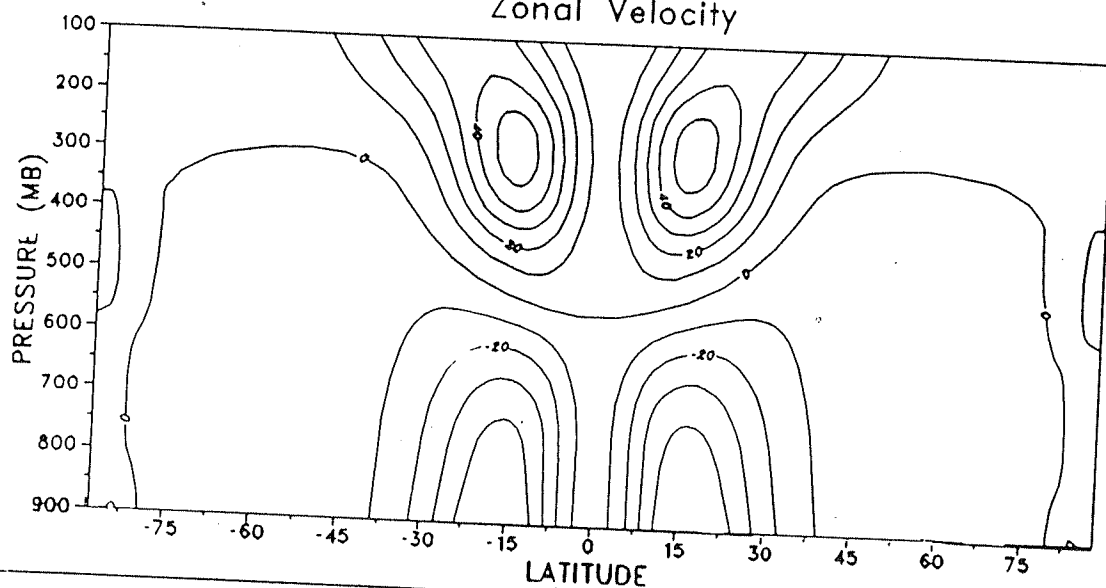


Fig.5.2c. (Top) Same as Fig.5.2a, except for vertical p-velocity. Interval 0.01 Pa s^{-1} .
Fig.5.3a. (Bottom) Same as Fig.5.2a, except for LM.

is to highlight the nonlinear effects as much as possible. However, in a subsequent study, we shall show that the Hadley circulation induced by a weaker heat source is characterized by more realistic wind speeds. An interesting feature to be noted in the steady-state nonlinear response, is that the easterlies in the tropical region have a large vertical depth. It can be seen that easterlies having speeds of -10 ms^{-1} extend even upto about 300 mb between 15°S and 15°N . The easterlies at the lower levels, near the equatorial region, have a maximum speed of about -25 ms^{-1} . It will be shown later that, the vertical transport of easterly momentum upwards by the nonlinear advection terms is considerably large in the region of the forcing. Another outstanding feature is the well marked core of strong upper level westerlies located at around 23°N and 23°S respectively. The equilibrium temperature in the NLM is shown in Fig.5.2b. The temperature field shows a gradual decrease in the poleward direction as well as in the vertical. The isotherms at a particular pressure level are almost meridionally flat near the region of forcing. This meridional flatness becomes broader as one proceeds vertically upwards. The vertical p-velocity (ω) distribution, which is symmetric w.r.t the equator, is shown in Fig.5.2c. The negative values of ω in the region of the forcing indicates that there is a large upward motion over this region. The maximum upward velocity is about 0.05 Pa s^{-1} at 500 mb, near the equator. The strong vertical motions over the forcing region results in considerable adiabatic cooling which was seen in the temperature field. The regions of positive ω on either hemisphere, suggest that the subsiding branches of the Hadley cell are situated at around 23°N and 23°S respectively. Although the ω field in the case of NLM is symmetric w.r.t the equator, the contours exhibit some asymmetry in the vertical direction. The adiabatic cooling due to ascent is well supported by both the ω and temperature fields which exhibit a latitudinal spread of the contours along the vertical axis.

We now evaluate the response in the LM and compare it with the response

already obtained in the NLM. The LM is constructed by omitting all the nonlinear terms from the equations in the NLM. The extraction of the nonlinear components from the thermodynamic energy equation 5.4 requires changes in the terms $\sigma\gamma + \frac{RT\bar{D}}{C_p}$. For this purpose, we represent γ and T at each vertical level, as a sum of their respective hemispheric mean values and the deviation from their means: $\gamma = \gamma_0 + \gamma'$ and $T = T_0 + T'$. Only the linear part of the term associated with the vertical advection is retained in the thermodynamic energy equation of the LM. The LM is forced using the same diabatic heating shown in Fig.5.1b and the steady state response is calculated. The zonal velocity field for the LM is given in Fig.5.3a. One notices that the low level easterlies are significantly larger in the LM than in the NLM. It is also clearly seen that in the case of LM, the easterlies are confined to the lower and middle troposphere and extend upto about 600 mb. The upper level westerlies have a vertical extent above the 500 mb pressure level. The position of the core of the westerly jet in the LM has shifted equatorward and is seen at around 17° N and 17° S respectively. The equilibrium temperature distribution in the LM is shown in Fig.5.3b. A comparison of the temperature fields in the LM and NLM reveals that the isotherms in the LM have larger magnitudes at the lower levels particularly over the forcing region. From the vertical structure of the temperature over the forcing region, it can be easily noticed that the isotherms in the LM do not exhibit broad latitudinal spreads, as seen in the case of NLM. The ω field for the LM (Fig.5.3c) shows that the maximum upward velocity is about 0.05 Pa s^{-1} at 500 mb. The vertical velocity distribution is nearly symmetric w.r.t the pressure co-ordinate. The ω field is quite small at the upper levels and the contours do not exhibit much latitudinal spreads. The vertical structures of the temperature and ω fields are consistent with each other. The large temperature values in the LM indicate that the absence of nonlinear vertical advection of temperature results in a decrease in the adiabatic cooling and hence a much warmer Hadley cell.

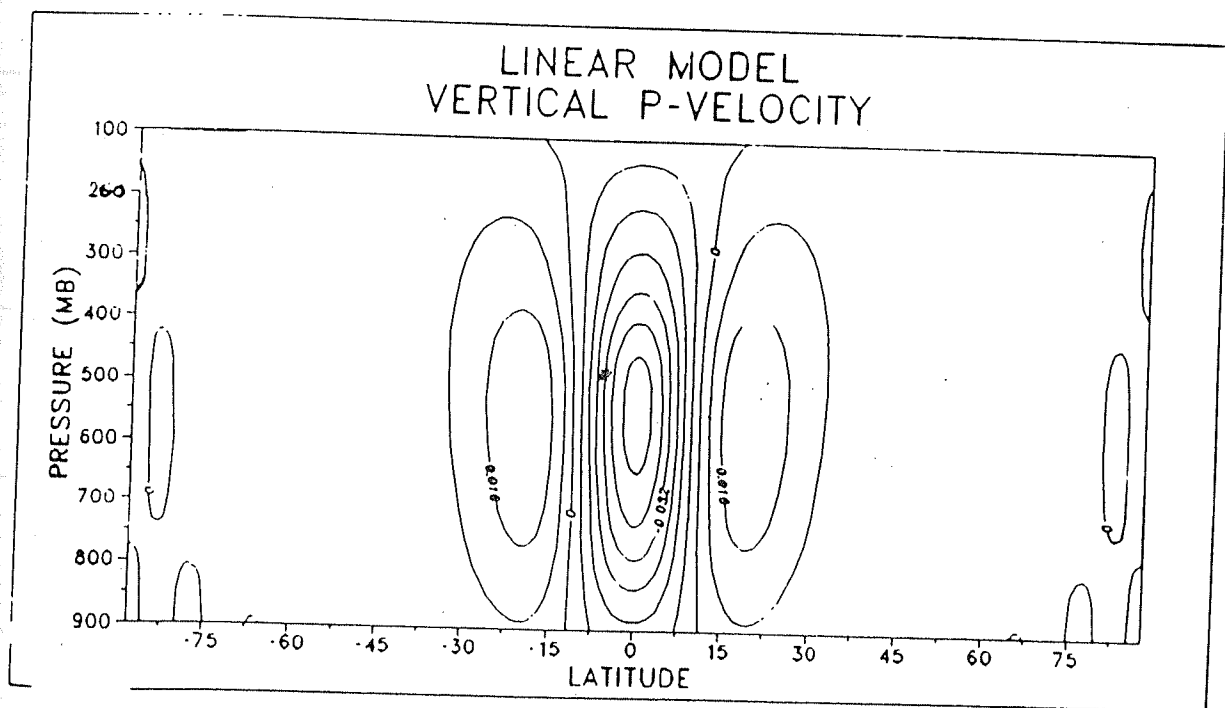
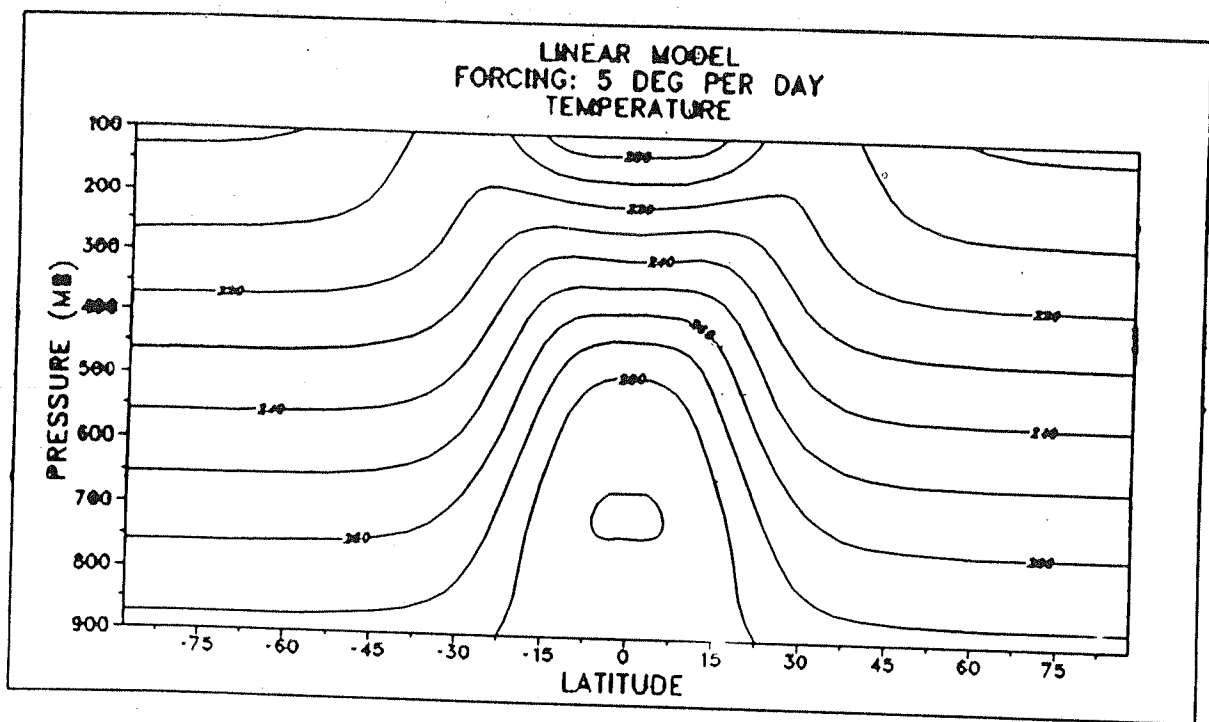


Fig.5.3b. (Top) Same as Fig.5.2b, except for LM.

Fig.5.3c. (Bottom) Same as Fig.5.2c, except for LM. Interval 0.008 Pas^{-1} .

We shall now examine the differences in the steady-state solutions between the NLM and LM and make an assessment of the impact of nonlinear terms on the time-mean Hadley circulation. The difference (NLM - LM) field for the zonal velocity is shown in Fig.5.4a. It can be seen from the difference field, that the winds are predominantly easterlies at the upper levels in the region of forcing. Even earlier, it was seen that the speed of easterlies at the lower levels was considerably smaller in the case of NLM than in the LM. In addition it was found that the easterlies remain confined to the lower levels in the LM, while they extended almost upto 300 mb in the NLM. The above mentioned features indicate that a large vertical transport of easterly momentum, over the forcing region, occurs in the NLM. It appears that this nonlinear vertical advection of easterly momentum can possibly act as a damping mechanism, by which the low level zonal winds get slowed down in the NLM. By comparing the positions of the upper level jets in the zonal wind field of NLM and LM, it is found that the core of the westerlies is located more poleward ($\sim 6^\circ$ latitude) in the NLM. This latitudinal displacement of the westerly jet, by the meridional advection term, is also evident from the difference field in Fig.5.4a. The difference field (NLM - LM) for the equilibrium temperature is shown in Fig.5.4b. Over the forcing region, one notices a large cooling that extends upto about 350 mb. The maximum cooling is about 10°K at around 500 mb. There is a smaller region of warming at the upper levels, with a maximum of 4°K at around 250 mb. The large cooling shown in the difference field indicates that the lower and midtropospheric temperatures in the LM are considerably higher as compared to the NLM. These high temperature values in the LM occur because of the neglect of nonlinear vertical advection of temperature and consequently absence of enough adiabatic cooling. It should be noted that only the linear part of the vertical advection term was retained in the thermodynamic energy equation of the LM. The difference field in Fig.5.4b also shows positive contours (max value 8°K) centered around 23°N and 23°S and

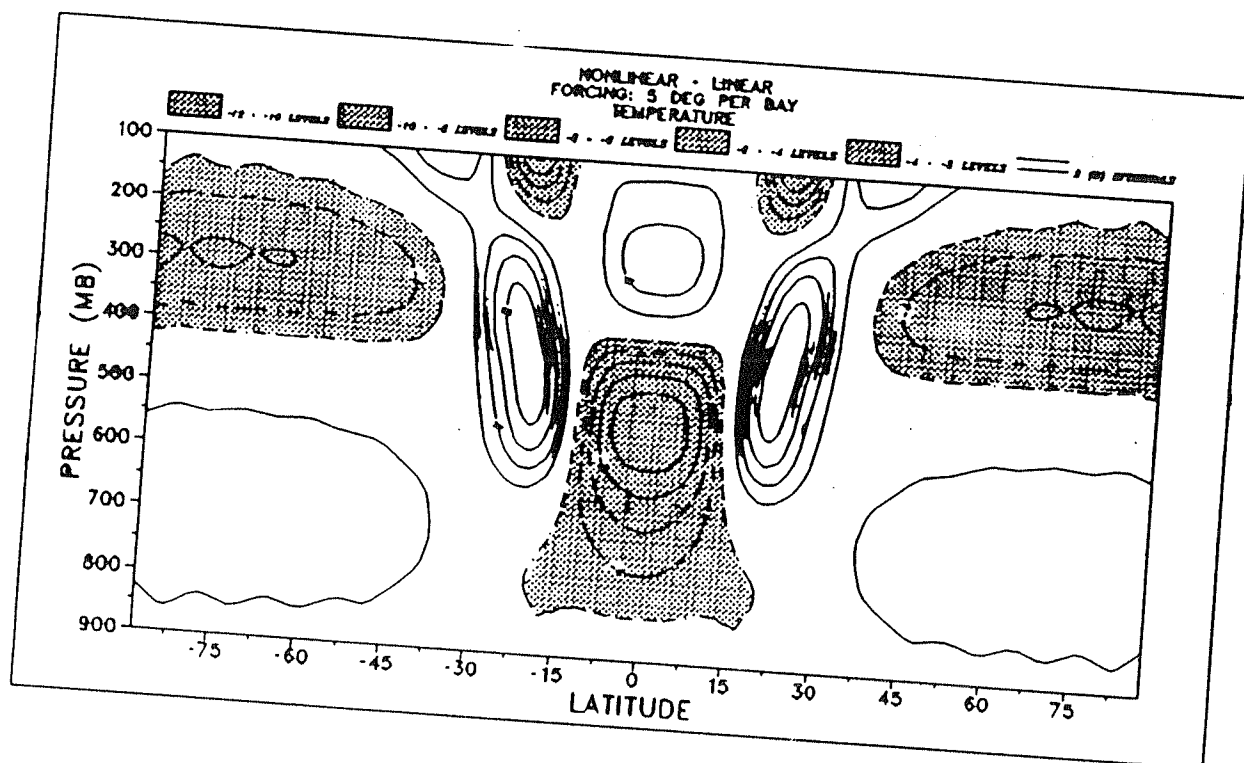
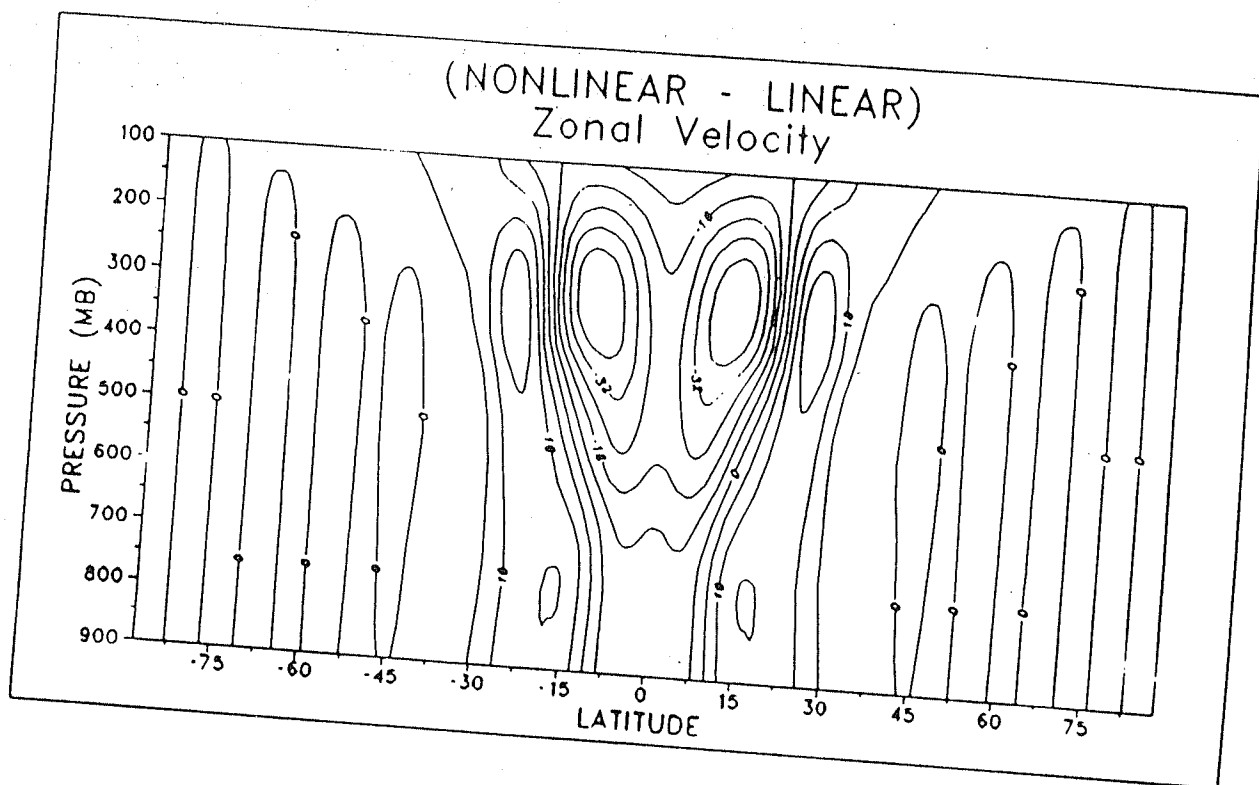


Fig.5.4a. (Top) Difference (NLM-LM) for zonal velocity. Strong forcing case. Interval 8 ms^{-1} .

Fig.5.4b. (Bottom) Difference (NLM-LM) for temperature. Strong forcing case. Interval 2°K .

located in the middle and upper troposphere. These contours are associated with the nonlinear adiabatic warming due to subsidence in the NLM. In short, Fig.5.4b shows that the neglect of nonlinear vertical advection term in the thermodynamic energy equation produces significant warming in the lower and middle levels over the forcing region. From the difference field for ω (Fig.5.4c) it is found that the nonlinear vertical advection terms can produce strong upward motions of the order -0.02 Pa s^{-1} , in the region of forcing.

Let us now examine a plot of the global mean kinetic energy (GMKE), which is defined as $\frac{1}{2g} \int \int (u^2 + v^2) p_* d\phi d\sigma$, versus time. This will be useful in estimating the changes in the kinetic energy associated with the nonlinear interactions (eg. the horizontal and vertical advection of momentum and the nonlinear vertical advection of temperature). The GMKE curves for the NLM and LM are shown in Fig.5.5. Initially, the GMKE starts monotonically increasing with time, because of the presence of transients and it later begins to flatten after having reached a steady state. It can be noticed from Fig.5.5 that, the curve A which corresponds to the NLM flattens at a lower value ($\sim 32 \times 10^5 \text{ Jm}^{-2}$) as compared to the curve B ($\sim 48 \times 10^5 \text{ Jm}^{-2}$) of the LM. The difference in the maximum GMKE between the curves A and B is about 35% of the maximum value attained in the LM (i.e., Curve B). One can immediately see that nonlinearities effectively dissipate the time-mean tropical Hadley circulation. There are two main reasons for damping of the GMKE in the NLM. We had seen before that, the presence of the nonlinear vertical advection of temperature term provides enough adiabatic cooling in the NLM. Since this nonlinear term is absent in the LM, a large warming occurs over the heating region, which is an additional source of kinetic energy generation in the LM. Secondly, one has to consider kinetic energy changes associated with the momentum transport by nonlinear advection terms. It was particularly seen that the nonlinear vertical advection of momentum can act as a dissipating mechanism by transporting easterly momentum, over the forcing region,

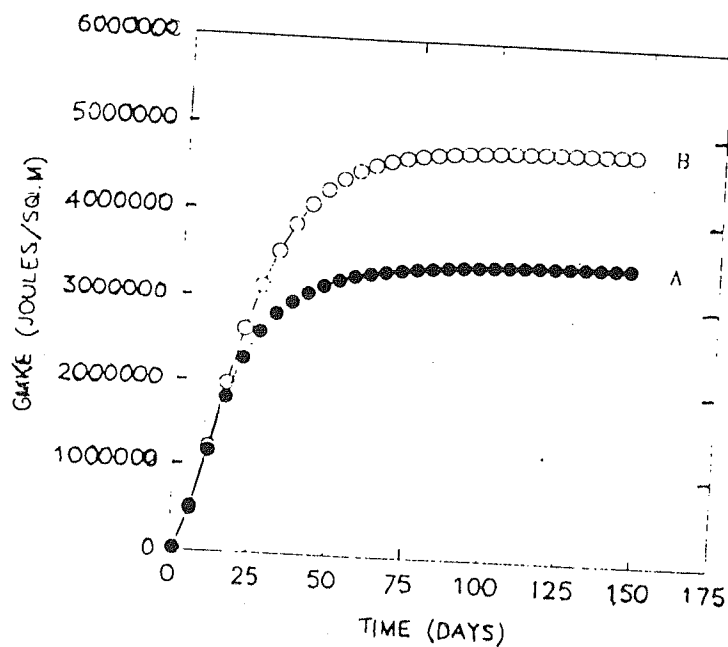
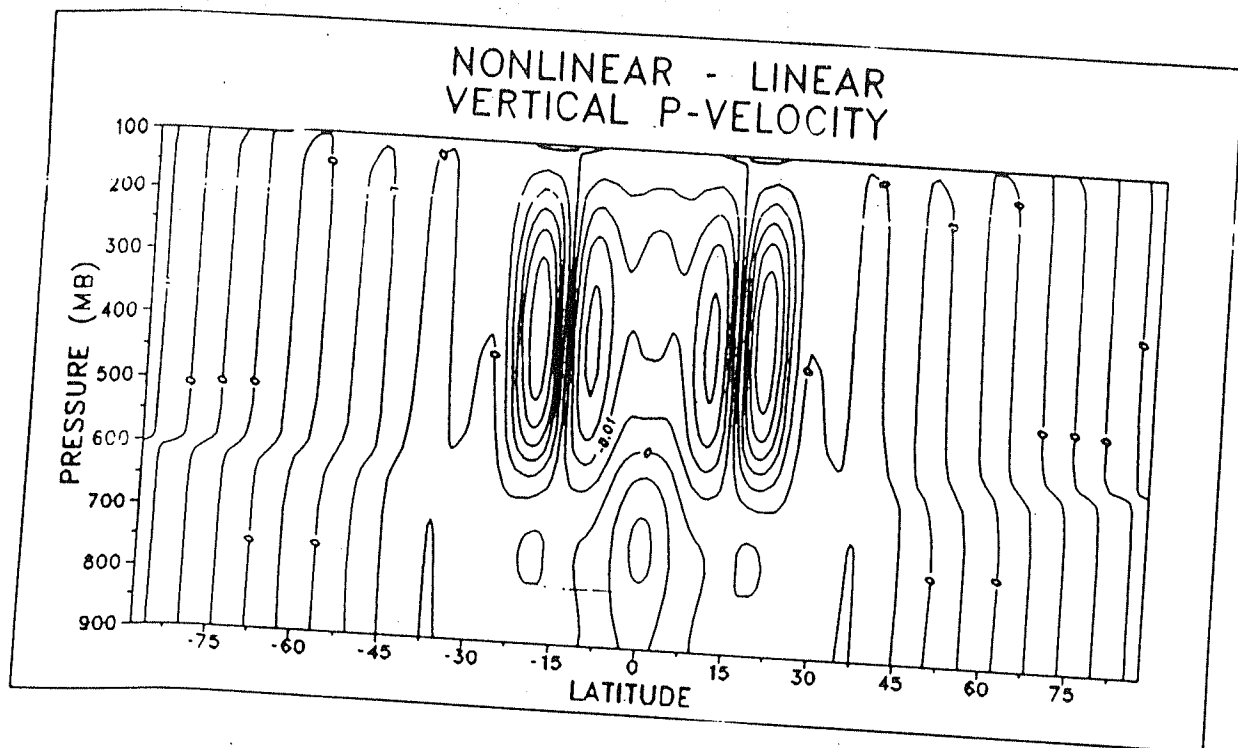


Fig.5.4c. (Top) Difference (NLM-LM) for vertical p-velocity. Strong forcing case. Interval 0.005 Pas^{-1} .

Fig.5.5. (Bottom) Time variation of GMKE in the strong forcing case. Curve A is in NLM and curve B is in LM.

from the lower to the upper levels. It appears that these two nonlinear effects can account for the lower values of GMKE in the NLM as compared to the LM.

We shall now estimate the angular momentum transport due to nonlinear meridional and vertical advection processes. Let M be the absolute angular momentum per unit mass about the earth's axis. Therefore,

$$M = \Omega a^2 \cos \phi + ua \cos \phi \quad (5.7)$$

We define $M_e = \Omega a^2 \cos \phi$ and $M_r = ua \cos \phi$. The angular momentum transport associated with the time-mean Hadley circulation are given by the terms $M1 = \frac{\hat{v}}{a} \frac{\partial \hat{M}_e}{\partial \phi}$, $M2 = \frac{\hat{v}}{a} \frac{\partial \hat{M}_r}{\partial \phi}$ and $M3 = \hat{\sigma} \frac{\partial \hat{M}_r}{\partial \sigma}$. The quantities with $(\hat{\quad})$ represent time-mean values. The term $M1$ is the Coriolis term, $M2$ represents the meridional advection of the relative angular momentum by the time-mean meridional wind and $M3$ represents the vertical advection of the relative angular momentum by the time-mean vertical component of the wind. Figs.5.6a, 5.6b and 5.6c show the latitude-pressure section of the terms $M1$, $M2$ and $M3$ respectively. From Figs.5.6a and 5.6b, it is seen that the contours of $M1$ and $M2$ are symmetric w.r.t the equator and have opposite signs at the lower and upper levels. In both the hemispheres, the values of $M1$ and $M2$ are positive at the lower levels and negative at the upper levels. This is because, the meridional wind (for eg., in the northern hemisphere) is northerly at the lower levels and southerly in the upper troposphere. It should also be noted that, $\frac{\partial \hat{M}_r}{\partial \phi}$ is positive in the northern hemisphere. It can be seen that the magnitude of the term $M2$ is quite large at the upper and lower levels. For instance at the upper levels, the maximum value of $M2$ is about $-750 m^2 s^{-2}$ while that of $M1$ is about $-400 m^2 s^{-2}$. The large values of $M2$ indicate that the nonlinear meridional advection effects are quite significant in the tropics. At the upper levels the contours of $M2$ are slightly pushed away from the equator as compared to the contours of $M1$. This indicates that the meridional advection term at the upper levels, tend to produce a poleward

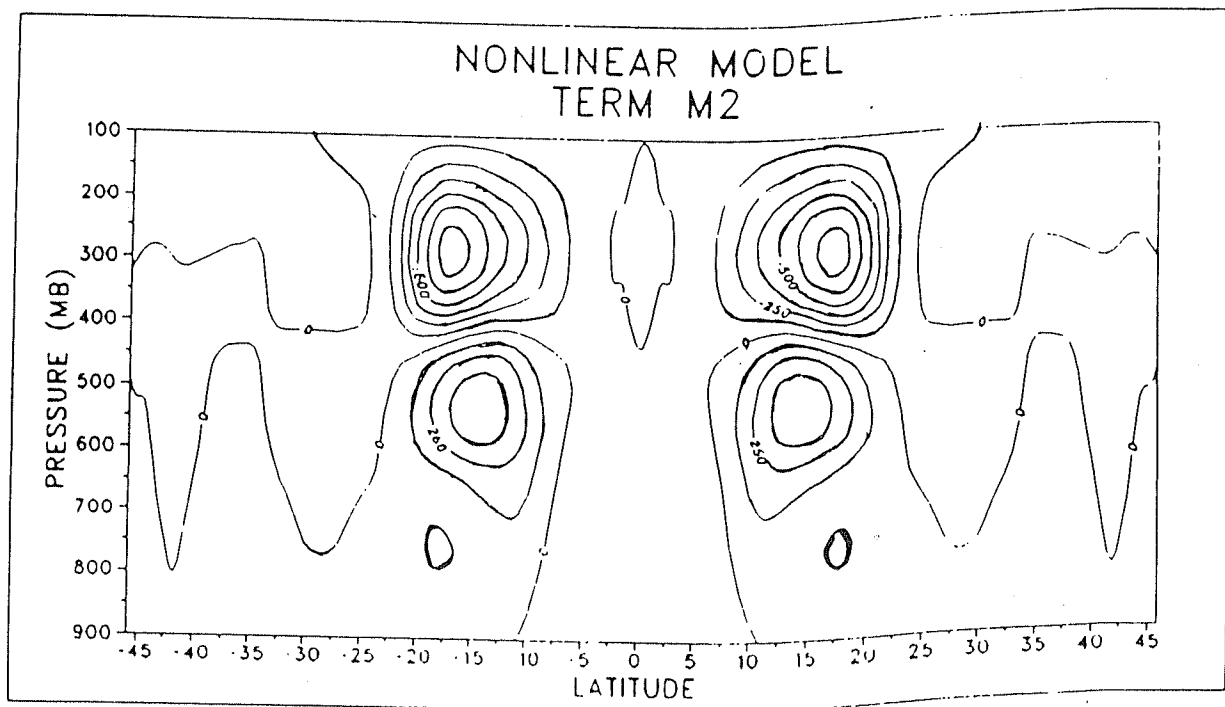
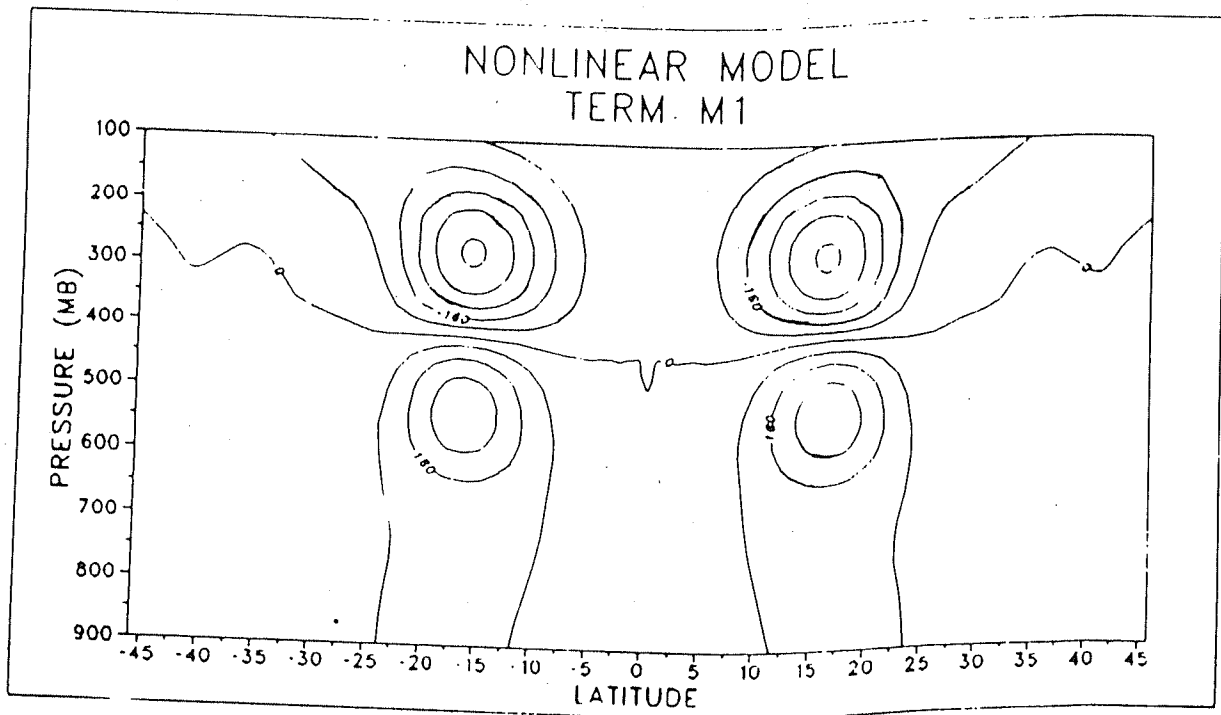


Fig.5.6a. (Top) Latitude-pressure section of term M1. Interval $80 \text{ m}^2 \text{ s}^{-2}$.

Fig.5.6b. (Bottom) Same as Fig.5.6a, except for term M2. Interval $125 \text{ m}^2 \text{ s}^{-2}$.

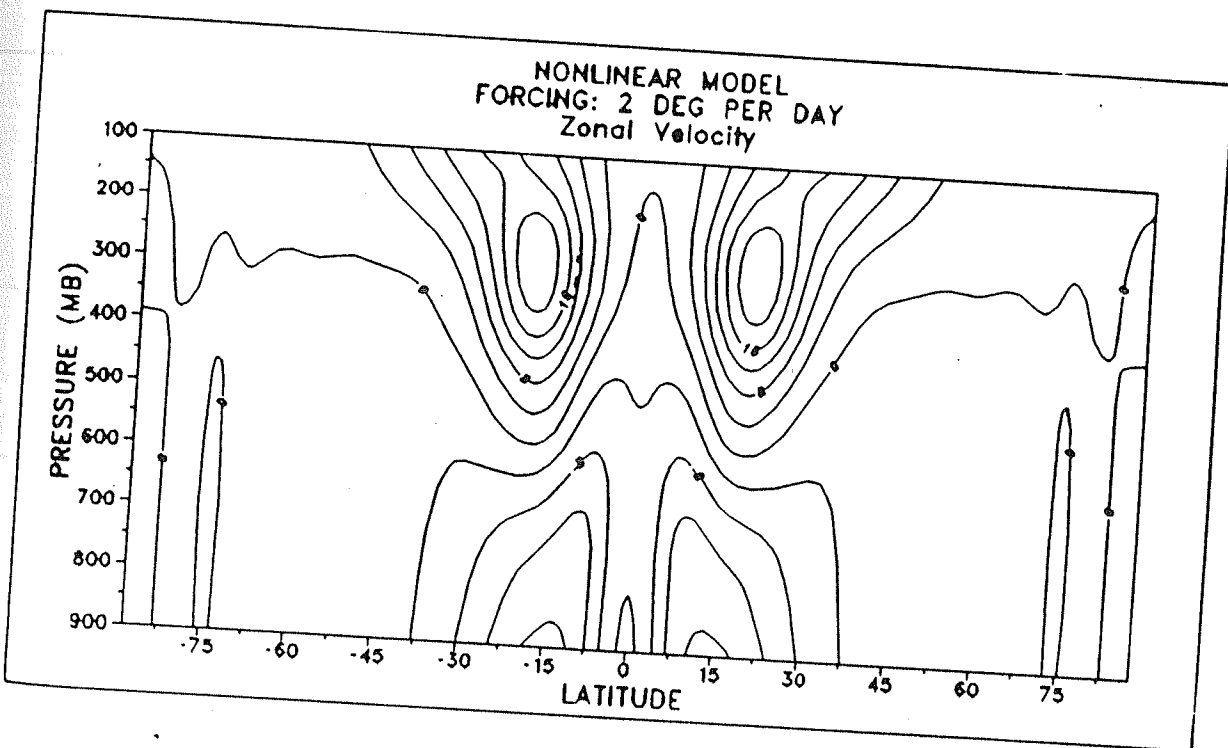
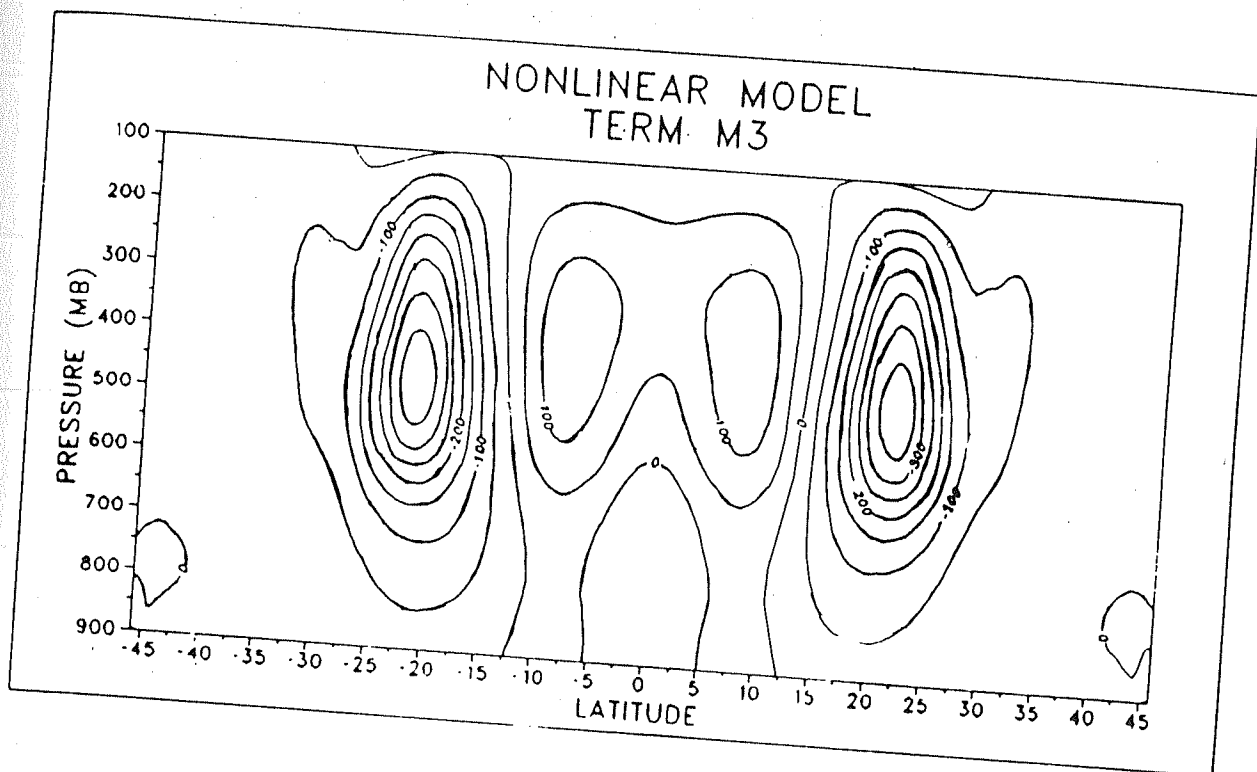


Fig.5.6c. (Top) Same as Fig.5.6a, except for term M3. Interval $50 \text{ m}^2 \text{ s}^{-2}$.

Fig.5.7a. (Bottom) Same as Fig.5.2a, except for weak forcing case. Interval 4 ms^{-1} .

displacement of the westerly jets in the NLM. It can be noticed from Fig.5.6c, that the distribution of M_3 is symmetric w.r.t the equator. The spatial distribution of M_3 can provide clue regarding the vertical transport of horizontal momentum in the nonlinear model. The values of M_3 , over the forcing region, show significantly large positive values in the middle and upper troposphere. The maximum positive value is about $100 \text{ m}^2 \text{ s}^{-2}$. It is easy to see that a transport of easterly momentum from the lower levels to the upper levels gives rise to positive values of M_3 . This is because both $\bar{\sigma}$ and $\frac{\partial \hat{M}_r}{\partial \sigma}$ are negative when easterly momentum is transported upwards, and hence their product is positive.

We have so far seen that nonlinear terms exert significant influence on the time-mean Hadley circulation induced by a strong heat source. We shall now investigate the impact of nonlinearities in the presence of a weak forcing. The structure of the weak forcing is identical to the strong heat source shown in Fig.5.1b, except that the maximum heating rate now is 2°K per day. The NLM and LM are forced using this weak heat source and integrated upto 150 days. The steady-state results are discussed below. Figs.5.7a and 5.7b, represent the time-mean zonal velocity distributions in the NLM and LM respectively. It can be seen that the response due to the weak forcing results in less intense mean meridional circulation in both the NLM and LM. The low level easterlies around 10°N is about -12 ms^{-1} in the NLM. The easterly winds in the LM over the same location have speeds around -15 ms^{-1} . The maximum speed of the upper tropospheric westerlies in the two models is almost the same ($\sim 20 \text{ ms}^{-1}$). The zonal winds in Fig.5.7a show that easterlies in the NLM extend from the surface upto about 450 mb, while in the LM (Fig.5.7b) the vertical extent of the easterlies is seen till 600 mb. However, the easterly momentum transport by nonlinear vertical advection is smaller as compared to the case of the strong forcing. The position of the upper level westerly jet in the LM is around 17°N and in the case of NLM it is located around 20°N . Thus the NLM shows a poleward shift in the upper level jet position by

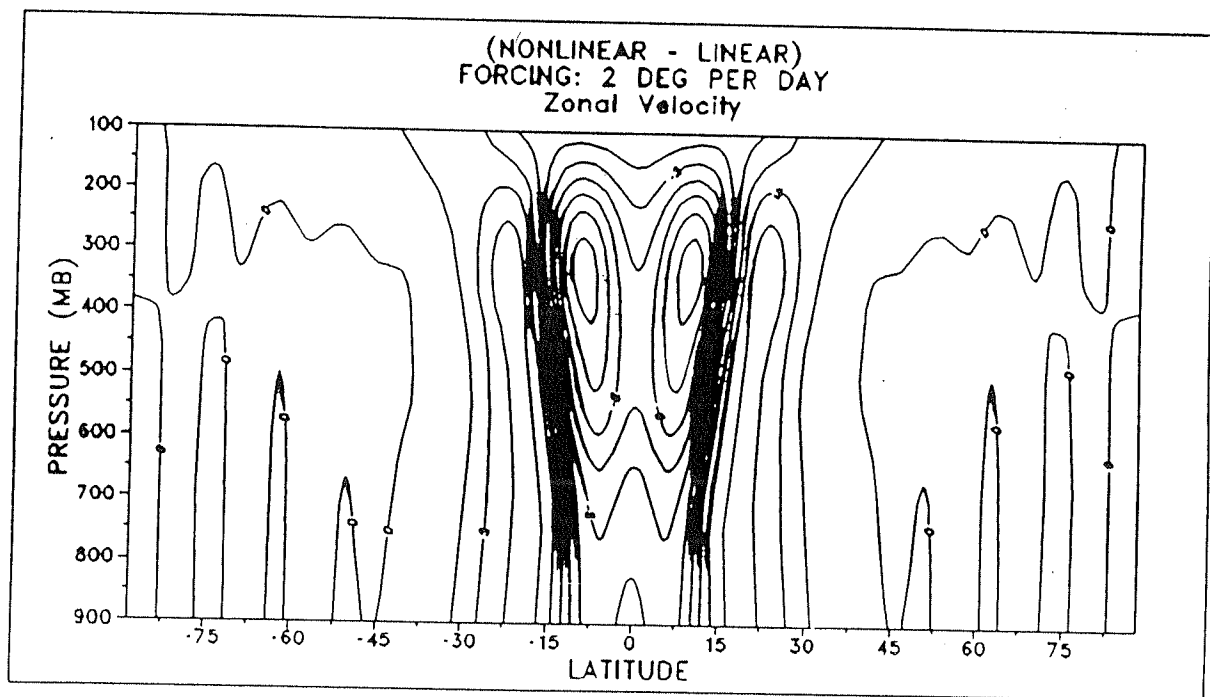
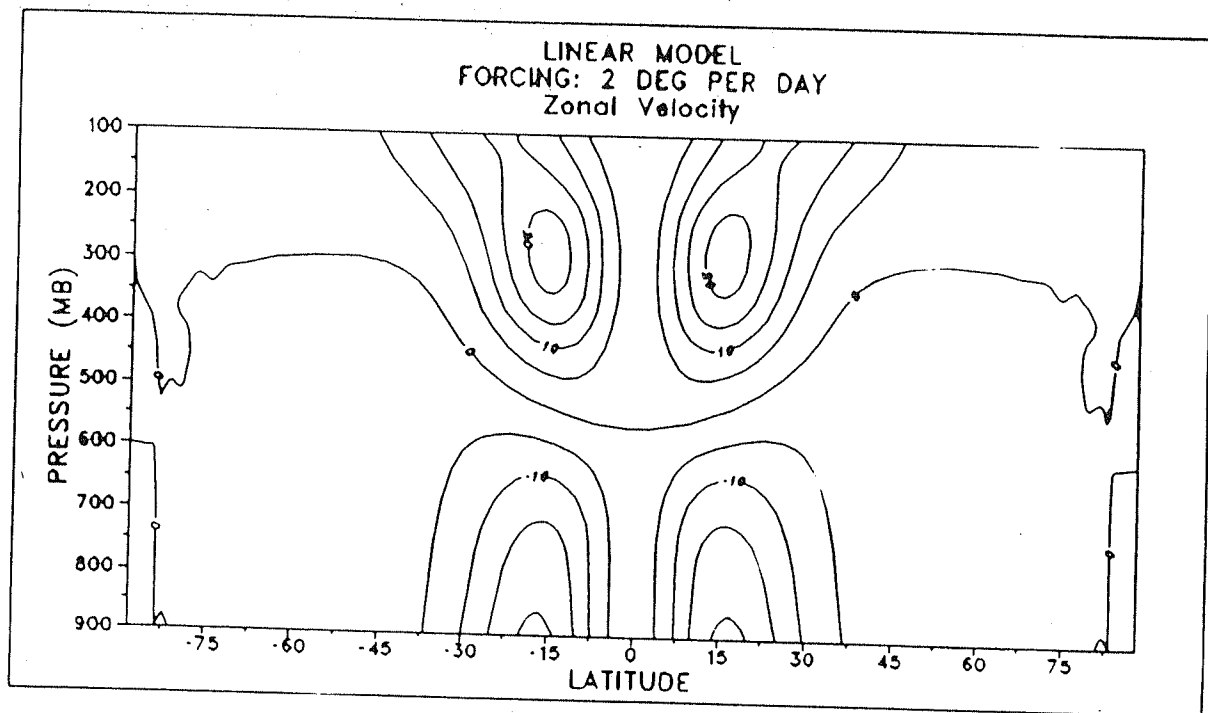


Fig.5.7b. (Top) Same as Fig.5.3a, except for weak forcing case. Interval 5 ms^{-1} .
Fig.5.8a. (Bottom) Same as Fig.5.4a, except for weak forcing case. Interval 1.5 ms^{-1} .

about 3° latitude, which is again small compared to the meridional shift seen in the case of the strong heat source. The difference field (NLM - LM) for the zonal velocity (Fig.5.8a), shows easterly predominance, at the middle and upper tropospheric levels, in the region of forcing. A maximum easterly speed of 9 ms^{-1} , associated with vertical transport of easterly momentum due to nonlinear advection, is seen at around 350 mb in Fig.5.8a. The difference field (NLM - LM) for temperature is shown in Fig.5.8b. The warming in the LM at the lower and middle troposphere, over the forcing region, has a maximum of about 1.6° K at 650 mb and a maximum cooling of 1.0° K is observed around 300 mb. Therefore for the weak forcing case, the differences in the equilibrium temperature between the NLM and LM have smaller magnitudes. The curves for GMKE (Fig.5.9) show correspondingly lower values. The GMKE values are one order lower than those in the case of the strong forcing. The GMKE curve saturates at about $63 \times 10^4 \text{ Jm}^{-2}$ in the case of LM and at about $57 \times 10^4 \text{ Jm}^{-2}$ in the case of NLM. The difference in the maximum GMKE between the curves A and B is only about 10 % of the maximum value attained in the LM. This shows that when the forcing intensity decreases the dissipation by nonlinearities becomes smaller.

5.5 Conclusions

A summary of the important results from this chapter is presented below. We have basically performed idealized forcing experiments, using both linear and nonlinear versions of a 5-level axisymmetric global spectral model, in order to understand the dynamics of the time-mean tropical Hadley circulation. The previous studies based on linear models have emphasized the need to employ cumulus friction for modelling the tropical Hadley cell realistically. However, the results of GCM simulations and nonlinear model calculations were quite contrary to those of the linear models. These

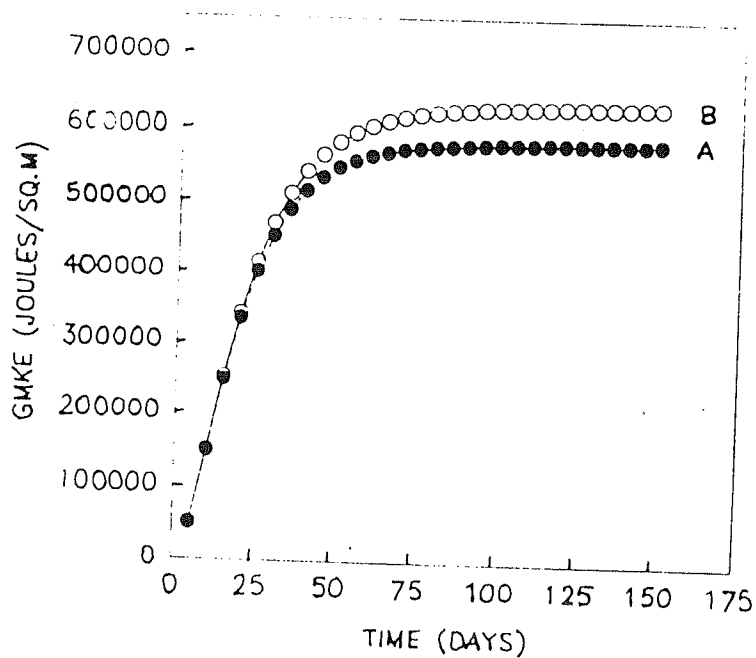
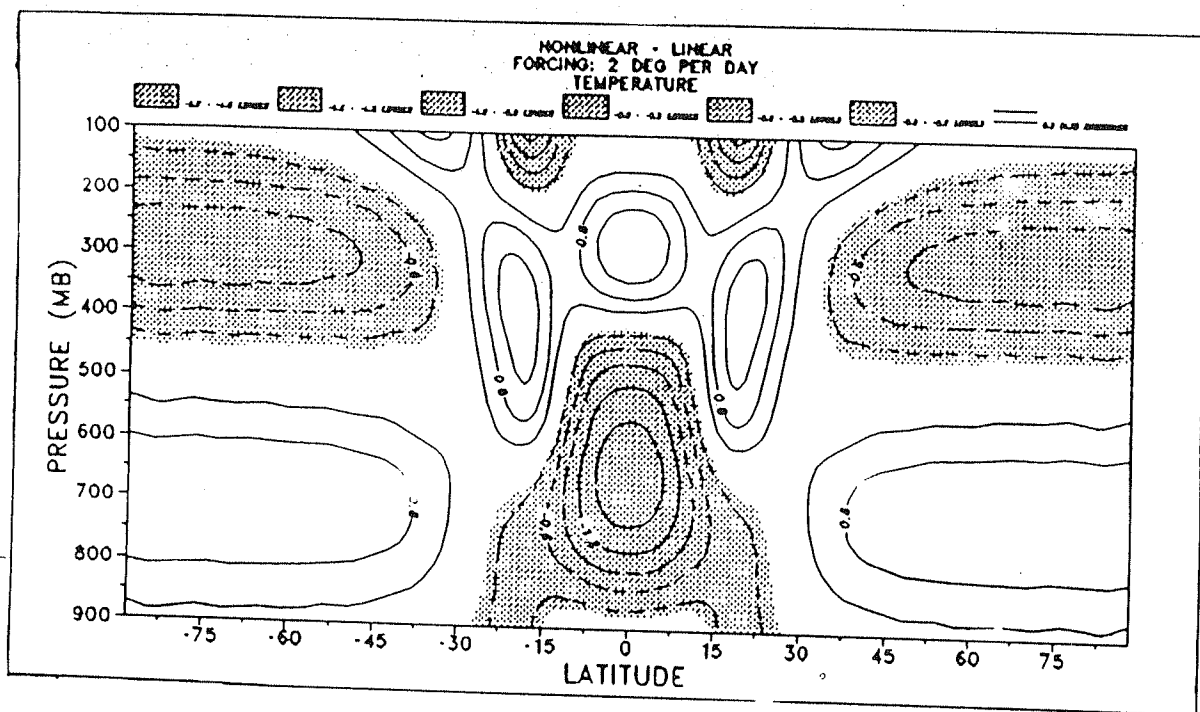


Fig.5.8b. (Top) Same as Fig.5.4b, except for weak forcing case. Interval 0.3°K .
Fig.5.9. (Bottom) Same as Fig.5.5, except for weak forcing case.

studies demonstrated that cumulus friction effects were only secondary, in determining the structure and intensity of the mean meridional circulations in the tropics. It is well known even from simple scale analysis of tropical atmospheric motions, that nonlinear advection effects are important in the low latitude regions. Therefore, it will be worth examining the impact of nonlinearities on the zonally symmetric circulations in the tropics. In our study, we have compared the linear and nonlinear solutions of the time-mean tropical Hadley circulation and delineated the effects caused by nonlinear terms. We have examined the steady-state zonally symmetric response forced by a strong heat source (maximum heating rate is 5° K per day) as well as a weak heat source (maximum heating rate is 2° K per day). The structure of the idealized heating is symmetric w.r.t the equator and has a maximum value at 500 mb and minimum at the bottom and top of the atmosphere.

It was found in the case of the strong heat source, that nonlinear terms produce a dominant impact on the time-mean Hadley circulation by transporting considerable flux of easterly momentum vertically upwards in the region of the strong forcing. The transport of horizontal momentum from the surface to the top of the atmosphere appeared to slow down the low level tropical trade winds in the NLM. Explicit calculation of the angular momentum transport by the vertical advection term also revealed that a significant fraction of the easterly momentum was transported upwards by nonlinear vertical advection. However, in the case of the weak forcing, the upward transport of easterly momentum by nonlinear vertical advection was smaller. In addition, it was found that the meridional advection terms displaced the core of the upper level westerlies, poleward by about 6° latitude. But in the case of the weak heat source, this poleward shift was smaller ($\sim 3^{\circ}$ latitude). The equilibrium temperature in the LM, showed large warming ($8-10^{\circ}$ K) in the lower and middle troposphere over the forcing region. The warming in the case of the weak forcing was about 1.5° K. This warming in the LM was a consequence of neglecting

the nonlinear vertical advection of temperature, due to which there was no adequate adiabatic cooling associated with the strong ascending motions. This extra warming in the LM generated a large increase in the global mean kinetic energy (GMKE). A comparison of the GMKE values in the LM and NLM, showed that the motions were strongly damped in the case of NLM. The damping in NLM is probably because of the two nonlinear effects (i) adiabatic cooling due to nonlinear vertical advection of temperature (ii) vertical transport of horizontal momentum. For the case of the weak forcing, the damping of GMKE was about three times smaller. In general, it was found that the effects of nonlinearities become less prominent when the amplitude of the diabatic heating decreases.

Chapter 6

The Tropical Low-Frequency Intraseasonal Oscillation and its Meridional Propagation

6.1 Introduction

The low-frequency intraseasonal oscillation, which is also referred to as the 30-40 or 30-50 or 40-50 day mode, is a coherent signal in the tropical atmosphere and accounts for much of the observed tropical intraseasonal variability. This low-frequency mode, which is an eastward propagating Kelvin wave, can be observed during all the seasons in an year. Our specific aim in this chapter is to examine the interaction between the equatorial low-frequency 30-50 day oscillation and the Indian summer monsoonal circulation.

6.1.1 Salient features of the low-frequency 30-50 day oscillation

We shall first describe some of the main characteristics of the 30-50 day oscillation, by presenting a review of the important observational findings. Madden and Julian

(1971) detected the tropical low-frequency oscillation, with a time-scale of 40-50 days, from several years of the observed zonal wind field at 850 mb and 150 mb pressure levels. A spectral analysis on long records of wind and precipitation from stations in the tropical Indian and Pacific oceans, separately for the winter and summer months was performed by Hartmann and Gross (1988). They found that the spectral peaks in the 40-50 day period range were statistically significant and exhibited strong seasonal variability. In a similar study, Lau *et.al* (1987) found the presence of 40-day and 20-day oscillations in the rainfall climatology over east Asia. An observational study by Madden (1986) reveals that in the Indian and western Pacific oceans, the eastward moving regions of enhanced convection associated with the 40-50 day oscillation force Kelvin-like waves to the east and Rossby-like waves to the west.

Studies using OLR data (a proxy for convection) have been carried out by Lau and Chan (1983), Lau and Phillips (1986), Knutson and Weickmann (1987) to investigate climate variability on the time-scale of 30-50 days. Using correlation techniques, possible relationships between the 500 mb height field and OLR were examined by Lau and Phillips (1986). They found that the 40-50 day mode was the dominant intraseasonal signal in the tropics. It was characterized by a convection zone propagating from western Indian ocean eastward to the dateline. They found that the tropical convection was strongest over the Indian ocean and western Pacific region. Lorenc (1984) and Chen (1988b) have analyzed the global velocity potential and divergence maps during the FGGE year. They found that the eastward propagating wave, with period 30-50 days and zonal wave number 1, was the dominant signal. Knutson and Weickmann (1987) performed global analyses of tropospheric winds and OLR fields, to investigate the life cycle of the 30-50 day atmospheric oscillation, for different seasons during 1979-84. They found that wavenumber-1 of the tropical divergent wind features propagate eastward around the globe throughout the seasonal cycle. The vertical structure of the oscillation varied with latitude. In the tropics, the upper and

lower tropospheric wind anomalies were about 180° out of phase. Poleward of about 20° , there was no pronounced phase-shift in the vertical. The convection anomalies were stronger over the Indian and western Pacific oceans than over tropical Africa and South America. Weickmann *et.al* (1985) analyzed several years of OLR and 250 mb circulation features and found that the strongest intraseasonal fluctuations in the tropics occurred over Indian ocean and close to the SPCZ. Based on the observations for the periods April-October (1979) and November (1982) - October (1983), Risbey and Stone (1988) have analyzed the zonally averaged atmospheric angular momentum and high cloud cover percent. Both the datasets revealed that the 30-60 day atmospheric oscillation was the dominant signal in the tropical as well as the subtropical belts. They have shown that the zonal mean tropical convection anomalies which drive the Hadley circulation, can influence the midlatitude weather systems.

Krishnamurti *et.al* (1988) have examined the fluxes of latent heat and sensible heat between the ocean and the atmosphere utilizing the observations from the global experiment. They found pronounced variance (0.5° - 1.0°) in the SST, on the time-scale of 30-50 days, over the equatorial western Pacific and the Bay of Bengal. On this time-scale, they found that the latent heat from the ocean to the atmosphere was about 20 - 30 Wm^{-2} . Their study indicated that the oscillations of both the wind and the SST contribute to a strong coupling of the atmosphere and the ocean on this time-scale. The seasonal and spatial variations of the observed tropical winds at 850 mb and 150 mb were analyzed by Gutzler and Madden (1989). They found that the intraseasonal oscillation in the global tropics exhibited two types of feature. Across the 'convective regime' that extends between the eastern Indian ocean and western Pacific ocean, the intraseasonal oscillation showed little seasonal variation and propagated eastward with a slower speed and elsewhere 'dry-regime' the oscillation underwent strong seasonal modulation and had faster eastward propagation speed. Chen and Yen (1986) showed that the low-level Somali jet exhibited a 40-50

day oscillation and intensified when the monsoon trough over northern India deepened. Since water vapour is carried eastward by the Somali jet, it was proposed that the low-frequency variability in the intensity of the jet can affect the monsoon rainfall over India. Weickmann and Khalsa (1990) noticed a slow propagation of convective activity from the Indian ocean to the western Pacific ocean on the time scale of the 30-60 days using OLR and satellite low-level moisture data. Hsu *et.al*(1990) have documented the intraseasonal oscillation during 1985-86 northern winter circulation. They found that the initiation of tropical convection in the Indian ocean resulted in the combination of a stationary wave over the maritime continent and an eastward propagating wave moving from the Indian ocean into the central Pacific. They also found that the wave train triggers a response in the meridional direction over the western Pacific. Lau and Chan (1988) and Wang and Murakami (1988) have analyzed the possible relationship between the intraseasonal and planetary scale interannual fluctuations in the tropical convection.

There are a few diagnostic studies of the intraseasonal oscillations using GCM outputs. Hayashi and Sumi (1986) performed numerical experiments using a GCM to investigate the 30-40 day oscillation in the tropics. The model was forced using a SST distribution and the results of the model integration showed the spontaneous appearance of a collective motion of convective activity, with an east-west wavenumber 1 that resembled the observed 30-40 day mode. The model oscillation showed a double structure consisting of a small scale structure (< 3000 km) and a larger scale (wave number 1). Both these structures propagated eastward with a speed of 15 ms^{-1} . Lau *et.al* (1988) have described the structure of the tropical intraseasonal oscillations of an idealized GCM with a zonally symmetric climate and fixed surface temperature. The simulated circulation patterns had a well-defined spectral peak in wavenumber 1 and a period of about 25 days. However the model's precipitation showed small

scale disturbances with wavenumber 2-5 that propagated eastward with a speed of 18 ms^{-1} . Eastward propagating disturbances of period 30-60 days were produced in a GCM integration by Swinbank *et.al* (1988). The structure of the disturbances resembled the slowly propagating Kelvin wave. The latent heat release from areas of active precipitation associated with the Kelvin wave reduced the static stability and hence slowed down the wave. The space-time spectral analysis of Hayashi and Golder (1986) showed that intraseasonal oscillations, in the northern summer, appeared in the GCM at GFDL. The wavenumber 1, with periods of 40-50 days and 25-30 days, which was the dominant spectral component agreed well with the FGGE data. Chao (1987) has demonstrated that the tropical intraseasonal oscillation should be viewed as an intrinsic instability, whose speed is a weighted mean of the speed of the Kelvin wave and that of the Rossby wave. A comprehensive study of the structure of the tropical intraseasonal oscillations appearing in a GFDL GCM has been carried out by Hayashi and Golder (1988). They found that the intraseasonal oscillations take the form of a Kelvin-Rossby wave pattern in the upper troposphere. Slingo and Madden (1991) have simulated the tropical intraseasonal oscillation using the NCAR model and shown that the vertical and horizontal structure of the simulated oscillation compares well with the observations. It was found that the zonal wind perturbations were characterized by an out-of-phase behaviour between the lower and upper troposphere which was most coherent in the convective regions of Indian ocean and west Pacific. The period of the simulated intraseasonal wave was around 25 days.

6.1.2 Theoretical explanations for the low-frequency wave

There are quite a few theoretical explanations for the slow eastward propagation of tropical convection. Chang (1977a) suggested that the eastward propagation is the manifestation of convectively driven equatorially trapped Kelvin waves. Davey (1984) has simulated an eastward propagating Kelvin wave, using a simple moist model of

the tropical atmosphere. The latent heating in the model was interactively determined and the saturation moisture content was closely linked to SST. Davey (1984) and Lau and Shen (1988) proposed that over the warm regions in the western Pacific and Indian oceans, the atmospheric moisture content being higher, lowers the static stability of the atmosphere. Therefore the intraseasonal oscillation slows down due to the reduction in the static stability. Many features of the tropical 40-50 day oscillation, including the modulation of the subtropical jet and the eastward and poleward propagations of zonal wind anomalies, have been reproduced by stratified models (eg. Anderson and Stevens (1987a)). Low-frequency modes resembling the tropical 40-50 day oscillations were reproduced in a zonally symmetric model by Anderson and Stevens (1987b). A simple theory for the 30-60 day oscillation has been presented by Emanuel (1987). The theory is based on the idea that the oscillation is a manifestation of an air-sea interaction instability driven by wind-dependent surface fluxes of moist entropy. Moist convection is treated as a means of rapidly redistributing the heat acquired by the sea surface in the vertical. Neelin *et.al* (1987) have proposed a mechanism by which feedback between zonal wind perturbations and evaporation can create unstable low-frequency modes that resemble the tropical 30-50 day oscillation. Wang (1988) showed that the tropical low-frequency waves could be simulated in a 2-layer model, which incorporates a circulation dependent heating based on boundary layer convergence. He showed that the slow eastward moving disturbance becomes unstable when the condensational heating which is jointly supported by the interior wave convergence and frictional convergence dominates over the dissipation due to longwave radiation and boundary layer viscosity. He showed that an increase in SST resulted in an increased growth rate for all wavelengths, but the maximum growth rate shifted to shorter wavelengths.

There are quite a few theoretical explanations based on wave-CISK (conditional instability of the second kind), which is a co-operative mechanism between

the planetary scale wave and the smaller scale cumulus convection, for the eastward propagation of tropical convection on the time-scale of 30-50 days. The underlying concept in the wave-CISK mechanism is that the planetary scale wave convergence supports the small scale convective activity which in turn drives the planetary scale circulation. Lau and Peng (1987) have shown that the observed eastward propagation of intraseasonal oscillation in the tropical atmosphere arises as an intrinsic mode of oscillation resulting from an interaction of convection and internal dynamics via the mobile wave-CISK mechanism. Through this mechanism, the heat source feeds on the intrinsic east-west asymmetry of equatorial waves. As a result, Kelvin waves are selectively amplified, which subsequently causes the heat source to propagate eastward. Based on the wave-CISK theory, Takahashi (1987) obtained the slow phase-speed of the intraseasonal oscillation. Using a simple linear shallow-water moist model on a sphere, Yamagata (1987) has shown that the mutual interaction of equatorial dynamics and convective activity produces a tropical mode which is consistent with the observed 30-50 day oscillation in the tropics. The CISK theory for tropical intraseasonal oscillations by Miyahara (1987) assumes that the CISK parameter is dependent on the SST distribution and is large over regions of high SST denoting stronger convective activity in these regions. He has shown that the unstable disturbance generated in the regions of high SST grows as it moves eastward. As the unstable disturbance propagates to regions of low SST, it decays with time. Hendon (1988) has investigated the impact of cumulus heating mechanism on equatorially trapped disturbances using both nonlinear and linear single vertical mode models. He found that in the nonlinear model, the growing CISK modes rapidly stabilized the atmosphere. The maximum stability occurred to the west of the CISK heating, thus leading to an eastward propagation with a speed of about 10 ms^{-1} . This mode had a substantial meridional velocity perturbation and resembled a coupled Rossby-Kelvin wave. This coupled Rossby-Kelvin mode explained many features associated with

the observed 40-50 day oscillation. Chang and Lim (1988) found that interactions between vertical modes in the tropical atmosphere could result in two type of CISK modes. They found that when the heating was maximum in the lower troposphere, an internal mode which was unstable was excited. This mode was stationary and had a deep vertical scale. However, when the maximum heating was located near the mid-troposphere, the CISK modes propagated eastward with a phase-speed of $15\text{-}20\text{ ms}^{-1}$. These modes resulted from an interaction of two internal modes and closely resembled the low-frequency oscillations in the tropics. Wang and Chen (1989) proposed that the unstable interactions between the boundary-layer frictional moisture convergence and associated latent heat release account for two important characteristics of the observed intraseasonal tropical disturbances. This mechanism explained the preferred zonal scale of wavenumber 1 and a vertical baroclinic structure which is asymmetric w.r.t the middle troposphere with largest amplitudes of the zonal wind and geopotential anomalies occurring in the upper troposphere. According to Sui and Lau (1989), tropical low-frequency oscillations having periods of 20-50 days are excited by the convective heating which is determined by the SST distribution. The period of these oscillations depends primarily on the vertical distribution of heating through mobile wave-CISK. They found that the 20 day period mode was excited by deep convection which had a maximum at 500 mb and above. On the other hand when the heating was confined between 500 mb and 700 mb, it was found that the 50 day period mode was excited. It was also found that heat fluxes from the ocean further destabilized the wave-CISK modes.

6.1.3 Meridional propagation of the low-frequency oscillation

Till now, we have discussed the various observational, diagnostic and theoretical studies pertaining to the eastward propagation of the tropical convective activity on

periods ranging from 30-50 days. An outstanding feature of this equatorial wave is its interaction with the mean meridional circulation during the Indian summer monsoon. During the months between June and August, the arrival of the low-frequency mode over the Indian longitudes is followed by a slow and distinct northward propagation of convective activity from the equator into the subcontinent. The meridional progression of the low-frequency intraseasonal perturbations, during summer (1979), over the Indian monsoon region is shown in Fig.6.1. There are several studies in the past which indicate that the summer monsoonal activity over India is being modulated by the low-frequency intraseasonal oscillation. The low-frequency variability of the Indian summer monsoon activity manifests in the form of onset, active and break cycles (Fig.6.2). In order to understand the behaviour of the active and break phases associated with the Indian summer monsoon, it is extremely important to investigate the mechanisms that govern the interaction of the equatorial low-frequency oscillation with the Indian summer monsoon circulation.

We present below a few important observational findings connected with the subseasonal low-frequency variability in the Indian summer monsoon. Yasunari (1979, 1980) examined the fluctuations in the cloud cover during the northern hemispheric summer and noted a meridional propagation of cloudiness anomalies, over the whole of Asian monsoon area, in the range of around 40 days. The northward movement was most apparent over India. He associated the fluctuation of the mode with the major active-break cycle over India. In a further study, Yasunari (1981) found that the geopotential and wind fields also exhibited the 40-day oscillation over the Indian summer monsoon region. The perturbations of geopotential and wind showed a marked northward movement towards the Himalayas confirming the association between the major active-break cycle of monsoon activity and the low-frequency variability in the tropics. Kasture and Keshavamurty (1987) performed a power spectrum analysis of the zonal wind over the Indian summer monsoon region and found that a large

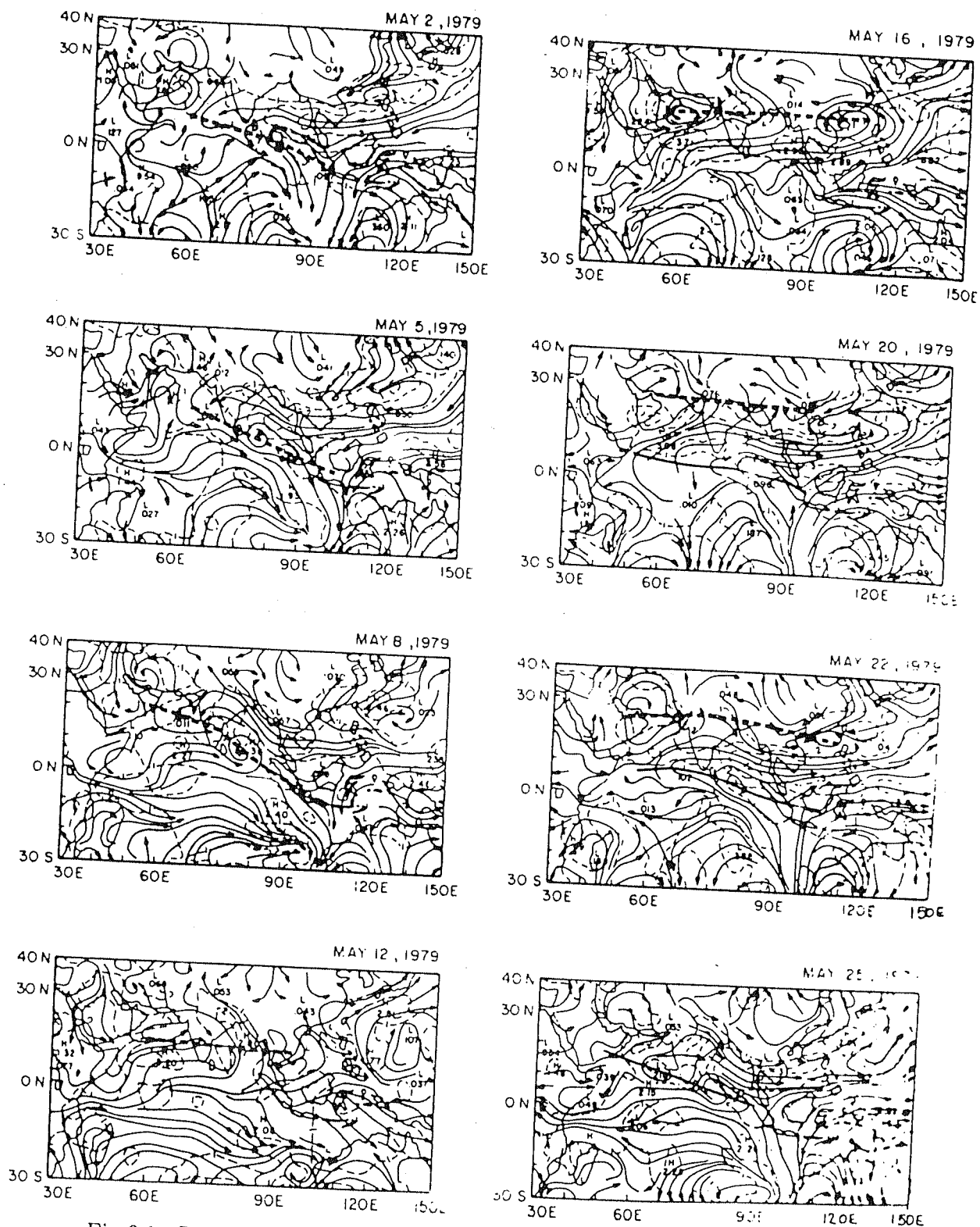


Fig.6.1. Streamlines (solid lines) and isotachs (dashed lines) showing the northward progression of the 30-50 day mode over the Indian summer monsoon region during summer (1979). (Adapted from Krishnamurti and Subrahmanyam (1982))

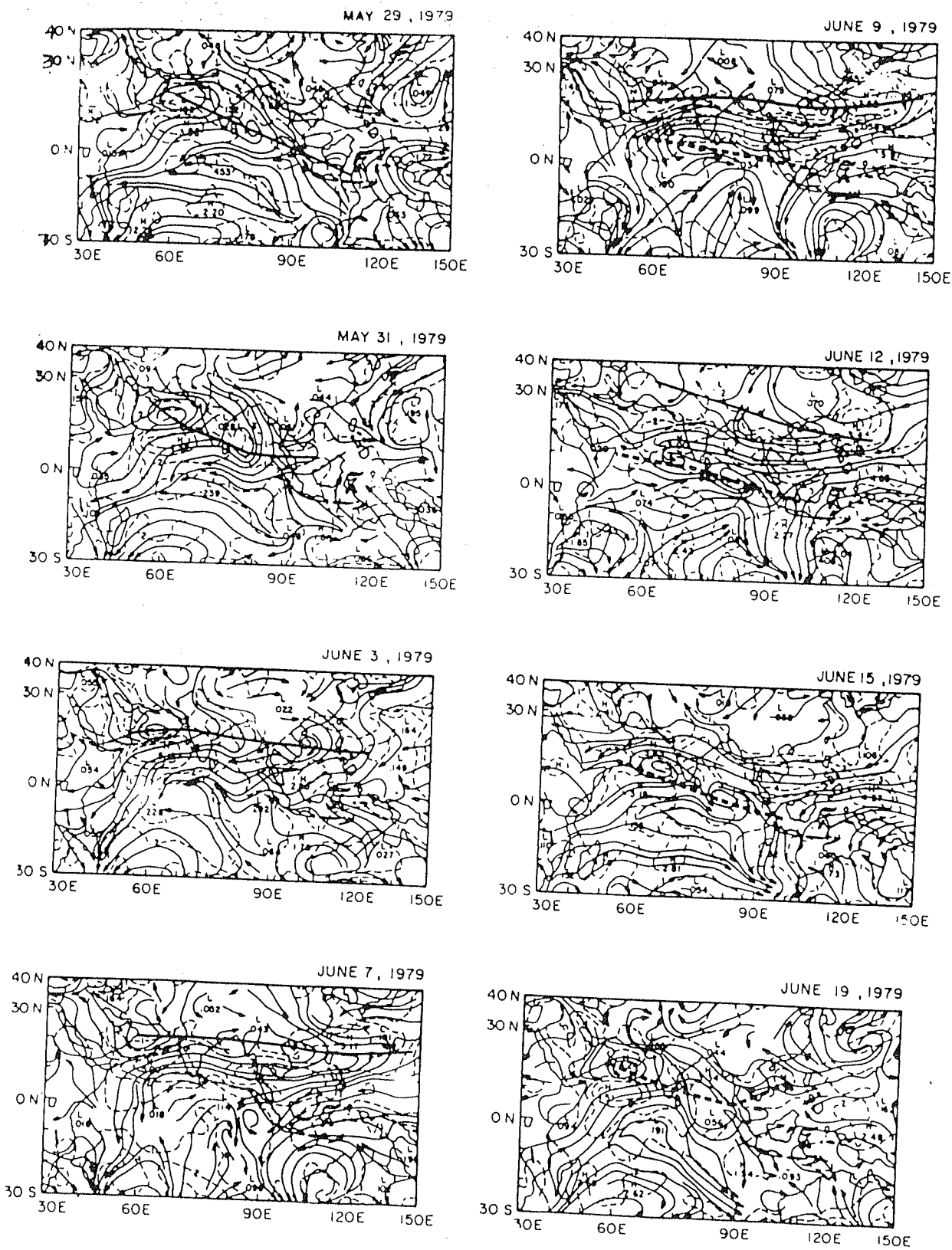


Figure.6.1

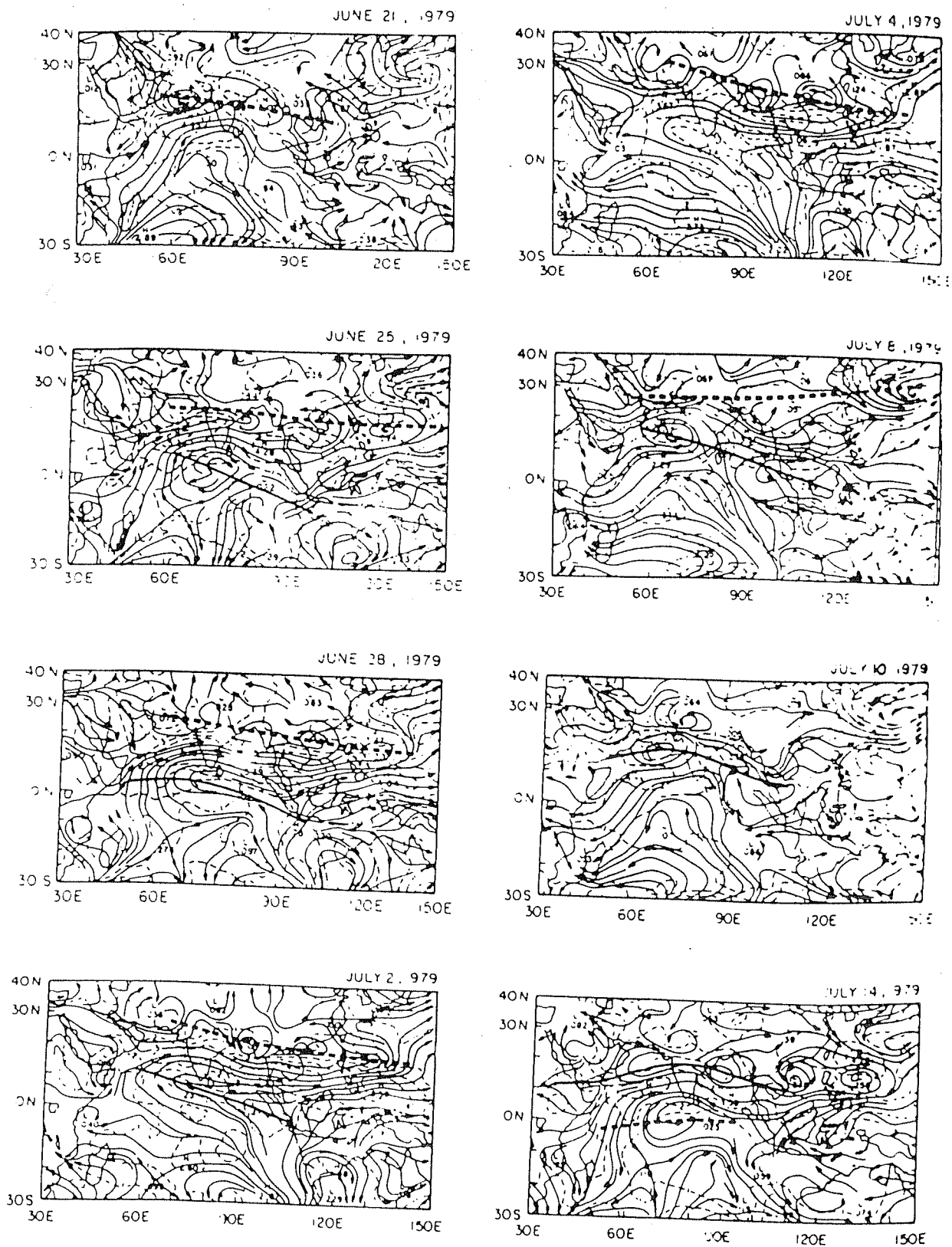


Figure.6.1

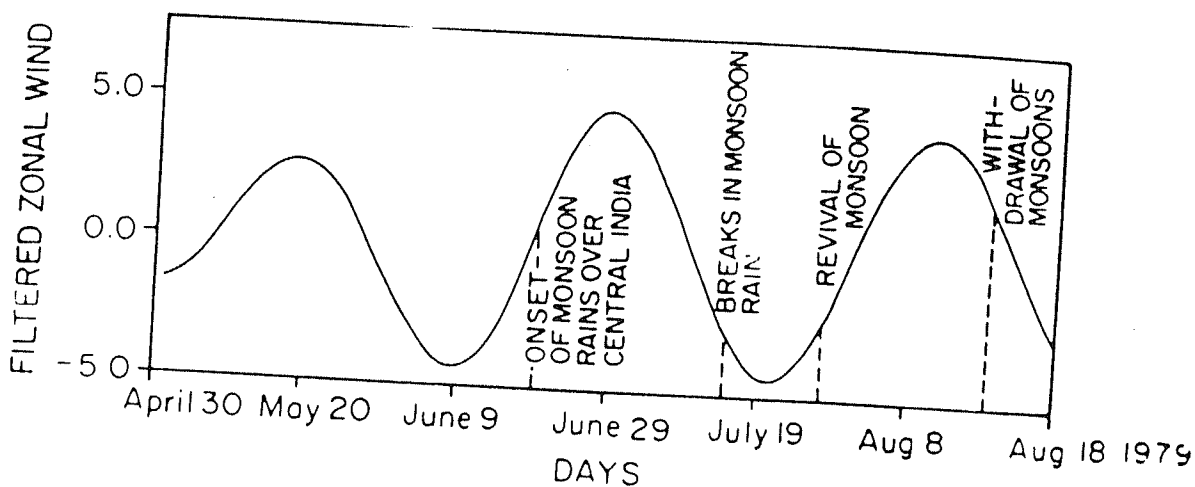


Fig.6.2. Filtered zonal wind data showing the low-frequency intraseasonal variability of the Indian monsoon activity during summer (1979). (Adapted from Krishnamurti and Subrahmanyam (1982))

power occurred on the time scale of 30-50 days. Based on cloud cover observations, Sikka and Gadgil (1980) found that during the months between June and September, the maximum cloud zone over India occurred mostly to the north of 15°N and a secondary maximum in the equatorial region. They found that a break in monsoon occurred when the maximum cloud zone in the northern latitudes disappeared for about 4 weeks. This cloud cover gets reestablished by a northward movement of the secondary maximum cloud zone from the equator. Krishnamurti *et.al* (1985) identified an eastward moving planetary scale divergent wave, having a period of 30-50 days, during the FGGE year. The amplitude of the signal was largest during the summer season over the monsoon region and the western Pacific ocean. As the oscillation traversed over eastern Pacific and Atlantic, its amplitude decreased. From their global and regional analyses, it was seen that the equatorial convective activity propagated northward over the Indian summer monsoon region. The OLR analysis by Murakami *et.al* (1986) and the diagnostic study based on GCM outputs by Lau and Lau (1986) also reveal similar results. Keshavamurty *et.al* (1986) inferred the meridional propagation of the low-frequency intraseasonal mode by calculating its 'meridional refractive index'. Observations by Knutson *et.al* (1986) suggest that both OLR and zonal wind at 250 mb exhibit the characteristics of a zonal wavenumber 1 structure. They found that the amplitude of the low frequency convection was large over the Indian monsoon region and tropical western Pacific. Near the region of strong convection, the intraseasonal oscillations propagate eastward at a speed of about 6 ms^{-1} , while they propagate at about 15 ms^{-1} over the drier regions of the tropics. Prominent northward propagation ($1\text{-}2 \text{ ms}^{-1}$) of OLR anomalies occurred in the Indian monsoon region. Keshavamurty *et.al* (1988) obtained a rough estimate of the northward phase speed of the intraseasonal mode to be around a few ms^{-1} .

Murakami (1980) subjected the OLR data over the winter monsoon region to an EOF analysis and found the existence of dominant peaks at about 15-30 days. The

15-30 day mode exhibited large deviations over Bay of Bengal, Indian ocean, Philippines and western Pacific regions. Krishnamurti and Subrahmanyam (1982) subjected the wind field at 850 mb, during the summer monsoon experiment (MONEX), to a time series analysis and confirmed the existence of a peak in the time range of 30-50 days. They have also shown that there is steady meridional propagation of a series of troughs and ridges that form at the equator and dissipate near the Himalayas. The meridional scale, propagation speed and amplitude of this mode are 3000 kms, 0.75° latitude per day and $3-6 \text{ ms}^{-1}$ respectively. Using FGGE data, Murakami and Nakazawa (1985a) found that, when active monsoons occur over South Asia, the Walker circulation becomes stronger resulting in strong low-level easterlies over the eastern Pacific and westerlies over the Indian ocean and western Pacific. During the break monsoon phase the equatorial Walker circulation weakens. Thus there exists a strong association between the south Asian monsoon activity and the equatorial Walker circulation. The global analysis of FGGE data by Krishnamurti and Gadgil (1985) and the OLR analysis by Lau and Chan (1985,86), revealed that the low-frequency weather systems propagate from the equator to the Himalayas during the northern summer. They also found that during the northern winter, the low-frequency oscillations exhibited a northward movement over the eastern Pacific. Chen *et.al* (1988a) studied the water vapour transport over the entire Asian monsoon region using the FGGE data set. They found that the movement of the water vapour convergence zone was linked with the eastward propagating 30-50 day oscillation. Using 70 years of daily precipitation records from 3700 stations in India, Hartmann and Michelson (1989) carried out a spectral analysis. They showed that the precipitation exhibits a dominant periodicity of about 40 days over most of South India during the northern summer. They showed that the structure of the oscillation had close resemblance with the tropical 40-50 day oscillation. Their study indicates that the active and break phases associated with the Indian summer monsoon are caused because of

its interaction with the equatorial 40-50 day oscillation.

In the past there have been a few theoretical attempts to understand the meridional propagation of the low-frequency intraseasonal convection in the tropics. Webster (1983) addressed the issue of meridionally propagating monsoonal low frequency waves. He showed that the temperature contrast between the warm land area to the north of the cloud zone provides a differential heating, which if modelled, with a detailed surface hydrology could provide realistic phase propagation. Webster and Chou (1980) have investigated the transients and low frequency variability associated with the monsoon system, using a zonally symmetric atmospheric model coupled to an interactive ocean. The ocean-continent heating and hydrological effects on the seasonal structure of the monsoon were discussed. Goswami and Shukla (1984) used the symmetric version of the Goddard Laboratory of Atmospheric Sciences (GLAS) climate model to study low-frequency fluctuations in the tropics and the transient behaviour of the ITCZ. They found that the interaction between the moist convective heating and the model dynamics produced a quasi-periodic behaviour in the Hadley circulation. The dominant time-scales occurred in the range of 20-40 days and the wave propagated to the position of maximum radiative heating. They found that the amplitude of the oscillation was large over the land as compared to that over the ocean. They suggested that the evaporation from the land surface plays a key role in generation and maintenance of this phenomenon. Goswami *et.al* (1984) used the symmetric version of the GLAS climate model to study the interaction of the CISK and the imposed SST in determining the position and structure of the ITCZ. They found that the ITCZ occurred over the region of SST maximum in most of the experiments. The issue of the interaction of the monsoon large-scale circulation and the near equatorial low-frequency oscillations has been addressed by Lau and Peng (1990). They have shown that this interaction generates unstable baroclinic disturbances having spatial scales of about 3000-4000 kms and periods of 5-6 days over the

monsoon region. They have also shown that the westward propagating disturbances generated over the monsoon region are the manifestation of heat-induced unstable Rossby waves. The large vertical wind shear and the plentiful supply of moisture leading to the reduction of the static stability favour the instability.

The studies by Webster(1983), and Goswami and Shukla (1984) emphasize the role of surface hydrology and land surface processes in determining the meridional propagation of the tropical low-frequency perturbations. One of the shortcomings in the above studies is that, the meridional phase speed is almost two times faster than the observed propagation rate. There is also a second school of thought (eg. Keshavamurty *et.al* (1988) and Krishnan *et.al* (1992)) in which the interplay between the monsoon basic flow and tropical cumulus convection is considered to be the primary physical basis that decides the meridional propagation of tropical low-frequency oscillation. Numerical experiments performed by Krishnan *et.al* (1992) using an axisymmetric version of a global spectral model suggest that cumulus heating through CISK reproduces the phenomenon of northward propagation fairly well. It has been shown that the perturbations which closely resemble the tropical low-frequency mode, migrate northward at the rate of about 0.5° latitude per day. In the next section we shall investigate the interactions between the monsoon circulation and the cumulus heating associated with the 30-50 day mode, and examine the phenomenon of northward movement of the low frequency mode.

6.2 Northward propagation in an axisymmetric global spectral model

We have used an axisymmetric version of a 5-level nonlinear global spectral model to study the meridional propagation of equatorial convective activity associated with the

low frequency intraseasonal oscillation. The motivation behind this study is to understand the interplay between the model dynamics and the interactively determined convective heating in producing the slow meridional migration of convective anomalies over the Indian summer monsoon region. The formulation of the axisymmetric 5-level global spectral model has already been described in Chapter V.

We shall begin with a description of the synoptic scale circulation features during the northern summer over the Indian monsoon region. The heating distribution during the northern summer over India exhibits a strong contrast in the meridional direction. The amplitude of heating is large over northeast India, north of Bay of Bengal, the foot hills of the Himalayas and over the elevated Tibetan plateau. This large thermal contrast, in the meridional direction, sets up the monsoonal Hadley circulation over the Indian subcontinent. The mean meridional circulation over India, is characterized by low-level south westerlies and upper tropospheric easterlies. The low-level cross-equatorial flow and the upper level anticyclonic flow over Tibet are outstanding features associated with the mean meridional circulation. A remarkable feature of the low-level south westerly winds over the Indian monsoon region is its large rotational component and significant cyclonic vorticity. Our aim is to study how the intraseasonal convective activity steers through this background flow. The phenomenon of low frequency northward movement of equatorial convection can be treated as a problem involving slow spatial and temporal evolution of perturbations superposed on a given basic flow. During the northern hemispheric summer, Yasunari(1979, 1980, 1981) noted a meridional propagation of cloudiness anomalies, over the whole of Asian monsoon area, in the range of around 40 days. The northward movement was most apparent over India. He suggested that the interaction between the low frequency oscillation and the Indian summer monsoon circulation produced the onset-active-break-revival-retrieval life cycle of the monsoonal activity. Sikka and Gadgil (1980) found that the maximum cloud cover over India fluctuated

on the time-scale of about 4 weeks during June-September. The time series analysis of Krishnamurti and Subrahmanyam (1982) using the MONEX wind data indicates that the 30-50 day oscillation is the most prominent subseasonal signal over the Indian monsoon region. They also showed that there is a steady meridional propagation of the 30-50 day mode at the rate of about 0.75° latitude per day. Hartmann and Michelson (1989) showed that the precipitation over south India exhibited a dominant variability on the time scale of 40-50 days. They related the active and break phases of the Indian summer monsoon with the equatorial 40-50 day oscillation.

We shall now describe the idealized experiments that were performed using the axisymmetric global spectral model. To begin with, we generate the monsoonal type of basic flow by forcing the axisymmetric global spectral model with an appropriate heating distribution. The heating is chosen in such a way that the maximum value occurs at around 26°N and at 200 mb in the vertical. The dissipation due to Rayleigh friction and Newtonian cooling, in the model, has a time-scale of 5 days. The initial condition corresponds to an atmosphere at rest. The initial temperatures at the different model levels correspond to their respective mean hemispheric values already mentioned in Chapter V. The model equations have been integrated for 25 days after switching on the heat source. The heating is kept fixed throughout the time of integration and the stationary response is first determined. The steady-state zonal velocity distribution is shown in Fig.6.3. The low-level westerly flow and the upper level easterlies resemble the structure of the monsoonal basic flow quite well. The maximum westerly flow (8 ms^{-1}) is at 700 mb and the maximum easterly (26 ms^{-1}) occurs at 100 mb. The low-level westerlies as well as the upper level easterlies peak at around 14°N . The arrival of the low-frequency wave over the Indian monsoon region triggers convective activity near the equatorial region which interacts with the large-scale monsoonal flow. Goswami and Shukla (1984) showed that the interaction between the moist convective heating and the model dynamics led to a quasi-periodic

fluctuation of the Hadley circulation in the range of 20-40 days. The modelling studies by Webster (1983) and Goswami and Shukla (1984) highlight the significance of surface hydrology in producing a meridional propagation of the ITCZ. Krishnan *et.al* (1992) performed experiments using an axisymmetric version of a global spectral model and found that, in the presence of cumulus heating (CISK), the convective anomalies near the equator propagated northward.

Having obtained a steady-state Hadley circulation that closely resembles the observed mean meridional circulation over the Indian summer monsoon region, we shall now examine the evolution of near-equatorial perturbations superposed on this background flow. In the axisymmetric model, the perturbations near the equator are generated by switching on an idealized equatorial heat source, that extends meridionally between 5°S and 5°N , and integrating the model for 5 days. Later on the equatorial heat source is turned off and cumulus heating (CISK) is imposed. The idea of introducing CISK is to study the interaction between the monsoonal basic flow and the convective activity. Charney and Eliassen (1964) who proposed the CISK mechanism, showed that in a conditionally unstable atmosphere, the interaction between the large scale motion and the cumulus convection works in such a way that the latent heat due to cumulus scale convection is derived from the large scale frictional convergence of moisture. The large scale motion in turn, is driven by the latent heat release from the cumulus clouds. Gadgil (1990) has shown that the variability of the ITCZ activity arises out of a nonlinear interaction between the small scale cumulus clouds and the synoptic scale motion. As already mentioned, the low-level circulation over India is characterized by strong cyclonic vorticity (see Fig.3.3.8d Chapter III). We now examine the interaction between this vorticity rich low-level circulation and the equatorial cumulus convection. The assumption in Charney's CISK, is that the rate of non-adiabatic cumulus heating is proportional to the relative vorticity at 900mb (ζ_{900}) and is given by

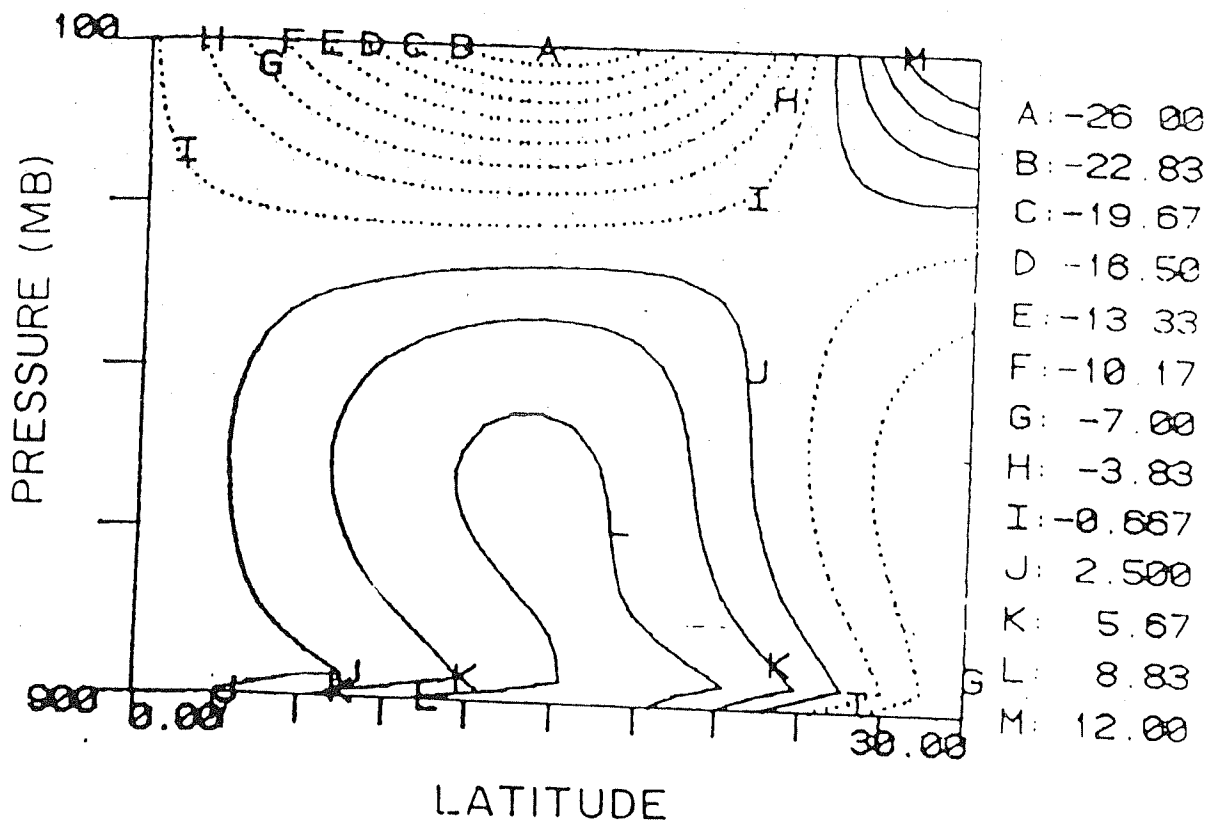


Fig.6.3. Model generated basic flow. Latitude-pressure section of zonal velocity (ms^{-1}).

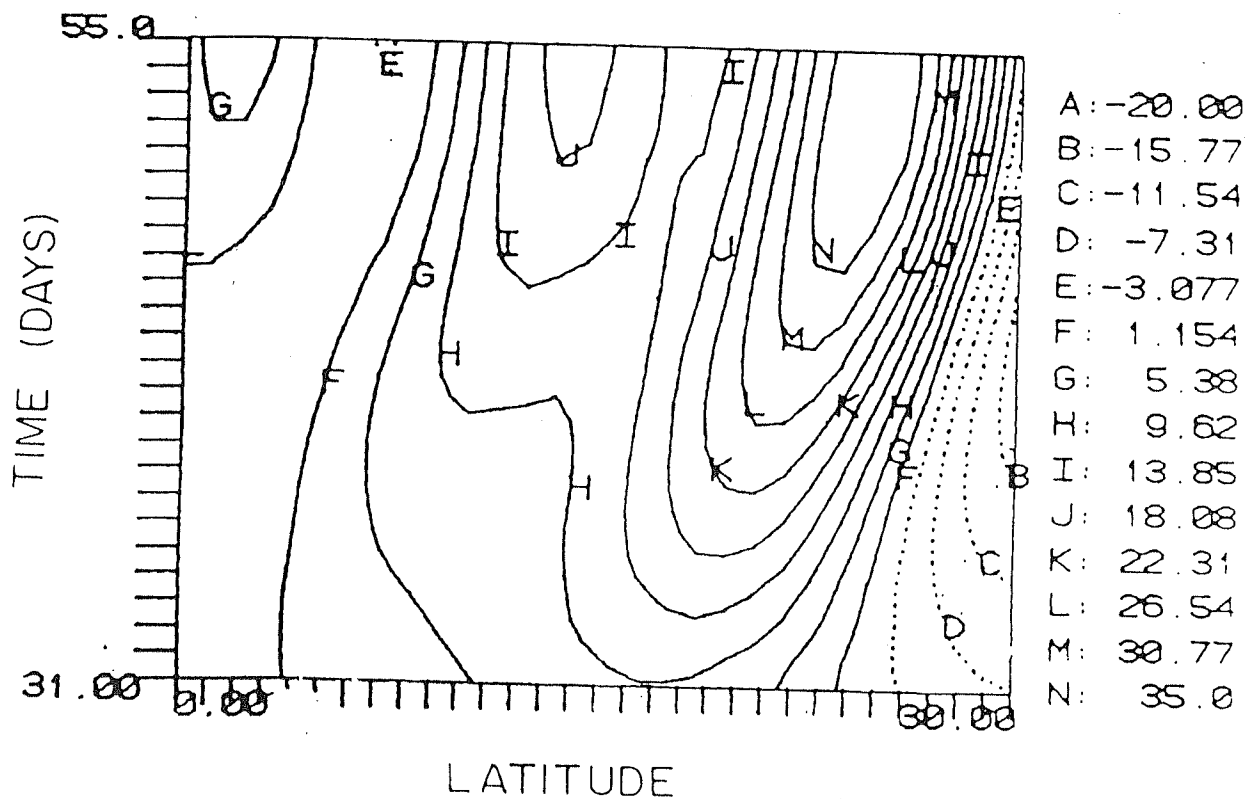


Fig.6.4. Latitude-time section of zonal velocity (ms^{-1}) at 700 mb.

$$\frac{\dot{Q}}{C_p} = H_f(p) \frac{p}{R} S \rho g \sqrt{\frac{K_e}{2f_0}} \sin(2\alpha_s) \zeta_{900} \quad (6.1)$$

where $\rho = 1.225 \text{ kgm}^{-3}$ is the density of air; $K_e = 10 \text{ m}^2\text{s}^{-1}$ is the eddy viscosity coefficient; $\alpha_s = 22.5^\circ$ is the angle between the surface geostrophic wind and the surface isobars; $g = 9.81 \text{ ms}^{-2}$ is the acceleration due to gravity; S is the static stability parameter; f_0 is the Coriolis parameter at 10°N ; $H_f(p)$ is the function $\frac{\pi}{2} \sin(\pi\sigma)$ which is used to distribute the heating in the vertical. This function has a maximum value at 500 mb and is zero at the surface and the top of the atmosphere. The value of S at 900 mb is $1.29 \times 10^{-6} \text{ m}^2\text{s}^{-2} P_a^{-2}$.

Figs.6.4 and 6.5 show the latitude-time cross-section of the zonal velocity and the relative vorticity distributions at 700 mb. Fig.6.6 shows the evolution of the relative vorticity at 900 mb. The time evolution in these figures is shown from day 31 till day 55. The distinct eastward tilt of the contours seen in the latitude-time cross-sections of Figs.6.4, 6.5 and 6.6 indicates that there is a northward movement of the perturbations. From Figs.6.5 and 6.6, it is seen that the trough at the lower levels advances northward with time implying the meridional propagation of the convective zone. We shall try to understand the physical mechanism by which this CISK induced northward propagation was produced. It can be seen that the basic flow, generated by the north-south heating contrast, has a strong meridional shear. The low level southwesterlies over the Indian summer monsoon region have a significant cyclonic vorticity. Therefore when CISK is introduced, the low level circulation tries to enhance the cumulus heating, which in turn modifies the large scale flow. This interaction works in a manner, so as to produce a phase difference between the perturbative wind field and the heating field. From Figs.6.4 and 6.5, it can be seen that there is a meridional phase difference between the vorticity field and the zonal wind field. It can be recalled that the vorticity perturbations (proxy for cumulus heating)

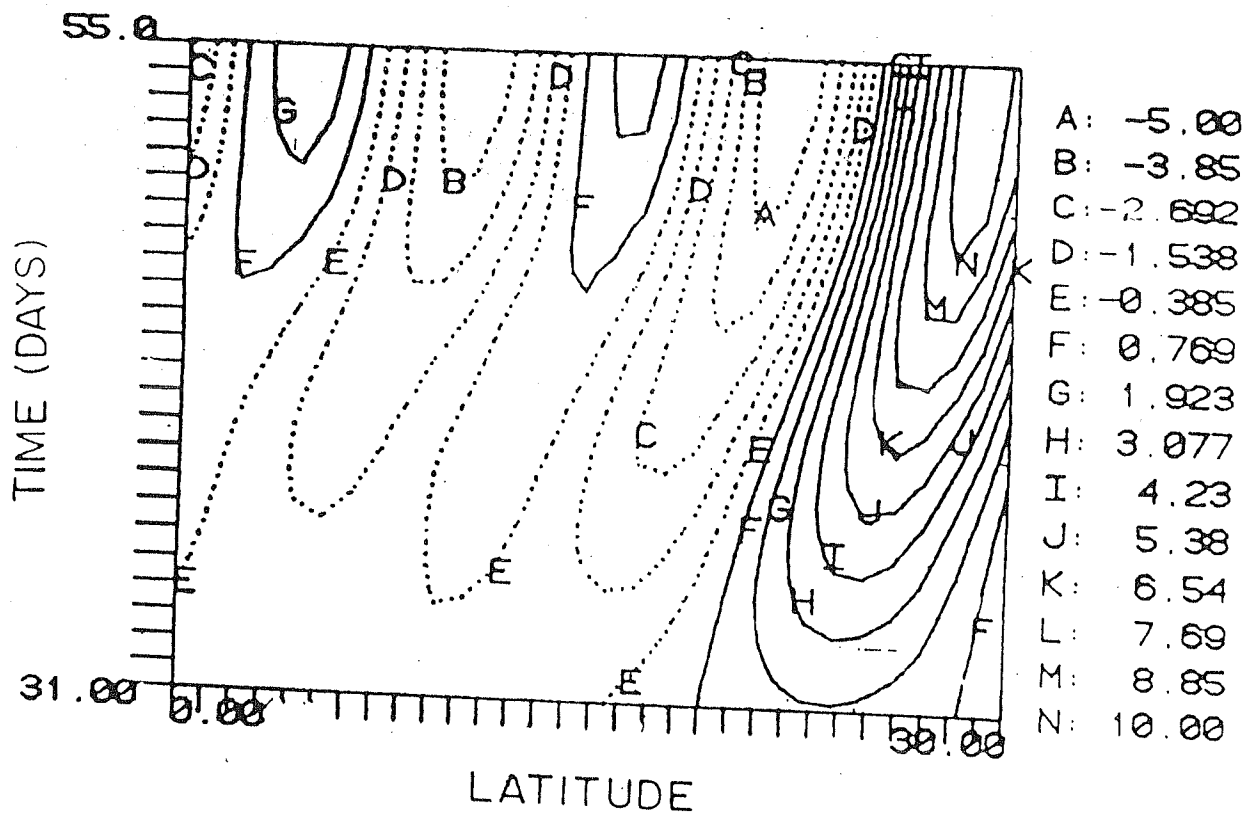


Fig.6.5. Latitude-time section of relative vorticity ($\times 10^{-5} s^{-1}$) at 700 mb.

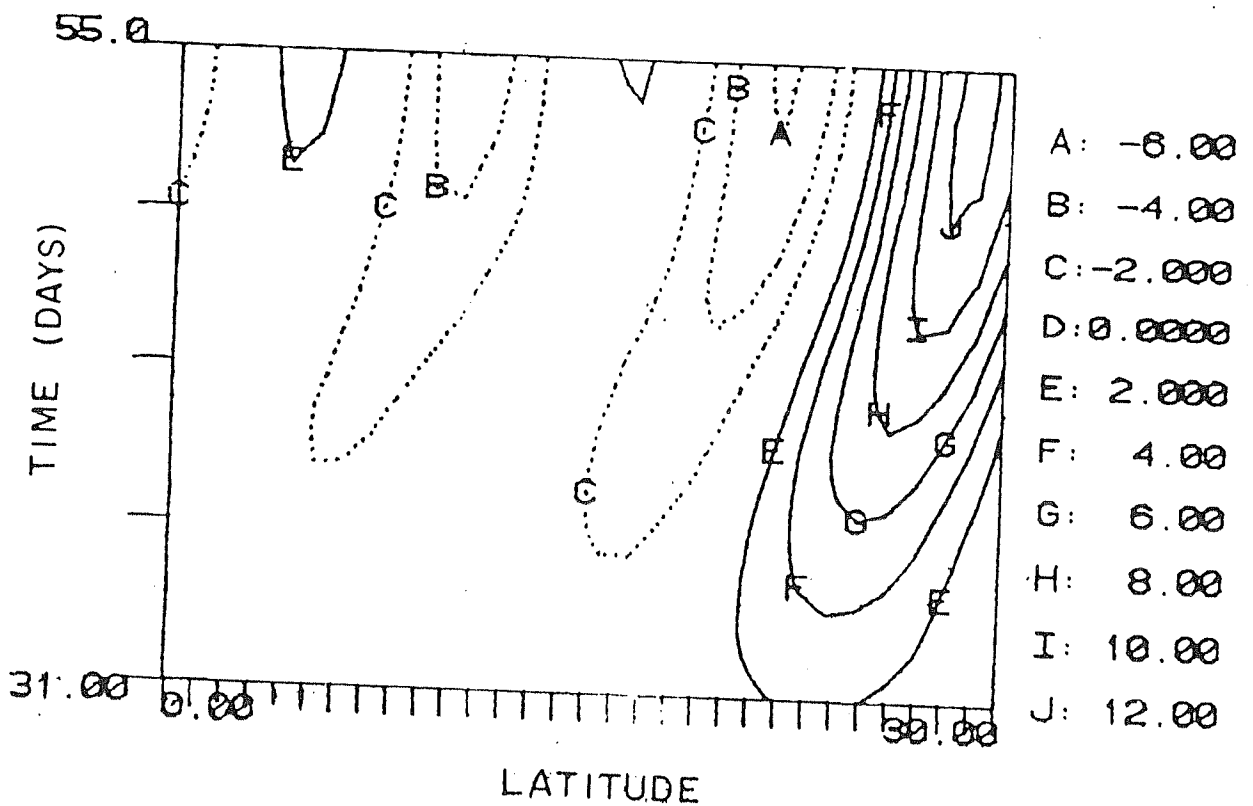


Fig.6.6. Latitude-time section of relative vorticity ($\times 10^{-5} s^{-1}$) at 900 mb.

are after all related to the latitudinal gradient of the perturbative zonal wind. Figs.6.4 and 6.5 show that the low level zonal wind field lags meridionally behind the vorticity field (perturbative cumulus heating): It is this meridional phase difference between the perturbations of zonal wind and cumulus heating that produces the northward migration of cumulus convection. The northward migration of convective activity obtained in our model, matches well with the observed meridional progression of intraseasonal low frequency transients over the Indian monsoon region. Observations suggest that the east-west oriented cloud bands appear quite prominently between $70^{\circ}E$ and $95^{\circ}E$ and extend upto 600 mb pressure level in the vertical. These cloud zones penetrate from the equatorial regions to about $30^{\circ}N$ in the Indian Monsoon region with a speed of around 1° latitude per day. From Figs.6.4, 6.5 and 6.6, the meridional propagation rate can be roughly estimated by calculating the slope of the tilt axis, which is about 0.5° latitude per day. We also find that the northward penetration of the convective activity is mostly in the lower and middle troposphere. The meridional propagation above the 500 mb pressure level is not very prominent. This result is in conformity with the observations of Kasture and Keshavamurty (1987). Further it is seen that there is no northward propagation of the convective anomalies beyond $32^{\circ}N$, even at the lower levels.

6.3 Concluding remarks

Many observational findings in the past have shown that the arrival of the equatorial low-frequency 30-50 day mode over the Indian summer monsoon region is characterized by a slow northward movement of convective activity over the Indian subcontinent. As a first step towards understanding the low-frequency variability of the onset, active and break cycles associated with the Indian summer monsoon, it is

extremely useful to study the physical mechanisms that govern this phenomenon of slow northward movement. In this chapter, a theoretical explanation for the meridional propagation of the low-frequency intraseasonal oscillation has been provided. Our study is based on idealized experiments using an axisymmetric 5-level global spectral model. To start with, a basic flow which closely resembles the time-mean Indian summer monsoon circulation, was generated in the model by forcing it with an appropriate heating distribution. Later on, near-equatorial perturbations were produced in the model, thereby mimicing the arrival of the 30-50 day mode over the Indian longitudes. The perturbations were actually generated in the model, by temporarily switching on an equatorial heat source. Having generated the perturbations, which are superposed on the basic flow, we investigated the impact of cumulus heating (CISK) on the perturbations. Our main interest was to examine the interaction between the time-mean basic flow and the cumulus heating associated with the low-frequency oscillation. The cumulus heating based on CISK was interactively determined from the low-level circulation. The assumption in CISK is that, the latent heat release by cumulus clouds is enhanced by the low-level frictional convergence of the large scale flow field and the latent heat in turn drives the large scale circulation. When the model was integrated in the presence of cumulus heating, it was found that the perturbations moved northward at the rate of about 0.5° latitude per day. The northward movement was most prominently seen at the lower levels. It was further found that the low level zonal wind field lagged meridionally behind the vorticity field (a proxy for cumulus heating (CISK)). The main conclusion of this study is that, the interactive cumulus heating (CISK) induces a meridional phase difference between the perturbations of zonal wind and the heating distribution, which is primarily responsible for the northward movement of the low-frequency intraseasonal convection over the Indian summer monsoon region.

References

1. Abbot, D.A., 1977: Hemispheric simulation of the Asian Summer Monsoon. *Pure. Appl. Geophys.*, 115, 1111-1130.
2. Anderson, J.R., and D.E. Stevens, 1987a: The response of the tropical atmosphere to low frequency thermal forcing. *J. Atmos. Sci.*, 44, 676-686.
3. Anderson, J.R., and D.E. Stevens, 1987b: The presence of linear wavelike modes in a zonally symmetric model of the tropical atmosphere. *J. Atmos. Sci.*, 44, 2115-2127.
4. Bender, C.M. and S.A. Orszag, 1978: *Advanced Mathematical methods for Scientists and Engineers*. McGraw-Hill, New York.
5. Bjerknes, J., 1969: Atmospheric teleconnections from the equatorial Pacific. *Mon. Wea. Rev.*, 97, 163-172.
6. Blackmon, M.L., Geisler, J.E., and Pitcher, E.J., 1983: A general circulation model study of January climate anomaly patterns associated with interannual variation of equatorial Pacific sea surface temperatures. *J. Atmos. Sci.*, 40, 1410-1425.
7. Bourke, W., 1974: A multi-Level spectral model. I. Formulation and Hemispheric Integrations. *Mon. Wea. Rev.*, 102, 687-701.
8. Bourke, W., McAvaney, B., Puri, K., and R. Thurling, 1977: Global modelling of atmospheric flow by spectral methods. *Methods in Computational Physics*, 17, 267-324.

9. Boyd, J.P., 1978: The effects of latitudinal shear on equatorial waves. Part.I: Theory and methods. *J.Atmos.Sci.*, 35, 2236-2258.
10. Cane, M.A., Munnich, M., and S.E.Zebiak, 1990: A study of self-excited oscillations of the tropical ocean-atmosphere system. Part.I: Linear analysis. *J.Atmos.Sci.*, 47, 1562-1577.
11. Chang, C.-P., 1977: Some theoretical problems of planetary scale monsoons. *Pure and Appl.Geophys.*, 115, 1089-1109.
12. Chang, C.-P., 1977a: Viscous internal gravity waves and low-frequency oscillation in the tropics. *J.Atmos.Sci.*, 34, 901-910.
13. Chang, C.-P., and H.Lim, 1988: Kelvin wave-CISK: A possible mechanism for the 30-50 day oscillations. *J.Atmos.Sci.*, 45, 1709-1720.
14. Chang, H.R., and P.J.Webster, 1990: Energy accumulation and emanation at low latitudes. Part II: Nonlinear response to strong episodic forcing. *J.Atmos.Sci.*, 47, 2624-2644.
15. Chao, W.C., 1987: On the origin of the tropical intraseasonal oscillation. *J.Atmos.Sci.*, 44, 1940-1949.
16. Charney, J.G., and A.Eliassen, 1964: On the Growth of the Hurricane Depression. *J.Atmos.Sci.*, 21, 68-75.
17. Chen, T.C., 1985: On the time variation in the tropical energetics of large-scale motions during the FGGE summer. *Tellus*, 37A, 258-275.
18. Chen, T.C., 1987: 30-50 day oscillation of 200-mb temperature and 850-mb height during the 1979 northern summer. *Mon.Wea.Rev.*, 115, 1589-1605.
19. Chen, T.C., and M.C.Yen, 1986: The 40-50 day oscillation of the low-level monsoon circulation over the Indian ocean. *Mon.Wea.Rev.*, 114, 2550-2570.
20. Chen, T.C., M.C.Yen and M.Murakami, 1988a: The water vapour transport associated with the 30-50 day oscillation over the Asian monsoon

- regions during 1979 summer. *Mon.Wea.Rev.*, 116, 1983-2002.
21. Chen, T.C., R.Y. Tzeng and M.C. Yen, 1988b: Development and life cycle of the Indian monsoon. Effect of the 30-50 day oscillation. *Mon.Wea.Rev.*, 116, 2183-2199.
 22. Cho, H.R., M.A. Jenkins and J. Boyd, 1983: A first order vorticity equation for tropical easterly waves. *J.Atmos.Sci.*, 40, 958-968.
 23. Chu, J.H., M. Yanai, and C.H. Sui, 1981: Effects of cumulus convection on the vorticity field in the tropics. Part.I: The large scale budget. *J.Meteor. Soc.Japan*, 59, 535-546.
 24. Colton, D.E., 1973: Barotropic scale interactions in the tropical upper troposphere during the northern summer. *J.Atmos.Sci.*, 30, 1287-1302.
 25. Cornejo-Garrido, A.G. and P.H. Stone, 1977: On the heat balance of the Walker circulation. *J.Atmos.Sci.*, 34, 1155-1162.
 26. Davey, M.D., 1989: A simple tropical moist model applied to the '40-day' wave. *Q.J.R.Meteorol.Soc.*, 115, 1071-1107.
 27. De Maria, M., 1985: Linear response of a stratified tropical atmosphere to convective forcing. *J.Atmos.Sci.*, 42, 1944-1959.
 28. Dickinson, R.E., 1971a: Analytic model for zonal winds in the tropics. I: Details of the model and simulation of the zonal mean troposphere. *Mon.Wea.Rev.*, 99, 501-510.
 29. Dickinson, R.E., 1971b: Analytic model for zonal winds in the tropics. II: Variation of the tropospheric mean structure with season and differences between hemispheres. *Mon.Wea.Rev.*, 99, 511-523.
 30. Eliassen, A., 1952: Slow thermally or frictionally controlled meridional circulation in a circular vortex. *Astrophys.Norv.* 5, 19-60.
 31. Emanuel, K.A., 1987: An air-sea interaction model of intraseasonal oscillations in the tropics. *J.Atmos.Sci.*, 44, 2324-2340.

32. Fein, J.S., 1977: Global vorticity budget over the tropics and subtropics at the 200 mb during the Northern Hemisphere Summer. *Pure Appl. Geophys.*, 115, 1493-1500.
33. Fennessy, M.J., L.Marx and J.Shukla, 1985: General circulation model sensitivity to 1982-83 equatorial Pacific sea surface temperature anomalies. *Mon.Wea.Rev.*, 113, 858-864.
34. Gadgil, S., 1990: Monsoon Dynamics. Hari Om Ashram Pretit Vikram Sarabhai Award Lectures, 45-58.
35. Geisler, J.E., 1981: A linear model of the Walker circulation. *J.Atmos.Sci.*, 38, 1390-1400.
36. Gill, A.E., 1980: Some simple solutions for heat induced tropical circulation. *Q.J.R.Meteorol.Soc.*, 106, 447-462.
37. Goswami, B.N., and J.Shukla, 1984: Quasi-periodic oscillations in a symmetric general circulation model. *J.Atmos.Sci.*, 41, 20-37.
38. Goswami, B.N., J.Shukla, E.K.Schneider and Y.C.Sud, 1984: Study of the dynamics of the intertropical convergence zone with a symmetric version of the GLAS climate model. *J.Atmos.Sci.*, 41, 5-19.
39. Graham, N.E., T.P.Barnett, R.M.Chervin, M.E.Schlesinger and U.Schlese, 1989: Comparisons of GCM and observed surface wind fields over the tropical Indian and Pacific oceans. *J.Atmos.Sci.*, 46, 760-788.
40. Gutzler, D.S., and R.A.Madden, 1989: Seasonal variations in the spatial structure of intraseasonal tropical wind fluctuations. *J.Atmos.Sci.*, 46, 641-660.
41. Hadley, G., 1735: Concerning the cause of the general trade winds. *Phil. Trans.*, 7, 58-62.
42. Hartmann, D.L., H.H.Hendon and R.A.Houze, 1984: Some implications of the mesoscale circulations in the tropical cloud clusters for large-scale dynamics and climate. *J.Atmos.Sci.*, 41, 113-121.

43. Hartmann,D.L., and J.R.Gross, 1988: Seasonal variability on the 40-50 day oscillation in wind and rainfall in the tropics. *J.Atmos.Sci.*, 45, 2680-2702.
44. Hartmann,D.L., and M.L.Michelson, 1989: Intraseasonal periodicities in Indian rainfall. *J.Atmos.Sci.*, 46, 2838-2862.
45. Hayashi,Y., and D.G.Golder, 1980: The seasonal variation of tropical transient planetary waves appearing in a GFDL General Circulation Model. *J.Atmos.Sci.*, 37, 705-716.
46. Hayashi,Y., and D.G.Golder, 1986: Tropical intraseasonal oscillations appearing in a GFDL general circulation model and FGGE data. Part I: Phase propagation. *J.Atmos.Sci.*, 43, 3058-3067.
47. Hayashi,Y., and D.G.Golder, 1988: Tropical intraseasonal oscillations appearing in a GFDL general circulation model and FGGE data. Part II: Structure. *J.Atmos.Sci.*, 45, 3017-3033.
48. Hayashi,Y., and A.Sumi, 1986: The 30-40 day oscillations simulated in an "Aqua Planet" model. *J.Met.Soc.Japan*, 64, 451-467.
49. He,H., J.W.McGinnis, Z.Song and M.Yanai, 1987: Onset of the Asian summer monsoon in 1979 and the effect of the Tibetan plateau. *Mon.Wea.Rev.*, 115, 1966-1995.
50. Heddinghaus,T.R. and A.F.Krueger, 1981: Annual and Interannual variations in the Outgoing Longwave Radiation in the tropics. *Mon.Wea.Rev.*, 109, 1208-1218.
51. Held,I.M., and A.Y.Hou, 1980: Nonlinear axially symmetric circulations in a nearly inviscid atmosphere. *J.Atmos.Sci.*, 37, 515-532.
52. Hendon,H.H., 1986: The time-mean flow and variability in a nonlinear model of the atmosphere with tropical diabatic forcing. *J. Atmos.Sci.*, 43, 72-88.

53. Hendon, H.H., 1988: A simple model of the 40-50 day oscillation. *J. Atmos. Sci.*, 45, 569-584.
54. Hodur, R.M., and J.S. Fein, 1977: A vorticity budget over the Marshall Islands during the spring and summer months. *Mon. Wea. Rev.*, 105, 1521-1526.
55. Holton, J.R., and D.E. Colton, 1972: A diagnostic study of the vorticity balance at 200 mb in the tropics during the northern summer. *J. Atmos. Sci.*, 29, 1124-1128.
56. Horel, J.D., and J.M. Wallace, 1981: Planetary scale atmospheric phenomena associated with the interannual variability of sea-surface temperature in the equatorial Pacific. *Mon. Wea. Rev.*, 109, 813-329.
57. Hoskins, B.J., and Karoly, D.J., 1981: The steady linear response of a spherical atmosphere to thermal and orographic forcing. *J. Atmos. Sci.*, 38, 1179-1196.
58. Hoskins, B.J., H.H. Hsu, I.N. James, M. Masutani, P.D. Sardeshmukh and G.H. White, 1989: Diagnostics of the global atmospheric circulation. Based on ECMWF analyses 1979-1989. WRCP-27, (WMO/TD - No.326).
59. Hoskins, B.J., and R.P. Pearce: Large scale dynamical processes in the atmosphere. Academic Press (1983).
60. Hsu, H.H., B.J. Hoskins, and F.F. Jin, 1990: The 1985/86 intraseasonal oscillation and the role of the extratropics. *J. Atmos. Sci.*, 47, 823-839.
61. Hunt, B.G., 1973: Zonally symmetric global general circulation models with and without the hydrologic cycle. *Tellus.*, 25, 338-354.
62. Julian, P.R., and R.M. Chervin, 1978: A study of the southern oscillation and Walker circulation phenomena. *Mon. Wea. Rev.*, 106, 1433-1451.
63. Kalnay, E., K.C. Mo and J. Paegle, 1986: Large-amplitude, short-scale stationary Rossby waves in the southern hemisphere: Observations and mechanistic experiments to determine their origin. *J. Atmos. Sci.*, 43, 252-275.

64. Kanamitsu, M., 1977: Monsoonal quasi-stationary ultra long waves of the tropical troposphere predicted by a real data prediction over a global tropical belt. *Pure. Appl. Geophys.*, 115, 1187-1208.
65. Kasahara, A., T. Sasamori and W. M. Washington, 1973: Simulation experiments with a 12-level stratospheric global circulation model. 1. Dynamical effect of the earth's orography and thermal influence of continentality. *J. Atmos. Sci.*, 30, 1229-1251.
66. Kasahara, A., 1984: The linear response of a stratified global atmosphere to tropical thermal forcing. *J. Atmos. Sci.*, 41, 2217-2237.
67. Kasahara, A., and P. L. Da Silva Dias, 1986: Response of planetary waves to tropical heating in a global atmosphere with meridional and vertical shear. *J. Atmos. Sci.*, 43, 1893-1911.
68. Kasture, S. V., and R. N. Keshavamurty, 1987: Some aspects of the 30-50 day oscillation. *Proc. Indian Acad. Sci. (Earth Planet Sci.)*, 96, 49-58.
69. Keshavamurty, R. N., 1968: On the maintenance of the mean zonal motion in the Indian summer monsoon region. *Mon. Wea. Rev.*, 96, 23-31.
70. Keshavamurty, R. N., 1982: Response of the atmosphere to sea surface temperature anomalies over the equatorial Pacific and the teleconnections of the southern oscillation. *J. Atmos. Sci.*, 39, 1241-1259.
71. Keshavamurty, R. N., and S. T. Awade, 1970: On the maintenance of the mean monsoon trough over north India. *Mon. Wea. Rev.*, 98, 315-320.
72. Keshavamurty, R. N., S. V. Kasture and V. Krishnakumar, 1986: 30-50 day oscillation of the monsoon: A new theory. *Beitr. Phys. Atmos.*, 49, 443-454.
73. Keshavamurty, R. N., V. Krishnakumar and S. V. Kasture, 1988: Northward propagation of the 30-50 day mode in the Indian Monsoon region. *Proc. Indian Acad. Sci. (Earth Planet Sci.)*, 97, 127-136.
74. Kinter III, J. L., J. Shukla, L. Marx and E. K. Schneider, 1988: A simulation of the winter and summer circulations with the NMC global spectral

- model. *J.Atmos.Sci.*, 45, 2486-2522.
75. Knutson, T.R., and K.M.Weickmann, 1987: 30-60 day atmospheric oscillations: Composite life cycles of convection and circulation anomalies. *Mon.Wea.Rev.*, 115, 1407-1436.
 76. Knutson, T.R., K.M.Weickmann and T.E.Kutzbach, 1986: Global-scale intraseasonal oscillations of outgoing longwave radiation and 250 mb zonal wind during northern hemisphere summer. *Mon.Wea.Rev.*, 114, 605-623.
 77. Krishnamurti, T.N., 1971: Tropical east-west circulations during the northern summer. *J.Atmos.Sci.*, 28, 1342-1347.
 78. Krishnamurti, T.N., 1985: Summer monsoon experiment - A review. *Mon. Wea.Rev.*, 113, 1590-1626.
 79. Krishnamurti, T.N., D.K.Oosterhof and A.V.Mehta, 1988: Air-sea interaction on the time-scale of 30-50 days. *J.Atmos.Sci.*, 45, 1304-1322.
 80. Krishnamurti, T.N., and D.Subrahmanyam, 1982: The 30-50 day mode at 850 mb during MONEX. *J.Atmos.Sci.*, 39, 2088-2095.
 81. Krishnamurti, T.N., N.Kanamitsu, W.J.Koss, and J.D.Lee., 1973: Tropical east-west circulations during the northern winter. *J.Atmos.Sci.*, 30, 780-787.
 82. Krishnamurti, T.N., P.K.Jayakumar, J.Sheng, N.Surgi and A.Kumar, 1985: Divergent circulations on the 30 to 50 day time scale. *J.Atmos.Sci.*, 42, 364-375.
 83. Krishnamurti, T.N., and S.Gadgil, 1985: On the structure of the 30-50 day mode over the globe during FGGE. *Tellus*, 37A, 336-360.
 84. Krishnamurti, T.N., and Y.Ramanathan, 1982: Sensitivity of the monsoon onset to differential heating. *J.Atmos.Sci.*, 39, 1290-1306.
 85. Krishnan, R., S.V.Kasture and R.N.Keshavamurty, 1992: Northward movement of the 30-50 day mode in an axisymmetric global spectral model.

- Current Science, 62, 732-735.
86. Krueger, A.F., and J.S. Winston, 1974: A comparison of the flow over the tropics during two contrasting circulation regimes. *J. Atmos. Sci.*, 31, 358-370.
 87. Kuo, H.L., 1956: Forced and free meridional circulations in the atmosphere. *J. Meteorology*, 13, 561-568.
 88. Kuo, H.L., and Y.F. Qian, 1982: Numerical simulation of the development of mean monsoon circulation during July. *Mon. Wea. Rev.*, 110, 1879-1897.
 89. Lau, K.M., 1981: Oscillations in a simple equatorial climate system. *J. Atmos. Sci.*, 38, 248-261.
 90. Lau, K.M., G.H. Yang and S.H. Shen, 1988: Seasonal and intraseasonal climatology of summer monsoon rainfall over east Asia. *Mon. Wea. Rev.*, 116, 18-37.
 91. Lau, K.M., and H. Lim, 1982: Thermally driven motions in an equatorial β -plane: Hadley and Walker circulations during the winter monsoon. *Mon. Wea. Rev.*, 110, 336-353.
 92. Lau, K.M., and H. Lim, 1984: On the dynamics of equatorial forcing of climate teleconnections. *J. Atmos. Sci.*, 41, 161-178.
 93. Lau, N.C., and K.M. Lau, 1986: The structure and propagation of intraseasonal oscillations appearing in a GFDL general circulation model. *J. Atmos. Sci.*, 43, 2023-2047.
 94. Lau, K.M., and L. Peng, 1987: Origin of low frequency (Intraseasonal) oscillations in the tropical atmosphere. Part I: Basic Theory. *J. Atmos. Sci.*, 44, 950-972.
 95. Lau, K.M., and L. Peng, 1990: Origin of low frequency (Intraseasonal) oscillations in the tropical atmosphere. Part III: Monsoon Dynamics. *J. Atmos. Sci.*, 47, 1443-1462.

96. Lau, K.M., and P.H.Chan, 1983: Short-term climate variability and atmospheric teleconnections from satellite observed outgoing longwave radiation. Part I: Simultaneous relationships. *J.Atmos.Sci.*, 2735-2767.
97. Lau, K.M., and P.H.Chan, 1985: Aspects of the 40-50 day oscillation during the northern winter as inferred from outgoing longwave radiation. *Mon.Wea. Rev.*, 113, 1889-1909.
98. Lau, K.M., and P.H.Chan, 1986: Aspects of the 40-50 day oscillation during the northern summer as inferred from outgoing longwave radiation. *Mon.Wea. Rev.*, 114, 1354-1367.
99. Lau, K.M., and P.H.Chan, 1988: Intraseasonal and interannual variations of tropical convection. A possible link between the 40-50 day oscillation and ENSO. *J.Atmos.Sci.*, 45, 506-521.
100. Lau, K.M., and S.Shen, 1988: On the dynamics of intraseasonal oscillations and ENSO. *J.Atmos.Sci.*, 45, 1781-1797.
101. Lau, N.C., I.M.Held and J.D.Neelin, 1988: The Madden-Julian oscillation in an idealized general circulation model. *J.Atmos.Sci.*, 45, 3810-3832.
102. Leibmann, B., and D.L.Hartmann, 1982: Interannual variations of outgoing IR associated with tropical circulation changes during 1974-78'. *J.Atmos. Sci.*, 39, 1153-1162.
103. Lim, H., and C.-P.Chang, 1981: A theory for midlatitude forcing of tropical motions during winter monsoons. *J.Atmos.Sci.*, 38, 2377-2392.
104. Lim, H., and C.-P.Chang, 1983: Dynamics of teleconnections and Walker circulations forced by equatorial heating. *J.Atmos.Sci.*, 40, 1897-1915.
105. Lim, H., and C.-P.Chang, 1986: Generation of internal and external mode motions from internal heating. Effects of vertical shear and damping. *J.Atmos.Sci.*, 43, 948-957.
106. Lindzen, R.S., 1967: Planetary waves on beta-planes. *Mon.Wea.Rev.*, 95, 441-451.

107. Lindzen, R.S., and S. Nigam, 1987: On the role of sea surface temperature gradients in forcing low-level winds and convergence in the tropics. *J. Atmos. Sci.*, 44, 2418-2436.
108. Longuet-Higgins, M.S., 1968: The eigenfunctions of the Laplace's tidal equations over a sphere. *Phil. Trans. Roy. Soc. London*, A262, 511-607.
109. Lorenc, A.C., 1984: The evolution of planetary-scale 200 mb divergent flow during the FGGE year. *Q. J. R. Meteorol. Soc.*, 110, 427-442.
110. Lorenz, E.N., 1967: Nature and theory of the general circulation of the atmosphere., WMO No. 218., World Meteorological Organization.
111. Madden, R.A., and P.R. Julian, 1971: Detection of a 40-50 day oscillation in the zonal wind in the tropical Pacific. *J. Atmos. Sci.*, 28, 702-708.
112. Madden, R.A., 1986: Seasonal variations of the 40-50 day oscillations in the tropics. *J. Atmos. Sci.*, 43, 3138-3158.
113. Manabe, S., D.G. Hahn and J.L. Holloway Jr, 1974: The seasonal variation of the tropical circulation as simulated by a global model of the atmosphere. *J. Atmos. Sci.*, 31, 43-83.
114. Manabe, S, J.L. Holloway, Jr., and H.M. Stone, 1970: Tropical circulation in a time-integration of a global model of the atmosphere. *J. Atmos. Sci.*, 27, 580-613.
115. Manabe, S., J. Smagorinsky and R.F. Strickler, 1965: Simulated climatology of a general circulation model with a hydrologic cycle. *Mon. Wea. Rev.*, 93, 769-798.
116. Matsuno, T., 1966: Quasi-geostrophic motions in the equatorial area. *J. Meteor. Soc. Japan*, 44, 25-42.
117. Miyahara, S., 1987: A simple model of the tropical intraseasonal oscillation. *J. Meteor. Soc. Japan*, 165, 341-351.

118. Murakami, M., 1983: Analysis of the deep convective activity over the western Pacific and southeast Asia. Part I: Diurnal variation. *J. Meteor. Soc. Japan*, 61, 60-76.
119. Murakami, T., 1980: Temporal variations of satellite-observed outgoing longwave radiation over the winter monsoon region. Part I: Long-period (15-30) oscillations. *Mon. Wea. Rev.*, 108, 408-426.
120. Murakami, T., L.X. Chen, and A. Xie, 1986: Relationship among seasonal cycles, low frequency oscillations and transient disturbances as revealed from outgoing longwave radiation. *Mon. Wea. Rev.*, 114, 1456-1465.
121. Murakami, T., L.X. Chen, A. Xie and M.L. Shrestha, 1986: Eastward propagation of the 30-60 day perturbations as revealed from outgoing longwave radiation data. *J. Atmos. Sci.*, 43, 961-971.
122. Murakami, T., and T. Nakazawa, 1985a: Tropical 45 day oscillations during the 1979 northern hemisphere summer. *J. Atmos. Sci.*, 42, 1107-1122.
123. Murakami, T., and T. Nakazawa, 1985b: Transitions from the southern to northern hemisphere summer monsoon. *Mon. Wea. Rev.*, 113, 1470-1486.
124. Neelin, J.D., 1988: A simple model for surface stress and low-level flow in the tropical atmosphere driven by prescribed heating. *Q. J. R. Meteorol. Soc.*, 114, 747-770.
125. Neelin, J.D., 1989: On the interpretation of Gill Model. *J. Atmos. Sci.*, 46, 2466-2468.
126. Neelin, J.D., 1990: A hybrid coupled general circulation model for El-Niño studies. *J. Atmos. Sci.*, 47, 674-693.
127. Neelin, J.D., 1991: The slow sea surface temperature mode and the fast wave limit: Analytic theory for tropical interannual oscillations and experiments in a hybrid coupled model. *J. Atmos. Sci.*, 48, 584-606.
128. Neelin, J.D., I.M. Held and K.H. Cook, 1987: Evaporation-wind feedback and low-frequency variability in the tropical atmosphere. *J. Atmos. Sci.*, 44,

2341-2348.

129. Nitta, T., 1983: Observational study of heat sources over the eastern Tibetan plateau during the summer monsoon. *J. Meteor. Soc. Japan*, 61, 590-605.
130. Oort, A. H., and E. M. Rasmussen, 1970: On the annual variation of the monthly mean meridional circulation. *Mon. Wea. Rev.*, 98, 423-442.
131. Oort, A. H., and J. P. Peixoto, 1983: Global angular momentum and energy balance requirements from observations. *Adv. Geophys.*, 25, 355-490.
132. Parker, D. E., 1973: Equatorial Kelvin waves at 100 mb. *Q. J. R. Meteorol. Soc.*, 99, 116-129.
133. Pearce, R. P., and U. C. Mohanty, 1984: Onsets of the Asian summer monsoon 1979-82. *J. Atmos. Sci.*, 41, 1620-1639.
134. Philander, S. G. H., 1983: El-Niño-Southern Oscillation phenomena. *Nature*, 302, 295-301.
135. Philander, S. G. H., T. Yamagata and R. C. Pacanowski, 1984: Unstable air-sea interactions in the tropics. *J. Atmos. Sci.*, 41, 604-613.
136. Philips, P. J. and A. E. Gill, 1987: An analytic model of the heat induced tropical circulation in the presence of a mean wind. *Q. J. R. Meteorol. Soc.*, 113, 213-236.
137. Pitcher, E. J., R. C. Malone, V. Ramanathan, M. L. Blackmon, K. Puri and W. Bourke, 1983: January and July simulations with a spectral general circulation model. *J. Atmos. Sci.*, 40, 580-604.
138. Plumb, R. A., and R. C. Bell, 1982: Equatorial waves in steady zonal flow. *Quart. J. Roy. Meteor. Soc.*, 108, 313-334.
139. Press, W. H., B. P. Flannery, S. A. Teukolsky and W. T. Vetterling, 1988: *Numerical Recipes: The Art of Scientific Computing*. Cambridge University

Press, Cambridge, 52pp.

140. Quiroz, R.S., 1983: The climate of the El Niño winter of 1982-83: a season of extraordinary climate anomalies. *Mon. Wea. Rev.*, 111, 1685-1706.
141. Ramage, C.S., 1968: Role of a tropical "Maritime Continent" in the atmospheric circulation. *Mon. Wea. Rev.*, 96, 365-370.
142. Rasmusson, E.M., and T. Carepenter, 1982: Variations in the tropical sea surface temperature and surface winds associated with the southern oscillation/El Niño. *Mon. Wea. Rev.*, 110, 354-384.
143. Rasmusson, E.M., and Wallace, J.M., 1983: Meteorological aspects of the El Niño-Southern Oscillation. *Science*, 222, 1195-1202.
144. Reed, R.J., and R.H. Johnson, 1974: The vorticity budget of the synoptic-scale wave disturbances in the tropical western Pacific. *J. Atmos. Sci.*, 31, 1784-1790.
145. Reeves, R.W., C.F. Ropelewski and M.D. Hadlow, 1979: Relationship between large-scale motion and convective precipitation during GATE. *Mon. Wea. Rev.*, 107, 1154-1168.
146. Riehl, H., and D. Soltwisch, 1974: On the depth of the friction layer and the vertical transfer of momentum in the trades. *Beit. Phys. Atmos.*, 47, 56-66.
147. Risbey, J.S., and P.H. Stone, 1988: Observations of the 30-60 day oscillation in zonal mean atmospheric angular momentum and high cloud cover. *J. Atmos. Sci.*, 45, 2026-2038.
148. Rosenlof, K.H., D.E. Stevens, J.R. Anderson and P.E. Ciesielski, 1986: The Walker circulation with observed zonal winds, a mean Hadley cell and cumulus friction. *J. Atmos. Sci.*, 43, 449-467.
149. Rowntree, P.R., 1972: The influence of tropical east Pacific ocean temperatures on the atmosphere. *Q. J. R. Meteorol. Soc.*, 98, 290-321.

150. Sankar Rao,M., 1969: On the steady state theory of global monsoons. *Tellus*, 21, 308-330.
151. Sardeshmukh,P.D., and I.M.Held, 1984: The vorticity balance in the tropical upper troposphere of a GCM. *J.Atmos.Sci.*, 41, 768-778.
152. Sardeshmukh,P.D., and B.J.Hoskins, 1985: Vorticity balances in the tropics during 1982-1983 El-niño-Southern Oscillation event. *Q.J.R.Meteorol. Soc.*, 111,261-278.
153. Sardeshmukh,P.D., and B.J.Hoskins, 1988: The generation of global rotational flow by steady idealized tropical divergence. *J.Atmos.Sci.*, 45, 1228-1251.
154. Sashegyi,K.D., and J.E.Geisler, 1987: A linear model study of cross equatorial flow forced by summer monsoon heat sources. *J.Atmos.Sci.*, 44, 1706-1722.
155. Schaack,T.K., D.R.Johnson and M.Y.Wei, 1990: The three-dimensional distribution of atmospheric heating during the GWE. *Tellus*, 42A, 305-327.
156. Schlesinger,M.E., and W.L.Gates, 1980: The January and July performance of the OSU two-level atmosphere general circulation model. *J.Atmos. Sci.*,37, 1914-1943.
157. Schneider,E.K., 1977: Axially symmetric steady-state models of the basic state for instability and climate studies. Part.II. Nonlinear calculations. *J.Atmos.Sci.*, 34, 280-296.
158. Schneider,E.K., 1987: A simplified model of the modified Hadley Circulation. *J.Atmos.Sci.*, 44, 3311-3328.
159. Schneider,E.K., and R.S.Lindzen, 1976: A discussion of the parameterization of momentum exchange by cumulus convection. *J.Geophys.Res.*, 81, 3158-3160.
160. Schneider,E.K. and R.S.Lindzen, 1977: Axially symmetric steady-state models of the basic state for instability and climate studies. Part.I. Linearized calculations. *J.Atmos.Sci.*, 34, 263-279.

161. Shapiro, L.J., 1978: The vorticity budget of a composite African tropical wave disturbance. *Mon. Wea. Rev.*, 106, 806-817.
162. Shukla, J., and M.J. Fennesy, 1988: Prediction of time-mean atmospheric circulation and rainfall: Influence of Pacific sea surface temperature anomaly. *J. Atmos. Sci.*, 45, 9-28.
163. Sikka, D.R., and S. Gadgil, 1980: On the maximum cloud zone and the ITCZ over Indian longitudes during the southwest monsoon. *Mon. Wea. Rev.*, 108, 1840-1853.
164. Silva Dias, P.L., W.H. Schubert and M. De Maria, 1983: Large-scale response of the tropical atmosphere to transient convection. *J. Atmos. Sci.*, 40, 2689-2707.
165. Simmons, A.J., 1982: The forcing of stationary wave motion by tropical diabatic heating. *Q. J. R. Meteorol. Soc.*, 108, 503-534.
166. Slingo, J.M., and R.A. Madden, 1991: Characteristics of the tropical intraseasonal oscillation in the NCAR community climate model. *Q. J. R. Meteorol. Soc.*, 117, 1129-1170.
167. Stevens, D.E., 1979: Vorticity, momentum and divergence budgets of synoptic-scale wave disturbances in the tropical Atlantic. *Mon. Wea. Rev.*, 107, 535-550.
168. Stone, P.H., W.J. Quirk, and R.C.J. Somerville, 1974: The effect of small scale vertical mixing of horizontal momentum in a general circulation model. *Mon. Wea. Rev.*, 102, 765-771.
169. Sud, Y. and A. Molod, 1988: The roles of dry convection, cloud-radiation feedback processes and the influence of recent improvements in the parameterization of convection in the GLA GCM. *Mon. Wea. Rev.*, 116, 2366-2387.
170. Sui, C.H., and K.M. Lau, 1989: Origin of low-frequency (Intraseasonal) oscillations in the tropical atmosphere. Part II: Structure and propagation of

- mobile wave-CISK modes and their modification by lower boundary forcings. *J.Atmos.Sci.*, 46, 37-56.
171. Sui,C.H., and M.Yanai, 1986: Cumulus ensemble effects on the large-scale vorticity and momentum fields of GATE. Part I: Observational evidence. *J.Atmos.Sci.*, 43, 1618-1642.
 172. Sumi,A., and T.Murakami, 1981: Large-scale aspects of the 1978-79 winter circulation over the greater WMONEX region. Part I: Monthly and season mean fields. *J.Meteor.Soc.Japan*, 59, 625-645.
 173. Swinbank,R., T.N.Palmer and M.K.Davey, 1988: Numerical simulation of the Madden and Julian oscillation. *J.Atmos.Sci.*, 45, 774-788.
 174. Takahashi,M., 1987: A theory of the slow phase speed of the intraseasonal oscillation using the wave-CISK. *J.Meteor.Soc.Japan*, 65, 43-49.
 175. Thomson,S.L., and D.L.Hartmann, 1979: "Cumulus friction" : Estimated influence on the tropical mean meridional circulation. *J.Atmos.Sci.*, 36, 2022-2026.
 176. Thomson,S.L., and D.L.Hartmann, 1980: Reply. *J.Atmos.Sci.*, 37, 2806-2808.
 177. Ting,M., and I.M.Held, 1990: The stationary wave response to a tropical SST anomaly in an idealized GCM. *J.Atmos.Sci.*, 47, 2546-2566.
 178. Vernekar,A.D., 1967: On mean meridional circulations in the atmosphere. *Mon.Wea.Rev.*, 95, 705-721.
 179. Wallace,J.M., and Gutzler, D.S., 1981: Teleconnections in the geopotential height field during the northern hemisphere winter. *Mon.Wea.Rev.*, 109, -812.
 180. Wallace,J.M., and Kousky, V.E., 1968: Observational evidence of the Kelvin waves in the tropical stratosphere. *J.Atmos.Sci.*, 25, 900-907.

181. Wang, B., 1988: Dynamics of tropical low-frequency waves: An analysis of the moist Kelvin wave. *J. Atmos. Sci.*, 45, 2051-2065.
182. Wang, B., and H. Rui, 1990: Dynamics of the coupled moist Kelvin-Rossby wave on an equatorial β plane. *J. Atmos. Sci.*, 47, 397-413.
183. Wang, B., and J. Chen, 1989: On the zonal-scale selection and vertical structure of equatorial intraseasonal waves. *Q. J. R. Meteorol. Soc.*, 115, 1301-1323.
184. Wang, X. L., and T. Murakami, 1988: Intraseasonal disturbance activity before, during and after the 1982-83 ENSO. *J. Atmos. Sci.*, 45, 3754-3770.
185. Washington, W. M., and A. Kasahara, 1970: A January simulation experiment with the 2-layer version of the NCAR global circulation model. *Mon. Wea. Rev.*, 95, 559-580.
186. Weare, B. C., 1986: A simple model of the tropical atmosphere with circulation dependent heating and specific humidity. *J. Atmos. Sci.*, 43, 2001-2016.
187. Webster, P. J., 1972: Response of the tropical atmosphere to local, steady forcing. *Mon. Wea. Rev.*, 100, 518-541.
188. Webster, P. J., 1973a: Remote forcing of the time-independent tropical atmosphere. *Mon. Wea. Rev.*, 101, 58-68.
189. Webster, P. J., 1973b: Temporal variation of low-latitude zonal circulations. *Mon. Wea. Rev.*, 101, 803-816.
190. Webster, P. J., and L. C. Chou, 1980: Seasonal structure of a simple monsoon system. *J. Atmos. Sci.*, 37, 354-367.
191. Webster, P. J., 1983: Mechanisms of monsoon low-frequency variability: Surface hydrological effects. *J. Atmos. Sci.*, 40, 2110-2124.
192. Webster, P. J., 1988: Mechanisms determining atmospheric response to sea surface temperature anomalies. *J. Atmos. Sci.*, 38, 554-571.

193. Webster, P.J., and H.R. Chang, 1988: Equatorial energy accumulation and emanation regions: Impact of zonally varying basic state. *J. Atmos. Sci.*, 45, 803-829.
194. Webster, P.J., and J.R. Holton, 1982: Cross equatorial response to midlatitude forcing in a zonally varying basic state. *J. Atmos. Sci.*, 39, 722-733.
195. Weickmann, K.M., G.R. Lussky and J.E. Kutzbach, 1985: Intraseasonal (30-60 day) fluctuations of outgoing longwave radiation and 250 mb streamfunction during northern winter. *Mon. Wea. Rev.*, 113, 941-961.
196. Weickmann, K.M., and S.J.S. Khalsa, 1990: The shift of convection from the Indian ocean to the western Pacific ocean during a 30-60 day oscillation. *Mon. Wea. Rev.*, 118, 964-978.
197. Whittaker, E.T. and G.N. Watson, 1950: *A Course on Modern Analysis*. Fourth Edition, Cambridge University Press, Cambridge, 347 pp.
198. Williams, K.T., and W.M. Gray, 1973: Statistical analysis of satellite observed trade wind clusters in the western north Pacific. *Tellus*, 25, 313-336.
199. Wilson, J.D., and M.K. Mak, 1984: Tropical response to lateral forcing with a latitudinally and zonally nonuniform basic state. *J. Atmos. Sci.*, 41, 1187-1201.
200. Wyrtki, K., 1975: El Niño - the dynamic response of the equatorial Pacific ocean to atmospheric forcing. *J. Phys. Oceanogr.*, 5, 572-587.
201. Yamagata, T., 1987: A simple moist model relevant to the origin of intraseasonal disturbances in the tropics. *J. Met. Soc. Japan*, 65, 153-165.
202. Yanai, M., and T. Maruyama, 1966: Stratospheric wave disturbances propagating over the equatorial Pacific. *J. Meteor. Soc. Japan*, 44, 291-294.
203. Yasunari, T., 1979: Cloudiness fluctuations associated with the northern hemisphere summer monsoon. *J. Meteor. Soc. Japan*, 57, 227-242.

204. Yasunari, T., 1980: A quasi-stationary appearance of 30-40 day period in the cloudiness fluctuations during the summer monsoon over India. *J. Meteor. Soc. Japan*, 58, 225-229.
205. Yasunari, T., 1981: Structure of an Indian summer monsoon system with a period around 40 days. *J. Meteor. Soc. Japan*, 59, 336-354.
206. Zhang, C., and P. J. Webster, 1989: Effects of zonal flows on equatorial trapped waves. *J. Atmos. Sci.*, 46, 3632-3652.

List of Publications

1. **R.Krishnan**, S.V.Kasture and R.N.Keshavamurty 1992: Northward movement of the 30-50 day mode in an axisymmetric global spectral model. *Current Science*, 62, 732-735.
2. **R.Krishnan** and S.V.Kasture, 1992: Impact of nonlinearities on the stationary Kelvin and Rossby waves in the tropical atmosphere. (Submitted to Q.J.R.Meteorol.Soc.).
3. **R.Krishnan** and S.V.Kasture and R.N.Keshavamurty: Linear and nonlinear studies of the dynamics of the time-mean tropical Hadley circulation. (Under preparation).
4. **R.Krishnan**, R.N.Keshavamurty and S.V.Kasture: Modelling the meridional progression of the low-frequency intraseasonal oscillation over the Indian summer monsoon region. (Under preparation).
5. **R.Krishnan**, R.N.Keshavamurty, and S.V.Kasture: Idealized studies of the dynamics of the Walker circulation. Meeting on Mathematical Modelling of the Ocean, June 1991, C-MMACS, National Aeronautical Laboratory, Bangalore - 37.
6. V.Krishnakumar, **R.Krishnan** and S.V.Kasture: A model study of the active and break monsoon conditions over western India. International Symposium on Evolution of Deserts, February 1992, Physical Research Laboratory, Ahmedabad - 39.
7. **R.Krishnan**, R.N.Keshavamurty, and S.V.Kasture: Diagnostic studies of the vorticity balance in the tropical upper atmosphere of a nonlinear global spectral model. National Symposium on Advances in Tropical Meteorology (Tropmet -92), February 1992, Space Application Centre, Ahmedabad - 53.
8. S.V.Kasture, **R.Krishnan**, R.N.Keshavamurty and V.Satyan: A model study of the northward propagation of zonal wind shear zone in the monsoon region. National Symposium on Advances in Tropical Meteorology (Tropmet-92), February 1992, Space Application Centre, Ahmedabad - 53.
9. **R.Krishnan**, R.N.Keshavamurty, and S.V.Kasture: Northward movement of the 30-40 day oscillation in an axisymmetric global spectral model. National Space Science Symposium, March 1992, Physical Research Laboratory, Ahmedabad - 39.